

SWINBURNE UNIVERSITY OF TECHNOLOGY

DOCTORAL THESIS

Analysis and Design of In-ear Devices

Author:
Philip KINSELLA

Supervisors:
Dr. Paul STODDART
Dr. Charles RANSCOMBE

*A thesis submitted in fulfillment of the requirements
for the degree of Doctor of Philosophy*

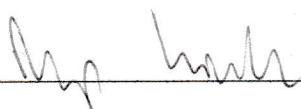
October 23, 2018

Declaration of Authorship

I, Philip KINSELLA, declare that this thesis titled, "Analysis and Design of In-ear Devices" and the work presented in it are my own. I confirm that:

- This work was done wholly or mainly while in candidature for a research degree at this University.
- Where any part of this thesis has previously been submitted for a degree or any other qualification at this University or any other institution, this has been clearly stated.
- Where I have consulted the published work of others, this is always clearly attributed.
- Where I have quoted from the work of others, the source is always given. With the exception of such quotations, this thesis is entirely my own work.
- I have acknowledged all main sources of help.
- Where the thesis is based on work done by myself jointly with others, I have made clear exactly what was done by others and what I have contributed myself.

Signed: _____



SWINBURNE UNIVERSITY OF TECHNOLOGY

Abstract

Faculty of Science, Engineering and Technology
Engineering

Doctor of Philosophy

Analysis and Design of In-ear Devices

by Philip KINSELLA

The human ear is the target for a wide variety of devices, such as earphones, hearing aids, Bluetooth devices, and even health monitors. However, the majority of these devices still rely on percentiles derived from anthropometric data, which can result in devices that are comfortable for only a relatively small proportion of the population. Customized devices aim to alleviate this discomfort by fitting the in-ear devices to the shape of the individual. However, using current customization processes, these devices can cost hundreds to thousands of dollars. With the advancement of 3D scanning and 3D printing there is the possibility to reduce these costs and make customization accessible. This research aims at bridging the gap between 3D scanning and 3D printing by developing an automated customization framework for in-ear devices. The difficulty with automating the customization of in-ear devices is the complexity of 3D scan data and the variation in shape among the population.

By assessing 3D scanning systems it was determined that automation systems were required to remove the need for an expert user and make the technology accessible for a larger proportion of the population. A custom-built 3D scanning was therefore developed that automatically captures and processes the data to reconstruct the shape of the individuals ear based on the principles of photogrammetry.

Using this 3D scanning system a database of 3D ears was constructed and a state-of-the-art statistical shape model (SSM) of the ear was generated which formed the basis for automating the customization of in-ear devices. Using the SSM, a constrained 3D mesh deformation process, known as As-Constrained-As-Possible (ACAP), was developed which takes the full 3D scan data and the SSM and deforms a CAD design such that the device is still functional and directly 3D printable.

The novelty of combining automated 3D scanning with statistical analysis and constrained 3D mesh deformation has allowed for a form of mass-customization to be developed which can operate without the need for user intervention. This could potentially lead to reduced cost and manufacturing time for hearing aids, or simply a more-accessible method for customized in-ear devices.

Acknowledgements

Firstly, I would like to express my sincere gratitude to my supervisors, Prof. Paul Stoddart and Dr. Charles Ranscombe for their support and motivation over the course of the PhD. I could not have imagined having a better team for my PhD study.

Besides my advisor, I would like to thank the rest of my thesis committee: Assoc. Prof. Scott Wade, Dr. Gianni Renda, and Prof. Romesh Nagarajah, for their comments and encouragement, which assisted me in getting over the hurdles in the research. My sincere thanks also goes to Prof. Peter Cadusch who provided invaluable support and knowledge over the course of the PhD. I would also like to thank Swinburne University of Technology and the ARC for part support of the project through the ARC Training Centre in Biodevices (grant number IC140100023) and all of the technology staff who provided knowledge and training in 3D scanning and 3D printing technologies.

Last but not the least, I would like to thank my family: my parents and to my brother for their support and encouragement, and especially to my own family for whom none of this would have been possible.

Contents

Declaration of Authorship	iii
Abstract	v
Acknowledgements	vii
1 Introduction	1
1.1 Automated Design of Customised Devices for the Human Ear	3
1.1.1 Mass-Manufacture versus mass-customization of Consumer Devices	3
1.1.1.1 Comfort and Functionality from customization	6
1.1.1.2 Improved Emotional Attachment to the Customised Device	7
1.1.2 Prevalence of Advanced 3D Imaging and Rapid Prototyping Technology	7
1.1.3 Why is Automation Necessary for Custom-Fit In-Ear Device Design?	8
1.1.4 The Human Ear	9
1.1.4.1 Standard customization of an In-Ear Hearing Aid	10
1.1.5 Methods for Automating customization	13
1.1.5.1 Automating Customised In-Ear Device Design	13
1.1.5.2 The Performance and Accuracy of Current Automation Systems	16
1.1.5.3 Complexities in automating hearing-aid design	17
1.1.6 Application to this research	18
1.1.7 3D Scanning Technology and It's Application to the Human Ear	19
1.1.7.1 Passive 3D Scanning Systems	19
1.1.7.2 Passive Systems for the Human Ear	20
1.1.7.3 Active 3D Scanning Systems	23
1.1.7.4 Active Systems for the Human Ear	24
1.1.7.5 Application to this research	25
1.1.7.6 Remaining Questions for Applicability to the Human Ear	26
1.1.8 Analyzing 3D Scan Data for Automating the Customization Process	27
1.1.8.1 Generating a Model of the Shape Variation	27
1.1.8.2 3D Non-Rigid Shape Matching for One-to-One Correspondences	28
1.1.8.3 Application to this Research	28
1.1.9 Design of In-Ear Devices For Automated Rapid Prototyping	29
1.1.9.1 Design of Customized In-Ear Devices	29
1.1.9.2 FDM, SLS and SLA 3D Printing	30
1.1.9.3 Achievable Surface Quality with SLA 3D Printing	30
1.1.9.4 Considerations for 3D Printing Speed	31
1.1.9.5 SLA Type Selection	31
1.1.9.6 Direct or Indirect 3D Printing	32
1.1.9.7 Ultra-Fast 3D Printing and the Considerations for Design	32
1.1.9.8 Automation of the 3D Printing Process	33
1.1.10 Literature Review Outcome	34
1.2 Aims and Objectives	35
1.3 Research Questions	36
1.4 Main Contributions	38

1.5	Thesis Overview	38
2	Determining the Optimal 3D Scanning System for the Outer Ear	41
2.1	Qualitative Evaluation of 3D Scanning	41
2.2	3D Scanner Requirements for Mass-Customization	42
2.3	Passive 3D Scanning	43
2.3.1	Equipment and Experimental Setup for Passive Imaging	44
2.3.2	Critical Imaging Parameters for the Passive System	45
2.3.2.1	Removing of Shadows	46
2.4	Active 3D Scanning Systems	47
2.4.1	Experimental Setup for Active 3D Scanning	47
2.5	3D Scanning Results	47
2.5.1	Structure From Motion	47
2.5.2	Artec EVA	49
2.5.3	Go!Scan	51
2.6	Discussion	51
2.6.1	Structure From Motion (SFM)	52
2.6.2	Structured Light 3D Scanner	54
2.6.3	Comparison of scanning technologies	55
2.6.4	Further Research	56
2.7	Conclusion	57
3	Development of a 3D Scanning system for the Ear	59
3.1	Requirements for the 3D Scanning System	59
3.2	Motion Design for the 3D Scanning System	59
3.2.1	Rail design for the motion constraint	61
3.3	Electronics Design for the 3D Scanning System	65
3.3.1	Controlling motion	65
3.3.2	Number of cameras	65
3.3.3	Controlling camera trigger	66
3.4	Calibration of the 3D Scanning System	66
3.5	Resulting 3D Scanning System for the Ear	68
3.6	Image Processing and Reconstruction	71
3.6.1	Processing Parameters for Each Stage	72
3.6.1.1	Camera Alignment:	72
3.6.1.2	Noise Removal:	72
3.6.1.3	Camera Optimisation:	73
3.6.1.4	Dynamic Calibration:	73
3.6.1.5	Dense Point Cloud Generation:	73
3.6.1.6	Mesh Generation:	74
3.6.1.7	Texture Generation:	74
3.7	3D Scanning Process	74
3.8	Validation of the 3D Scanning System	75
3.8.1	Camera Alignment	75
3.8.2	Dense Point Cloud	76
3.8.3	Mesh Generation	76
3.8.4	Repeatability	77
3.8.5	Variations in skin tone	77
3.9	3D Ear Database Construction	78
3.10	Discussion	79
3.10.1	Criteria Assessment	79

3.10.2	Repeatability	81
3.10.3	3D Ear Database	81
3.10.4	3D Scanning System Cost and the Possibility for Mobile Phone Technology	82
3.11	Future Research	83
3.11.1	Stationary Setup	83
3.11.2	Static Calibration	83
3.11.3	Custom 3D Reconstruction Algorithms	83
3.11.4	Possibility of Using Mobile Phone Technology	83
3.12	Conclusion	83
4	Establishing the Base Variance Using Statistical Shape Analysis	85
4.1	The Application of a SSM to Customization	85
4.2	Requirements for the Human Ear and this Research	88
4.3	Functional Map based 3D Statistical Shape Model Generation	89
4.3.1	What are Functional Maps?	89
4.3.2	Methodology for Generating a Statistical Shape Model	89
4.3.2.1	Preprocessing of the input 3D models	89
4.3.2.2	Groupwise Registration and Refinement using Functional Maps	90
4.3.2.3	Analyzing the Registered Data using Principal Components	95
4.4	Resultant Statistical Shape Model of the Human Ear	96
4.4.1	Modes of variation of the Statistical Shape Model	96
4.4.2	Selecting desired variance of the Statistical Shape Model	97
4.4.3	Variational Analysis of the Human Ear	98
4.5	Discussion	99
4.5.1	SSM Construction Process	99
4.5.2	SSM of the Human Ear	99
4.5.3	SSM Evaluation	100
4.5.4	Limitations of the SSM process	100
4.5.5	Applications to the goal of this research	101
4.5.6	Future Research	101
4.6	Conclusion	102
5	Deformation Constraints in CAD Designs to Streamline the Automation Process	103
5.1	Sample 3D Design for Testing the Constrained 3D Mesh Deformation	104
5.2	As-Constrained-As-Possible (ACAP) 3D Mesh Deformation	105
5.2.1	ACAP Mathematical Background	105
5.2.1.1	Derivation of the optimal rotation	106
5.2.1.2	Selection of weights	107
5.2.2	Incorporating volume preservation in ACAP	108
5.2.3	Form Preservation for ACAP	109
5.2.4	Form Preservation using constrained least squares Laplacian	109
5.3	ACAP 3D Mesh Deformation Applied to the Test Mesh	112
5.4	Discussion	115
5.4.1	ARAP Surface Deformation	115
5.4.2	ACAP 3D Mesh Deformation - Preserving Volume and Form	115
5.4.3	Advantages of the ACAP 3D Mesh Deformation	116
5.4.4	Further Work	116
5.5	Conclusion	116

6	Automated Customization of an In-Ear Device From 3D Scan Data	117
6.1	In-Ear Device and the Considerations For Automated Customization	117
6.1.1	Custom Shell and Electronics Module	119
6.2	Design Considerations for Automation and 3D Printing	120
6.2.1	Design for the mean	120
6.2.2	Limitations of 3D scan data	120
6.3	In-Ear Device Design using the SSM as a Guide	121
6.3.1	Direct and Indirect Design using the SSM	121
6.3.2	Direct Design of an Earphone to the Mean Shape of the SSM	121
6.3.2.1	Creating the Custom-Fit Shell Using Sub-D Modelling	122
6.4	Pre-Processing the In-Ear Device for the Automation Framework	123
6.5	Transferring a Deformation Field from the SSM to the In-Ear Device	123
6.6	Customized In-Ear Device using Variations in the SSM	127
6.7	Customized In-Ear Device from 3D Scan Data	128
6.7.1	3D Printed Customized In-Ear Device	130
6.8	Discussion	130
6.8.1	Fitting the SSM to a New 3D Scan	131
6.8.2	ACAP Mesh Deformation and it's Limitations	131
6.8.3	3D Printed In-Ear Device	132
6.9	Conclusion	132
7	Discussion and Conclusion	133
7.1	3D Scanning the Human Ear	134
7.1.1	Improvement in Processing and Capture Time	135
7.1.2	Dedicated 3D Reconstruction Algorithms	135
7.2	Statistical Shape Models and their Application to Product Design and Customiza- tion	136
7.2.1	Establishing Correspondences Using the Full 3D Scan Data	136
7.2.2	Quantitative Assessment of the SSM	136
7.2.3	Relevance to the Overall Aim of this Thesis	137
7.3	ACAP Mesh Deformation for Automatic Customization	137
7.3.1	Applying Constraints using ACAP	137
7.3.2	Advantages and Disadvantages of ACAP	138
7.3.3	Relevance to the Aim of this Thesis	138
7.4	Automated Customization of In-Ear Devices	138
7.4.1	Advantages of the ACAP Automated Customization Process	139
7.4.2	Limitations of the ACAP Automated Customization Process	139
7.4.3	Quantitative Assessment of the Automated Customization Process	139
7.5	3D Printing and Mass-Customization	139
7.5.1	3D Printing Time and the Potential for Improvement	140
7.5.2	3D Printing Materials for In-Ear Devices	140
7.6	Automated Customization and the Research Questions	140
7.7	Future Research	140
7.7.1	Soft Body Modelling for In-Ear Device Design	141
7.7.2	Further Constraints for the ACAP Process	141
7.7.3	Functional Map Based Statistical Shape Modelling	141
7.7.4	User Studies on Comfort for In-Ear Devices	141
7.7.5	Automatic Post-Processing of SLA-Based 3D Printed Parts	141
7.8	Conclusion	142

List of Figures

1.1	A selection of earphone styles and the silicone inserts that are used to account for variations in size and shape.	1
1.2	The process for creating a custom-fit in-ear device using the traditional in-ear mould and manual manipulation.	2
1.3	The process for creating a custom-fit in-ear device using the new direct 3D scanning technology, removing the need for moulding of the ear canal.	2
1.4	The proposed mass-customization process, showing the automation of the 3D scanning and 3D data customization. This process removes the need to have trained individuals manually manipulate the 3D scanner or the 3D data.	2
1.5	Breakdown of the main topics in this research and their sub-components.	3
1.6	Types of customization showing the standard "one-size-fits-all" to the extreme bespoke (Campbell, 2006).	5
1.7	Comparison of standard "one-size-fits-all" earphone (left) with the personalized or customized version (right).	5
1.8	The three capabilities to make mass-customization work, adapted from Piller and Tseng (2010).	6
1.9	The anatomy of the human ear where the main focus of this research is in the outer ear and ear canal (Netter, 2017).	9
1.10	Anatomical regions of the pinna (Image obtained from Geoface (2016))	9
1.11	Sample of variation among ears	10
1.12	Sample of the variation of hearing aids that are available and their placement within the ear.	11
1.13	Customization process for hearing aids (Adapted from Slabaugh et al. (2008 <i>b</i>)).	12
1.14	A flow chart showing the process of customizing a hearing aid using moulding, laser scanning and mesh processing. The manual section, which is the focus of this research is highlighted (Adapted from Slabaugh et al. (2008 <i>b</i>)).	12
1.15	A step-by-step illustration of the detailing process for creating a custom-fit hearing aid from 3D scan data in (a) to final product in (i). (Adapted from Slabaugh et al. (2008 <i>b</i>))	13
1.16	A step-by-step illustration of the modelling process which takes the custom-fitted shape in Figure 1.15 and adds to features for functionality, i.e. wall thickness, vents, and mounts.	13
1.17	Automated approach using a rule based system illustrating the feature detection and application of pre-defined rules (Adapted from Sickel et al. (2011)).	14
1.18	Key features of a hearing aid impression which are used to guide the expert system through the automated customization process.	15
1.19	Feature detection on a hearing aid impression by analysing the variation in contours (Slabaugh et al., 2008 <i>b</i>).	15
1.20	Predicting the customized shape from a statistical model (Adapted from (Unal et al., 2011)).	16
1.21	The proposed deformative customization approach showing the introduction of functional design deformation.	18
1.22	The process of reconstructing a 3D shape from a collection of 2D images.	20

1.23	3D ear reconstruction from a single image using a 3D morphable model Li et al. (2012).	21
1.24	3D ear reconstruction using stereo-vision, showing the wireframe 3D model(left) and the rendered 3D model (right) (Sun et al., 2003).	22
1.25	3D head reconstruction using an industrial passive 3D scanning rig (Ten-24, 2009).	23
1.26	Diagram showing the typical accuracy at different operating distances of the most common 3D imaging technologies (Pears et al., 2012).	24
1.27	Active 3D scanning of the face (Wickramaratne et al., 2009).	25
1.28	Generalized steps for constructing a SSM.	27
1.29	Functional map based 3D shape matching. The shape (a) is matched with (b-e), the surface colour represents matching areas with the target shape. Notice the colour similarity even with large pose variation (Ovsjanikov et al., 2012).	28
1.30	In-ear device design and 3D printing for mass-customization	29
1.31	Types of customized earphones to inform the design process.	29
1.32	Types of SLA based 3D printing, showing the different means by which to cure the photosensitive resin (Frey, 2017).	30
1.33	The pixelation effect caused by DLP and mask-based SLA in comparison with laser-based approaches (Formlabs, 2017a).	31
1.34	Indirect 3D printing of earphones using 3D printed moulds and injection moulding. Adapted from the processes discussed in Formlabs (2018)	32
1.35	The Formlabs Form Cell, an automated approach to SLA 3D printing Formlabs (2017b).	33
1.36	Post-processing steps for taking a 3D printed SLA component to be functional.	34
1.37	Thesis objectives split into the three main areas of 3D scanning, 3D data analysis, and 3D printing.	36
2.1	Variations in the shape of the human ear, and a sample of the texture taken from multiple keypoints. Each keypoint has a 4 pixel diameter that shows the similarity in texture between regions around the ear.	44
2.2	The exposure triangles: Changing the ISO, aperture, or shutter speed can impact the image quality (Gray, 2018).	45
2.3	Variations in image quality as a result of environmental changes with the introduction of a lightbox and a ring light	46
2.4	Sample images from the structure from motion process. Showing 4 out of 15 images.	48
2.5	Camera positions recovered from Agisoft PhotoScan Pro using the captured 15 images. The blue plane is representative of the position and angle of the camera.	48
2.6	Result from SFM reconstruction. The process has produced the overall shape, however, there is a lack of detail in the result.	49
2.7	Ear reconstruction from the Artec EVA, showing three views of the output mesh	50
2.8	The inner ear region as captured by the Artec EVA	50
2.9	3D scanning result from the Creaform Go!Scan, the desired area is marked in black.	51
3.1	Capture Area: The target within the green area is the focus for this research and requires segmentation from the full result.	60
3.2	Camera Dolly: Used to provide smooth and controlled motion to a mounted camera.	61
3.3	Showing the different focus caused by linear motion. Due to the distance of the cameras this would cause blurring	61
3.4	Curved camera dolly: Manufactured from aluminium and typically manual.	62

3.5	Curved rail concept: Similar concept to the mechanical curved rail but has components for adapting motorized control.	62
3.6	To manufacture the curved rail, it is split into 4 sections for 3D printing on a 200x200x200 mm volume 3D printer.	63
3.7	Assembled platform: Showing the mounted wheel bearings and the stepper motor on the rear of the platform	64
3.8	Assembled rail: Showing the rail and the intended positioning of the platform. The three wheel bearings slot into the curved section on the rail and are constrained there. The belt drive mounts on each end and any rotatory motion of the pulley wheel is transferred to the timing belt.	64
3.9	Arduino and RAMPS controller: Used to program stepper motors and digital inputs and outputs	65
3.10	One vs two view camera system illustrating the reduced occlusion by using multiple views. The red is the visualization of expected occlusion.	66
3.11	Static calibration: A chessboard pattern is capture from the camera at different angles and the intrinsic and extrinsic parameters are recovered.	67
3.12	Dynamic calibration: Using a pattern of coded targets with known distances it is possible to recover the intrinsic and extrinsic parameters during each scan . . .	68
3.13	Final design: showing the full rail, platform and camera mounts. The cameras are placed vertically to maximize the pixels used. The rail is mounted on aluminium profile to set the desired height and the calibration grid placed at the pre-defined distance from the cameras.	69
3.14	Manufactured system: showing the fully manufactured system with the 3D printed rail and platform, and the lighting equipment	70
3.15	Sample images from the custom 3D scanning system. Showing a sample of the total 76 images.	70
3.16	Steps for processing the raw images into a 3D model using Agisoft Photoscan. . .	71
3.17	Process for generating the 3D scan data.	75
3.18	Alignment of the images, showing the position of the cameras and the resultant sparse point cloud.	75
3.19	Dense point cloud: the fully reconstructed model from the sparse point cloud, showing some high frequency noise and minor occlusion.	76
3.20	Textured mesh: fully textured and noise free model with some minor occlusions that will not impact this research.	76
3.21	Showing the repeatability achieved with the system. The green and yellow colour show minor variations and blue and red show larger negative and positive variations respectively. The scale is a metric signed distance in centimetres. .	77
3.22	Invariance to skin colour. Some minor occlusions are visible in the left hand image caused by the image acquisition, and some errors in the lobe due to the position to the calibration grid. However, the overall reconstruction is accurate and smooth	78
4.1	The normal distribution showing the amount of variance within each standard deviation. The median line represents the mean shape.	86
4.2	A SSM of the human body. Showing $\pm 3\sigma$ and consecutive principal components from 1 to 10. The model consists of 6449 vertices.	87
4.3	The SSM of Figure 4.2 highlighting the ear region, showing that the output data is not sufficient to model the ear.	87
4.4	The process for generating a statistical shape model consisting of pre-processing, groupwise registration, statistical analysis and variance analysis.	89

4.5	Pre-processing the input mesh showing the uniform distribution of vertices and faces in the output mesh while maintaining the overall features. In order from the left: Original mesh, Orientation field, Position field, Uniform output.	90
4.6	The process of generating point-to-point correspondences from functional maps. Convert input mesh to basis functions, calculate rough correspondences, generate functional maps and refine into consistent correspondences.	91
4.7	Definitions of the angles and the area appearing in the discrete Laplace-Beltrami operator (Rustamov, 2007).	92
4.8	Example of basis functions on the surface of two ears illustrating the similarities in certain basis functions.	92
4.9	Reconstruction of a 3D model using the Laplace-Beltrami basis functions, showing the improved level of detail with increased basis functions (Lévy, 2006). . . .	93
4.10	Showing the process of transferring a function on the source shape to the target using the calculated functional map.	93
4.11	Consistent point-to-point refinement vs regularized thin-plate-spline: CPD refinement (Rodola et al., 2015) and our approach using regularized TPS deformation.	94
4.12	The registration error of the standard coherent point drift algorithm on the raw point data versus the refined correspondences using the functional maps. Scale is between -3mm and +3mm.	95
4.13	The cumulative variance of the principal components with 95% variance reached after 27 principal components.	96
4.14	Statistical shape model of the human ear showing the individual modes of variation between -2σ and $+2\sigma$ standard deviations.	97
4.15	Accounting for 95% of the variation within the dataset between -2σ and $+2\sigma$ standard deviations	97
4.16	The distance from the mean shape to $+2\sigma$, visualized as a scalar field on the mean shape. The distances are in millimetres.	98
4.17	Distance from the mean shape to -2σ deviation, visualized as a scalar field. The distances are in millimetres.	98
4.18	Concept of this research showing the use of the constructed SSM as the base for a prediction framework of the customized shape.	101
5.1	Sample 3D mesh design to test the mesh deformation algorithms, designed to have a hemispherical bump to evaluate the effective preservation of the local rotations and a rectangular cavity to explore preservation of the form.	105
5.2	A one-ring neighbourhood of a vertex, i , showing the edge length, e_{ij} , to connected vertices, j	106
5.3	Test Piece Deformation: The yellow region remains fixed and the red region is deformed using uniform weights and cotan weights (Sorkine and Alexa, 2007).	107
5.4	Cotangent weights in the one-ring neighbourhood of a vertex (Sorkine, 2005).	108
5.5	Tetrahedral mesh, shown in red, generated to preserve the volume of the mesh during the ACAP deformation.	109
5.6	Spanning Tree: a minimum representation of the connectivity in a 3D mesh region such that repeated edges are eliminated in the selected region (Masuda et al., 2007).	110
5.7	Process for generating a customized in-ear device from CAD data using the ACAP 3D mesh deformation process.	112
5.8	Test Piece Deformation: the red region remains fixed and the yellow region is deformed 0.5mm in the X-axis, and -1mm in both the Y and Z axes.	113

5.9	ARAP mesh deformation showing the self-intersections (pink) that arise due to the lack of volume information.	113
5.10	ARAP process including the volume information in the form of the tetrahedral connectivity, showing that self intersections are avoided, but the form region is distorted.	114
5.11	ACAP process showing the preservation of both volume and rotation with the critical component being the preservation of the form of the designated region. .	114
6.1	Styles of in-ear earphones. Various designs aim to improve comfort or sound quality by exploiting different areas of the ear for mounting or sound isolation. .	118
6.2	Custom-fit earphones produced using moulding, 3D scanning and manual processing of the scan data (Snugs, 2017).	119
6.3	The Beats urBeats2 that will be used to test the customized earphone (a) and the approximate dimensions that were measured manually (b).	119
6.4	A Sub-D model of a torus (a), showing the control points that are used to deform the shape (b).	121
6.5	A Sub-D model of a torus (a), showing the control points that are used to deform the shape (b).	122
6.6	A Sub-D model of a torus (a), showing the control points that are used to deform the shape (b).	122
6.7	Preprocessing the earpiece for the ACAP customization framework, showing the segmentation of the form region in red and the black region, the custom-fit region in black and the free region in gray.	123
6.8	(a) The mean shape of the SSM with (b) an input 3D scan, showing (c) the spatial and topological difference from the scan to the SSM.	124
6.9	(Left) The mean of the SSM registered to (Middle) an input 3D scan, showing (Right) the overlapping areas after registration. Further refinement is required as the SSM did not fully predict some areas of the shape.	125
6.10	SSM fitting process; showing the change from the SSM (a), to the input 3D scan (b), and the fitted 3D scan (c), and finally error in the fitting process shown in mm (d).	126
6.11	Generation of the deformation field, showing the change in shape from the mean (left), to the fitted input 3D scan (middle), and the deformation field (right). Colours represent the magnitude of the deformation in mm, however, the actual deformation field is in three dimensions (X,Y,Z)	126
6.12	(a) The mean shape from the SSM with the registered earpiece, (b) the mean shape with the area in contact with the earpiece, (c) the earpiece with the area in contact with the SSM. The indices of the contact areas are used to transfer the deformation from the SSM to the earpiece.	127
6.13	Testing the ACAP mesh deformation process showing the change in shape from the mean to $\pm 2\sigma$ in the SSM using 95% of the variance in the principal components.	128
6.14	SSM fitting showing, (a) mean shape, (b) input 3D scan, (c) registered scan to SSM, and (d) the fitted SSM.	129
6.15	The full ACAP process, showing (a) the mean shape with the earpiece, (b) the input 3D scan with the deformed earpiece using ACAP, and (c) the relative change in shape with the old earpiece being shown as transparent.	129
6.16	Sample 3D print of a customized in-ear device, showing the sample part (a), the beats insert (b), and the 3D printed in the ear (c).	130

7.1 Requirements for automating the customization of in-ear devices relating to 3D scanning, statistical shape model (SSM) development, customization algorithms, and 3D printing. 134

List of Tables

1.1	Outer ear anthropometrical data (Dreyfuss, 1960), see Figure 1.10 for the location of the anatomical regions.	10
1.2	The performance of the method by Sickel et al. (2011) showing the detection rate and the tolerance.	17
1.3	Achieved improvement in time compared to an expert user by using the automation system of Sickel et al. (2011).	17
1.4	Research questions to be addressed relating to the ability to 3D scan the ear and the processes for applying the data to customization and direct 3D printing. . . .	37
2.1	Comparison of 3D scanning technologies relative to the established criteria. Each criteria is weighted with relevance to this research. Weights are from 1-3 and the score is from 1-5 where 1 is a low score and 5 is the highest score. . . .	52
3.1	The distribution of ages within the 3D ear database showing a relatively spread out range.	79

Chapter 1

Introduction

The human ear is the target for a number of consumer and medical devices, including earphones, hearing aids, bluetooth monitors, direct language translators (iTranslate, 2018), and even health monitors for sleep (Nguyen et al., 2016), biometrics (Nakamura et al., 2018), and heart rate monitoring (Park et al., 2015; Palladino, 2016). The human ear also has a highly complex and varied shape, which has been determined to be probably unique between individuals (Iannarelli, 1964). This research asks the question, if the human ear has such a wide variation in shape, is it possible to produce a custom-fit earpiece for each individual? With the recent advances in 3D scanning and 3D printing technology it seems feasible that mass-customized in-ear devices are a possibility.

Decomposing the range of in-ear devices into their parts shows similarities, i.e. each device comprises an outer shell with or without a soft silicone insert, electrical sensors, and acoustic channels in the case of audio devices. Although there are many variations of both earphones and hearing aids, the principal of delivering sound to the ear canal remains the same.



FIGURE 1.1: A selection of earphone styles and the silicone inserts that are used to account for variations in size and shape.

In 2018, in-ear devices are becoming more akin to smart devices through the advancement in connectivity, sound quality, and functionality. In-ear devices, including hearing aids, are able to connect and communicate with more devices such as smartphones, tv's, or sound systems allowing for more control of the sound quality, in particular, the directionality and filtering of sound to accommodate social situations with multiple people conversing or significant background noise (hear.com, 2018). However, there still remains the issue of comfort and fit, and as these devices become more intelligent, the likelihood of prolonged exposure increases. This therefore heightens the need for mass-customization. In a mass-manufacture scenario, the consumer is supplied with different sizing, typically small, medium, and large (see Figure 1.1) to account for variation in shape. In the case of custom-fit devices such as professional in-ear monitors, and custom-fit hearing aids, the process requires a direct mould of the individual's ear-canal, and the subsequent manual processing into the final product (Slabaugh et al., 2008a). Figure 1.2 details the steps in this process showing the initial ear mould taken

by a professional, which is then 3D scanned and the data manually processed into the final customized shape.



FIGURE 1.2: The process for creating a custom-fit in-ear device using the traditional in-ear mould and manual manipulation.

The customized shape is then 3D printed and the electronics assembled. The combination of 3D scanning and 3D printing technology creates the perfect platform for consumers to access customized in-ear devices. With modern 3D scanning technology, the traditional moulding process can be replaced with a 3D scan that digitizes the shape of the participants ear-canal (Lantos Technologies, 2018). However, the process to acquire this data still relies on a well-trained individual to manipulate the typically handheld 3D scanner. Referring to Figure 1.3, the use of 3D scanning technology as the medium for acquiring the shape of an individuals ear has altered the paradigm by which a custom-fit in-ear device is designed and manufactured. The introduction of a 3D scanner removes the need for moulds, making the process digital manipulation of a 3D scan.

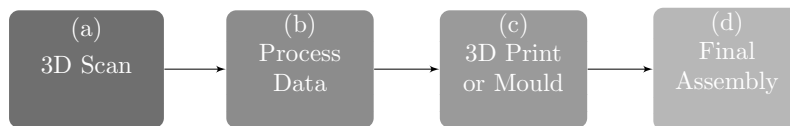


FIGURE 1.3: The process for creating a custom-fit in-ear device using the new direct 3D scanning technology, removing the need for moulding of the ear canal.

Figure 1.3 shows the alteration in the process due to the introduction of direct 3D scanning, illustrating the removal of the need for moulding of the ear canal. Although the technology by which to capture the shape of the human ear is advancing, the processes to create the final custom-fit in-ear device from the 3D scan data is, to the best of our knowledge, still predominantly manual. There is research aiming to automate or semi-automate the custom-fit design process through the embedding of machine learning to replicate or guide the steps performed by the human expert (see Figure 1.3 b). The need for a trained expert to manually process each custom-fit in-ear device limits its accessibility through additional costs and processing time. Therefore, this research aims to achieve mass-customization through the full automation of not only the 3D scanning process but the in-ear device customization. Figure 1.4 shows the proposed mass-customization approach in this thesis, where, through the use of custom-built 3D scanning systems and automation algorithms, it is possible to 3D print on-demand custom-fit in-ear devices.

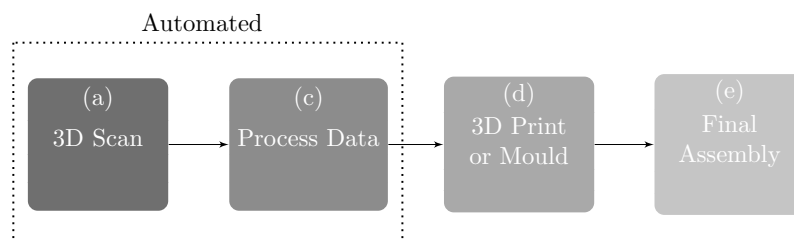


FIGURE 1.4: The proposed mass-customization process, showing the automation of the 3D scanning and 3D data customization. This process removes the need to have trained individuals manually manipulate the 3D scanner or the 3D data.

The introduction of direct 3D scanning in Figure 1.3 removed the need for moulding and is one of the driving forces behind the realisation of mass-customization. The following section introduces the reader to mass-customization, automation systems and the background theory behind the current state-of-the-art. This allows for formulation of the research questions and objectives to achieve the process in Figure 1.4.

1.1 Automated Design of Customised Devices for the Human Ear

What is the point of automating customization? With the current level of 3D scanning and 3D printing technology there is the ability to develop this automation system, but is there a need? This sections aims to build the background information that establishes the research questions and will guide the remainder of this work. Figure 1.5 shows the breakdown of the research topics and the broadness required to understand mass-customization for in-ear devices.

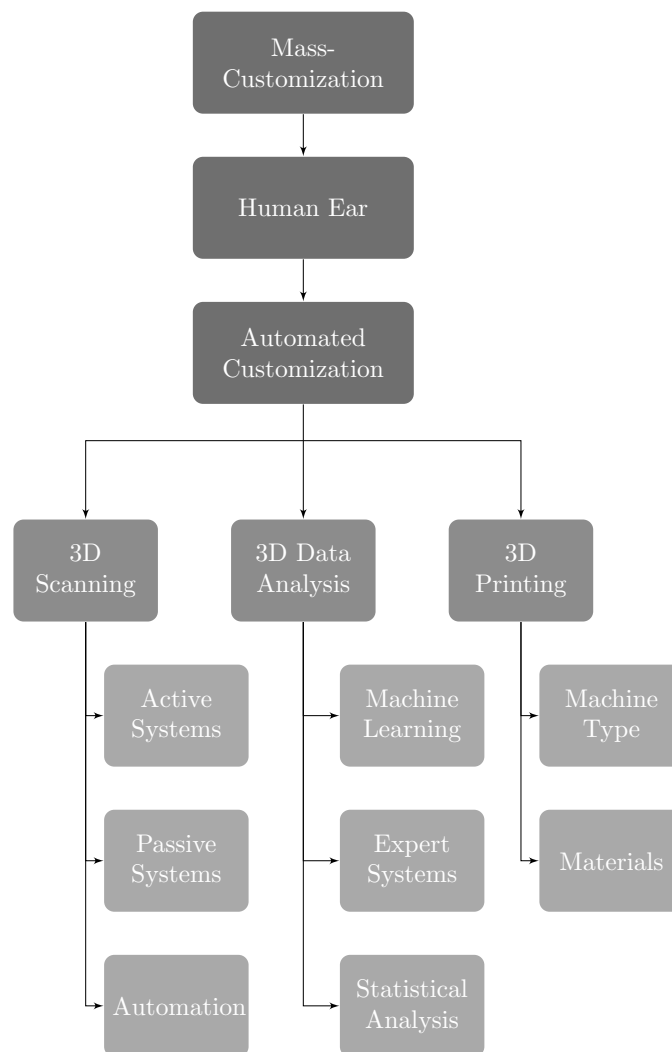


FIGURE 1.5: Breakdown of the main topics in this research and their sub-components.

1.1.1 Mass-Manufacture versus mass-customization of Consumer Devices

Mass-manufacturing, or mass-production, is the high volume production of standardized products using dedicated and often automated manufacturing systems. The initial high costs of

mass-manufacturing a product is offset by the high volume and low unit costs (Tanenbaum and Hollstein K, 2016). While mass-manufacturing has allowed for widespread adoption of consumer products at a relatively low-cost, there will generally be consumers that like the product and consumers that don't like the product, based on their own interpretation of the aesthetics or features. Mass-customization, on the other hand, requires further classification. Pine (1993) and Piller and Tseng (2010) define mass-customization as "developing, producing, marketing and delivering goods, and services with enough variety and customization that nearly everyone finds exactly what they want". For this research, mass-customization is the "development, production, marketing and delivering of goods that fits to an individuals shape". As such, the individual needs become more subjectively related to comfort and fit. The concept of mass-customization can be broken down to further clarify the approach of this research.

Gilmore and Pine (1997) propose the four faces of customization as collaborative, adaptive, cosmetic and transparent. Collaborative customization is the design of a product to fit the direct needs of the consumer with the end product determined by the user. Adaptive customization, on the other hand, offers a single product but provides the consumer with customizable options, for example in the earphone industry a standard earphone is supplied with a small, medium and large silicone earpiece to account for the variation in shape of the human ear. This can also be seen with many product where various interchangeable colours are provided, allowing the individual to select the colour which best suits their personal preference. This approach is the most utilised version of mass-customization in industry as it allows for traditional mass-manufacturing technologies to be used whilst maintaining the consumer benefits of partial customization, i.e. allowing the consumer to express their own individual style or preference through the combination of various mass-produced components. However, in terms of this research, the goal is a completely individualised product, therefore, adaptive customization is not applicable.

Cosmetic customization provides the consumer with a standard product with methods for altering its presentation such as varying colour or imagery. While this approach provides a somewhat unique aesthetic for a product it is not applicable to this research as the shape of the device is not altered. Finally, transparent customization is the provision of goods or services without letting the consumer know explicitly that those goods or services have been customised for them (Gilmore and Pine, 1997). In this approach, industries endeavour to predict the behaviour of the consumer and provide goods to potentially meet those needs. In terms of classification, this research lies between collaborative and adaptive customization where a consumer's collaboration is required to provide their 3D shape and the adaptive nature is in providing a single electronics interface that is varied with the custom-fit shell.

The variation in types of customization can also be determined based on the number of customisable features and available choices (see Figure 1.6) including personalisation, modularisation and bespoke. Personalisation is defined as a process that changes the appearance or functionality of a product to increase its personal relevance to an individual (Blom, 2000), which can include relatively simple concepts such as printing a name or image on a mug to fitting the shape of a hearing-aid to an individuals ear. Bespoke design is the extreme of customization, wherein, a product has been designed from its outset with one customer in mind and solely aims to satisfy the requirements of that individual. Modularisation, on the other hand, is the median between personalisation and one-size-fits-all where a single product is provided but the customer can configure it to fit their specific requirements, such as an earphone with small, medium and large silicone earpieces to account for the size variation of the human ear.

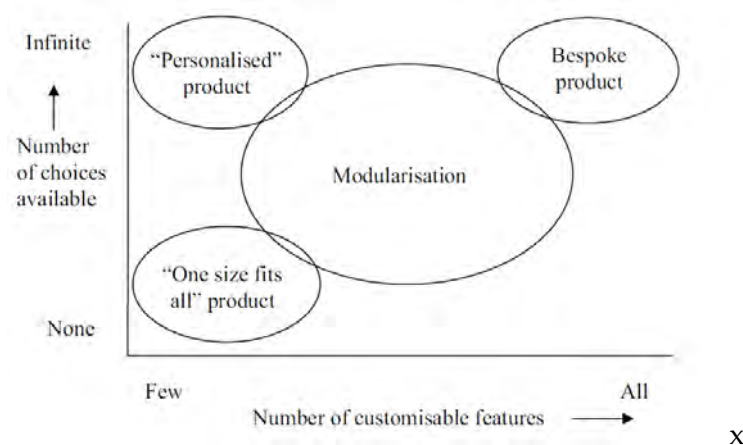


FIGURE 1.6: Types of customization showing the standard "one-size-fits-all" to the extreme bespoke (Campbell, 2006).

This research aims to custom-fit the shape of the in-ear device to an individual's ear with no alteration to the electronics. Contrary to standard in-ear devices, custom-fit devices follow the complex curvature of the ear to potentially improve comfort and quality.



FIGURE 1.7: Comparison of standard "one-size-fits-all" earphone (left) with the personalized or customized version (right).

As can be seen in Figure 1.7, the standard earphone consists of a base shape with a rubber shell that can be interchanged, whereas, a customised earphone adapts to the full shape of the ear. The custom-fit earphone, in this case, is being referred to as "personalized" as the electronics are not customized to the individual, which would be the case for a bespoke product. With mass-customization, the aim is to produce these customized devices at a scale and cost similar to mass-manufacturing. The complexity here is, how can a system be developed that takes account of the variation in human body shape and also the shape and functionality of the product? In order to give the reader an understanding of the novelty of mass-customization, the following section discusses the current method for customized in-ear devices.

While the concept of providing a customized product to each individual seems simple, its success in both a business and technological aspect is highly complex. Piller and Tseng (2010) describe the three capabilities of achieving mass-customization as Solution Space Development, Robust Process Design, and Choice Navigation (see Figure 1.8).

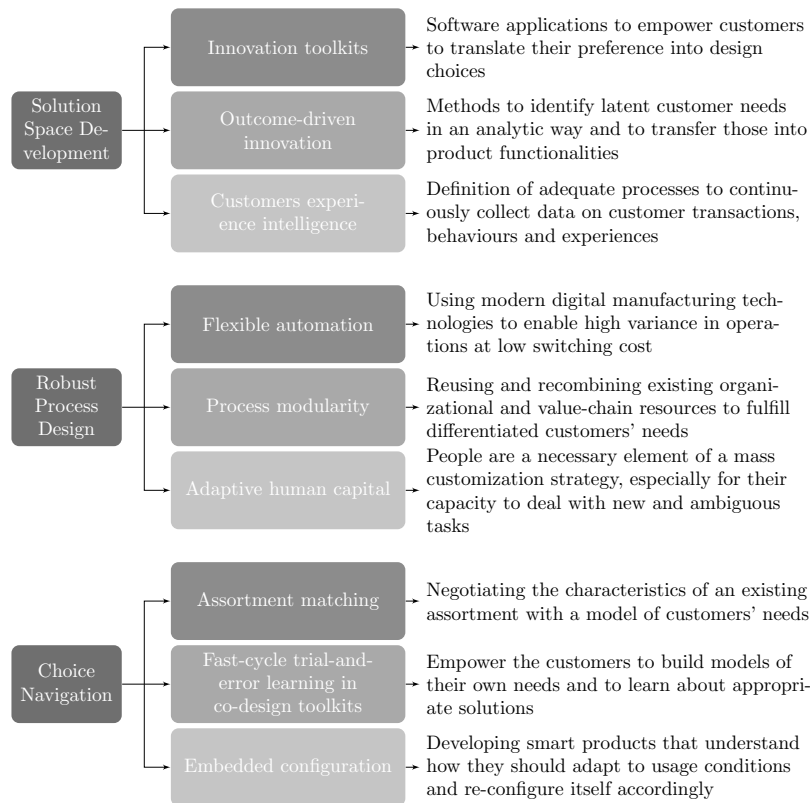


FIGURE 1.8: The three capabilities to make mass-customization work, adapted from Piller and Tseng (2010).

The solution space aims to identify the product attributes along which customer needs mostly diverge, this is related to providing software to empower the user in selecting and understanding their own needs (Piller and Tseng, 2010). While this is an important aspect of mass-customization it is not applicable to this research. Robust process design is the aspect that is most relatable to this research, particularly in providing flexible automation means that enables high product variance at low switching cost.

1.1.1.1 Comfort and Functionality from customization

An interesting aspect of the work by Piller and Tseng (2010) is their understanding that often, the consumer does not understand their own needs. This is reinforced by the understanding that the consumer has only since recently had access to mass-manufactured products, meaning that if the user were to be able to request a completely customized product, would they be able to vocalize their own needs? Traditionally, in-ear devices provide silicone earpieces in the form of small, medium, and large in order to account for variations in shape between individuals. However, what if a particular individual falls between small and medium, or medium and large, or completely outside of the typical range? Then there is no possibility with standard mass-manufacturing that an in-ear device is going to be perfectly comfortable for that individual. With mass-customized in-ear devices there is a certain subjectivity to the comfort and fit, in that the user may not understand the benefits due to the long-term exposure to mass-manufactured in-ear devices. This is verified in the research by Naddeo et al. (2015) and Brown and Cole (2009) where they determined that knowledge and control can affect a users perception of comfort. Specifically, the three most important parameters are prior experience, personal knowledge about the comfort experience, and the expectation of perceivable comfort.

This means that a user that has had no experience with custom-fit in-ear devices may expect more from the process, which could result in a poor perceived comfort level. On the other hand, a user that has experience with custom-fit hearing aids created through traditional moulding means may perceive the comfort level as greater due to a more realistic expectation level. As such, it is a considerable task to not only establish a quantitative comfort assessment, but even a qualitative assessment is dependent on the individuals that participate in the assessment.

While it is important to understand the complexity of evaluating comfort, the assessment of the achievable comfort levels through this automated customization approach is outside the scope of this research. This research is focused on the feasibility to automatically fit an in-ear device to an individual's unique shape using 3D scan data. This research will move forward with the understanding that by customizing an in-ear device to an individual, the perceived comfort should be increased.

As 3D scanning can digitise the complex shape of the human body there is now the means to analyse how the human body varies and use this data to redefine the small, medium, and large sizing based on gender, race, age or other factors. Alternatively, by digitising the 3D shape of individuals it provides a means to produce a custom-shape for that individual. In this approach, the complexity is now, how can we take the 3D scan data and produce a functional product that fits the specific individual?

In terms of functionality, Konkle and Bess (1974) analysed the audiological benefits of custom-fit hearing aids versus stock moulds. In their study, it was found that custom-fit hearing aids provide a better acoustic seal on the ear canal which in turn improves the acoustic transfer of low-frequency sounds as opposed to stock moulds where low-frequency noise seeped through gaps in the acoustic seal.

1.1.1.2 Improved Emotional Attachment to the Customised Device

Mugge et al. (2009) illustrate that customizing a product will increase the match with individual preferences (functional and aesthetic). Customization will also enhance the product's ease of use and reflect the individual's personal or group identity. Customization is also a way of expressing ownership of the product. Mugge et al. (2009) hypothesise that consumer involvement in the customization process results in an emotional bond with the product. They state "the more that consumers can act as co-designers of their product, the more effort they will invest in the product and the stronger the emotional bond is likely to become". By assessing the process in Figure 1.4, it can be assumed that the participation of an individual in the 3D scanning could promote a positive emotional response towards the mass-customization process. However, this requires that the experience be user-friendly, which further justifies the need for automation of the 3D scanning process in Figure 1.4.

1.1.2 Prevalence of Advanced 3D Imaging and Rapid Prototyping Technology

There is massive innovation taking place in the 3D scanning and 3D printing industry, but, there is little understanding about the link between the two. 3D scanning is the digitisation of real life objects such as people or products. This means that by using 3D scanning it is possible to develop a virtual 3D model of practically any object. The benefits of combining 3D scanning and 3D printing are clear: while 3D scanning allows for real-life objects to be made virtual, 3D printing allows for virtual objects to be made real. However, the process of taking the 3D scan data to be prepared for 3D printing is currently highly laborious due to noise, occlusion, or surface reconstruction errors. The repairing of these errors requires a well-trained individual to process the data. With 3D scanning and 3D printing seeing continuing innovation, there

are opportunities to use the technology for previously unconsidered applications. In industry there is a growing number of companies promoting a novel solution to customization, such as Normal (Hardawar, 2014), OwnPhones (Ownphones, 2014), and Metamason (Crunchbase, 2013), each offering a customization methodology using 3D scanning and 3D printing. It should be noted that while these companies promoted a method for mass-customization, they have since closed or ceased operations.

There is a lot left to be understood about the link between 3D scanning and 3D printing as these innovations are highly specialised and still require a skilled individual at some stage in the process. There is no apparent holy grail for customization as the range of applications is so broad that there will possibly never be a technology that can adapt to each situation. In order to advance the customization culture, a system is required to assist industrial engineers in developing a solution for their customised products, as current solutions are confined to niche applications and have been developed by small companies that have invested their time. By analyzing the process of mass-customization as a whole, it can be seen that by developing innovative methods for 3D scanning, 3D data analysis, and 3D printing, it may be possible to achieve mass-customization (see Figure 1.4) across a broad range of applications, therefore promoting industrial growth and a more customised culture.

1.1.3 Why is Automation Necessary for Custom-Fit In-Ear Device Design?

It has been discussed that customization is necessary for in-ear devices as it potentially provides improved comfort, functionality and emotional connection. However, in order to make the technology more accessible and reduce the time and cost involved, the process for creating a custom-fit in-ear device must be majority automated. It should be clarified that the goal here is mass-customization, which endeavours to make the technology available to the broader population as opposed to expert moulded products which provide the desired fit but are relatively expensive and time intensive. Mass-customization, for this research, constitutes the provision of a product that fits to the unique shape of the individual and requires the individual to participate in the process by providing their 3D data as input. Standard methods for manufacturing require a trained expert to manually augment the input 3D scan data to output a functional product. While this has been the standard approach it is only possible for a small proportion of the population due to the cost and time required by the expert user. Therefore, in order to truly achieve mass-customization, critical stages of the design process should be performed by a computer as opposed to a trained expert.

This research will be referring to this as an automation system, however, in the literature it can be found under expert systems, knowledge-based systems (KBS), rule-based systems (RBS), knowledge-based expert systems (KBES), and rule-based expert systems (RBES). For this research, automation system was chosen due to the process which was derived as part of this thesis and will be discussed in detail herein. To summarise, an expert system replicates the processes performed by the trained expert where the raw 3D scan data is processed into a functional product using a system of rules developed by the expert which rely on features or landmarks detected on the surface of the 3D scan data. There are many complications involved in this process as it mimics a typical human process and is reliant on accurate detection of landmarks on possibly noisy 3D scan data. This research aims to circumvent the complexities of the replicative approach by re-envisioning it as a morphometric process where the goal is to morph an already functional product to fit the 3D scan data as opposed to constructing a functional product from 3D scan data.

1.1.4 The Human Ear

To assist the reader, a brief introduction to the anatomy of the human ear is given in order to cover some of the terminology used throughout this work. The human ear has many anatomical regions, however, the main focus of this research is the outer ear which contains the pinna and ear canal. A full breakdown of these anatomical regions can be seen in Figure 1.9.

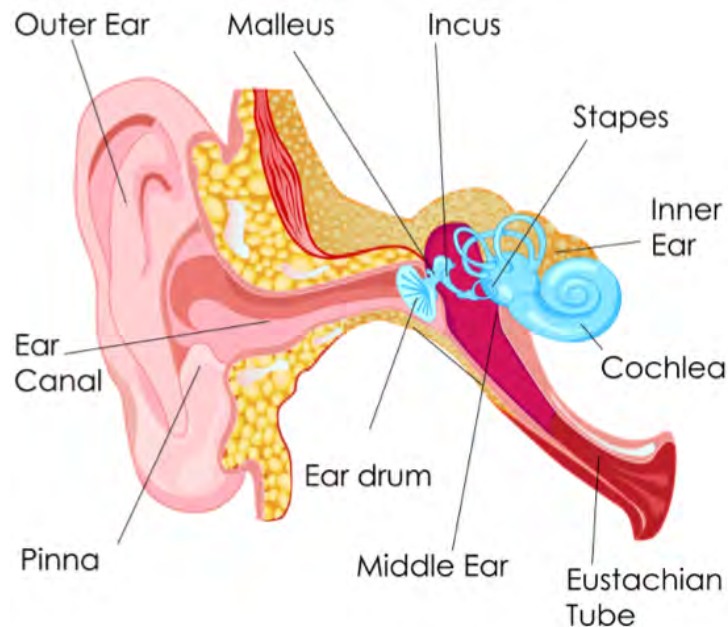


FIGURE 1.9: The anatomy of the human ear where the main focus of this research is in the outer ear and ear canal (Netter, 2017).

The outer ear acts as a funnel to conduct air vibrations to the eardrum (VMC, 2018) while also adding directionality to the incoming sound. The pinna is the most noticeable area of the human ear and can be segmented into multiple anatomical regions, see Figure 1.10.

The segmented pinna in Figure 1.10 shows the complex shape that is the human ear, consisting of 11 anatomical regions. In fact, the outer ear has such a high level of variance that it can potentially be used to identify individuals, in what is known as ear biometrics (Iannarelli, 1964). Burge and Burger (1997) have shown that biometrics based upon the ear are viable in that ear anatomy is probably unique in each individual and that features based upon measurements of that anatomy are comparable over time.

Table 1.1 shows a sample of anthropometric data taken from a study in Dreyfuss (1960). These measurements were taken manually by a trained expert from anatomical landmarks on the participants ear. However, while this provides useful information for how the shape of the ear varies, it is only a linear measurement between two points that can be

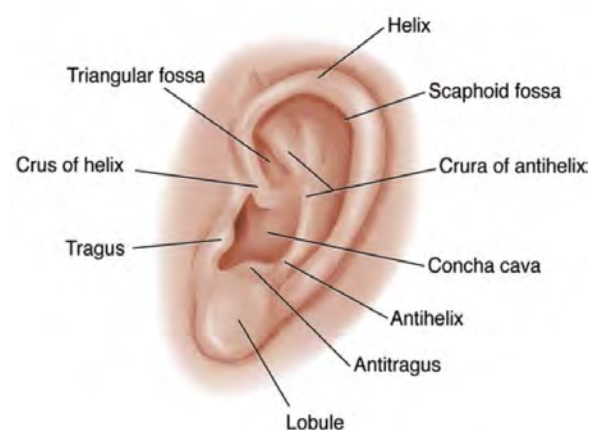


FIGURE 1.10: Anatomical regions of the pinna (Image obtained from Geoface (2016))

TABLE 1.1: Outer ear anthropometrical data (Dreyfuss, 1960), see Figure 1.10 for the location of the anatomical regions.

Dimensions		Averages			Standard Deviation			KEMAR	50% Male	50% Female	Average
		12 Male	12 Female	Overall	12 Male	12 Female	Overall				
Ear Length	cm	6.85	6.24	6.55	0.59	0.38	0.58	5.89	6.35	5.84	6.10
Ear length above tragon	cm	3.30	3.07	3.19	0.41	0.20	0.34	2.7	3.04		
Ear breadth	cm	3.77	3.36	3.57	0.24	0.27	0.33	3.1	3.55	3.3	3.42
Ear protusion	cm	2.28	2.03	2.16	0.22	0.23	0.26	1.85	2.10		
Ear protusion angle	deg	156.7	155.1	155.9	8.6	9.7	9.0	158			
Vertical tilt front view	deg	3.0	2.7	2.9	3.2	3.6	3.1	7			
Vertical tilt side view	deg	7.6	4.7	6.2	2.8	3.4	2.8	6			
Concha volume	cm ³	4.65	3.94	4.3	0.76	0.81	0.85	4.0			
Concha length	cm	2.73	2.53	2.63	0.23	0.20	0.24	2.45			
Concha length, tragon to lower notch	cm	1.74	1.62	1.68	0.16	0.16	0.17	1.82			
Concha breadth	cm	1.88	1.72	1.8	0.21	0.21	0.22	1.57			
Concha breadth tragon to helix	cm	1.82	1.65	1.73	0.27	0.22	0.25	1.39			
Concha depth	cm	1.29	1.29	1.29	0.12	0.08	0.10	1.33			

difficult to identify accurately. From the sample images in Figure 1.11, it is difficult to pinpoint a specific point in the image that constitutes the concha, tragus or lobe.



FIGURE 1.11: Sample of variation among ears

With the introduction of 3D scanning technology there exists the potential to move away from 2D measurements, and to provide full 3D shapes to guide the anthropometric design process. In the following section, the reader is introduced to the current perspective on customization and mass-customization with a focus on in-ear devices. Following this, current research on automating the customization process is discussed and the gaps in the research are established. From this each critical section from the automation literature is analyzed individually in order to determine the appropriate path for this research.

1.1.4.1 Standard customization of an In-Ear Hearing Aid

To understand the novelty of this research, it is important to outline how in-ear device customization is achieved in practice, particularly hearing aids are discussed due to the availability of research information. There are many variations of hearing aids available such as behind-the-ear (BTE) or invisible-in-the-canal (IIC) devices and are typically differentiated by cost, size and placement within the ear. BTE hearing aids place the electronics behind the ear and have a standardised rubber module to transmit the sound to the ear-canal. In-the-ear (ITE), on the other hand, place the electronics and speaker within the ear and the device's shape is adapted to the user's ear. The complexity here is fitting the required electronics within a small space and taking account of the variation in human ears. Other variations of ITE hearing aids

typically aim to reduce the size of the module in order to be placed further within the ear, either for visual purposes to reduce the possible stigma on the user, or to improve sound quality and comfort. Figure 1.12 shows some samples of the various hearing aids that are available in the market and their placement within the ear.



FIGURE 1.12: Sample of the variation of hearing aids that are available and their placement within the ear.

Customization of hearing-aids is currently achieved through the use of moulding, 3D scanning, digital manipulation, and 3D printing (see Figure 1.13). In this process an expert is required at several stages (see Figure 1.13). The primary stage involves taking a mould of the customer's ear canal where an expert will inject silicon rubber into the individual's ear canal and remove the hardened mould. The mould is then digitized using a 3D scanner, typically in the form of a 3D laser scanner. Finally, the digitized mould is processed by a trained expert into the shape of the hearing aid. The custom-fit hearing aid shell is then 3D printed and the electronics are added. The critical sections here, relative to this research, is the processing of the data into the functional hearing aid, which can be split into two sections, detailing and modelling (Slabaugh et al., 2008b).

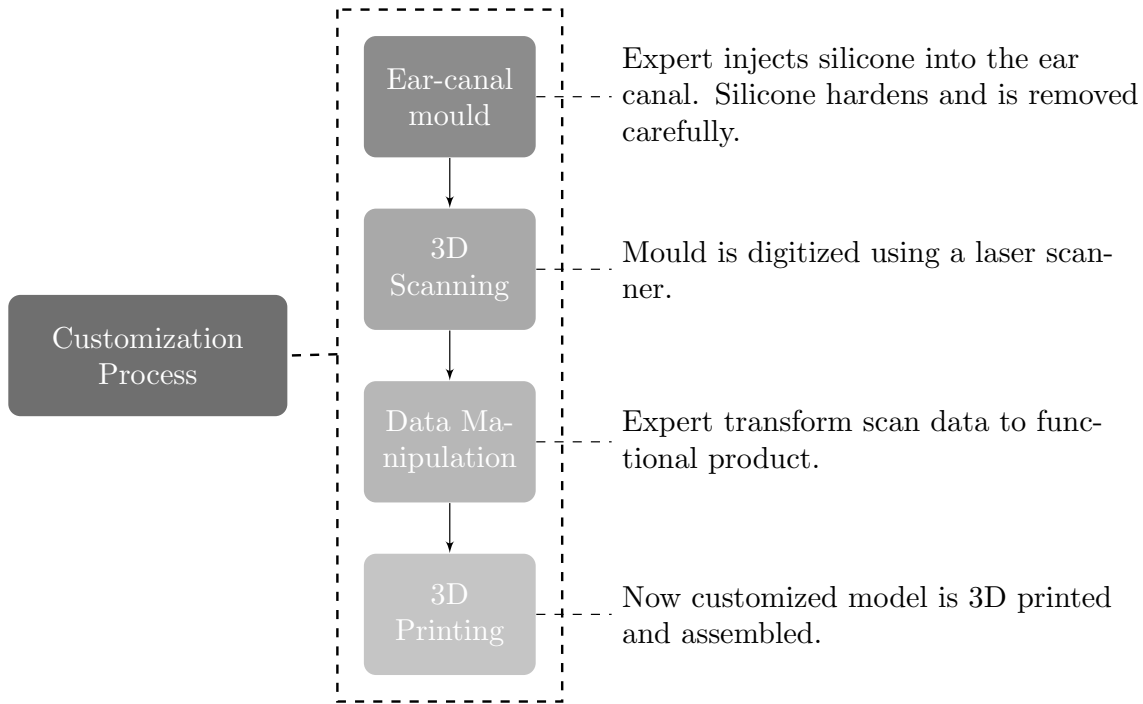


FIGURE 1.13: Customization process for hearing aids (Adapted from Slabaugh et al. (2008b)).

With the introduction of direct 3D laser scanning of the ear canal (Lantos Technologies, 2018), the moulding of the ear canal and consecutive 3D scanning of the mould is redundant. What is critical to this research is the manual stages which take the 3D scan data and process it into the final customized shape for manufacture. These steps, known as detailing and modelling, can be seen highlighted in Figure 1.14.

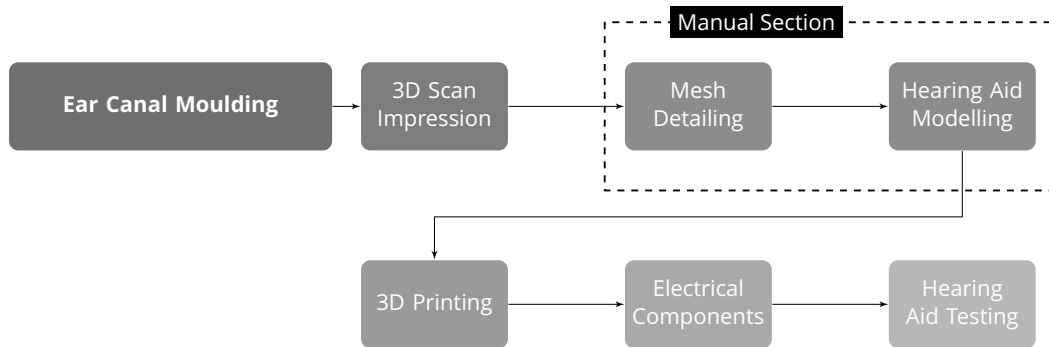


FIGURE 1.14: A flow chart showing the process of customizing a hearing aid using moulding, laser scanning and mesh processing. The manual section, which is the focus of this research is highlighted (Adapted from Slabaugh et al. (2008b)).

The detailing stage, shown in Figure 1.15, incorporates topology correction, surface smoothing, and cutting. When the ear canal mould is digitized the surface can contain defects which require remeshing or topology correction. The surface will typically contain some noise in the form of surface errors which are then smoothed to create a continuous curvature. The cutting process removes parts of the impression that are not required for the hearing aid, typically cutting through the tragus, antitragus and anticymba (see Figure 1.15 c for the placement of these cuts). Depending on the style of hearing aid, further cutting can be performed to remove part of the cymba for In-the-ear (ITE) devices and the crus for In-the-canal (ITC) devices.

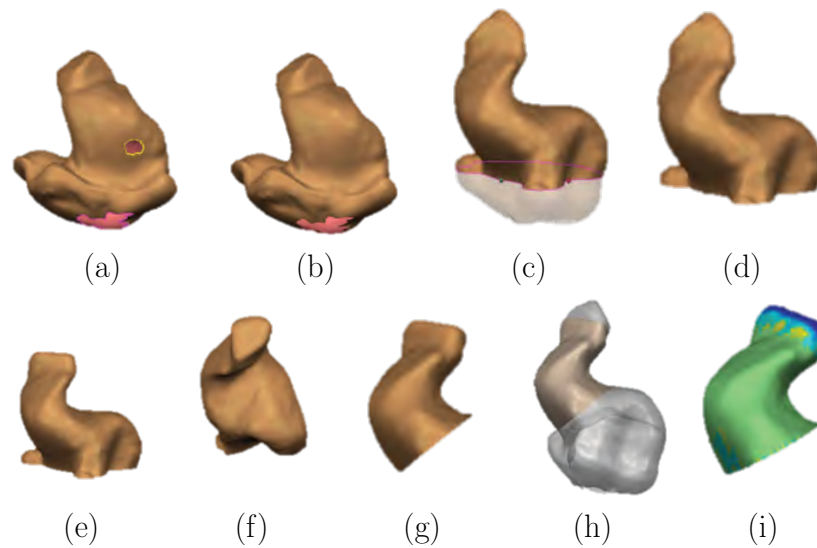


FIGURE 1.15: A step-by-step illustration of the detailing process for creating a custom-fit hearing aid from 3D scan data in (a) to final product in (i). (Adapted from Slabaugh et al. (2008b))

From the detailing procedure, the custom-fit hearing aid shell is complete, however, it is not yet functional. Modelling is performed to incorporate the necessary features to create a functional hearing aid including the shell thickness, vent and electronics placement.

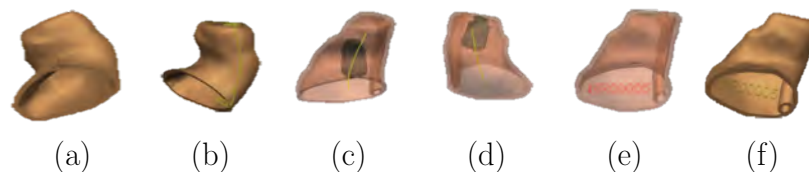


FIGURE 1.16: A step-by-step illustration of the modelling process which takes the custom-fitted shape in Figure 1.15 and adds to features for functionality, i.e. wall thickness, vents, and mounts.

As can be seen in Figure 1.16, the hearing aid shell is thickened to the desired range and the electronics module is placed in the necessary location. A vent is then added to reduce the pressure in the ear canal. It is the stages of detailing and modelling that are to be automated as this process is typically performed by an expert. There are many complexities involved in this process which are outlined in the following section.

1.1.5 Methods for Automating customization

For this research, the interest is in how can the process for designing and manufacturing custom-fit in-ear devices be automated. From the previous section the objective for automation was outlined and from this a thorough review of the literature was performed in order to gain the necessary knowledge to automate in-ear device design and achieve mass-customization.

1.1.5.1 Automating Customised In-Ear Device Design

As the area of automating the process of customization is so novel there are few research papers directly related to the topic or the methods for automation are kept from publication due to the commerciality of the process. A group from Siemens Audiologische Technik GmbH

(Slabaugh et al., 2008b; Baloch et al., 2010; Unal et al., 2011; Unal, 2010; Zouhar et al., 2009; Sickel et al., 2011) have produced the majority of work on automation of the customization of in-ear devices. This section will discuss the progression of their work and the comparison with other literature. Slabaugh et al. (2008b) illustrated the applicability of feature detection on 3D scans to the automation of typically manual parts of the hearing-aid manufacturing process (see Figure 1.14).

In their latest work, Sickel et al. (2011) extend on the previous work on automation by employing an expert system and feature detection. An expert system is one which aims to replicate the processes performed by an expert user, i.e. the manual section in Figure 1.14. In their research, Sickel et al. (2011) outlined the complexity of automatically designing prosthesis as maintaining the overall core functionality, which for hearing aids is amplifying the sound, and to ensure that the component fits to the anatomy of the patient. Sickel et al. (2011) aim to replicate the expert user in the form of rules that are performed by a computer program, specifically, given an unprocessed ear-canal scan represented as a triangulated mesh, the goal is to transform it into the desired shape through a series of transformations constrained by a pre-defined set of rules.

$$S_{Final} = T_R(S_{Scan})$$

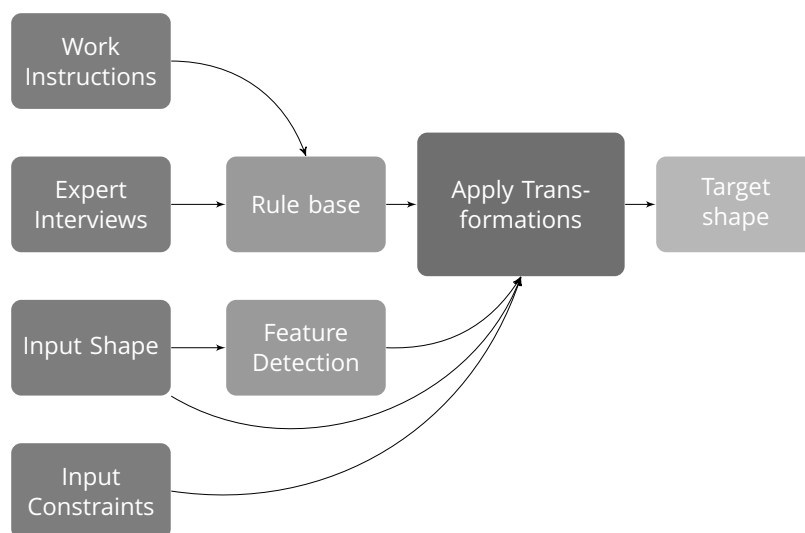


FIGURE 1.17: Automated approach using a rule based system illustrating the feature detection and application of pre-defined rules (Adapted from Sickel et al. (2011)).

The process for determining the placement of key features is driven by the detection of anatomical features on the surface of the ear-canal impression. Specifically, Sickel et al. (2011) detect the following features, which were deemed distinctive among individuals in terms of their shape, and their relative size, depth and/or location.

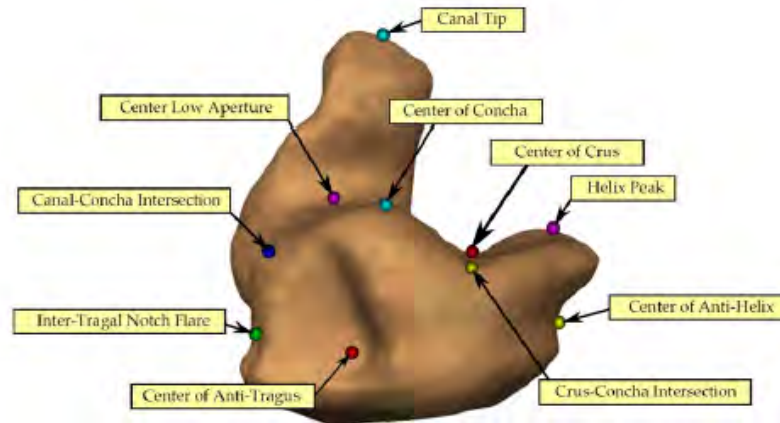


FIGURE 1.18: Key features of a hearing aid impression which are used to guide the expert system through the automated customization process.

Sickel et al. (2011) identify 44 anatomical features in total by using generic features such as peaks, concavities, elbows, and ridges, and a set of derived features from a combination of these. Collectively, Sickel et al. (2011) define these anatomical features as the Canonical Ear Signature (CES), which is the distinctive information which constitutes a person's ear canal. Comparatively, Slabaugh et al. (2008b) rely on feature recognition on ear-canal scans in order to automate the detailing and modelling processes in Figure 1.15 and Figure 1.16. However, contrary to Sickel et al. (2011) they recognize features on the surface of the canal scan through contour analysis.

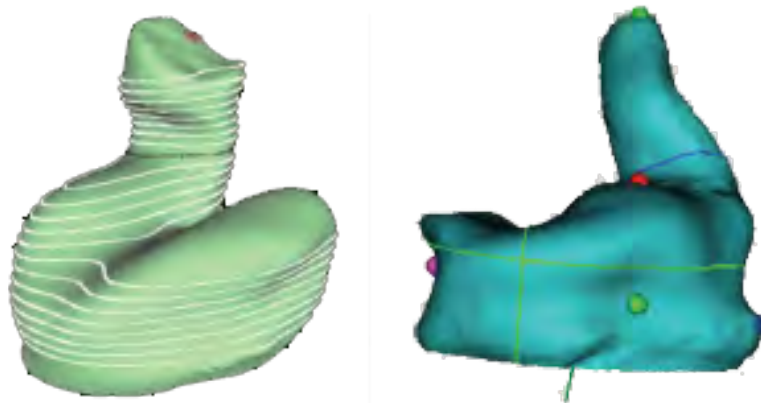


FIGURE 1.19: Feature detection on a hearing aid impression by analysing the variation in contours (Slabaugh et al., 2008b).

No further information is given on the achieved quality or accuracy, the information is merely given as a possibility to in-ear device manufacture. The method by Sickel et al. (2011) and Slabaugh et al. (2008b) can be classed as a generative approach to customization. In the generative design approach, the final customized design is generated successively from raw 3D scan data, following the same steps as the expert user. Alternatively, Unal et al. (2011) introduced the use of 3D statistical analysis to guide the customization process. In this approach, a database of raw 3D scans and manually constructed target shapes is generated, which is then statistically analyzed to generate the principal components (PC). Unal et al. (2011) use the statistical model as a means to transform a raw 3D scan to the customized shape using a predictive model from the PC's following the steps in Figure 1.20.

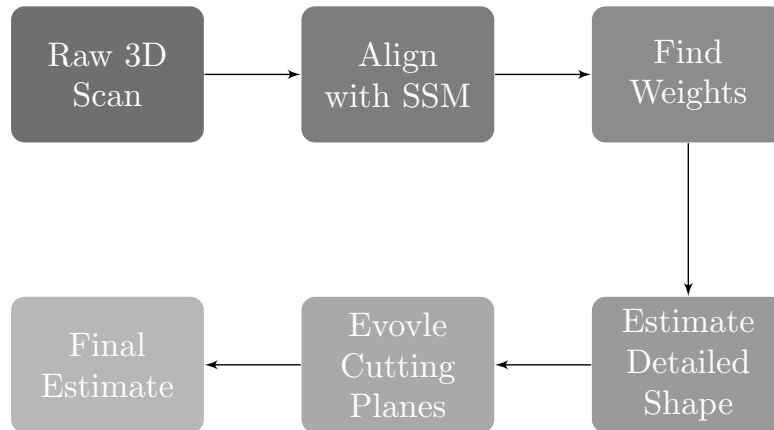


FIGURE 1.20: Predicting the customized shape from a statistical model (Adapted from (Unal et al., 2011)).

While it is still necessary to perform the detailing and modelling stages as per Figure 1.15 and Figure 1.16. The use of a statistical model circumvents the need for detection of landmarks on the surface of the raw 3D scan in order to transform the input data into the desired customized shape. However, it should be noted that the use of statistics is a limitation in some aspects. As stated by Unal et al. (2011), for some individuals with highly varying ear canal shape and length, it was not possible for the system to automatically place the necessary cutting planes, resulting in a failure. It was proposed by Unal et al. (2011), that the addition of anatomical landmarks could pose an improvement to the process. The approach by Unal et al. (2011) can be classed as a morphometric approach where the goal is to use pre-learned statistical models to morph the input data into the desired shape. Comparatively, the generative and morphometric approaches aim to achieve the same goal but by different means. The morphometric approach uses pre-defined data as a guide for predicting the output shape, whereas, the generative approach uses a set of pre-defined rules that successively generate the output shape. While the two approaches achieve the same goal there are advantages and disadvantages to consider for mass-customization which are discussed in Section 1.1.6.

1.1.5.2 The Performance and Accuracy of Current Automation Systems

Research by Sickel et al. (2011) and Unal et al. (2011) is at the forefront of automating custom-fit in-ear device design. The method by Sickel et al. (2011) relies on the detection of features on the surface of 3D scanned ear-canal impressions and pre-defined rules that aim to replicate an expert user. In order to evaluate their system, a dataset of 198 ear-canal impressions were tested against ground truth data established from an expert user. Curve features, however, were evaluated qualitatively by the expert user due to the absence of ground truth data. Their feature detection system was evaluated against feature point placement (δ_p), cut plane location (δ_{loc}), cut plane orientation (δ_{or}), area sensitivity (δ_{sen}) and area specificity (δ_{spe}). The combination of these features constitutes the replication of the expert user. For the interpretation of the results, experts provided error tolerances for various features equating to a 3mm tolerance for location and 15deg tolerance for orientation, which were used to define two additional performance metrics, detection rate (Δ_{det}) and tolerance rate (Δ_{tol}). Detection rate is computed as the percentage of test cases for which the algorithm successfully detects the corresponding feature and the tolerance rate is computed as the percentage of test cases for which the detected feature is within the acceptable tolerance.

Their results indicate an acceptable performance for most features with an overall mean tolerance rate of 87% for points and 83% for planes. The full results can be seen in Table 1.2.

TABLE 1.2: The performance of the method by Sickel et al. (2011) showing the detection rate and the tolerance.

Performance Measure	Feature Type	Rate in %
δ_{det} (detection)	3D Point	98.6
	3D Point	98.6
δ_{tol} (tolerance)	3D Point	87.0
	3D Plane	82.0

Of interest here is not the accuracy of the detected features, seen in Table 1.2, but how the system performs for the automation of the customization process. The critical table here is Table 1.3 which shows that the automation approach achieves less than 10% reduction in time when compared with the expert user and it was established that the system was not able to reach full automation of the hearing aid manufacturing approach.

TABLE 1.3: Achieved improvement in time compared to an expert user by using the automation system of Sickel et al. (2011).

Automated	Total Time (s)	Time Difference (s)	Ratio (%)
No	652	-	100
Yes	597	55	91.6

Comparatively, the method by Unal et al. (2011) does not provide time improvements compared to an expert user but does provide the estimated error compared to ground truth data. Specifically, the maximum distance between the ground truth data and the estimated shapes from the statistical model were $5.0 \pm 1.7 \text{ mm}$, and $3.6 \pm 0.9 \text{ mm}$ for the final shape.

1.1.5.3 Complexities in automating hearing-aid design

With the state-of-the-art failing to reach full automation it is necessary to understand why in order to determine the most appropriate path for this research. Sickel et al. (2011) outline the complexities with automation as:

- Poorly acquired 3D scans with gaps and excessive noise.
- Misuse of the framework. The rigidity of the generative, rule-based system, can lead to errors if the steps are not performed in the correct order.
- Translating special design instructions into rules or constraints requires re-programming the framework.
- Determining acceptability in custom-fit due to the subjectivity in user comfort and expectations.

One of the main complexities that Sickel et al. (2011) encountered is the excessive noise in the 3D scan data. As their system relies on the detection of feature points on the surface of the scan data it is a requirement that the scan data be smooth and consistent across consecutive scans. The predictive method could potentially be more robust to noise input 3D scan data as the statistical model is typically learned on noise-free data. The method by Sickel et al. (2011) also relies on a step-by-step process that is synonymous with the process of the expert user, however, depending on the user there is no guarantee that the pre-defined steps will be followed in the correct order by the user, which was found to cause errors in their automation process. It is known that each individual has a potentially unique ear-canal shape, and

can sometimes require specific hearing aid designs determined by an audiologist. One of the complexities experienced by Sickel et al. (2011) was applying these special instructions to their pre-defined rule-based system.

1.1.6 Application to this research

By analyzing the literature, the methods for automating the customization of in-ear devices can be split between generative and morphometric. The generative approach aims to construct the final customized shape successively from raw 3D scan data, whereas, the morphometric approach predicts the customized shape from a learned statistical model. A disadvantage of both approaches is the need to detect landmarks on the surface of the scan data to place cutting planes to form the functional customized shape. The functional customized shape, in this case, contains the wall thickness, acoustic vents, and electronic mounts (see the detailing steps in Figure 1.15). While both methods are able to output a customized product, there are clear disadvantages. For example, the predictive model, while powerful, works on a relatively sparse set of detected landmarks. Similarly, the generative method attempts to replicate the expert user through the placement of cut-planes and other CAD functions guided by the detection of anatomical landmarks. These disadvantages pose the following questions:

- *How do we statistically analyze the full 3D scan data to form a predictive model, without the use of landmarks?*
- *Can we use already fully functional CAD designs as opposed to performing the processes after customization?*

Similar to the process of Unal et al. (2011), a statistical model will be used to guide the customization process and incorporate robustness in the estimation of the final shape from noisy input 3D scan data. Typically, the final functional product has to be formed through the use of cutting planes and detailing steps (see Figure 1.15). However, in reality products are designed using computer aided design (CAD) software, not by placing cutting planes at anatomical landmarks. Therefore, this research will aim to adapt standard CAD designs with a statistical shape model (SSM), such that, a functional product is deformed using the SSM. This introduces a new class of automated customization which is being defined as deformative customization. The new automated deformative customization approach is outlined in Figure 1.21.

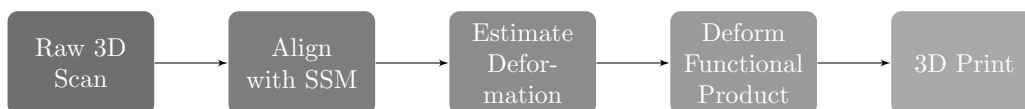


FIGURE 1.21: The proposed deformative customization approach showing the introduction of functional design deformation.

From Figure 1.21 the path to mass-customization has been determined. In order to achieve this a review of the methods for 3D scanning the human ear, using machine learning for statistical analysis and mesh deformation, and 3D printing is required. The following section analyzes the literature on 3D scanning, with a particular focus, where possible, on the human ear. Section 1.1.8 discusses machine learning for automation and statistical analysis and Section 1.1.9 discusses the design of customized in-ear devices and the use of 3D printing to achieve mass-customization.

1.1.7 3D Scanning Technology and It's Application to the Human Ear

From the previous section it was discussed that one of the difficulties in achieving fully automated customization was dealing with noise in the 3D scan data. To ensure successful completion of the goal of this research, the current state of 3D scanning and its application to the human ear was researched.

3D scanning is a critical component of this research, however, depending on the complexity and material of the object to be scanned there are advantages and disadvantages to the various 3D scanning methods. There are two types of 3D scanners, contact and non-contact. Of interest to this research are non-contact 3D scanning methods, which can be further classified into active and passive scanners.

1.1.7.1 Passive 3D Scanning Systems

Passive 3D scanning relies solely on 2D images to extract 3D depth information from a scene without the assistance of an external source such as projection of light patterns onto the scene. Several techniques exist to recover 3D scene information from a single or multiple images:

Shape from focus: Vary the camera focus and estimate the pixel-wise depth from image sharpness.

Shape from shading: Uses the shadows in a grayscale image and the known reflectance map to recover 3D shape

Shape from texture: Recovers the 3D shape only if the object is covered by a regular surface pattern. Surface normal and distance are then estimated from the perspective effects in the images.

Shape from stereo disparity: The scene is imaged from two viewpoints and the difference (disparity) is calculated based on the corresponding pixel positions in the images.

Shape from focus, shape from shading, and shape from texture, are all techniques that can use a single image to recover the 3D shape. However, such methods are often not practical in terms of either robustness or speed or both. Therefore, this research will focus on shape from stereo disparity or more commonly referred to as multiple-view passive 3D scanning. With multiple-view 3D scanning, the scene is observed from two or more viewpoints by either multiple cameras at the same time (stereo) or a single moving camera at different times (structure from motion) (Pears et al., 2012). Stereo is the simultaneous capture of multiple viewpoints using two or more cameras with the most common being binocular stereo vision which relies on two viewpoints. This can be extended to three cameras, trinocular stereo, or can even include unlimited cameras distributed around the viewing sphere of the desired object. In contrast to this, structure from motion (SFM) uses a single moving camera where the image sequence is captured over a period of time. The advantage here is that a single camera can be used to reconstruct an object of small to unlimited size. Figure 1.22 illustrates the process for reconstructing the 3D shape of an object from a sequence of images.

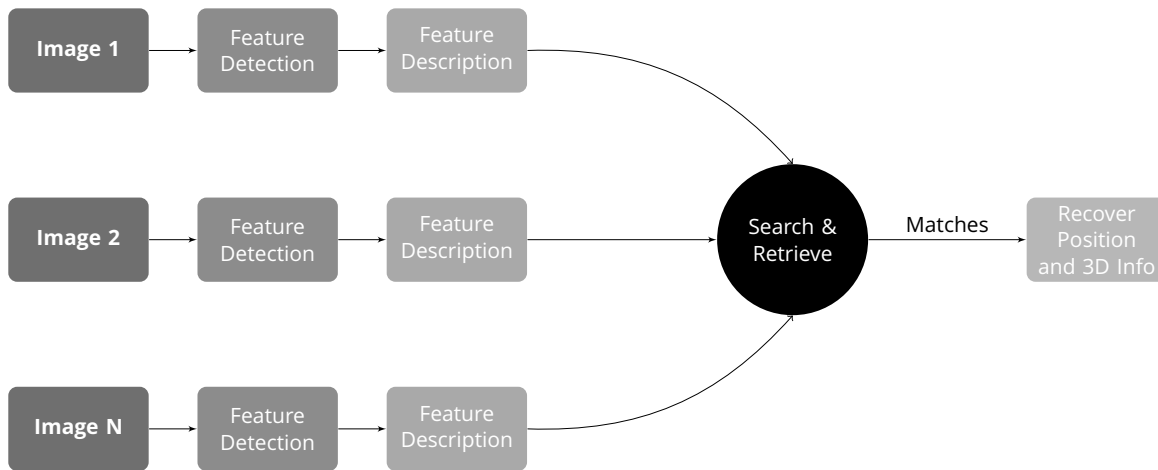


FIGURE 1.22: The process of reconstructing a 3D shape from a collection of 2D images.

As can be seen in Figure 1.22, the standard approach for passive imaging involves the detection of features/keypoints within an image, the description of these features, and then the search and retrieval of matching features between images. The recovered matches are then used to determine the position of the cameras relative to each other and the 3D scene information. The reader is directed to Pears et al. (2012) for an overview of passive 3D imaging, detailing the processes for detection, description, search and retrieval, and reconstruction. As this research is focused on passive 3D imaging in regards to robustness to occlusion, low level of texture, and automation, the applicable research will be discussed in the following section.

1.1.7.2 Passive Systems for the Human Ear

This section aims to identify key research on passive 3D reconstruction of the ear, or similar regions, in order to assess its viability to this research. On the single image approaches, some research has attempted to overcome the limitations and complexities to successfully reconstruct the ear. Cadavid and Abdel-Mottaleb (2008) used shape from shading from video sequences in order to reconstruct and recognize the ear. In this approach a set of frames is extracted from a video clip and the ear region segmented. Then the 3D ear models corresponding to each frame are derived using the shape from shading technique. In order to align the models, the iterative closest point (ICP) algorithm is used and cross validation is performed for recognition. The shape from shading method using video sequences does successfully construct a 3D model of the ear; however, the technique is highly sensitive to lighting variations as it relies on illumination and reflectance in order to derive the 3D model.

Li et al. (2012) and Li et al. (2015) aim to improve the 3D ear reconstruction process by employing a 3D ear morphable model (3DEMM). A morphable model, also known as a statistical shape model (SSM), is a statistical representation of an object containing the dimensional variation within the trained dataset. The complexity with a 3DEMM is that each vertex must be meaningfully corresponded across each mesh within the dataset, given the high variability in shape and size of the human ear it is not a simple task to construct. 3DEMM provide priori information which can be used to assist in the 3D reconstruction process as a full representation can be constructed from low level input such as a single image. Li et al. (2012) detect key anatomical landmarks on the ear image which are then registered to the 3DEMM and the final shape is constructed. This process is similar to Unal et al. (2011) and Sickel et al. (2011), but in two dimensions. It therefore falls into the same disadvantages, i.e. the detection accuracy of the anatomical landmarks.

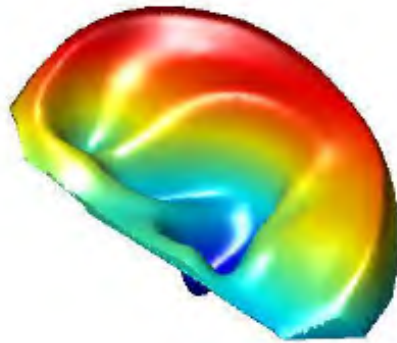


FIGURE 1.23: 3D ear reconstruction from a single image using a 3D morphable model Li et al. (2012).

In consecutive research, Li et al. (2015) aim to improve the alignment and registration process for the 3DEMM by using contour detection on the ear as opposed to feature point detection which they determine significantly reduces the workload as there is no longer the need to manually label dozens of feature points. While the 3DEMM is a powerful representation of the variation of the ear and can allow the user to reconstruct the 3D shape from a single image, the construction of the database and 3DEMM is a significant disadvantage. Li et al. (2012, 2015) use the UND J2 database (Yan and Bowyer, 2007; UND, 2007), which contains 1800 3D profile of the human ear. While this is the largest public 3D (and corresponding 2D) ear dataset, the 3D shape is acquired from a single viewpoint and by analyzing the data it was seen that the majority contain self occlusion or hair which makes the data unreliable for this research. The purpose of the UND database is for biometric analysis typically in the form of ear recognition which does not require highly detailed or full 3D scan data. However, the goal of this research is automated product design, which at its outset requires highly detailed 3D scans in order to generate an accurate fit.

In the multi-view passive 3D reconstruction, Sun et al. (2009) use a stereo camera setup consisting of two Canon EOS 450D digital cameras with a resolution of 4272x2848 pixels. To obtain dense feature points in the images, Sun et al. (2009) employ the Harris corner detector (Harris and Stephens, 1988) and describe each feature point using the DAISY descriptor (Tola et al., 2010). To determine accurate matching points the epipolar constraint and euclidean similarity metric are used (see Pears et al. (2012) for more information on epipolar geometry and similarity matching metrics). The resultant 3D model is highly dense consisting of 5000-8000 vertices.



FIGURE 1.24: 3D ear reconstruction using stereo-vision, showing the wireframe 3D model(left) and the rendered 3D model (right) (Sun et al., 2003).

Of interest here is the automatic nature of the 3D reconstruction without priori information. Sun et al. (2009) have shown that a feature description and matching approach can successfully reconstruct the human ear, however, similar to Li et al. (2012, 2015) the data is taken from a single plane as a stereo camera setup was utilised. Comparatively, Zeng et al. (2009) utilised the same stereo camera setup but employed a variation in feature description and matching, obtaining 2000-3000 vertices per mesh which can be considered a quasi-dense 3D reconstruction. Liu and Yan (2007) aim to reconstruct the entire ear region by capturing and reconstructing 10 views, however, their feature detection and matching algorithms require manual interference and produce a sparse output of 300-600 vertices, which is insufficient for the purpose of this research.

Research from Sun et al. (2009) and Zeng et al. (2009) have shown that it is possible to densely and accurately reconstruct the human ear using passive 3D reconstruction and this has also been verified in industry (Ten-24, 2009).

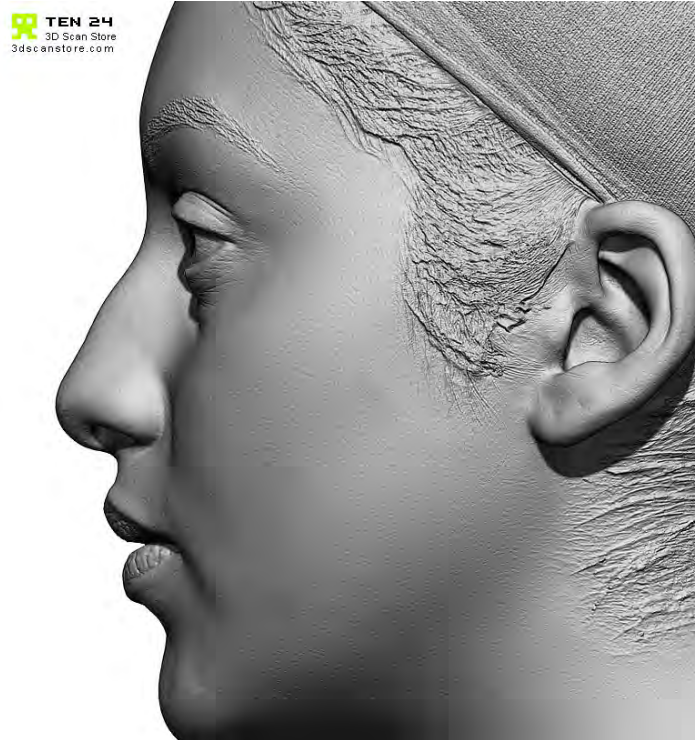


FIGURE 1.25: 3D head reconstruction using an industrial passive 3D scanning rig (Ten-24, 2009).

It should be noted that the industrial system by Ten-24 (2009) consists of over 170 DSLR cameras with a cost value of over \$100,000. One of the main difficulties seen in the literature is the dense matching of feature points across images due to the low-texture of the human ear, however, it has been shown that feature description approaches are successful in obtaining a quasi-dense and dense reconstruction of the ear. For this research several questions remain about the reliability and repeatability of the passive 3D reconstruction process, in the literature there were no discussion on the inherent noise in the scan data due to the inaccuracies in the 3D reconstruction process or the ability of the process to consistently output the same accuracy. There was also no discussion on the ability of the algorithms to account for variations in skin tone as all of known research has used Caucasian skin tone. These concerns will be evaluated further in Chapter 2. The following section assesses the literature on active 3D scanning systems for the human ear.

1.1.7.3 Active 3D Scanning Systems

One of the disadvantages of passive 3D scanning is the necessity to match feature points across images, which can result in erroneous matches. The process is also highly sensitive to variations in lighting and shadows. Active 3D scanning systems avoids this process by using external information, such as a projection device. In comparison to passive stereo-vision, active systems exchange one camera by a projector, which projects a spot, stripe, or patterned area onto the target object (Pears et al., 2012). This alleviates the complexities of establishing correspondences as the 3D information is recovered based on the distortion of the projected pattern, meaning active 3D imaging systems can generate a model of surface geometry even when the surface appears featureless while remaining relatively insensitive to ambient illumination and surface color (Pears et al., 2012). Active 3D scanners can be based on different operational principles; the three most common commercial systems are time-of-flight, interferometry, and triangulation.

Time of flight 3D scanners are based on the principle of accurate timing from a signal leaving the system to when it is reflected back, however, due to the large operating distance and level of accuracy achieved, time of flight systems are not applicable to this research (See Figure 1.26). Interferometry is based on the principle of phase difference between a beam of light of known length and unknown length. The interference pattern caused by the combination of the out of phase beams can be measured to define the distance to the object. While interferometry has a very high level of accuracy, achieving resolutions of micro-meters; the operating distance is much too small to be applicable to 3D scanning of the human ear.

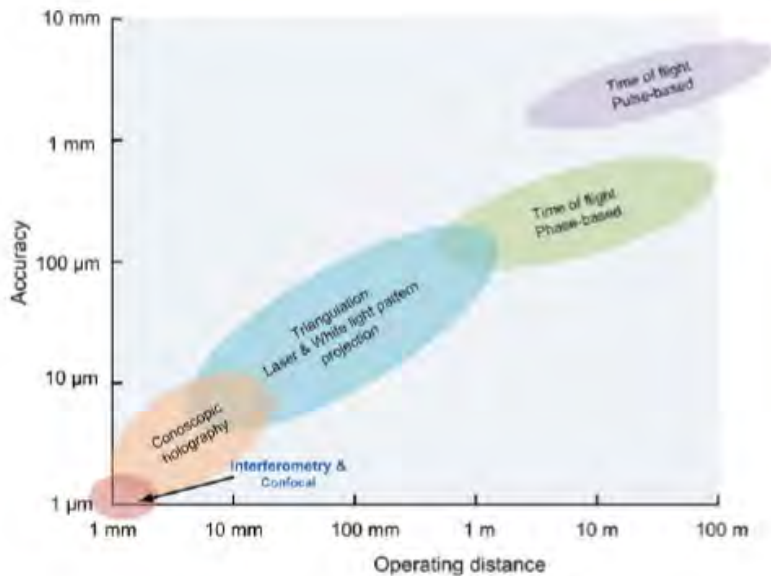


FIGURE 1.26: Diagram showing the typical accuracy at different operating distances of the most common 3D imaging technologies (Pears et al., 2012).

Both active and passive 3D scanning systems are based on the same geometric principle of triangulation, namely intersecting light rays in 3D space (Pears et al., 2012). As discussed previously, the most common active 3D imaging systems are based on spot, stripe, and area projection. Spot scanners are the simplest active 3D scanning system where a collimated laser beam is projected onto the target and the knowledge of both projection and collection angles (α and β) relative to a baseline (H) determines the 3D coordinate of the point on the surface (Pears et al., 2012).

This research will not focus on spot scanners due to the slow nature in acquiring the target surface point-by-point, however, it is a good start in understanding the functioning principles of active 3D scanning systems. Stripe or line scanners aim to acquire more information per frame by projecting a line instead of a spot. However, following similar triangulation principles as the spot scanner. The complexity with these systems is the necessity to translate or rotate the systems in order to capture the full view. Area based methods project many planes of light simultaneously and use a coding strategy to recover the underlying 3D structure.

1.1.7.4 Active Systems for the Human Ear

For active 3D scanning of the human ear the majority of literature focuses on laser stripe scanning which could be due to the low cost and simplicity of operation. Coward et al. (1997, 2000, 2002) use a laser stripe scanning system in order to reconstruct the human ear. The application of the 3D reconstruction is in the detection of anthropometric landmarks for studying the variation between left and right ears, and determining the correct positioning of prosthetic ears on

a patient's face. In their system, the participant is placed on a rotating platform and the laser and camera are held stationary. The laser stripe is captured at 1° intervals, constituting 60,000 points for a full face and a precision of 0.5mm.

Liu et al. (2015) also use a laser scanning system for the reconstruction of the human ear. However, contrary to Coward et al. (1997), Liu et al. (2015) keep the participant stationary and translate the laser beam across the ear using a rotating mirror. While this is more compact, it only captures a planar view of the human ear which could possibly be more occluded. Whereas Coward et al. (1997) captured the full-view of the ear, Coward et al. (1997) does not determine the time to acquire the full-view of the ear, however, Liu et al. (2015) have a scan time ranging from 0.2s to 6.0s depending on the number of desired images and resolution of the laser increments.

While the laser scanning systems have successfully reconstructed the ear, the stripe based method has a significant issue regarding self-occlusion due to the angle between the laser and the camera. As the human ear contains complex curvature and protrusions it may not be possible to reconstruct certain parts of the ear from a single viewpoint.

To circumvent the redundancy with laser scanning systems, area-based methods capture the entire region simultaneously. However, there is no literature with a direct application to the human ear but a significant contribution towards 3D face reconstruction. Wickramaratne et al. (2009) designed and built an active 3D scanner for the face based on fringe projection and triangulation, achieving submillimeter accuracy, the result of which can be seen in Figure 1.27.

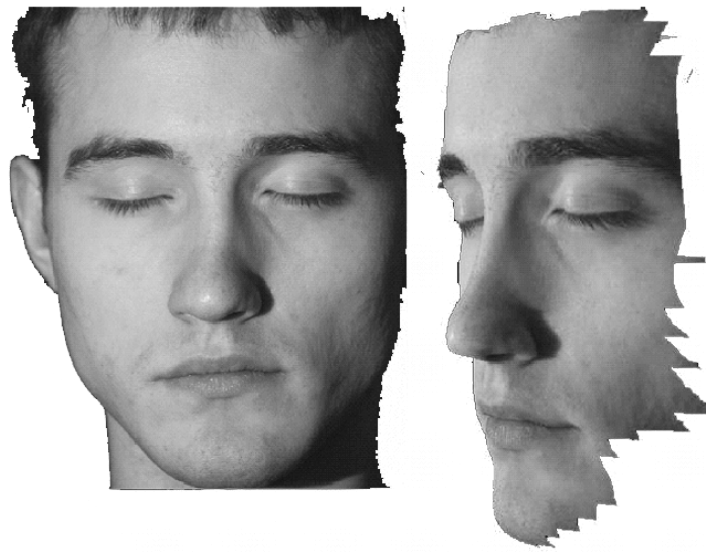


FIGURE 1.27: Active 3D scanning of the face (Wickramaratne et al., 2009).

Similarly, Zhang and Yau (2007); Oujii et al. (2013) reconstruct the human face using active 3D scanning. Of interest here is the ability of active systems to reduce the redundancy of laser stripe based systems whilst remaining highly detailed. As no research has explicitly used area-based method for the ear this will require further evaluation in Chapter 2.

1.1.7.5 Application to this research

It has been shown that both passive and active 3D scanning systems have reconstructed the human ear with varying levels of complexity and resolution. Passive systems are highly modular and inexpensive as they can use widely-available camera technology. Modularity is a valuable parameter as the systems can easily adapt to various 3D scanning applications and

rely primarily on advances in reconstruction algorithms to improve the quality. The difficulty with passive systems is their variance under environmental conditions and the computational complexity in reconstructing the overall 3D geometry from the 2D input. The resultant output is also more prone to noise when compared with active 3D scanning systems.

Active systems are advantageous in smooth, texture-less regions as they do not rely on correspondences between multiple views of the same object. The disadvantage of active systems is the need to move the system to acquire the full 3D object. While it is possible to acquire a 3D shape from a single view, there is no angle that will prevent occlusion with the human ear due to its complexity. Contrary to passive systems, to use multiple active systems to capture the full 3D shape requires synchronization as projection of a pattern onto the surface creates destructive interference. For passive systems, the placement of multiple cameras around the scene is much more cost effective but requires strict control of the environmental conditions.

1.1.7.6 Remaining Questions for Applicability to the Human Ear

From analyzing the available literature on passive and active 3D scanning systems, the following questions remain which are critical to this research:

1. Are Active or Passive systems more appropriate for the human ear?
2. What level of automation can be achieved?
3. What is the effect of variations in skin tone on the 3D reconstruction?

The advantages and disadvantages of both passive and active systems was discussed in the previous section. While active systems produce high quality and accurate surfaces, they are susceptible to occlusion and require a trained individual to manually move the system around the target to construct the full 3D geometry. While you can position multiple active systems around the target, it requires synchronization due to the destructive interference of the projected pattern. Passive 3D scanning systems, on the other hand, are more susceptible to noise but are much more modular and relatively inexpensive. A key advantage of passive systems, which will be discussed in Chapter 2, is the ability to improve reconstruction accuracy with software alone. This makes passive systems somewhat future proof, as improvements in algorithms can be directly applied to the system, similarly with improvements in imaging technology.

Throughout the literature there was minimal discussion on the automation of the 3D scanning process. By positioning multiple passive systems around the target, the acquisition of the required data is completely automatic and instant. However, the complexity is in processing the data. While this is a complex process, there are multiple software packages available to allow for some automation, this will be discussed in Chapter 2. For active 3D scanning systems, the processing of the data is handled by the software and can even be performed in real-time, the difficulty for automation is in the motion of the system and ensuring that all critical angles are captured so as to minimize the occlusion.

A critical issue with both active and passive systems is the reconstruction of dark and textureless regions. Throughout the literature, all examples were of caucasian skin tone. Of interest to this research is the ability of both active and passive systems to handle darker complexions. These remaining questions will be answered in Chapter 2 and Chapter 3. The following section aims to understand how the 3D scan data can be used in a product design scenario, particularly machine learning for automated customization.

1.1.8 Analyzing 3D Scan Data for Automating the Customization Process

In the previous sections the methods for 3D scanning the human ear were discussed. However, in order to accomplish the goal of this research, which is automating the design and manufacture of custom-fit devices for the human ear, it is necessary to further analyze this 3D scan data. In Section 1.1.5 the current processes for automating customization were discussed, this section aims to gather further information on employing machine learning for the generation of statistical shape models as per Unal et al. (2011) and the possibility for using the statistical analysis for product design.

1.1.8.1 Generating a Model of the Shape Variation

It has been determined that a statistical shape model (SSM) will form a critical component of this research due to the advantages shown in Unal et al. (2011). What is remaining to be understood is the complexity in generating the SSM for the human ear. From the literature a SSM can be constructed following the steps in Figure 1.28.

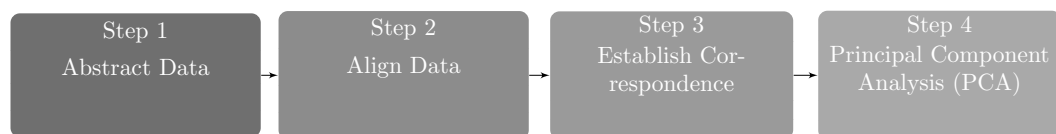


FIGURE 1.28: Generalized steps for constructing a SSM.

Abstracting the data is the first step in the generation of a SSM and was added due to the broadness in data sources that SSM's are learned on. For example, a SSM can be generated from point clouds, mesh or surface data (Paulsen et al., 2002; Dalal et al., 2007; Dalal and Wang, 2012), from volumetric data for medical analysis (Heimann and Meinzer, 2009), and even from lower dimensional spaces (Unal et al., 2011; Rustamov et al., 2013).

The next step is the alignment of the dataset, this can be through biased registration where all the models are registered to a randomly selected model in the dataset, or a groupwise registration process can be used. Registration in a groupwise scenario is highly complex, especially in the presence of non-rigidity. In simple terms, registration is the transformation of multiple three-dimensional datasets into the same coordinate system so as to align overlapping components of the data (Tam et al., 2013). One of the most widely used methods for registering or aligning 3D data is the Iterative Closest Point (ICP) (Besl and McKay, 1992).

With all of the models in the dataset now aligned, i.e. they have the same coordinate system and overlapping regions. It is now required to establish the correspondence which is a one-to-one mapping from one model to the next. This is one of the most complicated steps for generating a SSM as there are numerous issues:

1. Noise in the data
2. Non-rigidity or pose variations
3. Holes or partiality in the data

The goal for this research is the use of the full 3D scan data as the basis for SSM as it may potentially result in a more accurate model for product design. Therefore, methods that rely on sparse representations of the model, i.e. landmarks or subsampling, will not be considered. Non-rigidity is an important consideration as the shape of the human ear is so varied that it may be required to establish an accurate correspondence. For a full overview of methods and considerations for establishing correspondences between 3D shapes, the reader is directed to Van Kaick et al. (2011).

1.1.8.2 3D Non-Rigid Shape Matching for One-to-One Correspondences

Due to the amount of available literature on 3D shape matching, this research will focus on methods for dense non-rigid shape matching that do not rely on pre-learned data. Functional map based 3D shape matching (Ovsjanikov et al., 2012) is a state-of-the-art method for establishing correspondences across 3D shapes. Functional maps are based on the principle of establishing a mapping between real-valued functions as opposed to spatial points on a surface. By mapping between real-valued functions it removes the spatial constraint and makes the correspondence pose-invariant as shown in Figure 1.29.

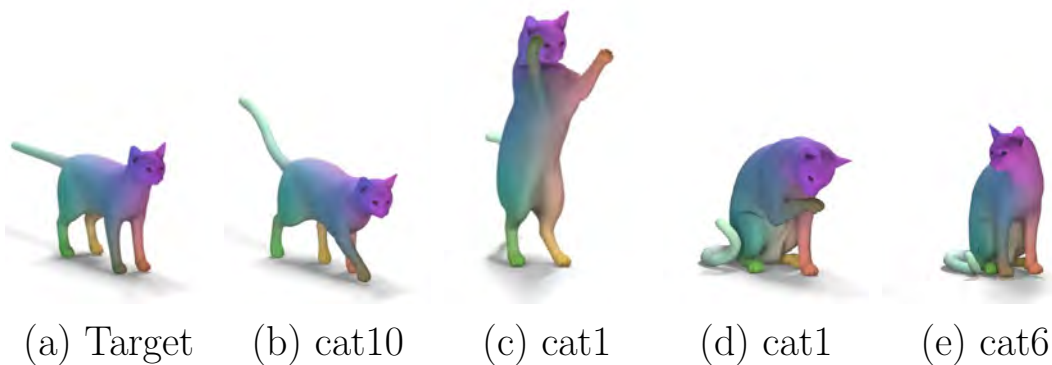


FIGURE 1.29: Functional map based 3D shape matching. The shape (a) is matched with (b-e), the surface colour represents matching areas with the target shape. Notice the colour similarity even with large pose variation (Ovsjanikov et al., 2012).

The functional map framework can potentially be an improvement over methods in the spatial domain such as the widely-used non-rigid Coherent Point Drift (Myronenko and Song, 2010), the validation of which will be discussed in Chapter 4. One of the key advantages of the functional map framework is its extensibility with new feature descriptors or manifold learning algorithms. The functional map framework has been applied to the analysis of variation within a dataset (Rustamov et al., 2013), however, it is difficult to relate the resultant variation analysis to a standard SSM. More recently, the functional map framework has been extended to improve the reliability and robustness of the correspondences (Nogneng et al., 2018; Mandad et al., 2017; Rodolà et al., 2017; Vestner et al., 2017), the framework has also shown applicability to machine learning where the goal is to improve the robustness of the correspondences through the use of a pre-defined training set (Defferrard et al., 2016; Bronstein et al., 2017).

1.1.8.3 Application to this Research

By assessing the literature, it was found that to construct a SSM an accurate and meaningful correspondence has to be established. As it is desired to use the full 3D scan data as the source for the SSM, this presents a difficult task due to the variations in topology and density of the 3D scan data. The functional map framework presents a state-of-the-art method for establishing correspondences in the presence of pose and shape variations. The review of the literature has laid the foundations for how we statistically analyze the full 3D scan data, without the use of landmarks?. Chapter 4 establishes the use of the functional map framework for the generation of a SSM from 3D scan data to answer this research question. The following section aims to wrap up the remainder of questions for this research relating to the design of in-ear devices and 3D printing for mass-customization.

1.1.9 Design of In-Ear Devices For Automated Rapid Prototyping

Section 1.1.5 discussed the process of automating the customization of in-ear devices, and Section 1.1.7 and Section 1.1.8 detailed how 3D scanning can digitize the shape of the ear and how that data can be processed for automation. This section aims to illustrate the final step of the mass-customization process which describes the design of the in-ear device and the process for 3D printing.

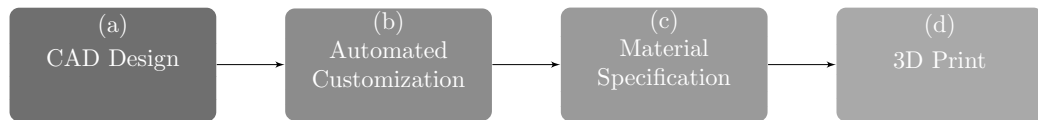


FIGURE 1.30: In-ear device design and 3D printing for mass-customization

The customization process in Figure 1.30 (b) is the novelty of this research and the methods in the literature have been discussed in Section 1.1.5. This section aims to discuss the design of in-ear devices (Figure 1.30 (a)) and the processes for manufacturing the customized device using 3D printing (Figure 1.30 (d)) and the available materials (Figure 1.30 (c)). It should be noted that the advancement of the 3D printing materials and processes are outside the scope of this research. The purpose of the inclusion of this information is to provide a full overview of how the automated customization process fits together.

1.1.9.1 Design of Customized In-Ear Devices

Current technology that use the ear are; earphones (outer and in-ear), Bluetooth devices, hearing aids, direct language translators (iTranslate, 2018), and even health monitors for sleep (Nguyen et al., 2016), biometrics (Nakamura et al., 2018), and heart rate monitors (Park et al., 2015; Palladino, 2016). For customization it is important to understand how these devices interact with the human ear to determine the best possible design.



FIGURE 1.31: Types of customized earphones to inform the design process.

From Figure 1.31, three types of customized earphones are shown. Figure 1.31 (a) shows the Snugs (Snugs, 2017) brand which are made through moulding and manual data editing. Figure 1.31 (b) and (c) are customized options made through the use of 3D scanning technology. It should be noted that both Normals (Hardawar, 2014) and Ownphones (Ownphones, 2014) have ceased operations. For this research, the range of customized earphones have shown that typically the outer shell which fits to the ear is the only custom component and standard earphone electronics are simply mounted into the custom shell. In regards to hearing aid design, a similar approach can be followed. For this research, a custom shell will be created to be fitted to available earphones in order to demonstrate the customization process. Particularly, the

design of Figure 1.31 (a) is to be adapted for mass-customization. Given that the process for Snugs is manual, the advantages of the automated approach will be directly relatable.

1.1.9.2 FDM, SLS and SLA 3D Printing

With the type of customized earphones assessed, it is important to consider how the devices will be manufactured. With mass-customization it is not possible to use standard mass-manufacturing process due to the unique nature of each device. 3D printing is essential to produce the one-off devices for each individual. However, the type of machine is dependent on the requirements.

Fused deposition modeling (FDM) is one of the more widely used 3D printing technologies due to its relatively low cost and wide-availability. FDM 3D printers work by melting and extruding thermoplastic filament through a nozzle. The deposition of material is built up over layers. While this process is widely-used, it has the lowest resolution and accuracy of the three technologies. Selective Laser Sintering (SLS), on the other hand, uses a high-powered laser to fuse small particles of polymer powder. Similarly, this is a layer-by-layer process where a new layer of powder is set after each layer. The benefit of SLS is there is no need for support structures and it is ideal for complex geometrics, including interior features, undercuts, thin walls, and negative features (RedStack, 2017). A disadvantage of SLS is the relatively low variation in available materials with the machine typically working with Nylon.

The final type of 3D printer, Stereolithography (SLA), is the oldest but still one of the most popular. SLA uses a laser to cure a liquid resin into hardened plastic in a process called photopolymerization. Parts that are printed using SLA have the highest resolution and accuracy, the clearest details, and the smoothest surface finish of all the available 3D printing technologies. One of the key advantages of SLA 3D printing is the wide-availability of materials, from hard engineering plastics to soft silicone-like.

1.1.9.3 Achievable Surface Quality with SLA 3D Printing

Surface quality is a key criteria for 3D printing, particularly in-ear devices where the 3D printed device is expected to be used as the end-product. Contrary to alternative 3D printing techniques, such as FDM and SLS, SLA based 3D printing achieves a very smooth surface finish. This has been quantitatively verified in Choudhari and Patil (2016). Within the SLA based machines there are variations which must be considered, including laser SLA, DLP SLA, and mask SLA, see Figure 1.32. The choice of SLA type impacts the achievable level of detail and the printing speed.

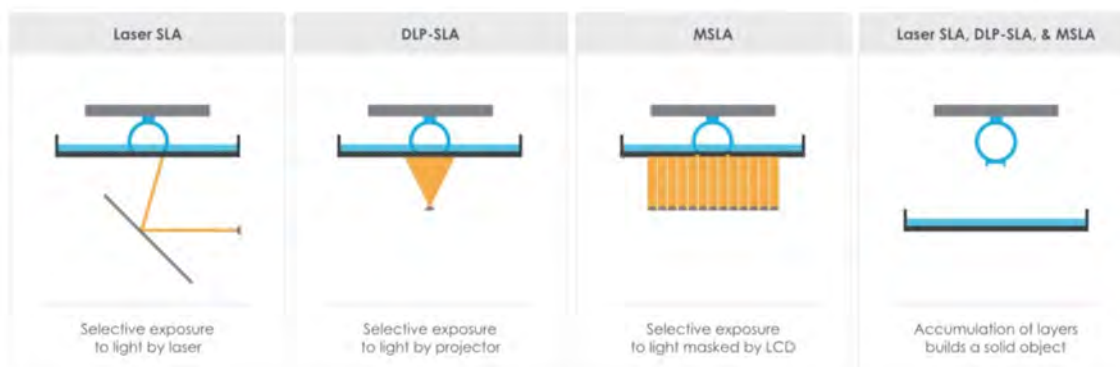


FIGURE 1.32: Types of SLA based 3D printing, showing the different means by which to cure the photosensitive resin (Frey, 2017).

As per Figure 1.32, the three types of SLA 3D printing are laser, DLP, and mask. In Formlabs (2017a), a comparison of surface quality was performed using laser and DLP-based SLA. It was determined that laser-based methods provide superior surface quality due to pixelation effect of DLP and mask-based approaches as seen in Figure 1.33. With all 3D printing technology there is the layering effect where horizontal lines are visible. However, it was established that with DLP and mask-based approaches, there are also vertical lines due to the pixelation effect, which creates a less aesthetic surface when compared to laser-based methods.

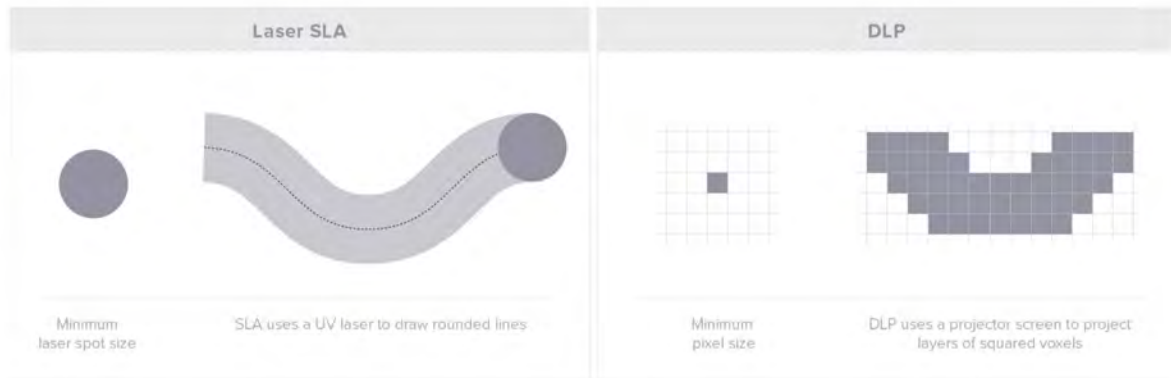


FIGURE 1.33: The pixelation effect caused by DLP and mask-based SLA in comparison with laser-based approaches (Formlabs, 2017a).

It can be seen in Figure 1.33 that the motion of the laser-based methods do not cause pixelations, comparatively, the stationary DLP and mask-based approaches cause pixelation due to the technology limitation. The selection of the machine type is dependent on the application and the degree to which pixelation of the surface affects the end result.

1.1.9.4 Considerations for 3D Printing Speed

Speed is an important aspect of mass-customization, although it should be noted that standard 3D printing times for the customized in-ear device in Chapter 6 using the widely available Form2 3D printer (Formlabs, 2017c) is approximately 1 hr 30 minutes. As the automated customization process discussed in Chapter 6 takes less than 5 minutes, and even adding 25 minutes for post-processing, the time to delivery using this process would be 2 hrs.

1.1.9.5 SLA Type Selection

Depending on the type of machine that is selected, there can be significant improvements to the 3D printing time, although with some compromises. As discussed in Section 1.1.9.3 there are three types of SLA based 3D printers; laser, DLP, and mask. Laser based SLA is the slowest of the three as it must trace the path of the model using an XY scanning galvanometer. Therefore, the larger the part is, the longer the 3D printing time. This is also relevant for 3D printing of multiple parts in a batch. However, as discussed in Section 1.1.9.3, the laser based machines produce the finest surface quality and level of detail.

DLP and mask based SLA operate in a similar manner. DLP SLA based 3D printing projects the desired pattern onto the surface of the resin where it solidifies, and the process then repeats this layer-by-layer. Contrary to laser-based methods, this process does not need to trace a path and it therefore has a much faster layer curing time when, and it does not vary with part size. Similarly, mask based SLA 3D printing solidifies the entire layer at the same time, but the method for projection is different than DLP SLA. In this method, an LCD screen is used to display a mask, UV light of the designated wavelength is then passed through the screen. Due

to the masking effect of the LCD screen, pixels that are dark will absorb the light, and pixels that are transparent will transmit the light. Both DLP and mask-based SLA achieve similar layer curing time, the main source of variation is the difference in power of the projected light source. See Figure 1.32 for an overview of each technique.

1.1.9.6 Direct or Indirect 3D Printing

It has been stated in Chapter 6 that the 3D printing time for the customized in-ear earphone is approximately 1 hr 30 minutes. This is assuming a direct 3D printing of the in-ear device. By directly 3D printing the in-ear device, the part can be immediately used after post-processing. Another process exists, which is being deemed indirect 3D printing, where the a means for the component to be manufactured is 3D printed. This means that the 3D printer will output a custom mould for the device, from which the customized device is created using injection moulding. This processes is detailed in Formlabs (2018) and detailed in Figure 1.34.

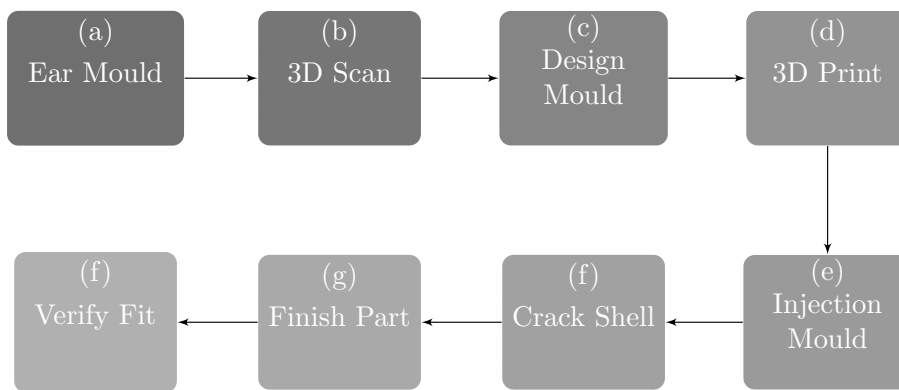


FIGURE 1.34: Indirect 3D printing of earphones using 3D printed moulds and injection moulding. Adapted from the processes discussed in Formlabs (2018)

The advantage of the indirect process is the ability to use standard injection moulding materials, including medical grade silicone. This alleviates some of the issues in terms of quality with 3D printed parts. However, the need to injection mould introduces additional time and manual labour in the process. As detailed in Formlabs (2018), the curing of the silicone adds an additional 25-30 minutes to the process, and requires the use of a pressure chamber for optimum results. Following the curing, the 3D printed mould needs to be removed, which is typically a manual process. When the moulded part is free it may need additional post-curing which is estimated at 5-10 minutes in a specially designed chamber at 60°. Alternatively, the part can be left in ambient conditions for 8-12 hours to perform the post-curing.

While the indirect method has advantages in terms of material properties, the additional time and manual labour is a disadvantage for mass-customization.

1.1.9.7 Ultra-Fast 3D Printing and the Considerations for Design

Recently, a new approach to SLA 3D printing has been introduced, being called ultra-fast 3D printing or continuous 3D printing. In this approach, the main time consuming components of the SLA process have been optimized such that the component can be printed continuously, rather than layer-by-layer. With SLA 3D printing, the main time-consuming component is the resetting of the material after each layer. This involves the printed part lifting out of the resin, a wiper blade resetting the resin and the part lowering for the next layer, for a full overview of SLA based 3D printing the reader is directed to Varotsis (2017).

One of the emerging ultra-fast 3D printing technologies is the CLIP, which stands for continuous liquid interface production (Tumbleston et al., 2015). CLIP works by projecting light through an oxygen-permeable window into a reservoir or vat of UV-curable resin. The advantages here is that there is no need to reset the material after each layer and the process can work continuously.

The CLIP process is considered a bottom-up process, where the part is pulled out of the liquid resin vat. Alternatively, there is the top-down process where the part is lowered into a vat of resin. The benefit of this approach is there are no issues with layer adhesion, and depending on the material properties and projection power, it is possible to print continuously, as shown in Gizmo3DPrinters (2017). With speeds of 3 mm per minute, it would be possible to 3D print a set of earphones in approximately 10-15 minutes. With commercial speeds reaching 3 mm per minute, the focus is now on what materials can be 3D printed that are suitable for the ear.

1.1.9.8 Automation of the 3D Printing Process

Automation has been the theme of this research. However, it was discussed in Chapter 1, that automation of the 3D printing process is not a goal, due to time restrictions. This is also based on the understanding that the remaining process to be automated for SLA 3D printing is the post-processing. In the SLA 3D printing process, the typically manual tasks are; calibrating the platform, loading material, and post-processing. The majority of available SLA-based 3D printers have already automated the platform calibration and material loading, for example the Form2. The remaining process to be automated for SLA 3D printing is the post-processing. This is an exceptionally difficult task and it is not known if there are any potential solutions due to the variability of support structures and part shape. To create a functional component from SLA-based 3D printing requires the post-processing steps in Figure 1.36.



FIGURE 1.35: The Formlabs Form Cell, an automated approach to SLA 3D printing Formlabs (2017b).

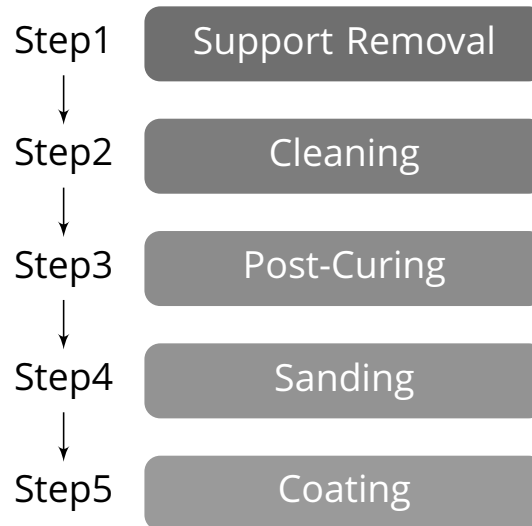


FIGURE 1.36: Post-processing steps for taking a 3D printed SLA component to be functional.

One of the most advanced automated systems for SLA 3D printing is the Form Cell (Formlabs, 2017b) seen in Figure 1.35. In this process, the printing and some of the post-processing operations are completely automated. For post-processing, the cleaning and post-curing of the part are now automated. The remaining post-processing operations that require manual intervention is the removal of the support structures, sanding of the surface, and any optional surface coating. It should be noted that support removal can occur before the cleaning process or after the post-curing process. To the best of our knowledge, there are no known solutions for this problem and remains an area for future research.

1.1.10 Literature Review Outcome

To achieve mass-customization of in-ear devices, a broad understanding of 3D scanning, 3D data analysis and processing, and 3D printing is required. The aim of the literature review was to determine the gaps in knowledge in order to direct this research. In Section 1.1.5 the principles of automating the customization of in-ear devices was discussed and the current state-of-the-art literature was assessed. From this, it was seen that, there are generally two types of customization, generative and morphometric. The generative approach aims to completely replicate the steps performed by a trained expert, whereas, the morphometric approach aims to predict the target shape using statistical analysis. The generative approach requires the detection of landmarks on the surface of the 3D scan data which is highly sensitive to noise. The morphometric approach, on the other hand, circumvents the need to detect landmarks on the surface of the 3D scan data. However, the morphometric method by Unal et al. (2011) still requires the modeling process (see Figure 1.16) to generate the functional product. It was determined that, if it were possible to use a standard CAD designed product with a predictive statistical shape analysis, it would circumvent the need detect landmarks on the surface and would allow for direct 3D printing from the statistical model.

To achieve this requires knowledge of machine learning for 3D statistical shape model (SSM) generation and 3D data processing. The literature discussed in Section 1.1.8 has shown that the generation of a 3D SSM is highly complex, as it requires each vertex on the training data to be in meaningful correspondence. For the human ear, this may pose a difficult task due to the highly varying shape. It was determined that the functional map framework presents the best possible approach for establishing a one-to-one correspondence in a dataset of 3D

scanned ears. The derived method for generating a 3D SSM of the human ear is detailed in Chapter 4.

1.2 Aims and Objectives

This research aims at bridging the gap between 3D scanning and 3D printing by developing advanced tools that will automate the manufacture of customized products. This consists of tool-sets for automating the manipulation of CAD designs relative to 3D scan data using statistical shape models and constrained 3D mesh deformation techniques. Using these advanced tools it is possible to develop mass-customization of products, which as stated, is the process of creating something unique to each individual. The overall objective of this thesis is to determine the feasibility of applying digital automation systems to the design of customized in-ear devices from 3D scan data. Particularly, the methods and processes will be tested against a custom-fit in-ear earphone design. This objective is subdivided into three goals:

1. The assessment and automation of current 3D scanning technology for the human ear.
2. The development of algorithms that automate the customization of in-ear devices relative to 3D scan data.
3. The verify of the automation algorithms through a case study of a custom-fit in-ear earphone.

In order to customize a 3D in-ear device it is critical to be first able to digitize the area in a realistic manner such that it can be further used for statistical analysis, and with automation as the key criteria of this research, the process must be majority automated. Therefore, 3D scanning must be optimized and further developed for this purpose. By digitizing the 3D shape of the human ear it is possible to develop algorithms to perform similar actions to the expert user which could automate the customization process. Following this, the customised shape can be 3D printed to create a functional in-ear device shell. These stages are elaborated in Figure 1.37.

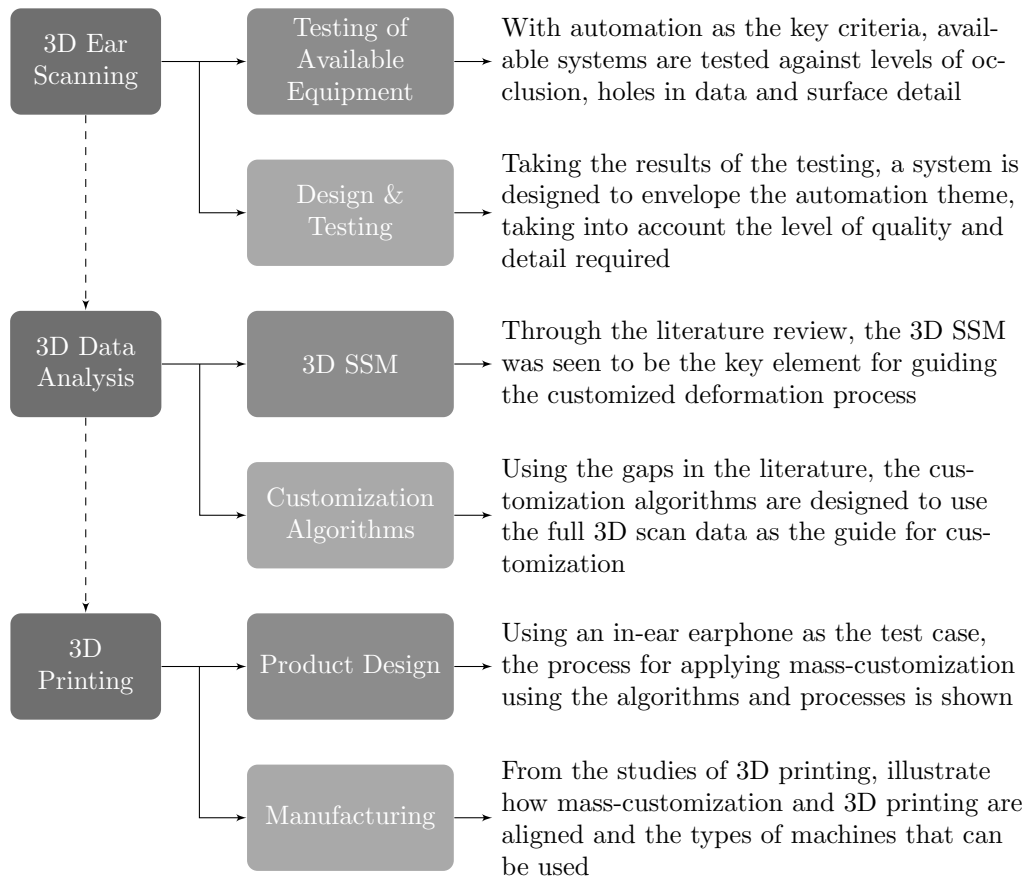


FIGURE 1.37: Thesis objectives split into the three main areas of 3D scanning, 3D data analysis, and 3D printing.

1.3 Research Questions

In Figure 1.37, the three main areas of this thesis are 3D scanning, 3D data analysis, and 3D printing. Each of these areas is further broken down into objectives that were determined to be critical for mass-customization. For 3D scanning, an assessment of available technologies is required to understand the level of automation available and the limitations in terms of level of occlusion and detail in capturing the human ear. It should be noted that this assessment is restricted to technologies that were available at the time and comprises two high end active 3D scanners and standard imaging cameras (see Chapter 2). By understanding the limitations of currently available technologies it is possible to construct a system that will be optimized for mass-customization.

A 3D statistical shape model (SSM) will form the basis for automatically customizing the in-ear device. To construct a SSM, a database of 3D scans is required to analyze the variance. As such, the 3D scanning system will be used to generate the required data that will be the cornerstone for mass-customization. By understanding the gaps in current methods from the literature review in Section 1.1, algorithms were developed that use the SSM as a guide for which to deform a product design. In the final section, an in-ear earphone is designed to test the mass-customization algorithms. Each of these sections aims to answer research questions related to current gaps in the published literature and industry practice, in order to address the novelty and importance of the outcome, as summarized in Table 1.4

TABLE 1.4: Research questions to be addressed relating to the ability to 3D scan the ear and the processes for applying the data to customization and direct 3D printing.

AIM	RESEARCH QUESTIONS	OBJECTIVES	METHODOLOGY	
Development of a method for automated customization of in-ear devices from 3D scan data	Q1	What is the most applicable 3D scanning method for the ear?	Assessment of current 3D scanning systems	Propose most automated 3D scanning approach
		Development of an automated 3D scanning system	Apply chosen approach for 3D SSM	
	Q2	How do we statistically analyze the full 3D scan data, without the use of landmarks?	Analyze the 3D scan data to assess the variance in shape	Apply non-rigid 3D shape matching and statistical analysis techniques
			Adapt the SSM for use in product design	Use of 3D mesh deformation techniques to morph the product design
	Q3	How do we use already fully functional CAD designs as opposed to performing the processes after customization?	Research and create a method to deform the product relative to the SSM, whilst preserving original design features	Scoping study of constrained 3D mesh deformation techniques
			Develop algorithms that can deform CAD designs to 3D scan data	Apply constrained 3D mesh deformation using the SSM as a guide
	Q4	What are the limitations, for design, using this customization process?	Design of an in-ear device, particularly in-ear earphone	Use CAD programs to design an earphone, using available models as a guide
			Detail any limitations from this design process	From the customization process, assess the complications or limitations

Question 1 revolves around a critical component of this research, using 3D scanning technology to develop a 3D database of human ears. Question 1 was derived due to the variation in 3D scanning technologies and the complexities in 3D scanning the human ear. An outcome of this question is a summary of 3D scanning technologies and a database for statistical analysis of the human ear. In terms of novelty, successful completion of research question 1 will result in a completely automated method of 3D scanning the human ear, from capture to full processing. However, it should be noted that the main focus of this research is the generation of the automation algorithms. The 3D scanning system is a necessity for the successful completion of the following research questions.

Question 2 has been introduced due to the observation that variations in the human ear have been taken either by hand or through the use of 2D images and presented in table form (see examples in Table 1.1). However, by using a 3D database of human ears, captured from 3D scanning equipment, it becomes possible to analyse and present this data in three dimensions. The outcome of which is invaluable when designing devices which must adhere or conform to highly varying topology.

Question 3 is related to the main objective of this research, which is the development of a method for automatic customization of in-ear devices based on 3D scan data. 3D scan data, in its raw form, consists of points in 3D space, however, by incorporating the SSM it is possible to introduce consistency and guide the deformation of a pre-designed product. The methodology for this is discussed in Chapter 4 and Chapter 5.

Question 4 aims to apply the mass-customization approach to an in-ear earphone design and outline the advantages and limitations of the process in a realistic scenario. The methodology for 3D printing the custom-fit devices was discussed in Section 1.1.9, including types of machines, materials, and limitations with a sample customized in-ear device in Chapter 6. It should be noted, that the automation and development of the 3D printing technology is not a goal of this thesis.

1.4 Main Contributions

Through in-depth analysis of 3D scanning and automation systems the following contributions to knowledge have been made and are discussed throughout the thesis.

1. Design and testing of an automated 3D scanning system for the human ear based on low-cost multiple-camera photogrammetry.
2. Development of a 3D database of the human ear that can be used for SSM and anthropometric analysis.
3. Development of a state-of-the-art framework for non-rigid Statistical Shape Model (SSM) generation; circumventing the complications with currently available systems (outlined in Chapter 4).
4. Development of a 3D mesh deformation based automation framework for design of custom-fit in-ear devices that does not rely on prior knowledge of anthropometrics and is completely automatic (detailed in Chapter 5).

1.5 Thesis Overview

This thesis consists of seven chapters that show the progression of the research. Due to the broad nature of this research the thesis has been structured so as to assist the reader in understanding the overall goal of this research whilst maintaining a readable flow.

- **Chapter 2: Determining the optimal 3D Scanning System for the Outer Ear**
This chapter aims to illustrate the complexity involved in 3D scanning the human ear by assessing various 3D scanning technologies and determining the optimal approach for this thesis relating to the ability to automate the process, the occlusion/holes in the data and achievable surface quality. It should be noted that accuracy is not assessed in this case due to the complexity in generating ground truth, or digitally comparable, sample, which is discussed and reasoned throughout Chapter 2 and Chapter 3
- **Chapter 3: Design of a 3D scanning System for the Human Ear**
From Chapter 2, the optimal 3D scanning approach has been selected and this chapter develops the system that will 3D scan the human ear based on a set of predefined requirements that are expected to be important for mass-customization, the reasoning for which is discussed in Chapter 2.
- **Chapter 4: Establishing the Base Variance using Statistical Shape Analysis**
This chapter is a milestone for this research as it constitutes the basis for customization that has been established. In this chapter, the methodology for generating a full 3D Statistical Shape Model (SSM) is discussed, resulting in, to our knowledge, the most detailed 3D SSM of the human ear to date.
- **Chapter 5: Deformation Guides in CAD Designs to Streamline the Automation Process**
In this chapter the methodology for adapting the automation system to various in-ear device designs is outlined. It is shown that by manually defining regions on the 3D CAD design that are deformable or rigid, it is possible to generate a range of different products completely automatically.
- **Chapter 6: Automated Customization of an In-Ear Device From 3D Scan Data**
This chapter combines the knowledge in Chapter 5 and Chapter 6 to illustrate how to use the SSM and 3D mesh based deformation to generate a completely customized in-ear device from a previously unseen 3D scan.

- Chapter 7: Discussion and Conclusions
In this chapter the mass-customization process is discussed, outlining the advantages and detailing the limitations.

Chapter 2

Determining the Optimal 3D Scanning System for the Outer Ear

From the literature review in Section 1.1, it was seen that several techniques are able to scan the ear with varying levels of quality. However, there was no definitive answer to the research question:

What is the most applicable method for 3D scanning the ear?

The purpose of this chapter is to select a 3D scanning technology that will be optimized for this research. In industry, 3D scanners have been developed that can scan the ear canal (Lantos Technologies, 2018) and all of the known research has focused on in-ear devices for the ear canal (Sickel et al., 2011; Unal, 2010; Unal et al., 2011). While this is important for in-the-canal hearing aids, it limits the system to being solely in the canal. With the variety of in-ear devices discussed in Chapter 1, it is important to be able to reconstruct the outer ear as well as the canal. Therefore, this research will focus on the 3D scanning of the outer-ear in order to develop an automated customization framework for devices that fit to the concha (see Figure 1.9). The remainder of this research will focus on methods for accurately and reliably scanning the entire outer ear region, including behind-the-ear, and the entrance to the ear canal.

A full overview of 3D scanning technologies and their applications to the human ear can be seen in Section 1.1.7. To recap, there are two areas of 3D scanning which are explored in this section, passive and active. Passive 3D scanning does not project a light source or pattern onto the target and can be categorized as either multiple view approaches, or single view approaches. Single view approaches rely on information sources such as shading, texture, and focus and are known as shape from shading, shape from texture and shape from focus respectively. Single view approaches are outside the scope of this research as they are typically not practical in terms of robustness or speed or both (Pears et al., 2012). The main focus of this research, for passive systems, is multiple view. With multiple view approaches the scene is observed from two or more viewpoints, either by a single moving camera (structure from motion) or multiple cameras stationed around the scene (multiple view stereo).

Active 3D scanning systems, on the other hand, are typically handheld systems that project a pattern onto the target and record the distortion. To capture the entire object, the systems have to be moved around the target object manually or can be synchronized to project and capture from multiple views in succession. Alternatively, the active 3D scanning unit can be mounted to a robotic arm system do which automates the capture motion and removes human error from the process (Artec3D, 2015).

2.1 Qualitative Evaluation of 3D Scanning

In this chapter, the 3D scanning equipment is to be assessed qualitatively due to the lack of a ground truth sample. This means that there is no common object by which to compare

the different 3D scanning technologies. ISO 20685-2:2015 states that, "to verify or specify the accuracy of body scanners, a calibrated test object with known form and size is used". This means that an object of known dimensions, either 2D measurements or full 3D data, is used to compare the 3D scanning equipment. For this research, the objective is to determine how the systems perform in the 3D acquisition of the human ear, particularly the complex occluded regions, not the achievable accuracy in the hardware, so a standard calibration object is not sufficient.

After much research into the issue of quantitative assessment, it was determined that for it to be applicable to this research the calibrated object should be a 3D ear. This means that a highly accurate 3D scanning method, possibly magnetic resonance imaging (MRI), would be used to digitize a 3D ear. This digital 3D model would then be 3D printed and scanned by the active and passive systems. This would give a digital means by which to assess the 3D reconstruction of both active and passive systems. However, after much consideration it was determined that the 3D printed object would require full skin texture due to the limitation of passive systems on the 3D scanning of textureless surfaces. At the time of this research, it was not feasible to 3D print in full texture and access to an MRI machine was limited. Therefore, it was determined that the assessment of the 3D scanning systems would be qualitative. This was justified based on the understanding that the 3D scanning was developed as a means for achieving customization and is not the main novelty of this research.

Quantitative assessment, where possible, is provided. For active 3D scanning systems, it is known from the specifications that the achievable accuracy is 0.1mm. Whereas for passive 3D scanning systems, the accuracy is dependent on a number of factors including the image quality, the placement of the cameras and the object being scanned. To provide a quantitative means by which to assess the passive systems, the root-mean-square reprojection error is provided which details how accurately the reconstructed 3D shape projects back to the 2D images.

2.2 3D Scanner Requirements for Mass-Customization

In this chapter, the objective is to discover the most applicable 3D scanning method for mass-customization. Applicability, for this research, is determined by the feasibility of the 3D scanning system to fit within an automation system, meaning the capture and processing of the data can be performed without expert interference. Applicability is also being determined by the quality of the captured 3D data. Quality in this chapter is not a quantitative measure due to the lack of a ground truth comparison but rather an evaluation of the captured detail and the completeness of the data.

The following are the methods for assessment of the 3D scanning techniques and for the capturing the data. Broadly, this consists of using a range of 3D scanners to scan the ear and rate the performance against a set of critical parameters that were deemed important for mass-customization. In order to correctly answer research question 1 (see Table 1.4), further exploration into each technique was required. To objectively analyse each 3D scanning technique, criteria of assessment are established here and will be used in the following section to determine the suitability of each scanning method for the human ear. These include quality and scanning criteria.

Surface quality: For this purpose, the surface quality is determined visually by the overall smoothness and similarity to the scanned object. While this is not a quantitative assessment, due to the lack of a ground truth, it provides a means of comparison.

Holes/Occlusion: Holes can be identified as regions that the scanning system was unable to reconstruct. Software is typically used to fill in these holes, however, this is undesirable

for this research as it is an approximation of the surface and may not be an accurate representation, and/or requires operator intervention. Holes in the data is linked to occlusion, in that, it was most likely not reconstructed correctly due to occlusion.

Captured detail: This is similar to surface quality, however, is more related to the ability of the 3D scanning system to reconstruct minor details with high resolution. For example, a high level of detail would be given to a system that can reconstruct the hairs on the human face. This is not critical to this research, of overall importance is the ability of the 3D scanning system to reconstruct critical details such as the inner ear region.

The scanning criteria were established based on the processes of acquiring the 3D data and not the quality. These are related to the applicability of the system to fit within a mass-customization system. They are as follows:

Scanning time: This is the time to acquire the entire region of interest. This is not including the processing time and is related to the time it takes to start and stop the acquisition process.

Ease of use: The ease of use criteria is subjective and can vary depending on the user's expertise, however, for this research the ease of use is determined as the simplicity in acquiring the data and not the use of the accompanying software as each 3D scanning system will typically have its own software package.

Processing time: The processing time is the time taken to make the 3D data usable for the purposes of this research, which includes 3D reconstruction, noise removal, cropping the region of interest, and making the result watertight, meaning there are no holes in the data.

Automatability: This is the percentage of the process that can be automated. It is known that 3D scanning involves a majority of steps including the acquisition of the data and the processing of the data into the 3D reconstruction. The ability of any of these processes to be automated is advantageous to the overall goal of this research.

Using this criteria, both passive and active systems are tested against a human ear.

2.3 Passive 3D Scanning

Structure from motion (SFM) is the simultaneous recovery of 3D structure and camera pose (position and orientation) from image correspondences typically taken from a single moving camera, but can also be applied to multiple cameras (Pears et al., 2012). There are three critical areas of SFM:

Correspondence: Which pixels between images are deemed to be the same point from different viewpoints.

Motion and reconstruction: Determination of camera motion, pose, and the reconstructed 3D position of the observed points.

Segmentation: Removal of dynamic objects in the scene or the highlighting of the region-of-interest.

The main difficulty with all passive 3D scanning systems is the correspondence problem, which is typically viewed as a search and retrieval, i.e. for a point in the reference image, where is the corresponding point in the target image. This is especially difficult when considering the human ear or to be more specific, human skin. This is due to the fact that human skin has a low texture, meaning the colour does not vary much within a given area. SFM has typically been applied to building or landscape reconstruction where there are clearly defined areas and multiple textures that are relatively simple to track. However, when considering the human ear, there are several areas of similar texture that can be difficult to track, as illustrated in Figure 2.1.

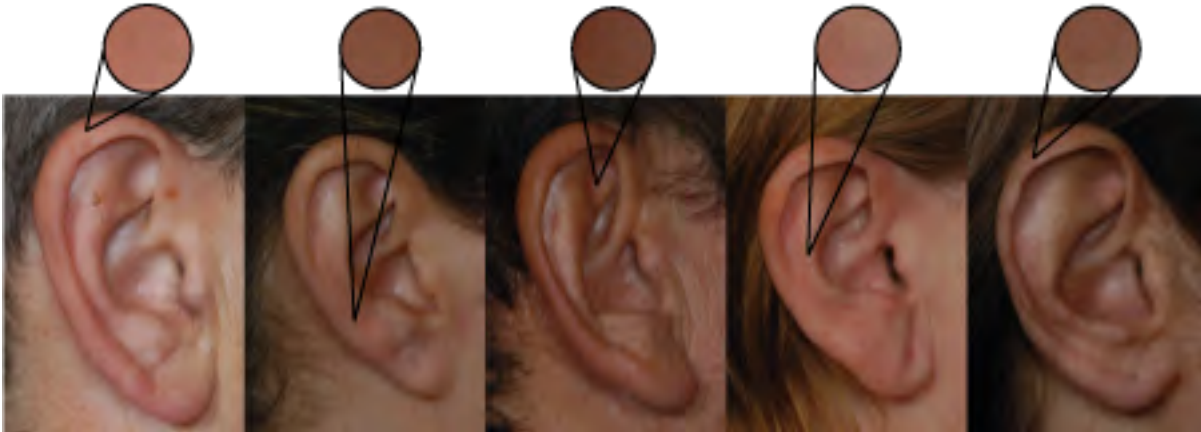


FIGURE 2.1: Variations in the shape of the human ear, and a sample of the texture taken from multiple keypoints. Each keypoint has a 4 pixel diameter that shows the similarity in texture between regions around the ear.

It is clear from the images in Figure 2.1 that the passive reconstruction of areas with low texture is difficult. However, as discussed in Section 1.1.7, the use of feature description and advanced reconstruction algorithms has successfully reconstructed the ear. For a full overview of passive 3D imaging please review Section 1.1.7.

2.3.1 Equipment and Experimental Setup for Passive Imaging

To assess the passive reconstruction method, the following equipment is used:

Camera: Canon 1200D DSLR

Ring Light: Voking LED macro ring light

Software: Agisoft PhotoScan

The Canon 1200D DSLR is an entry level camera with an 18MP APS-C CMOS sensor which equates to an image resolution of 5184×3456 pixels. The Canon 1200D is equipped with an 18-55 mm lens and an aperture range of 5.5 to 22. The 18-55 mm focal lens provides the capability to test the range of distances that the data can be taken, optimally the distance should be minimal to ease the process of acquiring the data. Agisoft Photoscan is a stand-alone software product that performs photogrammetric processing of digital images and generates 3D spatial data (Agisoft, 2006).

To capture the data, the participant is sat in a chair. 15 images are then captured to form the full viewing sphere of the participants right ear. A selection of the captured images and the position of the cameras can be seen in Figure 2.4 and Figure 2.6 respectively.

2.3.2 Critical Imaging Parameters for the Passive System

Prior to testing the passive system, the following parameters must be assessed in order to ensure that the output quality is optimal. From Section 1.1.7, the results achieved in the literature were discussed, however, the imaging parameters used were not discussed. As different combinations of imaging parameters produces highly varying results, it is important to adjust them to fit the environment and scanning object. Lighting conditions are the most crucial and the imaging parameters in Figure 2.2 must be adjusted to compensate for environmental and shooting conditions. The goal of this adjustment is to produce an image that is sharp, i.e. contains no blurring due to depth-of-field issues, and has even light distribution.

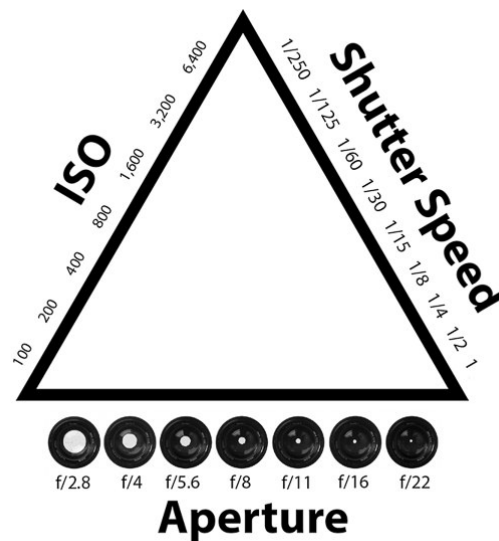


FIGURE 2.2: The exposure triangles: Changing the ISO, aperture, or shutter speed can impact the image quality (Gray, 2018).

These three parameters are known as the exposure triangle and determine how light or dark an image will appear when it's been captured by the camera. The aperture is the diameter of the hole by which all light must pass through before reaching the image sensor. The bigger the hole, the more light that reaches the sensor. Aperture is quantified as an f-stop and is a ratio that relates to the size of the opening (Gray, 2018).

The shutter speed is how long the image will be exposed for, or how long the shutter will remain open to allow light to enter (Gray, 2018). Care must be taken when the target is dynamic as a slow shutter speed will result in blurring. As the target for this research is a seated individual the shutter speed does not have to be set to the fastest which will allow for a smaller aperture to give a larger depth-of-field without losing light intensity. The final parameter is the ISO, and it controls the sensitivity of the camera's sensor to the given light. Higher values of ISO mean the sensor does not need to collect as much light to reach the desired exposure, and vice versa for a low ISO. However, care must be taken as at higher ISO values there is a significant amount of noise or grain introduced in the image (Mansurov, 2018).

The combination of these parameters creates the depth-of-field, which refers to the range of distances that appears acceptably sharp. Or, in other words, it is the farthest and nearest points which are in acceptable focus. This is crucial for passive 3D imaging as feature or intensity correspondences are key. Therefore, sections of images that appear blurred will be unreliable for matching.

All DSLR cameras available have an automatic mode which aims to select the best parameters for the scene based on some metrics, however, this can be unreliable when using multiple views as the image parameters may not be the same across all images. For this research, the image parameters are set manually through iterative assessment of the image quality. This means that a captured image is assessed based on whether the target area is sharp and has a sufficient depth-of-field and that there are no shadows present. For the acquisition of the images in this chapter, the imaging parameters were selected as; an ISO of 1600, an aperture of 8, a shutter speed of 1/200, and a focal length of 47.

2.3.2.1 Removing of Shadows

A disadvantage of passive 3D scanning systems is its sensitivity to environmental conditions. As discussed in Section 1.1.7, passive 3D scanning systems rely on correspondences between consecutive frames of the same object. Therefore, changes in lighting or colour can affect the overall reconstruction. In particular, if shadows are present on the target object they will be reconstructed as flat surfaces. To improve the overall reconstruction process for passive systems the environment must be controlled. To accomplish this, lighting equipment is used to illuminate the scene. Particularly, a 135W lightbox was placed near the target to ensure that there was sufficient diffuse lighting for the scene.

To ensure that there were no shadows in the view of the camera an 18 LED ring-light was used. A ring-light is a piece of equipment that is placed around the front of the camera lens and illuminates the scene. The effectiveness of the ring-light is in reducing the shadows in the field of view of the camera. Figure 2.3 shows examples of the image quality under the different lighting conditions.



FIGURE 2.3: Variations in image quality as a result of environmental changes with the introduction of a lightbox and a ring light

From the images in Figure 2.3, it can be seen that by using appropriate lighting equipment, a uniform and shadow free environment was created for passive 3D scanning. When a small aperture is used with the camera it limits the amount of light that can enter but also increases the depth-of-field. Therefore, significant external lighting is required to ensure adequate image quality. In Figure 2.3 (a), it can be seen that at an aperture of 8, an ISO of 1600 and a focal distance of 47 mm the light is not sufficient to capture the image. It should be noted that these images were taken in a room with overhead fluorescent lighting and no external ambient lights. Figure 2.3 (b), introduced a lightbox to the side of the camera to create sufficient diffuse lighting. However, due to the angle of the lighting relative to the camera, a shadow was formed in the inner-ear region. Figure 2.3 (c) shows the scene with a lightbox and a ring-light.

As can be seen, there are no visible shadows in the scene relative to the camera viewpoint. As the ring-light is mounted on the front of the camera lens, all objects in the field-of-view of the camera are practically free from shadow, which is an ideal scenario for passive 3D scanning. However, care must be taken to not over-saturate the scene.

2.4 Active 3D Scanning Systems

Active 3D scanning, contrary to passive, projects a light source onto the target and measures the deformation. Both active and passive 3D scanning systems are based on the same principle, intersecting light rays in 3D space. However, active systems typically replace one camera of a passive system with a projection device, which can be a digital video projector or a laser.

From Section 1.1.7, it was discussed that laser systems have been primarily used for the reconstruction of ears. It was determined that due to the relatively slow nature of the systems and quality of the results seen in the literature, that area based 3D scanners would be tested for the ear. Specifically, two variations of area-based 3D scanners are used to determine the validity of active approaches for the human ear.

Structured Light 3D Scanner: Creafom Go!Scan G1 (Creafom, 2012)

Structured Light 3D Scanner: Artec Eva (Artec, 2012)

The Creafom Go!Scan is a white light (LED) 3D scanner that can capture with a resolution of 0.5 mm and an accuracy up to 0.1 mm. The Artec EVA, on the other hand, has the same resolution and accuracy, but also has a working distance between 0.4-1.0 m with a field of view of 214×148 mm at its closest range. Contrary to the Creafom, the Artec EVA uses a flash bulb as opposed to an LED for its structured light source.

2.4.1 Experimental Setup for Active 3D Scanning

Similar to the process in Section 2.3.1, the participant is sat in a chair and the active systems are manually moved around the participant's ear until the desired region is covered. One of the advantages of the active systems is the continuous feedback during the scanning process, this gives the user an understanding of the acquired surface. Compared to the passive system, it is not known until the data is processed whether enough images have been taken.

2.5 3D Scanning Results

By performing the process discussed in the previous section, the following results were obtained.

2.5.1 Structure From Motion

To acquire the images the Canon 1200D was used to capture 15 images of a participant's ear. As this is only to test the viability of the SFM process the resolution of the images is not of critical concern. To capture the images, the camera was placed at 15 different positions to around the participants right ear. The sequence to capture the images took approximately 1 minute, however, it should be noted that should 15 cameras be used simultaneously then the capture would be instant.



FIGURE 2.4: Sample images from the structure from motion process. Showing 4 out of 15 images.

Agisoft PhotoScan Pro was used to process the images into a 3D reconstruction. The result of this process can be seen in Figure 2.5 and Figure 2.6. Figure 2.5 shows the recovered camera positions from the SFM process.

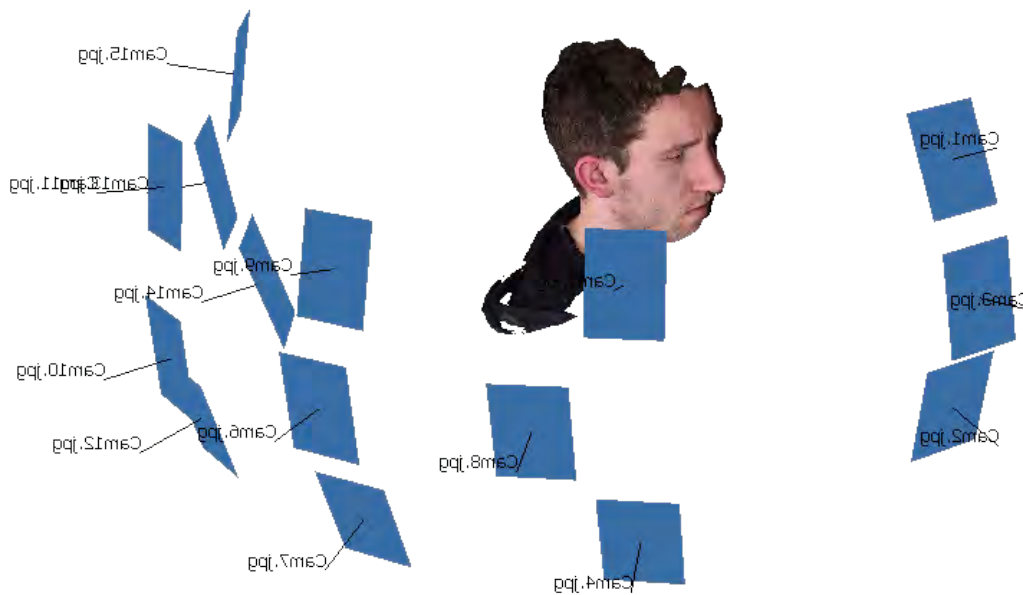


FIGURE 2.5: Camera positions recovered from Agisoft PhotoScan Pro using the captured 15 images. The blue plane is representative of the position and angle of the camera.

As can be seen in Figure 2.5, the camera positions cover the majority of the viewing angles for the participants ear. It is possible to gain even more detail in the images through the addition of more viewing angles, however, this proves sufficient to illustrate the applicability of SFM to the reconstruction of the human ear.

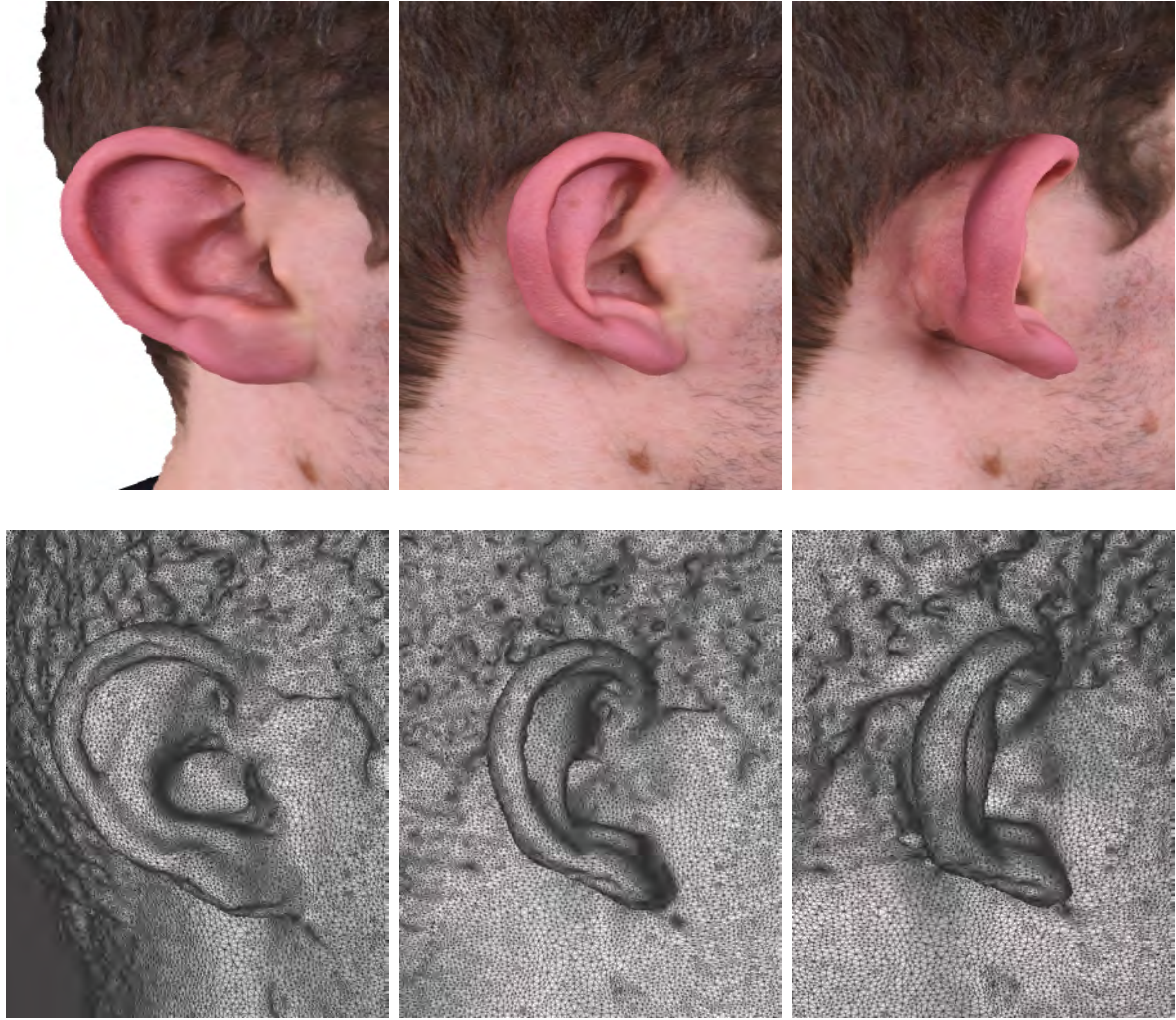


FIGURE 2.6: Result from SFM reconstruction. The process has produced the overall shape, however, there is a lack of detail in the result.

The 3D reconstruction process took approximately 11 minutes. This includes matching points between images (1 minute 44 seconds), aligning the cameras (7 seconds), dense reconstruction (3 minutes 20 seconds), mesh generation (3 minutes 32 seconds) and texture generation (1 minute 57 seconds). It should be noted that texture generation is optional and not a requirement for the proposed customization approach. The overall output quality is a watertight mesh consisting of 524,452 faces and 264,259 vertices. The root-mean-square (RMS) reprojection error is 1.4 pixels.

2.5.2 Artec EVA

To capture the participant's ear the system was held at the optimum distance, as determined through software feedback which is between 400-600mm. The system was then gradually moved around the participant's ear, capturing different angles to try to minimize the occlusion. It should be noted that it is difficult to maintain a similar scanning path between consecutive 3D scans due to human error.

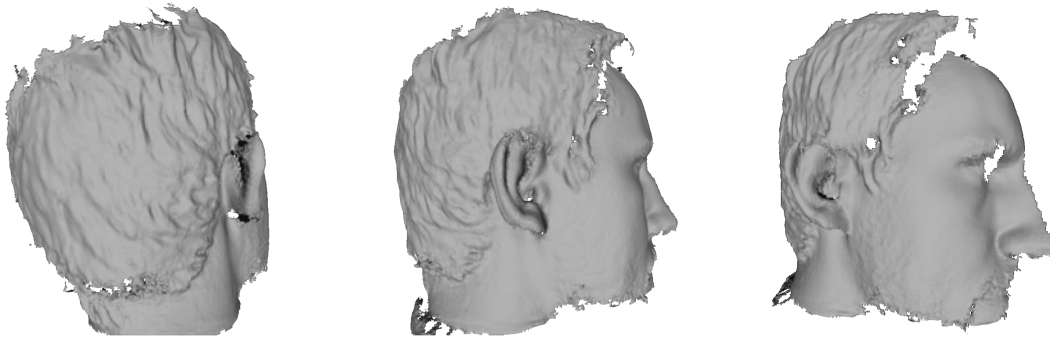


FIGURE 2.7: Ear reconstruction from the Artec EVA, showing three views of the output mesh

From the Figure 2.7, it can be seen that the surface quality is excellent, however, there is a substantial amount of occlusion and holes in the data that would need to be repaired manually. The output mesh had a density of 194639 faces, however, this is not an accurate measure of quality. The scanning process took approximately 10 seconds and the output seen in Figure 2.7 did not require any extra process as the system was able to reconstruct the mesh in real-time. Of particular interest to this research is the inner ear region, which the Artec EVA was unable to scan, therefore, limiting its application to this research (see Figure 2.8).

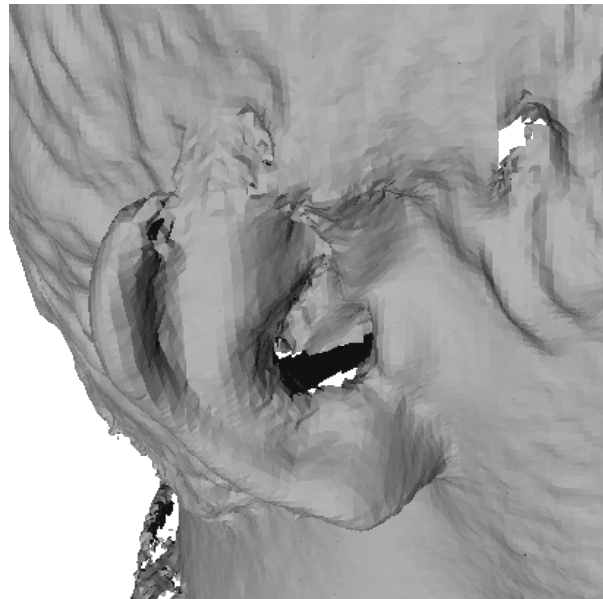


FIGURE 2.8: The inner ear region as captured by the Artec EVA

It should be noted that it may be possible to acquire this region if the Artec EVA is positioned at a certain angle. However, in terms of automation, it is difficult to constrain this process to ensure that the inner-ear region is consistently scanned. The robotic method by Artec3D (2015) would potentially be a solution to this problem, however, the cost is substantial.

2.5.3 Go!Scan

To fully test the structured light approach, the Creaform Go!Scan G1 was tested which follows the same principle as the Artec EVA. Contrary to the Artec EVA, the Creaform Go!Scan G1 requires a calibration procedure to be performed when the system has been left idle or powered off. To calibrate this system, a checkerboard pattern was captured at different distances and angles. The resultant 3D scan can be seen in Figure 2.9



FIGURE 2.9: 3D scanning result from the Creaform Go!Scan, the desired area is marked in black.

Tracking was a serious issue using the Go!Scan as several attempts were required to obtain the data. This could be a limitation of the system as it has a part size range from 50mm to 500mm and a scanning area of 143x108mm, which the ear is just below.

2.6 Discussion

This initial exploration clearly identified the advantages and disadvantages of the two techniques. The overall results can be seen in Table 2.1 and the reasoning behind the marking is discussed in the following sections.

TABLE 2.1: Comparison of 3D scanning technologies relative to the established criteria. Each criteria is weighted with relevance to this research. Weights are from 1-3 and the score is from 1-5 where 1 is a low score and 5 is the highest score.

	Quality Criteria			Scanning Criteria				Totals
	Surface Quality	Holes/Occlusion	Captured Detail	Scanning Time	Ease of Use	Processing Time	Automate-ability	
Weights	2	2	1	3	2	1	3	
Passive SFM	3	5	4	5	5	2	4	59
Active Artec EVA	5	3	4	5	5	4	2	55
Active Creaform Go!Scan	5	1	2	5	5	4	2	49

The criteria are weighted as they do not have the same relevance to this research. The weights are in the range 1-3, where 1 is normal and 3 is extremely important. Time to scan and automate-ability were given a weighting of 3. This was deemed acceptable as the process must be fast enough to deal with the dynamic nature of the human body. The automate-ability is also critical to this research and was deemed important to the success of the overall goal.

Ease of use, holes/occlusion, and surface quality were given a weighting of 2. As the scanning process must be used to scan hundreds to thousands of individuals it was deemed important that the process be simple. Holes/occlusion is important to this research as the resultant data must be usable and of sufficient quality for customization and automation. The processing time and capture-able detail were deemed to have normal importance. The processing time was given a weighting of 1 as it is not of critical importance. As the processing of 3D scan data is highly computational intensive, reduction in processing time can be achieved through high-end processors or even cloud computing. Captured detail was also given a weighting of 1 as it is not critical to the end goal of this research, captured detail is referring to the resolution obtained, for example, reconstructing the hairs on the individual's face. Of higher importance is the surface quality and not the capture-able detail.

The individual processes are then rated from 1-5, where 1 equates to a poor performance in that area and vice versa for the higher values. The following section will now discuss each scanning technique against the criteria of assessment in order to justify the marking in Table 2.1.

2.6.1 Structure From Motion (SFM)

The SFM approach successfully output a 3D reconstruction of the participants ear. With regards to the criteria of assessment, the goal is to assess this process against the surface quality, holes/occlusion, and captured detail.

2.6.1.0.1 Surface Quality: The surface quality from the SFM process is average. Surface quality, for this research, is a subjective measure which is defined as the similarity to the target object and perceived noise level in the data. It is possible to test the surface quality on a quantitative level by using a ground truth comparison which is scanned and then compared digitally. However, this was not possible for this research due to limitations in available objects. Analysing the result in Figure 2.6, the surface is rough in certain areas and not consistent with the target surface. This can be said to be a limitation of the passive 3D reconstruction algorithms. However, the data taken was not completely optimized and was merely a test of the process.

2.6.1.0.2 Holes/occlusion: There are no visible holes in the output, however, there is a relatively high level of noise particularly in the inner ear region. This could be due to partial

occlusion from a lack of images in that particular region or a combination of the imaging parameters. By increasing the resolution of the images the inner ear region it is more likely to be reconstructed due to the increase in available information. One of the advantages of SFM is the ability to add or remove images as necessary, making the system highly modular.

2.6.1.0.3 Captured detail: The captured detail is a measure of the accuracy to the target surface, i.e. the visibility of a hair in the reconstructed mesh. For the SFM approach, the level of detail was deemed medium with the system able to reconstruct the complex external ear region with the majority of noise only in the internal ear. Of important to this research is that the captured object be occlusion free, and from the results in Figure 2.6 it can be said that the multiple view approach of SFM presents a potential solution to this problem.

Overall, it can be seen that for the quality criteria the SFM has delivered average performance. It should be noted, however, that this was a simple test of the process without optimization of the imaging parameters and manual motion of the camera. By optimizing the imaging parameters and acquisition process the overall reconstruction should improve. For the scanning criteria it is also necessary to assess the process based on time to scan, ease of use, processing time, and automatability.

2.6.1.0.4 Scanning time: The system was relatively efficient in capturing the data, taking approximately 1 minute to capture the full ear. However, manually moving the camera can affect the repeatability and quality of the images due to human error in the positioning and motion of the camera. The advantage of SFM with regards to the scanning time is the expandability of the systems without affecting the overall scanning. Adding a second camera would not increase the scanning time, and by using multiple stationary cameras the scanning time could be effectively instantaneous.

2.6.1.0.5 Ease of use: The ease of use parameter, to reiterate, is not a function of the use of the software but capturing of the data. The SFM process therefore has a very high ease of use, using standard cameras that the majority of users would be experienced with. However, while the use of the camera itself is simple, the knowledge required to set up the imaging parameters can dramatically affect the overall scanning quality and creates a difficulty with using the approach in different environments. If the system is moved from one environment to another it may be necessary to reconfigure the imaging parameters.

2.6.1.0.6 Processing time: The processing time was slow compared to the real-time active systems with the results in Figure 2.6 taking approximately 11 minutes to fully process. While this time is significant it should be noted that this is dependent on the computing power available, and can be reduced depending on the number of images required for processing. The SFM approach must calculate matching features between images, on average the technique calculates from 20,000 to 100,000 features per image and aims to match them with the images deemed acceptably similar. Therefore, for each image there is a significant amount of processing required to generate the camera positions and alignment. After the process the dense reconstruction is calculated which takes the output from the previous process and outputs a high resolution reconstruction. This is a pairwise process which calculates a depth-map for each image pair deemed matching. The combination of these approaches is the main computationally intensive resource and is not easily overcome. However, with advances in processing algorithms and the use of cloud computing it is possible to do these high intensity calculations relatively easily.

2.6.1.0.7 Automatability: The automatability parameter is strictly relevant to this research. The aim of this research is to automate the process of customizing in-ear devices. Therefore, it is desirable that the scanning process also be automated. The SFM process is applicable to automation, meaning that the acquisition and processing can be performed using algorithms. The SFM software provides an interface for plugins that can be used to automate the processing of the images and outputting the mesh. With the steps for processing the raw images into a 3D model remaining the same it allows for simple scripting to perform the same operation for new data. This is dependent on the consistency in the process and the variation in image quality that may be seen.

Overall, the SFM process scored very well across the criteria of assessment and the resultant 3D mesh seen in Figure 2.6 is comparable in quality to that of a high-end active 3D scanning system seen in Figure 2.7 which illustrates the power of passive approaches given that the reconstruction was performed with a single camera. The main concern remaining with SFM is its application to scanning different textures relating to variations in skin tone. From the known published literature in Section 1.1.7 there are no references to the 3D scanning of different textured skin using passive 3D scanning and is therefore a remaining area of research required, which will be assessed in Chapter 2. Given that the algorithms successfully output a 3D reconstruction of the ear, it is now viable to invest time into fully optimizing the system.

2.6.2 Structured Light 3D Scanner

Similar to the SFM process, the active 3D scanning systems were assessed against the same criteria.

2.6.2.0.1 Surface Quality: For active systems it was seen that the surface quality was very high and representative of the target shape. As the system projects a pattern on the surface it can be said to record the true shape, whereas, the passive 3D scanning systems approximate the shape by matching features between frames. The active systems therefore scored the highest in terms of surface quality.

2.6.2.0.2 Holes/occlusion: Both active 3D scanning systems had consistent holes in the inner ear region, which is not desirable as the inner ear region is the main interest of this research. It should be noted that only a single pass was performed to capture the data. It can be said that if the system was at a specific angle it may have been able to capture the inner-ear data. However, it seems likely that the inner-ear may span a range of sizes and positions that is not possible for the majority of active 3D scanning systems to capture due to the projection angle. As active 3D scanning systems are continually improving, this limitation may be overcome in the near future. However, the issue stands for the systems that were tested.

2.6.2.0.3 Captured detail: The active systems captured the highest detail out of the 3D scanning approaches which was anticipated due to the projection of a pattern onto the target surface.

Overall, the active systems scored very high on the quality criteria. However, their inability to scan the inner-ear region limits their applicability to this research. It should be noted, however, that if the projection and camera of the active 3D scanning systems was specifically designed to be applicable to the inner-ear region, then the output quality would be very high. In terms of processing criteria, the active systems must be assessed on time to scan, ease of use, processing time, and automatability.

2.6.2.0.4 Scanning time: The active 3D scanning systems were able to scan the data at a much faster rate than the SFM approach, taking approximately 8 to 10 seconds. It should be noted that one pass of each technique was performed, and the time is dependent on the expertise of the user. In practice, the active 3D scanning systems typically require multiple passes or a highly experienced user to fully reconstruct the area.

2.6.2.0.5 Ease of use: Similar to the SFM approach, the active systems are rated on the ease of use of acquiring the data not use of the software. The acquisition process for both active systems involved the pressing of a button to start the process and pressing the button again to stop the process. However, contrary to the SFM approach, the active systems reconstruct the data in real-time. To do this, the systems must track the 3D position of the target which can be subject to loss of tracking depending on the complexity of the surface and the expertise of the user.

This was a severe issue with the Creaform Go!Scan which required multiple trials in order to output a successful pass. This was not an issue with the Artec EVA, and can therefore be said to be a function of the reconstruction algorithms and not the scanning process. The loss of tracking hinders the ease of use of the system and the necessity to redo the scanning process is undesirable for this research.

2.6.2.0.6 Processing time: As discussed previously the active systems were able to reconstruct the data in real-time. The output of this process can be seen in Figure 2.7 and Figure 2.9. By their nature, active systems reconstruct the entire field of view, therefore there will always be unwanted or redundant data in the scan that must be removed. Contrary to the SFM process, there is no process to automate this. To take the reconstructed data and output a usable mesh the result must be manually segmented, which depending on the software or experience level of the user, it can take 5-10 minutes. Automated approaches could be constructed based on the principle of detecting keypoints on the surface and using them to guide the segmentation, however, this would introduce unwanted complexity in the process.

2.6.2.0.7 Automatability: The active 3D scanning systems that were tested are handheld 3D scanning systems that rely on manual motion to capture the desired data. It is possible to automate the motion process using robotics (Artec3D, 2015), however, the cost of the robotics may outweigh the advantage of the automation. Similar to SFM, it is possible to place multiple active systems around the target object. However, the systems must be synchronized to capture the data successively as the simultaneous projection would cause destructive interference. With the cost of active systems being in the range of \$15,000-30,000, multiplicity of the systems is a considerable cost. Another limit of the active approach is the difficulty in automating the processing of the data. The automatability for active 3D scanning systems is therefore low.

Overall, the active 3D scanning systems performed very well and achieved a very high surface quality, however, both systems suffered from holes, particularly in the inner-ear region. The output data consisted of 200,000 faces, which is a very dense 3D mesh. However, much of the detail is outside the region of interest and therefore limits the applicability of the systems to this research.

2.6.3 Comparison of scanning technologies

To compare the 3D scanning technologies it is important to reiterate the purpose of this research, which is, to automate the manufacturing process of custom fit products. To fully accomplish this, the 3D scanning process must also be automatable. While not a direct goal of

this research, it is important to the overall concept that the process be free from a need for expert users.

From the initial experimentation in Figure 2.6, it was seen that the passive system had an average surface quality with considerable noise in some areas and a comparably high processing time. However, the process can be highly automated and can be said to be future proof. This means that the systems can be easily and cost effectively adapted to future improvements. With new cameras the overall quality will be improved. Also, improvements in algorithms can be directly applied to the process. The passive nature of the system allows for modularity in the capture of the data, making it possible to use a single moving camera or multiple stationary cameras positioned around the subject. The active 3D scanning systems, on the other hand, exhibited very good surface quality, highly representative of the target shape, and had a very low processing time with the data being reconstructed in real-time. The remaining processing involved simple, but time-consuming, segmentation of the region-of-interest.

From the results in Table 2.1, it can be seen that SFM was awarded the highest overall score, achieving its highest marks in automatability, scanning time, and holes/occlusion. The active approaches, on the other hand, scored their highest marks in surface quality, captured detail, scanning time, and ease of use. Comparatively, SFM was given a higher value in holes/occlusion due to its ability to reconstruct the data from as little as two image frames. This allows for occluded areas to be more easily accessed. Active systems, on the other hand, have to project a pattern at a certain angle which restricts the areas that can be scanned as the projector and camera are rigid and therefore can only reconstruct areas that simultaneously fall within the view of both the camera and the projector. SFM also scored higher in automatability due to its ability to automate the processing of the data, which is highly applicable to the end goal of this research. The active systems were not able to be automated unless automatic segmentation algorithms were developed, which was deemed outside the scope of this research. The active systems scored higher in surface quality as they achieved a very good approximation of the surface. However, by optimizing the SFM process the surface quality could potentially be comparable to the active systems. Optimization in this sense, is the use of higher resolution images and controlling the overlap between consecutive images so the entire ear region can be scanned without occlusion. Therefore, the following chapter describes the development of a custom 3D scanning system based on the principles of SFM.

2.6.4 Further Research

The testing and evaluation described in this chapter have given an understanding of the applicability of active and passive systems to the 3D scanning of the human ear. However, during this processes several issues were discovered that need to be further assessed in the following chapter. These difficulties include, dealing with human hair, variations in skin colour, and controlling motion, data capture and data processing.

Dealing with human hair: From this testing process it was discovered that 3D scanning has a particular challenge with human hair. To understand this problem it should be noted that human hair is not only on the outer surface but also present in the ear-canal, particularly with older people. External hair, such as from the scalp, can be removed from the scanning process using a simple hair net, however, for hair in the inner-ear this is a much more difficult problem. It is not possible to mask this hair in the data and if it remains in the scanning process it may resolve itself as bumps or sharp regions in the inner-ear, which is a problem for the application to this research.

Variations in skin colour: In the above testing a caucasian skin color was used due to the availability. However, in the literature in Section 1.1, there has been no discussion of the performance with people of darker complexion. It is known that active systems have

difficulty in reconstructing regions of black colour, due to the absorption of the projected light. There has also been no known published research on using passive systems for varying skin tones. Therefore, this must be tested in the following chapter.

Controlling motion, capture, and processing: From the testing it was determined that the SFM method was most promising for further exploration. This decision was based largely on the grounds of the modularity and automation capabilities of the system. The following chapter will explore how to control the motion, capture and processing of the SFM system.

2.7 Conclusion

The aim of this chapter was to assess 3D scanning techniques against a set of criteria in order to answer the research question:

What is the most applicable method for 3D scanning the ear?

It was seen that both active and passive 3D scanning system were successful in reconstructing part of the human ear with advantages and disadvantages. The passive 3D scanning system reconstructed the overall shape but lacked detail in some key areas. Whereas, the active 3D scanning system was not able to scan the inner-ear region but the remainder was in very high quality. By analyzing each technique with the established criteria it was seen that the passive 3D scanning was deemed more applicable to the overall goal of this research. However, there are still several areas in the SFM process that must be improved in order to fully answer the above research question, including improved surface quality, processing time, and data capture. The remaining improvements will be addressed in the following chapter and the resultant data will be shown to fully answer the above research question.

Chapter 3

Development of a 3D Scanning system for the Ear

In the previous chapter it was seen that SFM was the most appropriate 3D scanning system for the human ear due to its flexibility in capturing the data, lack of occlusion, and ability to be automated. However, the result seen in Figure 2.6 is not sufficient for this research, but requires optimization of the imaging parameters and the acquisition process. This chapter illustrates the design, prototyping, and testing of an improved 3D scanning system following the passive SFM approach.

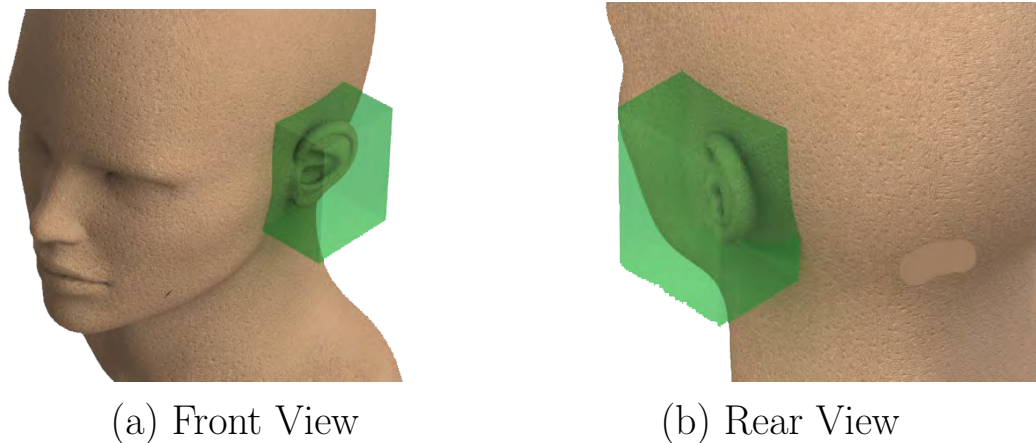
3.1 Requirements for the 3D Scanning System

It was outlined previously that to be applicable to this research the 3D scanning process must be consistent, fast, and automated. With the overall goal of this research being to automate the process of manufacturing custom-fit products, removing the need for a trained expert is essential. A fast scan time was deemed necessary due to the dynamic nature of the human body. However, to our knowledge there has not been a quantitative limit proposed in the literature and therefore it will be set to a maximum of 10 seconds per scan. This should be sufficient to gather the necessary data while also limiting the motion artefacts in the results. Automation is the key requirement here; with the goal being overall automation of the customization process it is beneficial that the scanning process be highly automated. It should be noted that the scanning system is being developed as a means to automate the customization of in-ear devices and is not the main novelty of this research. Due to the inability of available 3D scanning systems to reconstruct the human ear (see Chapter 2, a custom system is required. The following section discusses the proposed system design that aims to achieve these requirements and is split between the design of the motion system, the electronics, and the calibration respectively.

3.2 Motion Design for the 3D Scanning System

To begin the design of the system it is necessary to reiterate the overall scanning requirements, i.e. what is it that we want to achieve with the custom build 3D scanner. To be applicable to this research, it is necessary to scan the ear in full, meaning behind-the-ear and the inner-ear region. Therefore the 3D scanning system must be capable of viewing and reconstructing the full ear, the required viewing area is highlighted in Figure 3.1.

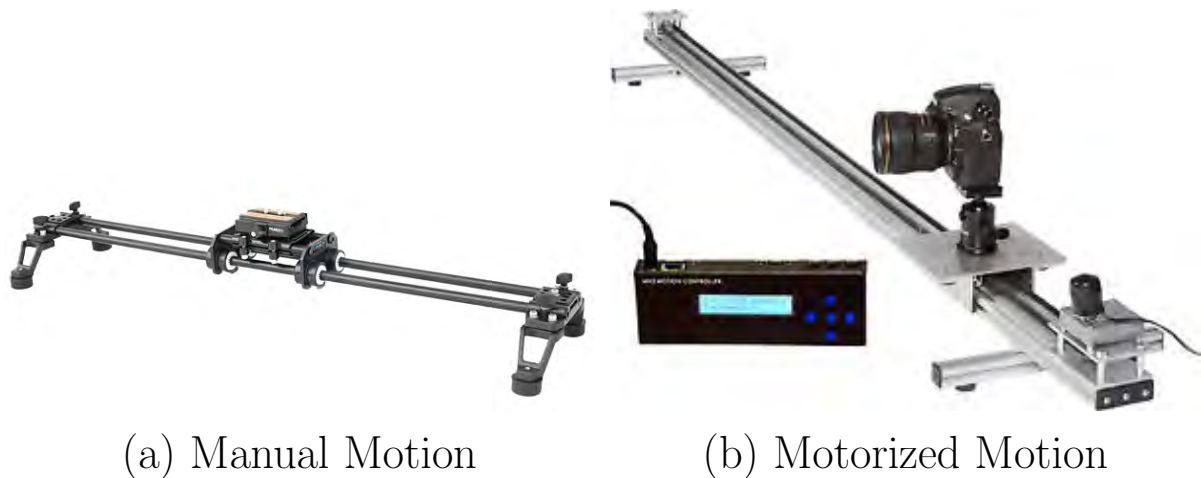
FIGURE 3.1: Capture Area: The target within the green area is the focus for this research and requires segmentation from the full result.



In Chapter 2 the capture of the data was manual, meaning that the user moved the camera to a start position, controlled the motion during the capture, and then triggered the end. This process, while simple, cannot be deemed repeatable as variations in the start and end point will create more or less data. Also, during the capturing process it was observed that consistently moving a camera from one point to another is not a simple task for a human, there will always be variations in the captured data, whether this is due to human error in camera positions or variations in the path of motion. Therefore to establish repeatability in the scanning process it is required to control the motion and the capturing of the data using electro-mechanical systems. By controlling the motion and capture parameters it also allows the user to control the speed, however, there will be a limit to what can be accomplished as a faster scan time will lead to less data due to the limited frame-rate of standard DSLR cameras.

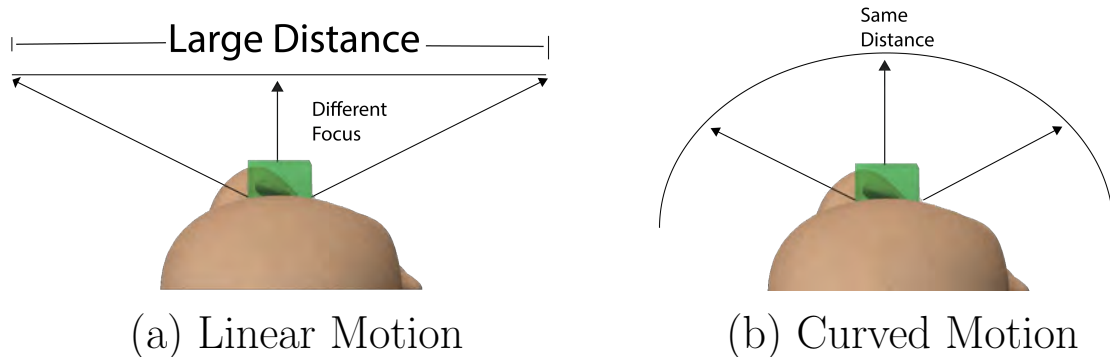
It has been determined that to automate the scanning process, the motion and capture must be controlled. One could do this by mounting a camera onto a robot arm and constructing a virtual path, however, the cost of the robot arm limits its applicability to low-cost manufacturing. In photography there is a piece of equipment known as camera dolly (see CameraGrip (2017) for examples), which is used to provide a smooth motion for capturing time-lapse images or videos. This is achieved through the use of smooth rails rails which the DSLR camera is mounted on, and the motion is provided manually or electro-mechanically. A manual system can be seen in Figure 3.2 (a) and motorized system in Figure 3.2.

FIGURE 3.2: Camera Dolly: Used to provide smooth and controlled motion to a mounted camera.



Linearity in the motion is not desirable, as per Figure 3.1, it is required to capture the region behind the ear. If this were accomplished using only linear motion the distance would be so large that the target may move out of focus, as illustrated in Figure 3.3 (a). In order to keep the image consistently sharp, the camera should remain at a constant distance from the target. To achieve this the camera rail should be curved, as seen in Figure 3.3 (b).

FIGURE 3.3: Showing the different focus caused by linear motion. Due to the distance of the cameras this would cause blurring



By using a curved rail it constrains the motion to a set path which is ideal for instilling repeatability in the process and also for maintaining consistency in the results.

3.2.1 Rail design for the motion constraint

With this concept in mind it is now necessary to design and manufacture a curved rail. To achieve this the concept was designed in 3D CAD software and manufactured using 3D printers. It should be noted that, to the best of our knowledge, there are currently no available motorized curved camera dollies. The few curved systems available are purely manual and typically very expensive, an example of which can be seen in Figure 3.4 .

FIGURE 3.4: Curved camera dolly: Manufactured from aluminium and typically manual.



The rail consists of a curved track to guide the cameras, a platform on which to mount the cameras, and wheel bearings that will provide the smooth motion of the platform along the track. Wheel bearings are standard components, therefore, the platform and rail were designed around 18 mm radial wheel that are 5 mm thick. The necessity for controlled motion created a difficulty when designing the curved camera dolly. The majority of available linear motorized camera dollies use a belt driven system where a motor is placed on the platform or at the start point and the platform is moved using the belt drive, as seen in Figure 3.2 (b).

The design used in this research aimed to adapt the curved system in Figure 3.4 with the motorized system in Figure 3.2 (b). To transmit the motion to the platform it is proposed to place a motor on the platform, behind the camera system, and to secure the pulley on each end of the rail. Contrary to Figure 3.2 (b), it is not possible to mount the motor at the end of the system as the curvature would cause the belt to interfere with the platform. By mounting the motor on the platform it increases the overall weight but also allows for a higher weight to be pulled. The rail in Figure 3.5 is the conceptualization of this process.

FIGURE 3.5: Curved rail concept: Similar concept to the mechanical curved rail but has components for adapting motorized control.

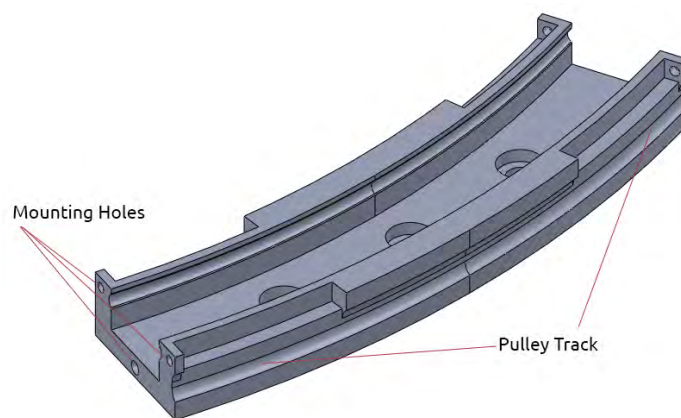


The radius of the rail is 150mm, this was chosen due to the minimum focal distance of the cameras, this distance could be reduced by using macro lenses , however, it is sufficient for the

purpose of this research. The total arc length of the rail amounts to 540mm. Manufacturing of the rail posed a difficulty due to the overall size and curvature. It was not possible to use standard manufacturing methods to create this rail as it would cause a significant amount of waste material and therefore be highly expensive. In order to manufacture the rail, the use of 3D printing technology is ideal. However, due to the limited size of available 3D printing machines, it was decided to split the rail into several parts and then assemble them afterwards.

To split the rail, the arc was divided into 4 evenly spaced sections and mounting holes on both sides and underneath were added. Each section was then 3D printed using PLA plastic, which was chosen due to the ease of printing and the overall size of the parts. In future work, it would be more beneficial to print in ABS or Nylon due to their enhanced mechanical properties.

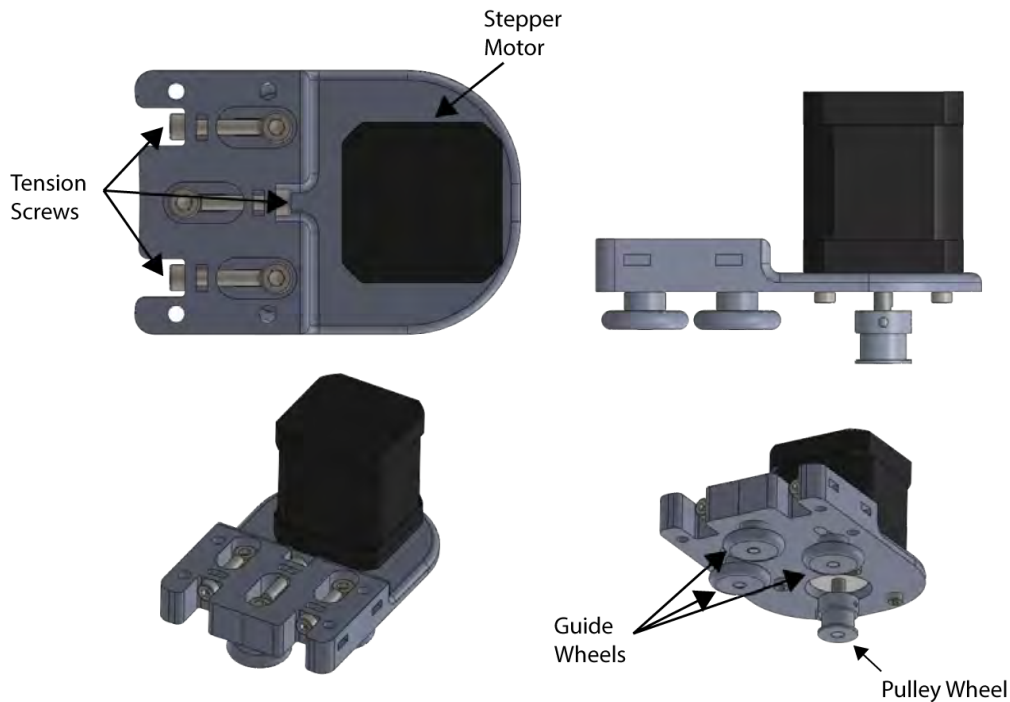
FIGURE 3.6: To manufacture the curved rail, it is split into 4 sections for 3D printing on a 200x200x200 mm volume 3D printer.



To join the rails, three mounting holes were added on each side; one on the bottom and one on each side. This was to ensure rigidity and strength as the weight of the camera system could cause the joints to break. It can be seen, in Figure 3.6 that there is a curved section at the back of the rail, this has been designed to account for the pulley. There are also box sections cut out behind each mounting hole to allow for a screwdriver or allen key to be used.

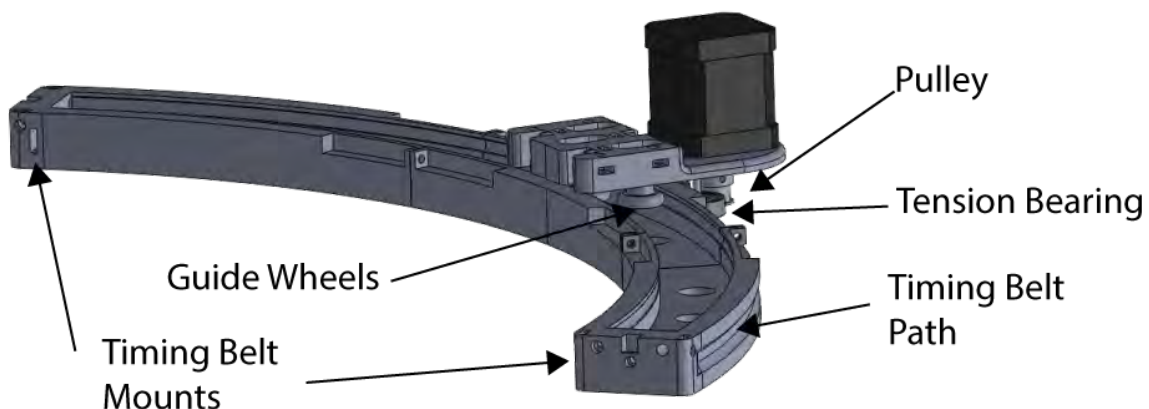
With the rail designed it was then necessary to design the platform on which to mount the camera system and the wheel bearings. To ensure that the platform follows the curvature of the rail, a three wheel system was used, as seen in Figure 3.7. To account for the wheel bearings there are three slots which allow for varying levels of tension to be achieved. There are four holes on the sides that will accommodate the camera mounts and the rear of the system is where the motor will be mounted.

FIGURE 3.7: Assembled platform: Showing the mounted wheel bearings and the stepper motor on the rear of the platform



To transmit the motion, a Nema17 stepper motor is used, as illustrated in Figure 3.7. A GT2 timing belt is used in conjunction with the Nema17 pulley and is mounted on each end of the rail and placed around the pulley wheel, as annotated in Figure 3.7.

FIGURE 3.8: Assembled rail: Showing the rail and the intended positioning of the platform. The three wheel bearings slot into the curved section on the rail and are constrained there. The belt drive mounts on each end and any rotatory motion of the pulley wheel is transferred to the timing belt.



The final design consists of the guide rail that has sections on each end to mount the pulley, the platform holds the motor and has three wheel bearings positioned inside the rail for smooth motion and two bearings outside the rail to provide tension to the timing belt. The

design was then printed using an Ultimaker 3D printer in PLA plastic for testing. One of the advantages of the sectioned method is the ability to extend the path as needed, by 3D printing an extra section, the path can be extended simply by mounting the new section and extending the timing belt length. The original design incorporated three sections, however, during testing it was determined that a fourth was required to fully cover the region of interest. The remaining components incorporate the electronics and will be discussed in the following sections.

3.3 Electronics Design for the 3D Scanning System

The previous section outlined the mechanical system that will constrain and provide smooth motion to the camera platform. The following section shows the electronic components that are required in order to transmit and control the motion, and to trigger the camera imaging.

3.3.1 Controlling motion

As discussed previously, the motion is generated through a Nema17 stepper motor that is mounted on the camera platform, the motion is then transmitted using a belt drive mounted on each end of the rail.

However, it is now required to control the stepper motor. To do this an Arduino Mega with a RAMPS controller was used. An Arduino is a programmable micro-controller unit that can be used to perform a multitude of tasks, while the RAMPS controller is an extension of the Arduino specifically designed to control stepper motors.

A stepper motor is controlled by providing a set of functions that tell the motor how many steps to take and in what direction. To do this a driver is required, which can be seen in Figure 3.9.

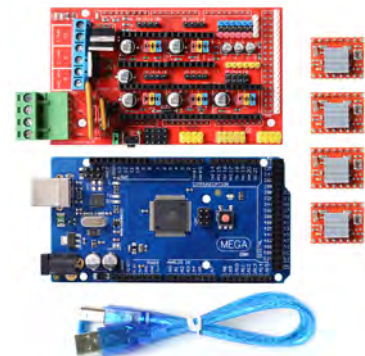


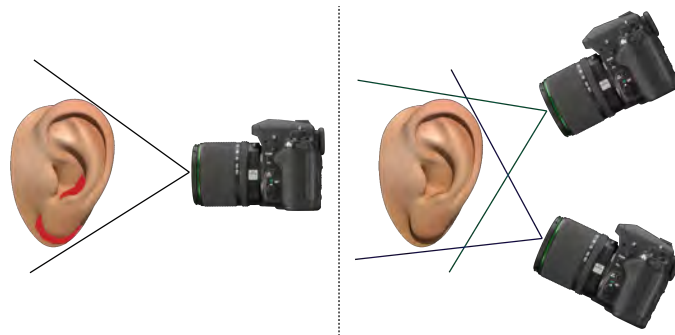
FIGURE 3.9: Arduino and RAMPS controller: Used to program stepper motors and digital inputs and outputs

3.3.2 Number of cameras

For the experiment in Chapter 2 a single moving camera was used. However, there are no limits on the number of cameras that can be used in a passive 3D scanning setup. The system can be setup to use a single moving camera or to have multiple cameras stationary around the object. Of critical importance is to cover areas of occlusion, meaning areas that are not visible from a single viewpoint. If part of the region is not visible to the camera then there is no possibility for it to be accurately reconstructed.

From the result in Chapter 2 (Figure 2.6), the inner-ear region lacked detail, which was attributed to occlusion experienced by the camera. By analyzing the shape of the ear it can be determined that a minimum of two moving cameras should be used to avoid occlusion in the results. Due to the complex curvature and self occlusions of the ear it is not possible to view some areas from a single viewpoint, as illustrated in Figure 3.10 .

FIGURE 3.10: One vs two view camera system illustrating the reduced occlusion by using multiple views. The red is the visualization of expected occlusion.



The 3D scanning system developed in this research will therefore use two Canon 1200D DSLR cameras mounted on the curved rail seen in Figure 3.8.

3.3.3 Controlling camera trigger

In Chapter 2, the camera was manually triggered, meaning the user explicitly pushed a button to capture each image. However, now that the cameras are being mounted on a motion rig, it was required to trigger the cameras for each individual image remotely.

There are two possible methods to trigger the camera externally; via USB or through a special remote control. As this system used two cameras, triggering via USB is not recommended as the signals must be sent sequentially, meaning that there could be issues with synchronization of the cameras. As the acquired images are to be used in a feature matching procedure it is important that they are of the same object at different viewpoints. However, if the cameras are not synchronized there can be discrepancies in the positioning which can cause issues in the matching procedure.

Therefore, an external remote was built to trigger the cameras. An external triggering remote works by grounding the electrical signal in the audio port of the DSLR cameras. The process used the Arduino Mega seen in Figure 3.9. The Arduino Mega can be programmed to ground a signal and therefore be used to trigger the cameras. By doing so it allows the user to trigger the motion and the capture of the cameras in a synchronous manner. This is a simple but effective method for triggering the cameras and can also be extended to be completely wireless by using the wireless extension board available for the Arduino.

3.4 Calibration of the 3D Scanning System

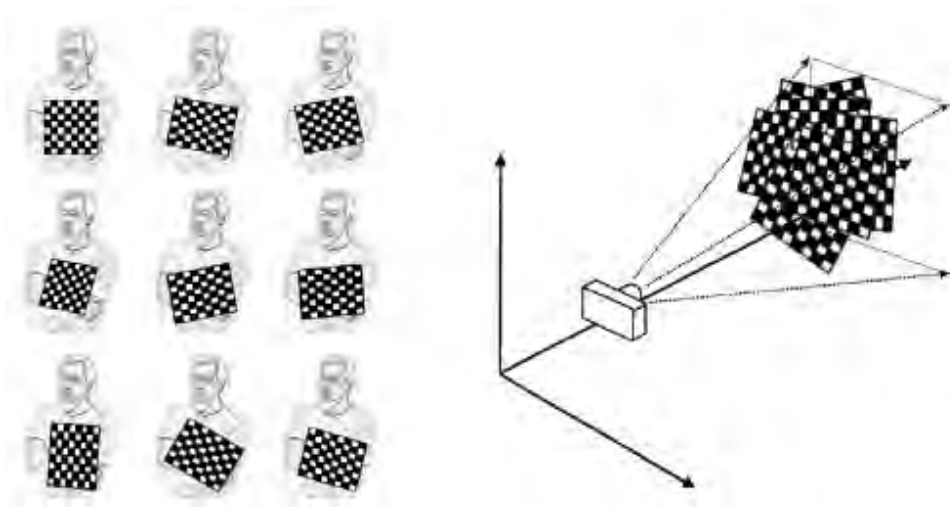
Calibration is an extremely important process for all 3D scanning technologies. It is required to take the arbitrary 3D positions recovered by the reconstruction and make them metric, meaning that the scanned object is to scale. To calibrate a camera the intrinsic and extrinsic parameters must be recovered (Beyeler, 2015; Laganière, 2014). Intrinsic parameters refer to the focal length, optical centre, skew, and lens distortion for the specific camera. These parameters constitute the camera intrinsic matrix that can be used to take camera coordinates to world coordinates. Extrinsic parameters, on the other hand, define the location and orientation of the camera with respect to the world frame.

By knowing both the intrinsic and extrinsic parameters it is possible to do a full 3D metric reconstruction. There are two methods to achieve this using passive 3D scanning systems, static and dynamic. Static calibration is performed prior to any 3D scanning and is similar to hard-coding in programming terminology. This means that the calibration for that particular camera at that focal length is now fixed. Therefore, if the system is moved or bumped then the

calibration procedure must be performed again. The advantages of static systems is that the calibration procedure typically only needs to be performed once and is relatively simple for systems with a low camera number. The more cameras that a system has the more difficult the calibration procedure will be as the cameras must resolve their extrinsic parameters relative to each other, meaning that for a system with 5 cameras, each camera must have its world position defined relative to the other cameras.

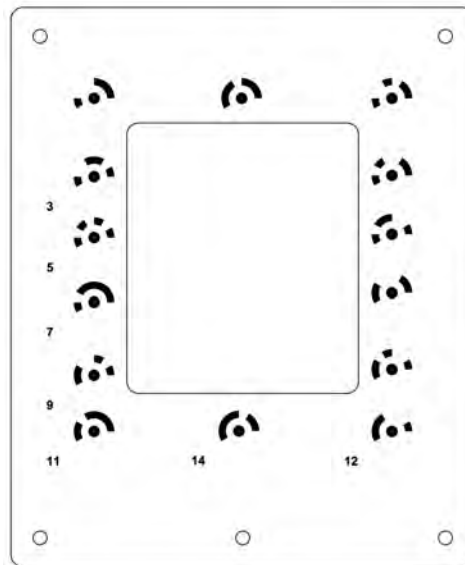
Static calibration can be performed by capturing images of a known pattern, such as a chessboard pattern as shown in Figure 3.11. The goal of this procedure is to recover the extrinsic and intrinsic parameters discussed earlier.

FIGURE 3.11: Static calibration: A chessboard pattern is capture from the camera at different angles and the intrinsic and extrinsic parameters are recovered.



Dynamic calibration, on the other hand, calculates the calibration parameters during each consecutive scan. To do this there must be an object of known size placed in the scene. For this research, coded targets were placed in the scene with a known distance between each of the targets. The targets were designed to be positioned around the ear during the scanning process, as seen in Figure 3.12. The coded targets also serve additional purposes of stabilizing the subject during scanning, and automating the post-processing.

FIGURE 3.12: Dynamic calibration: Using a pattern of coded targets with known distances it is possible to recover the intrinsic and extrinsic parameters during each scan

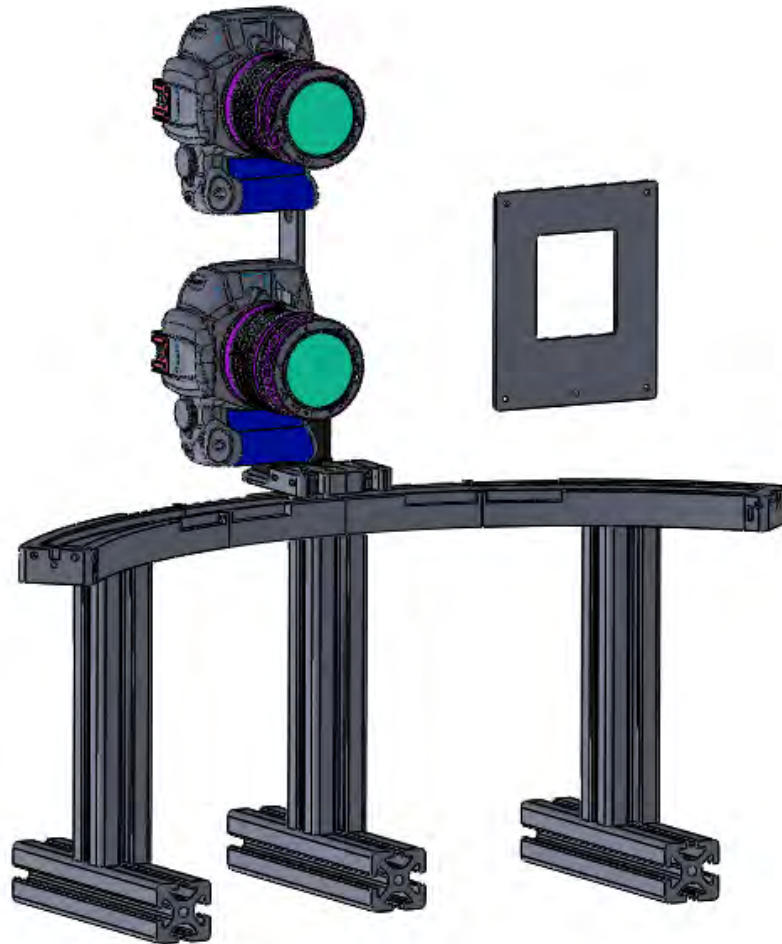


The 12-bit concentric circle coded targets (Agisoft, 2014), seen in Figure 3.12, are detected by the algorithms (Wijenayake et al., 2014) and refer to numeric values. For example, the left side of the calibration grid, from the top to bottom, equate to the numbers 1,3,5,7,9, and 11 respectively. The right side of the grid equate to the numbers 2,4,6,8,10, and 12 respectively. These targets are tracked by consecutive frames of the cameras and as the distance between each target is known, it is possible to reconstruct the 3D scan to scale. There are also other methods for dynamically calibrating a system, for example, by placing an object of known size in the scene, such as a coin, if the coin is detected in the images then it is possible to scale the resultant 3D scan to be metric. However, for this research the dynamic calibration with the coded target grid in Figure 3.12 was used. It is known that to collect the necessary data for this research that the system will have to be moved between locations, therefore, it is not viable to perform static calibration each time. It should be noted, however, that static calibration can be performed at any time and the system is not limited to any particular calibration procedure.

3.5 Resulting 3D Scanning System for the Ear

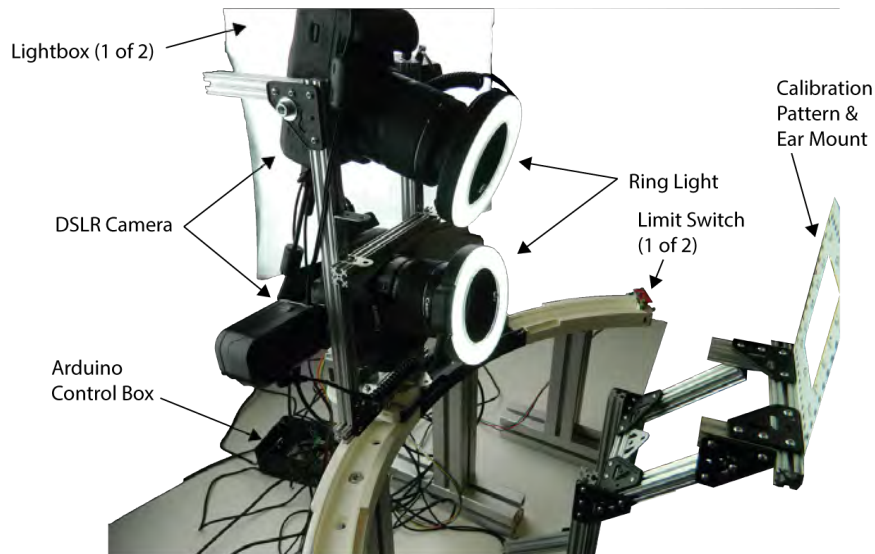
From Section 3.2.1, it was determined that to accurately and reliably reconstruct the human ear, a curved motorized camera rail will be constructed based on the design in Figure 3.8. To transmit the motion a Nema17 stepper was placed on the camera platform and controlled using an Arduino Mega and a RAMPS board (seen in Figure 3.9). It was determined that two cameras were necessary to avoid occlusions in the inner-ear regions. Therefore, both cameras had to be triggered from the Arduino, as discussed in Section 3.3.3. In terms of lighting, two lightboxes were placed on either side of the ear to provide diffuse lighting to the target and a ring-light was mounted on each camera to remove shadows from the ear region. To stop the motion, limit-switches were placed at either end of the rail in order to signal to the Arduino when to stop the stepper motor. A 3D CAD design of the final system can be seen in Figure 3.13.

FIGURE 3.13: Final design: showing the full rail, platform and camera mounts. The cameras are placed vertically to maximize the pixels used. The rail is mounted on aluminium profile to set the desired height and the calibration grid placed at the pre-defined distance from the cameras.



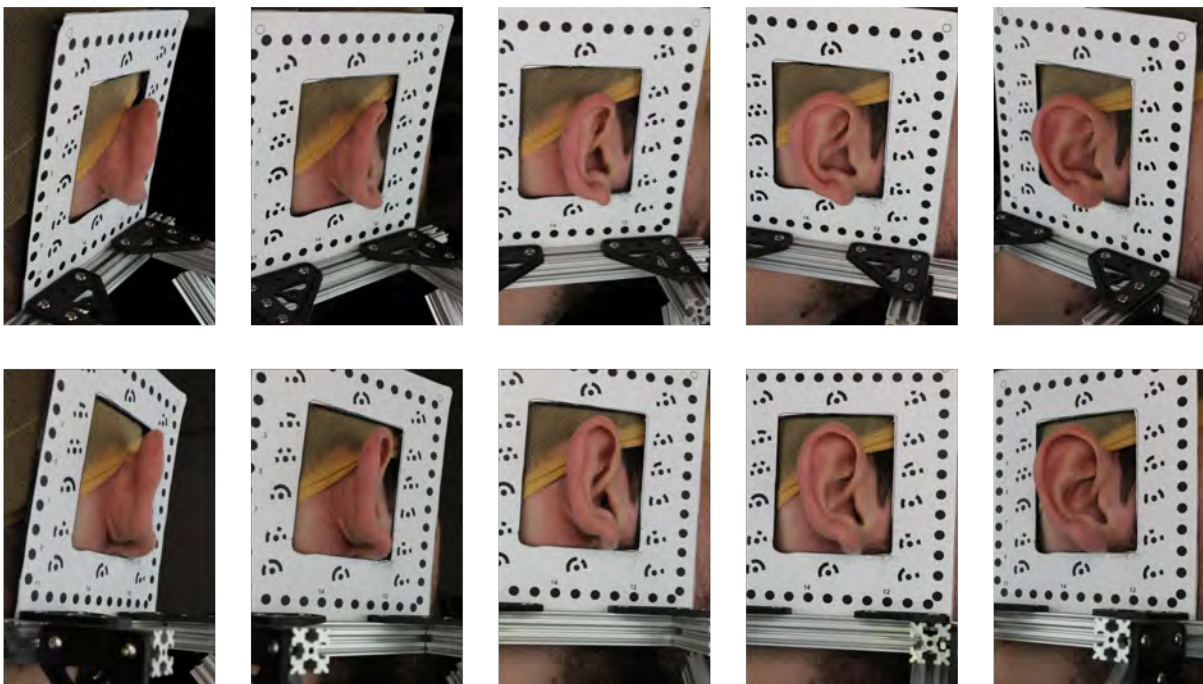
The fully printed and assembled system can be seen in Figure 3.14. It should be noted that the original system consisted of three rail sections, however, during the testing process it was determined that a longer rail was required due to the size of the cameras. To accomplish this a second middle section was 3D printed and assembled to the rail. A testament to the modularity was the simplicity in extending rail without having to redesign any components.

FIGURE 3.14: Manufactured system: showing the fully manufactured system with the 3D printed rail and platform, and the lighting equipment



From the initial testing of the system the maximum number of images that can be captured is 76. This is a limitation of the camera and can be improved if required. The total time to acquire the images is approximately 8 seconds per side, which was one of the requirements in order to limit dynamic motion artefacts in the results.

FIGURE 3.15: Sample images from the custom 3D scanning system. Showing a sample of the total 76 images.

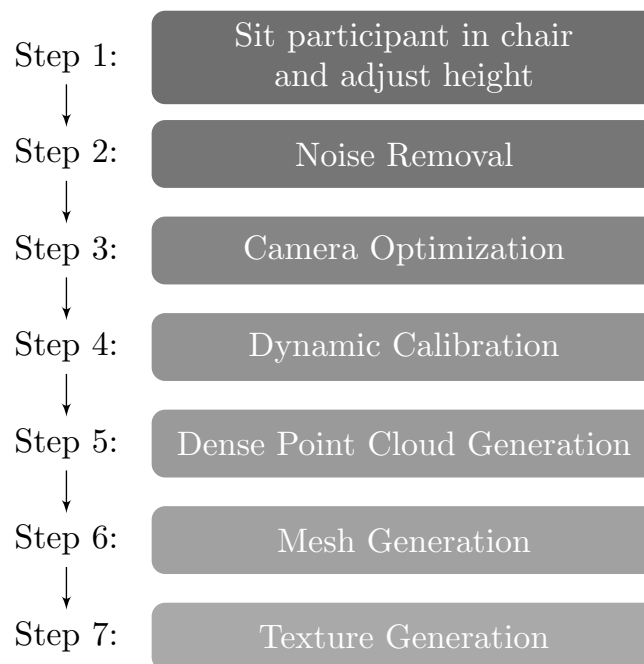


The images in Figure 3.15 shows the importance of the two cameras to minimize the occlusion in the images.

3.6 Image Processing and Reconstruction

To process the data commercial software Agisoft PhotoScan will be used. This software was chosen due to its availability and success in the initial experimentation. The software also has the capability to be automated which is highly applicable to this research. Passive 3D scanning relies solely on algorithms for the reconstruction, therefore, it is possible to programme a custom method specifically designed for the human ear, however, that is outside the scope of this research. The following are the steps required to accurately and reliably reconstruct the human ear and were established through numerous trials involving the processing of the data and the visual assessment of the results.

FIGURE 3.16: Steps for processing the raw images into a 3D model using Agisoft Photoscan.



Camera alignment is the process of approximating the intrinsic and extrinsic calibration parameters and establishing a sparse set of matches between the images. Agisoft Photoscan (Agisoft, 2006) provides multiple scales at which camera alignment can be performed; lowest, low, medium, high, and highest. The high resolution setting uses the images at the original scale whereas the highest resolution up-scales the images by a factor of 4. The lower resolutions downscale the image, medium by a factor of 4, low by a factor of 16, and lowest by a factor of 20. By decreasing the scale it improves the overall processing time but can miss certain important details.

After selecting the image scale, the algorithms detect feature points in the images and then describe these points using a feature descriptor. This process generates a set of feature vectors for each image which are then matched against each other using an approximate nearest neighbour approach. This process can be computationally intensive as the algorithms match upwards of 100,000 points per image from up to 76 images.

Once this process has resolved, the output is a 3D sparse point cloud of roughly 50,000 points and the camera intrinsic and extrinsic parameters. During this process there will be matching points that are erroneous due to low texture or regions with similar texture in the images. These points must therefore be removed and there are several functions which can achieve this, namely reprojection error, reconstruction uncertainty, image count, and projection

accuracy. Reprojection error measures the difference between the original pixel position and new pixel position after the 3D point is projected back to the image coordinates using the camera intrinsic matrix. A threshold is then applied to remove erroneous points, which for this research is 0.5 pixels. This research used the reprojection error as the noise filter.

After the noise is removed, the camera intrinsic parameters are optimized to fit the noise free data, this improves the approximation of camera coordinates and distortion coefficients. Following this, the dynamic calibration is performed (as discussed in Figure 3.12), where the coded targets are detected in the images and the known distances applied to determine the model scale. Steps 5-7 in Figure 3.16, takes the sparse point cloud from Step 1 and calculates a dense point cloud using processes similar to Furukawa and Ponce (2010). The dense point cloud does not contain any connectivity information, it is simply an unordered set of points. The next step is to calculate the connectivity information and generate the mesh. The final optional step is to calculate the texture information, this is the realistic colours. For the purposes of this research the colour is not necessary.

3.6.1 Processing Parameters for Each Stage

For this research, the following step-by-step process and parameters were used to reconstruct the human ear and generate the 3D ear database for statistical analysis.

3.6.1.1 Camera Alignment:

The first step of the SFM process, as outlined in Figure 3.16, is the alignment of the cameras. To achieve this, feature points are detected in the images and used to match across each image, such that a sparse point cloud is generated. In terms of processing parameters, the images are processed at high resolution, meaning the images are processed at the original size. The keypoint limit remains at 0, meaning there is no limit on the number of keypoints per image and the tiepoint limit is also set to 0. At this stage of the research, the system is processed at maximum quality to determine the limit of achievable quality. It is possible to alter these parameters to reduce the processing, however, quality is of more importance than speed at this stage. By processing the images using these parameters, the sparse point cloud density is in the range of 15,000-20,000 vertices.

Resolution: High

Keypoint Limit: 0

Tiepoint Limit: 0

It should be noted that, the achievable sparse point cloud density is dependent on the texture in the image and the resolution of the images. As the target object, in this case the human ear, has a relatively low texture, it is assumed the point density will be relatively low when compared to alternative applications such as aerial mapping, where there is a much higher level of texture in the images.

3.6.1.2 Noise Removal:

The sparse point cloud generated from the camera alignment will contain errors in the positioning of some of the points due to the inaccuracies in the matching process. There are several methods to remove these points, for this research the reprojection error was used. The reprojection error will remove all points above a certain distance threshold.

Reprojection Error: 0.5 pixels

3.6.1.3 Camera Optimisation:

With the erroneous points removed it is important to optimise the intrinsic and extrinsic matrices of each of the cameras. In this process, the focal length, skew factors, and lens distortion parameters are optimised relative to the remaining points in the sparse point cloud. If there were severe errors in the results this could have created a poor positioning for some of the cameras which would then require optimisation.

3.6.1.4 Dynamic Calibration:

As discussed in Section 3.4, this research used dynamic calibration, which is the generation of the scaling parameters to return a metric reconstruction. There are two steps to accomplish this, the detection of the coded targets in the images, and setting of the distance between each of the targets. As the distance between each of the coded targets is known, it is simply input into the program. Detecting the parameters is relatively simple with the only parameters to set being the type of target being detected and the tolerance.

Marker Type: Circular 12-bit

Tolerance: 30 pixels

3.6.1.5 Dense Point Cloud Generation:

Dense point cloud generation uses pair-wise depth map calculations to recover the detailed features from the images. This is the most computationally intensive section of the reconstruction. For each pair of images that have feature matches above a threshold of 100 matches, a depth map is calculated.

Similar to the sparse point cloud generation, there are two main parameters which will vary the output quality, which are, scale and depth filtering mode. The scale for the dense point cloud generation are ultra, high, medium, low, and lowest. Contrary, to the sparse point cloud generation, the ultra setting relates to the processing of the original size, while each following step implies downscaling by a factor of 4. At higher resolution the algorithm will be able to account for minute details on the surface of the target. However, the processing time can be extremely high, for example, processing a set of images from the 3D scanning system at ultra setting would take longer than 12 hours for the full 76 images.

For this research, there is a trade off between achievable resolution and acceptable processing times. It is not viable to spend 12-16 hours per dataset as the goal is to process over one hundred samples. Typically, if the SFM approach is being used to reconstruct a once-off object then the processing time is non-essential. However, for this research, the processing time is crucial. It should be noted that if higher computational power is available then it may be possible to reconstruct the ultra quality within a reasonable time. However, with higher resolutions there is also the possibility of increased noise.

The depth filtering modes relate to the overall smoothness of the dense point cloud, and have mild, moderate, and aggressive modes. Mild filtering will filter out some of the minor noise, while aggressive filtering will remove the majority of small feature and noise. For this research, the human ear consists of relatively smooth surfaces, therefore the aggressive filtering will be applied.

Scale: Medium

Depth filtering: Aggressive

3.6.1.6 Mesh Generation:

The dense point cloud is a high resolution representation of the target object with the majority of the detail required, however, there is no information on the connectivity between each of the points. Mesh generation is the process of generating the face data, which is the connections between each of the points. Mesh generation also constitutes the smoothing of the result and the removal of disconnected components. To generate the connectivity information the following parameters were used:

Surface Type: Arbitrary

Source Data: Dense Cloud

Face Count: Medium

The face count dictates the overall density of the mesh. It was determined that the medium face count provides sufficient resolution for the purposes of this research. To complete the meshing stage a smoothing algorithm was applied to remove any remaining high frequency noise. To ensure the final mesh be watertight, any open holes are closed and all disconnected components removed. This is an essential process for the statistical shape model and automation stage. It should be noted that through scripting, this process is automated between consecutive 3D scans.

3.6.1.7 Texture Generation:

Texture generation is non essential to this research, however, it may be useful for future research or for alternative applications. Texture generation, for this research, refers to the photo-realistic colours of the 3D mesh data. This step is performed by projecting the image colours onto the 3D mesh and blending between images.

Mapping Mode: Generic

Blending mode: Mosaic

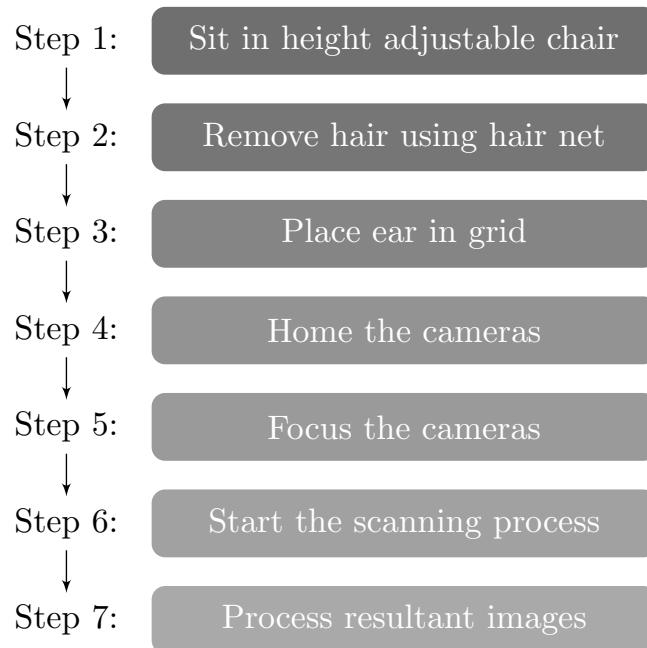
Texture size: 4096x1

Enable color correction: True

3.7 3D Scanning Process

For each 3D scan the process in Figure 3.17 is proposed to ensure that accurate and reliable results are obtained.

FIGURE 3.17: Process for generating the 3D scan data.



As the system is fixed, a height adjustable chair allows for variation in height to be accounted for. The process from setting up the participant to downloading the images takes approximately 2 minutes. Processing of the images accounts for the 3D reconstruction of the target and follows the step-by-step procedure described in Figure 3.16.

3.8 Validation of the 3D Scanning System

The following shows the results from each section of the 3D scanning process.

3.8.1 Camera Alignment

The camera alignment can be seen below. It is clear that when the resolution of the alignment process increases, the overall density of the sparse point cloud also increases.

FIGURE 3.18: Alignment of the images, showing the position of the cameras and the resultant sparse point cloud.

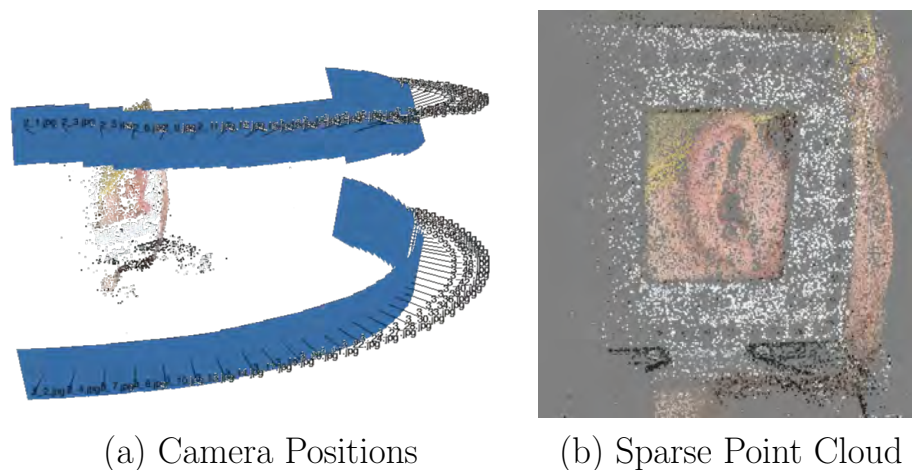
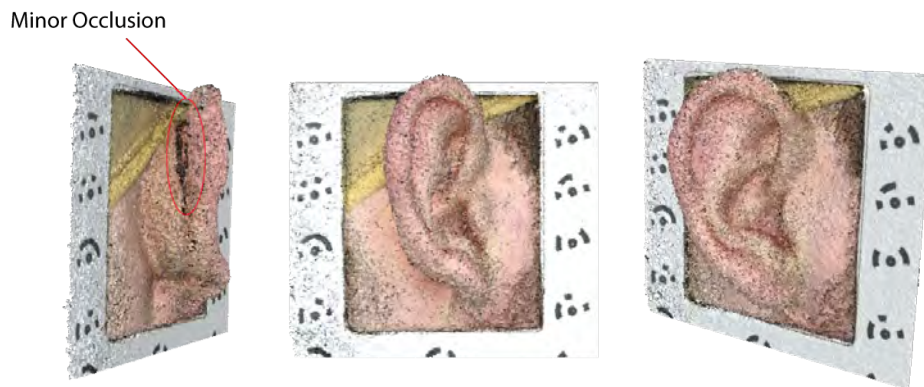


Figure 3.18 (a) shows the position of the images relative to the sparse point cloud. Figure 3.18 (b) shows the sparse point cloud after the noise removal process where points with a reprojection error above 0.5 pixels are removed.

3.8.2 Dense Point Cloud

Figure 3.19 shows the dense point cloud calculated from the camera alignment. As can be seen there is significantly more information, however, also containing some high frequency noise.

FIGURE 3.19: Dense point cloud: the fully reconstructed model from the sparse point cloud, showing some high frequency noise and minor occlusion.



In the inner-ear region, the data is occlusion-free. However, behind the ear it can be seen that there is some minor occlusion. Due to the variation in shape of the ear, it is very difficult to capture this data reliably. In order to capture this data, it may be required to capture the full head as opposed to one ear at a time.

3.8.3 Mesh Generation

From the dense point cloud in Figure 3.19, the final mesh can be constructed which contains the connectivity information from the point data. For this research a medium mesh resolution was used, which is approximately 50,000 faces. The mesh is fully textured and as can be seen in Figure 3.20, is relatively noise free.

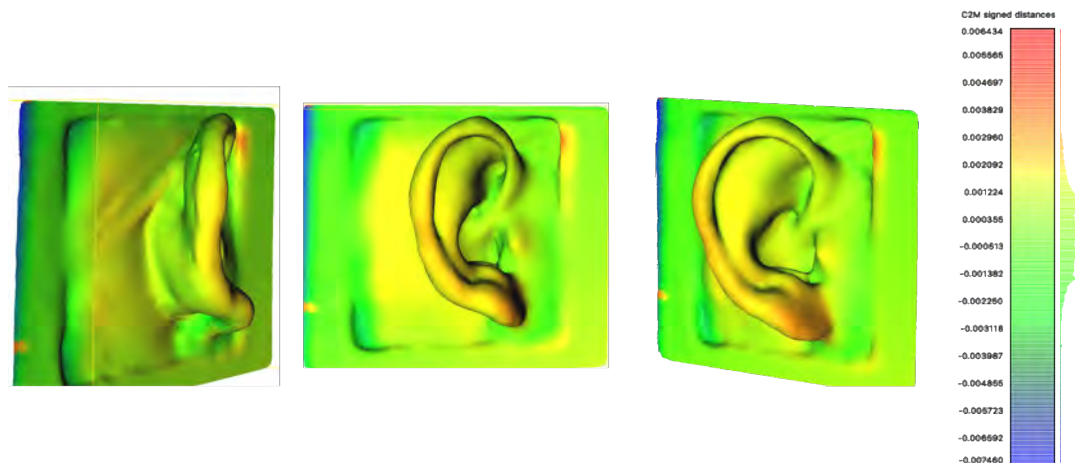
FIGURE 3.20: Textured mesh: fully textured and noise free model with some minor occlusions that will not impact this research.



3.8.4 Repeatability

An important criteria for this research is to test whether the system is repeatable, i.e. for a given subject, is the system accurate enough to reconstruct the same shape taken at different times. As the system relies on point-to-point matching, there is the possibility for variations in the overall reconstruction.

FIGURE 3.21: Showing the repeatability achieved with the system. The green and yellow colour show minor variations and blue and red show larger negative and positive variations respectively. The scale is a metric signed distance in centimetres.



To test this, a scan of a participant was taken and then repeated several minutes later. As can be seen in Figure 3.21, the majority of the variation is in the range of -0.2mm and $+0.2\text{mm}$ (yellow and green colours). From the test there was a discrepancy between the placement of the target's ear within the calibration grid which caused some minor issues. However, the registration algorithms were able to take account of this, the slight blue and red colour on the frame shows that the grid had to be shifted to align the two ears. As the process requires, an individual leaning against the frame, some of the distortion could be attributed to bending of the calibration grid.

3.8.5 Variations in skin tone

One of the important questions remaining from the literature review (Section 1.1) is, can passive 3D scanning systems accurately reconstruct variations in skin tone? It is known that even active 3D scanning systems struggle with extremely dark surfaces. Figure 3.22 shows a sample of the acquired dataset, overall the quality is comparable to caucasian skin tone. However, some minor occlusion occurred in the helix, as marked in Figure 3.22.

FIGURE 3.22: Invariance to skin colour. Some minor occlusions are visible in the left hand image caused by the image acquisition, and some errors in the lobe due to the position to the calibration grid. However, the overall reconstruction is accurate and smooth



As can be seen in Figure 3.22, the algorithms were able to accurately reconstruct the dark complexion of this subjects ear. There is some noise and minor holes in the data, which could be due to issues with the image acquisition. During the process the participant had their ear placed very close to the grid which may have caused issues in the alignment process. However, the overall reconstruction is successful and has the majority of the desired information such as the inner ear region.

3.9 3D Ear Database Construction

With the custom built 3D scanning system meeting the requirements for this research, it was possible to collect the data for a 3D ear database. As discussed previously, the 3D ear database is required to study the variation of the human ear and also to construct a statistical shape model (SSM) of the human ear.

A SSM is a valuable tool for analysing 3D data within a specified object population that can be used for determining best-fit, or for this research, a custom-fit. The negative aspect of the SSM is that the accuracy is dependent on the size and quality of the dataset. Using the 3D scanning system developed in this research the data quality was not an issue. However, there were limitations in the size of the database that could be constructed due to time constraints.

For this research, the goal was to gather a database of approximately 100 participants aged between 18-100 and of mixed gender. It was not possible to scan younger participants due a requirement for informed consent. It was also not feasible to use paid participation which constrained how many participants could be recruited. To gather the most participants in a limited time frame external public events were used.

The primary event was the Tech and Gadget Expo, where the 3D scanning system was setup and over a two day period was able to scan approximately 86 people. The majority of participants were Caucasian males with a relatively even spread of ages. The second event was the Swinburne Open Day, at which the system was setup and scanned approximately 30 people. Efforts were also made to recruit interested participants through email lists, which resulted in approximately 15 participants. All participation in the experimentation was conducted following the guidelines of the Swinburne Human Research Ethics guidelines and process (approval number 2013/309).

In total the 3D ear database, in Table 3.1, constitutes 118 people, of which 28 were women and 86 men with approximately 90% of the database being Caucasian.

TABLE 3.1: The distribution of ages within the 3D ear database showing a relatively spread out range.

Age Range	18-25	25-30	30-40	40-50	>50	Total
Men	10	14	24	15	23	86
Women	5	4	3	10	5	27

Unfortunately, there is a large discrepancy between male and female participants, which could be due to the event at which they were recruited. However, the age range is relatively even with each age group. In the literature there was no discussion of 3D scanning variations in skin colour and it remained a question for this research. As the remaining 10% of the 3D ear database are not Caucasian it allows for the testing of the algorithms, which, from the previous section, the SFM process was shown to successfully reconstruct coloured skin.

3.10 Discussion

The custom-built 3D scanning system has proven to be able to reliably and repeatedly reconstruct the human ear, from Figure 3.21 the overall variations can be seen to be within an acceptable range of ± 0.2 mm. The system has also proven to be able to reconstruct variations in skin colour, something which was not seen in the literature and remained a concern for this research. The clear advantage of the system is the minimal knowledge required for the user to acquire and process the resultant data, making it highly applicable to situations where expert users are not available or feasible. Reviewing the overall construction of the system, the design is high modular, meaning that the principle can be applied to a wide range of 3D scanning applications and this particular system has proven to be able to reconstruct the human face and even the inner mouth. 3D printing was necessary to manufacture the curved rail and with variations in the design different paths can be easily achieved. However, the system also lends itself to further development based on a stationary setup where multiple cameras placed around the desired target are used instead of moving cameras. Even with variations in the number of cameras the same algorithmic process can be applied to achieve the 3D reconstruction. The design can be said to be future proof, meaning that new technology can be easily integrated into the current system for improvements in the overall quality. For example, by investing in more advanced cameras the overall imaging quality would improve, or new algorithms for 3D reconstruction can be easily integrated through a software update and the improvements seen instantly. Contrary to active system which are constrained to a specific pattern and the improvements are typically only in speed, passive 3D scanning systems are much more flexible. The results in Figure 3.20 justify the decision to custom-build a 3D scanning system for the human ear and has achieved qualities that are not seen in commercial systems such as repeatability, ease of use and automation. In order to ensure consistency in the assessment of the custom-built system it was assessed against the same criteria as seen in Chapter 2.

3.10.1 Criteria Assessment

Similar to the processes seen in Chapter 2, the custom built 3D scanning system must be assessed against the same criteria in order to justify the use of passive 3D scanning for the ear.

Surface Quality: This is tested by visual inspection and is determined due to the overall smoothness and similarity to the target shape. For the custom built system, the surface quality is very high, with the output from the meshing procedure containing some high frequency noise, by using smoothing functions the overall surface quality is excellent. It should be noted that it was not possible to generate a ground truth dataset to quantitatively test the surface quality. As a statistical shape model (SSM) is used to approximate the 3D scan data, it is more critical that the level of occlusion be minimum as opposed to a high level of detail. The predictive nature of the SSM will allow for minor surface issues to be accounted for.

Holes/Occlusion: From the reconstruction process holes in the data are very rare and are only seen on target shapes with a high level of variation, for example in Figure 3.22. While the 3D reconstruction software has functions to account for holes in the data, it is an approximation and therefore not a true representation of the surface. When compared with the active 3D scanning systems in Chapter 2 Figure 2.7 and Figure 2.9, the holes in the passive system are much fewer and not in the critical areas within the inner-ear.

Captured detail: For the custom built system the captured detail is below that of the active 3D scanning systems. This is due to the approximation of the surface using image data, as opposed to using a projected pattern to measure the true surface. However, as the 3D scan data is to be used with a SSM, the captured detail is not as critical as the holes or occlusion. With improvements to the imaging quality and by possibly adding extra image viewpoints, the captured detail could potentially be improved.

Scanning time: With the curved rail and the stepper motor controlling the motion the time to acquire the images is consistent at approximately 8 seconds per ear. This time can be decreased, however, it should be noted that by changing the time there will be more or less data captured. As the frame-rate of the camera is fixed, by increasing the speed of the motor, less images will be captured, and vice versa. Alternatively a fixed array of cameras could be used which would capture the data instantaneously. However, the cost of the cameras becomes significant.

Ease of use: Once the system is setup the ease of use is very high, requiring only to click "start" and then download the images. However, the process to setup the system requires knowledge of photography which restricts the ease of use of the system. If poor imaging parameters are set then the overall quality of the 3D reconstruction will be poor as well. Therefore, training must be provided to those that are setting up the system in different environments, or different targets, as the imaging parameters may need to be changed.

Processing time: For the full 76 images that processing time is extremely high, taking approximately 1 hour and 30 minutes per ear, with the following time per section:

Accurate Alignment: 32 Minutes

Dense Point Cloud: 59 Minutes

Mesh Generation: 1 Minute

Texture Generation: 4 Minutes 50 Seconds

This time was achieved on an Intel Core i7 2.3GHz with 8GB RAM. This processing power is average and a better processing time could potentially be achieved by using higher power computers or cloud computing.

3.10.1.0.1 Automatability: The process from acquisition to processing of the images is highly automated. To capture the images there is a simple one click system that has been programmed using the Arduino, all camera controls are automated and the only user control input is setting the directory for downloading the resultant images. Following this is processing of the images. While this is typically manual, the commercial software allows for custom plugins to be written that allow for majority automation. By writing the plugins in the Python programming language 100% of the processing was automated.

The automation program has been written to process batches of images, meaning that if a queue of 100 participants has been scanned it is possible to set up the interface to process all of these jobs with 100% automation. Using this approach, the 3D ear database has been processed with 100% automation.

3.10.2 Repeatability

One of the critical criteria for this research is testing whether the 3D scanning system is capable of outputting the same results reliably. The output of this process can be seen in Figure 3.21. The overall variation is minimal in the majority of areas, as can be seen by the green colour. It should be noted that the calculated distance is signed, therefore dark blue will represent extreme negative and dark red represents extreme positive. With the majority of the comparison in yellow and green colour, this shows that the overall variation between the models is minimal with the average range between +0.3mm and -0.5mm.

The overall range for variation is acceptable given that the SFM process works by matching feature points across images, meaning that variations in the acquired images will result in a different output.

3.10.3 3D Ear Database

The 3D ear database successfully achieved the goal of at least 100 participants ranging from 18-100 years of age. However, there were several issues with the acquisition and processing of the data that need to be addressed. In the lab setting the removal of hair was done using a wig cap, which is a nylon mesh material. However, for the external events mesh caps were not available and a different method needed to be used. This therefore caused some discrepancies between the lab results and the external results. It was seen that several participants had issues with the hair nets and the time to resolve these issues limited the number of participants that could be collected.

It was determined that for the external events there would be no hair nets used, instead the participant will aim to remove as much hair as possible from the scene. For the majority of participants this was satisfactory as 73% of the database were males with short hair. The choice to remove hair nets from the process affected the female participants and it was seen in the results. However, the internal ear-region is still visible which is the most important area for this research. With further time, more effort would be made to more reliably remove hair from the scene.

Aside from external hair there were also issues with internal hair in the ear region, particularly with older males. In the SFM process hairs in the internal ear region tend to inhibit the reconstruction process, resolving themselves as flat surfaces, which renders that data useless for the purposes of this research. This could not be avoided in the collection process as it was not possible to shave the participants.

3.10.4 3D Scanning System Cost and the Possibility for Mobile Phone Technology

It was discussed previously that the choice of two cameras for this research was to reduce occlusion and the use of a motion rail was to reduce the overall cost of the system. The full cost of the system developed in this chapter is under \$1000, however, it would be ideal to use a stationary system with multiple cameras as opposed to a motion rail. This would allow for a faster acquisition time and introduce greater consistency. In terms of cost, a commercial system consisting of over 170 DSLR cameras has been used to capture the full 3D human body. In this research, the maximum images that can be captured through motion is 76. It is highly likely that a number of those images are redundant and that the necessary cameras for reconstruction of the human ear or human head could be closer to 30-40. This would cost approximately \$20,000-30,000 which is comparable to the cost of some active 3D scanning systems. While this is a relatively high cost for the system the intention is not for the consumer to purchase the unit but to access it through commercial service providers.

There is the possibility to use widely available mobile phone technology to capture the data. However, the small image sensor is not comparable to a large DSLR image sensor which determines the achievable image quality. With the onset of machine learning there exists the opportunity to use mobile phone technology in the future, however, by reviewing the companies that used mobile phone technology to capture the 3D ear data (discussed in Section 1.1.2) it was determined that the limitations inhibit its applicability to this research. The limitations include, the necessity for the individual to scan themselves which is reliant on that individual having the experience or knowledge to do this successfully. With the variety of mobile phones available, it is difficult to instil consistency due to the variation in image sensor and processing algorithms. Allowing the user to 3D scan themselves is good for the business as it means there does not have to be a defined locality and the end-product can be delivered by mail. However, this removes control from the process so there needs to be a method for determining if the captured data is good enough for the purpose of customization which is highly complex to achieve. The limitations with mobile phone technology illustrates the benefits of using a high-end stationary DSLR camera rig.

Overall, the custom-built 3D scanning system has achieved the initial requirements and scored highly on the criteria of assessment from Chapter 2. However, there are still advantages and disadvantages to this setup. The system, while user friendly, does require knowledge of imaging parameters in order to setup the system for the given environment. This involves setting the desired aperture, ISO, and shutter speed. While many people are familiar with these parameters, it is uncertain whether an individual will be able to optimize them for passive 3D scanning. As the resultant output is dependent on the accuracy of these parameters it is essential that they be optimised for the given environment. One of the difficulties with this research was moving the system between locations in order to acquire enough data for the 3D ear database. In moving the system, it was seen that optimization of the imaging parameters was especially difficult as the output can be somewhat subjective or easily misinterpreted. The lab environment was considered the perfect setup where the lighting was consistent and the background noise could be controlled. However, at the public events the lighting was generally very high up and the system relied heavily on the lightboxes and ring-lights for the majority of the illumination. It was also not possible to control the background noise at the public events, meaning that there are people moving in and out of the background through some of the images. However, through the automation of the reconstruction process this background noise was taken account of and did not impact the overall result. The main difficulty, therefore, was the variation in imaging parameters between the lab environment and the public environment.

3.11 Future Research

While the 3D scanning system has accomplished the initial requirements and criteria, there are still some areas that require further work. However, for this research, the quality achieved is satisfactory and will allow for the overall goal to be completed.

3.11.1 Stationary Setup

The system used in this research consists of two cameras mounted on a custom-built curved rail that acquire 76 images of the human ear, which are then reconstructed. The motion to acquire the 76 images is substantial when considering the motion of the human body and the difficulty in holding perfectly still for a period of approximately 10 seconds, but the reconstruction process is able to account for slight motion. A two camera system was designed due to cost restraints and the uncertainty in applicability to 3D scanning the human ear. With the accurate and reliable power of the passive 3D scanning system fully tested it is now feasible to invest time and funding into further development. By using a stationary setup of multiple DSLR cameras, the capture time will be effectively instantaneous and it will also assist with the calibration and alignment procedure of the 3D reconstruction.

3.11.2 Static Calibration

Regardless of whether a stationary or moving system is used, it is possible to perform a static calibration. The dynamic calibration used to gather the database was beneficial as the system was moved between locations to acquire the data. By statically calibrating the system it removes the necessity for the dynamic calibration grid and will allow for a more relaxed acquisition process for the participant.

3.11.3 Custom 3D Reconstruction Algorithms

The algorithms used to perform the 3D reconstruction are proprietary to Agisoft PhotoScan, however, with the reconstruction power of passive 3D scanning fully tested it is now viable to invest time in the development of algorithms for specific applications of this research. Photogrammetry is a generic term for the 3D reconstruction of objects from 2D images, and the algorithms which perform this are general. As the target for this research is known, it is possible to apply machine learning or prior knowledge reconstruction to improve the performance and possibly quality.

3.11.4 Possibility of Using Mobile Phone Technology

There are opportunities to use existing mobile phone technology to perform the 3D scanning, particular with the majority of flagship mobile phones, such as iPhone X, containing more than one rear facing camera. Future research will involve the use of machine learning algorithms and mobile phone technology to determine the feasibility of a lower cost system to fit within the automated customization approach of this research.

3.12 Conclusion

From Chapter 2 the research question, *What is the most applicable 3D scanning method for the ear?*, was left open, as the passive 3D scanning system had to be optimized in order to prove its applicability to the 3D scanning of the human ear. In this section the design and construction of a 3D scanning system was outlined and qualitatively evaluated. The results proved that the

passive 3D scanning system is able to reliably and repeatedly 3D scan the ear with a relatively high level of detail and automation, therefore answering the research question.

Of significance here is the ability of the 3D scanning system to automate the capture and processing of the data, which is a desirable aspect for this research. The modularity and passive nature of the system lends itself to future improvements with new cameras or using a stationary system. The true test of the system was the construction of the 3D ear database which constitutes 86 men and 27 women. The age range of the participants can be seen in Table 3.1 with the majority of the database consisting of Caucasian males.

One of the unanswered questions from the literature was, can the 3D scanning system reconstruct variations in skin complexion?. It is known that both active and passive systems have difficulty with extremely dark texture-less areas. However, from Figure 3.22 it can be seen that the custom-built 3D scanning system can reconstruct dark complexion. The significance here is that in a production scenario, the 3D scanning system will be able to reliably reconstruct the target object regardless of the skin tone.

With the primary research question answered the following chapter will aim to setup and use the 3D ear database to analyze the variation in shape among the population and process it for use with the automated customization algorithm.

Chapter 4

Establishing the Base Variance Using Statistical Shape Analysis

In the previous chapter the 3D ear database was constructed which constitutes 100 3D scans of the human ear. As it stands the data consists of unordered points and faces in three-dimensional space, which can be transformed into a functional product through an expert user (see Figure 1.15 and Figure 1.16). However, as outlined, the process to accomplish this is not simple. This research aims to use 3D data in a way that to the best of our knowledge has not been fully demonstrated in product design and manufacture. The aim is the development of an automation system for manufacturing custom-fit products by using a statistical shape model (SSM) with constrained 3D mesh deformation. This chapter aims to answer a critical research question, which is:

How do we statistically analyze the full 3D scan data, without the use of landmarks?

While it has been said that a SSM is important to this research it has not been discussed in detail as to why it is important.

4.1 The Application of a SSM to Customization

Using the 3D ear database constructed in Chapter 3 in its current state, it is possible to complete the goal of this research, however, it could potentially be unreliable. As discussed in Section 1.1, research by Lee et al. (2016) attempted to inform the design process of in-ear devices through 3D fit analysis using 3D scan data. However, in their approach, it is not possible to determine if the selected data covers the full range of shape variation of the population as it does not use any statistical data. A SSM is a compressed representation of shape variation within a dataset and allows the user to construct the desired standard deviation for which to assess size and fit. By selecting, for example, 10 models from -3σ to $+3\sigma$ it is possible to design a product that will fit 99.7% of the population, as can be seen in Figure 4.1.

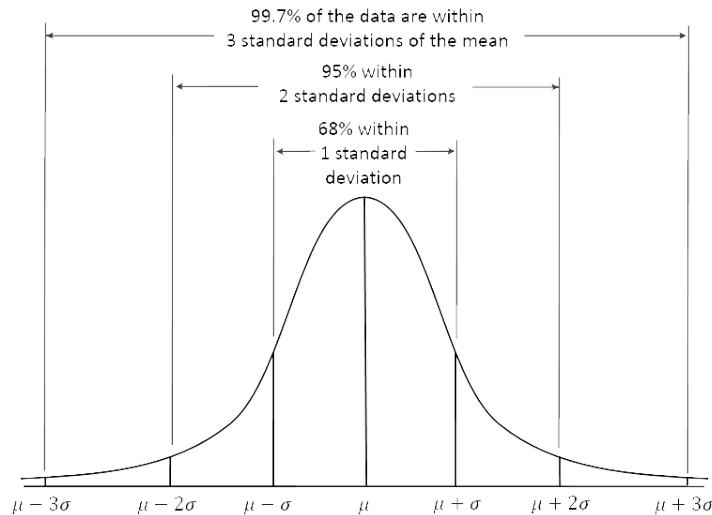


FIGURE 4.1: The normal distribution showing the amount of variance within each standard deviation. The median line represents the mean shape.

However, if the raw 3D scan data was used to assess the fit, as per Lee et al. (2016), it would be uncertain which models to use and if the chosen models were varied enough to cover the population. For example, if a dataset of 10 randomly selected participants was used to assess the fit of an in-ear device, there would be no knowledge of where those participants lie on the normal distribution in Figure 4.1. Therefore, the fit would not be suitable for someone outside of this range. Using a SSM for product design allows for the variation to be explicitly set, for example, to be between $\pm 2\sigma$ or $\pm 3\sigma$, where σ is the standard deviation.

Using a SSM for product design is a relatively novel process due to the complications in not only constructing the 3D database but in establishing and using the SSM. This chapter will, therefore, establish the methodology for generating a SSM that can be analyzed and used for product customization. Specifically, this chapter will demonstrate the complexity in establishing an accurate one-to-one correspondence among highly varied shapes, and in particular dense 3D scan data as opposed to sparse landmarks. The quantitative analysis in this chapter is therefore directed towards the establishment of the correspondences as opposed to the evaluation of the SSM. As a relatively small dataset was used in this research, it is likely that the evaluation will be poor when the aim is to show the accuracy of the correspondences when compared with standard approaches.

The example in Figure 4.2 shows a publicly available SSM of the human body consisting of 6449 vertices, whereas in Chapter 3, the output density of the ear region was above 20,000. While low resolution models may be suitable to applications such as basic sizing studies or pose tracking in computer vision, in this research, the objective is to use a SSM for form-fitting product design, which requires a much higher density mesh which limits the available algorithms that can be used.

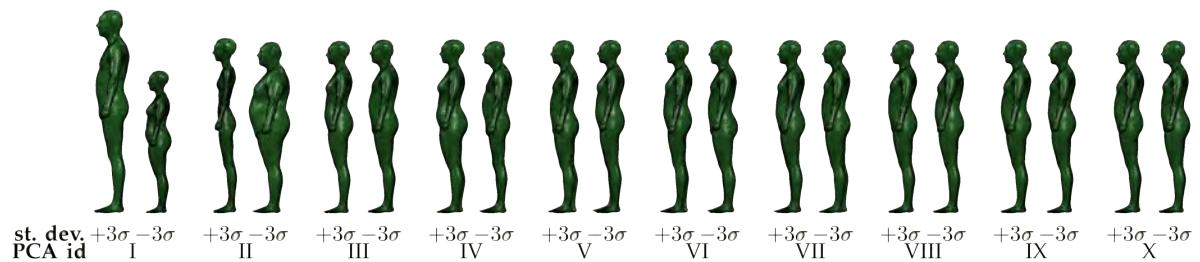


FIGURE 4.2: A SSM of the human body. Showing $\pm 3\sigma$ and consecutive principal components from 1 to 10. The model consists of 6449 vertices.

Figure 4.2 shows the current standard for SSMs. The SSM is shown with $\pm 3\sigma$ and the first 10 principal components that capture different features such as height (PC1) and weight (PC2). From the model, the first three principal components constitute 90% of the total variance within the dataset and by using the first ten principal components the total explained variance is 97%. Principal component analysis (PCA) is a statistical procedure that uses an orthogonal transformation to convert a set of observations of possibly correlated variables into a set of values of linearly uncorrelated variables called principal components. The variables in this case, are the positions of the corresponding vertices across each model. By performing PCA, as per Figure 4.2, it is possible to construct a model of the variance within the given dataset. However, as discussed, the outcome from the majority of available techniques is a relatively sparse model. From Figure 4.2, the output is a mesh with 6449 vertices which is a relatively low resolution model that is unsuitable for the present studies, however, may have alternative applications. As this research is focused on form fitting product design, the dataset must be of higher resolution.

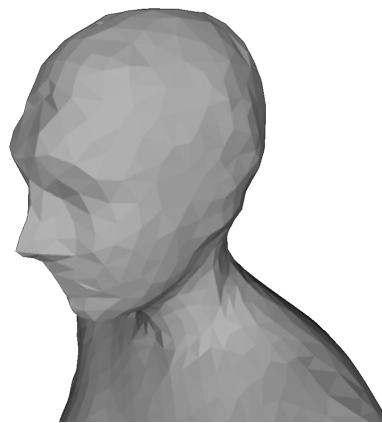


FIGURE 4.3: The SSM of Figure 4.2 highlighting the ear region, showing that the output data is not sufficient to model the ear.

By focusing on the ear region in Section 4.1 the detail is completely lost and unusable for the purpose of this research. In order to be applicable to this research, the output data must have high detail, meaning that each model in the 3D ear database from Chapter 3 should be used in full resolution or with minimal loss of quality. This creates a difficult problem as the majority of available algorithms are not suitable for high density meshes. The following section introduces the requirements for this research as established in this section and the algorithms that will be used are discussed in Section 4.3.

4.2 Requirements for the Human Ear and this Research

By analyzing the literature in Section 1.1.8 and focusing the available methods towards the data generated in Chapter 3, the following requirements were established in order to create a SSM that uses the full 3D scan data as its basis, as opposed to landmark data.

Dense:For this research, a one-to-one correspondence is required, meaning that for each point in the mean shape there should be a corresponding point in each model. Typical approaches for a SSM rely on landmarks placed on the surface to guide the registration and fitting (Dalal and Wang, 2012; Pishchulin et al., 2015). However, the excessive work required to train and detect landmarks limits the modularity of the approach. The difficulty with one-to-one correspondences is the increased complexity and overall computational resources required. The overall process for registering the 3D ear models will be outlined in Section 4.3.

Non-Rigid: This refers to the ability of the algorithm to account for large surface deformation in order to determine correct correspondences. For models with pose variation or high deformation it is necessary to include non-rigidity. By analyzing the 3D ear database generated in Chapter 3, non-rigidity was deemed necessary due to the large shape variation witnessed within the population for the human ear. Contrary to standard applications for SSMs such as bones or organs, the human ear is a relatively complex surface with many folds and ridges which creates difficulties for rigid registration. Also, for alternative applications to the human body such as the human hand, which has a high level of dynamic motion, it is beneficial to incorporate non-rigidity at an early stage.

Groupwise:This is not an essential parameter to this research but is beneficial to remove bias in the overall results. Groupwise refers to the process of generating the correspondences. Typically, this is a pairwise process where one model is chosen as the base, either the first model or a random model, and is then sequentially matched against the remaining models and the mean model is generated from the matching points, which creates a bias towards the chosen model. Groupwise registration aims to remove the bias by iteratively updating the mean shape by registering all of the models to a generic shape or chosen shape.

Non-Landmark Based: The majority of available statistical shape modelling algorithms rely on the use of landmarks, therefore, requiring a trained expert to train the detection algorithms and can actually be prone to errors or inaccuracies depending on the level of the expert. For this research, it is not viable to manual landmark each model within the dataset as there is no access to an individual with this skill level and the requirement for landmarking is counter-productive to the overall goal of automating the construction of custom-fit products. By creating a system that does not require landmarks it allows for modularity and rapid adaptation to regions other than the ear.

So, for this research, the overall aim is to generate a SSM using algorithms that non-rigidly determine a groupwise, dense correspondence without relying on landmarks. The chapter is broken up as follows; the chapter introduction summarized the concept of the statistical shape model discussed in Section 1.1, followed by the requirements for this research in Section 4.2, the methodology for generating a SSM is illustrated in Section 4.3 and the resultant SSM and analysis is outlined in Section 4.4 and Section 4.4.3 respectively.

4.3 Functional Map based 3D Statistical Shape Model Generation

In Section 1.1.8, the concept of the SSM was introduced with the theoretical background and current research. This section aims to focus this theory with a direct application to the aim of this research, which is to analyze the variance in a 3D database of human ears. In this instance, variance is referring to the change in shape between 3D models. The goal here is to establish, given a population of shapes in correspondence, what are the main modes of shape variation and how they contribute to ear shape.

4.3.1 What are Functional Maps?

From Section 1.1.8, it was discussed that in order to account for the large deformation between shapes it was necessary to follow the current state-of-the-art shape matching process known as Functional Maps (Ovsjanikov et al., 2012), which will be proven in a later comparison. As opposed to standard point-to-point matching, Functional Maps can be considered as a "transporter" that allow for information to be moved across shapes (Ovsjanikov et al., 2016). The main benefit of Functional Maps over point-to-point matching is that the mapping can be represented as matrices of linear transformations between basis functions on the shape. For more information on Functional Maps the reader is directed to Ovsjanikov et al. (2012, 2016); Rustamov (2007); Huang et al. (2014).

4.3.2 Methodology for Generating a Statistical Shape Model

Constructing a 3D SSM follows a very similar approach to the 3D reconstruction method seen in Chapter 3 which establishes correspondence through 2D feature point registration. However, the complexity of the process has now been increased as the registration data is three-dimensional. From Chapter 3, the output from the 3D scanning system was seen, however, this data is typically unordered. This means that between consecutive 3D scans it is uncertain whether a point that is in one model will be in the same position in the next model. For a SSM there needs to be a meaningful correspondence between points, therefore, similar to the passive 3D reconstruction process it is required to take the unordered point sets and find the corresponding points across each model. This research has generated a SSM through the following process:

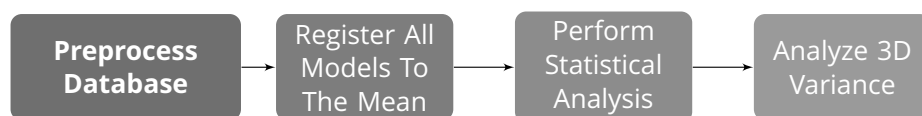


FIGURE 4.4: The process for generating a statistical shape model consisting of pre-processing, groupwise registration, statistical analysis and variance analysis.

4.3.2.1 Preprocessing of the input 3D models

As discussed previously, the output of the 3D scanning system is a high density 3D model of the target surface, in this case the human ear. However, the user has no control over the positioning or localised density of the vertex distributions. As the SSM process aims to generate a one-to-one correspondence between vertices, this discrepancy can result in poor registration. One of the requirements for this research was to generate the SSM using the dense representation of the scanned object, however, using the raw 3D scanning data results in poor registration. In order to alleviate the processing difficulty, the 3D models are pre-processed to uniformly distribute the vertices and faces across the mesh while preserving the overall features. To accomplish this, this research follows the approach of Jakob et al. (2015), which

produces a highly isotropic mesh while preserving sharp features. The critical steps to this process can be seen in Figure 4.5.

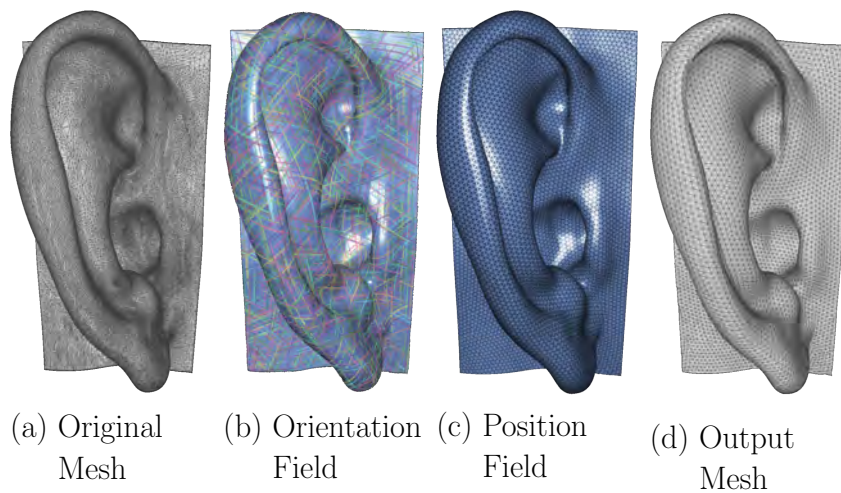


FIGURE 4.5: Pre-processing the input mesh showing the uniform distribution of vertices and faces in the output mesh while maintaining the overall features. In order from the left: Original mesh, Orientation field, Position field, Uniform output.

The original mesh can be seen in Figure 4.5 (a), following this is the visualization of the calculated orientation field (b), the position field (c), and the output mesh (d). Of interest here is the uniform distribution of vertices over the surface which will assist with the overall registration process. The original mesh consisted of 50,000 vertices, and the output consists of 16,000 uniformly distributed vertices with minimal loss of information. There is no upper limit to the number of vertices in this SSM approach, however, the higher the vertex count the longer the processing time will be. For this research, the vertices are refined to 5000 vertices, however, in a practical application the choice of upper limit should be determined based on visual quality. This means that the user should determine the appropriate number of vertices based on the loss of quality.

4.3.2.2 Groupwise Registration and Refinement using Functional Maps

Following the pre-processing stage, each of the input models must be registered to the mean shape. The mean shape can be iteratively refined from a random model in the dataset or a model can be selected that is close to the mean based on variance analysis. The selection of the mean shape is not overly critical to the output SSM, therefore, a random shape is selected and the mean shape is refined. The registration process for functional maps is as follows:

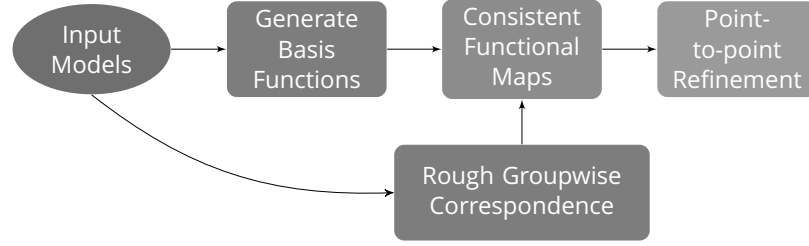


FIGURE 4.6: The process of generating point-to-point correspondences from functional maps. Convert input mesh to basis functions, calculate rough correspondences, generate functional maps and refine into consistent correspondences.

Generating Initial Correspondences for Functional Map Guidance: To calculate functional maps between shapes requires the estimation of rough or soft correspondences across models, this is simply an initial guess to guide the functional map generation and can be generated using standard feature matching approaches as per Rodolà et al. (2016) or through a free-form deformation as per Huang et al. (2014). Feature matching depends on the method for description to generate an accurate match, the descriptors need to be definitive enough to select from different vertices in the same region. While feature matching processes, such as Salti et al. (2014) and Li and Hamza (2013), are relatively robust, for areas with smooth surfaces or symmetry, the process can be error prone. Recent literature aims to embed machine learning in the feature detection and matching process to improve the robustness (Fang et al., 2015). Free-form deformation, on the other hand, uses the 3D position of the vertices as the matching information. In this approach, the input 3D model, is split into a volumetric grid and correspondences are established by deforming the grid to the closest point on the target shape (Modat et al., 2010). This research follows the process of Huang et al. (2014) as it generated an initial estimate that had fewer errors in the matching process when compared to the feature description approach.

Generating Basis Functions on the Shapes: The next stage of the functional map based registration is to generate basis functions for each model in the dataset. Following the procedure of Ovsjanikov et al. (2012), the Laplace-Beltrami basis function is chosen. Lévy (2006) and Rustamov (2007) discuss the advantages of the Laplace-Beltrami basis function for 3D shape analysis. The Laplace-Beltrami basis exhibits preferable behaviour for 3D shape registration including deformation invariance, which means that regardless of pose the basis functions will be the same (Rustamov, 2007). In Rustamov (2007), the discrete Laplace-Beltrami differential operator is described as; for a function f defined on the surface, the value of Δf is approximated as:

$$\Delta f(p_i) \approx \frac{1}{s_i} \sum_{j \in N(i)} \frac{\cot \alpha_{ij} + \cot \beta_{ij}}{2} [f(p_j) - f(p_i)] \quad (4.1)$$

$$m_{ij} = \frac{\cot \alpha_{ij} + \cot \beta_{ij}}{2} \quad (4.2)$$

$$L_{ij} = \begin{cases} \sum_k m_{ik}/s_i, & \text{if } i = j. \\ -m_{ij}/s_i, & \text{if } i \text{ and } j \text{ adjacent.} \\ 0, & \text{otherwise/.} \end{cases} \quad (4.3)$$

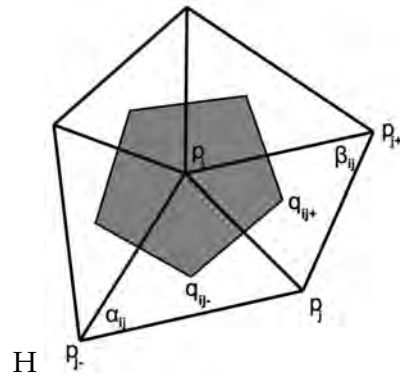


FIGURE 4.7: Definitions of the angles and the area appearing in the discrete Laplace-Beltrami operator (Rustamov, 2007).

s_i in Equation (4.1) is the area of the shaded region in Figure 4.7. The summation is over all vertex indices j adjacent with vertex p_i . Using the column-vector \vec{f} , the formula in Equation (4.1) can be written as a matrix-vector multiplication $\Delta f \approx L \vec{f}$, where L is the discrete Laplacian in Equation (4.3). Eigen decomposition of the discrete Laplacian L constitutes the Laplace-Beltrami basis functions, that will be used herein. For more information on Laplace-Beltrami basis functions the reader is directed to Rustamov (2007). Figure 4.8 shows the first 5 basis functions for two sample 3D ear models.

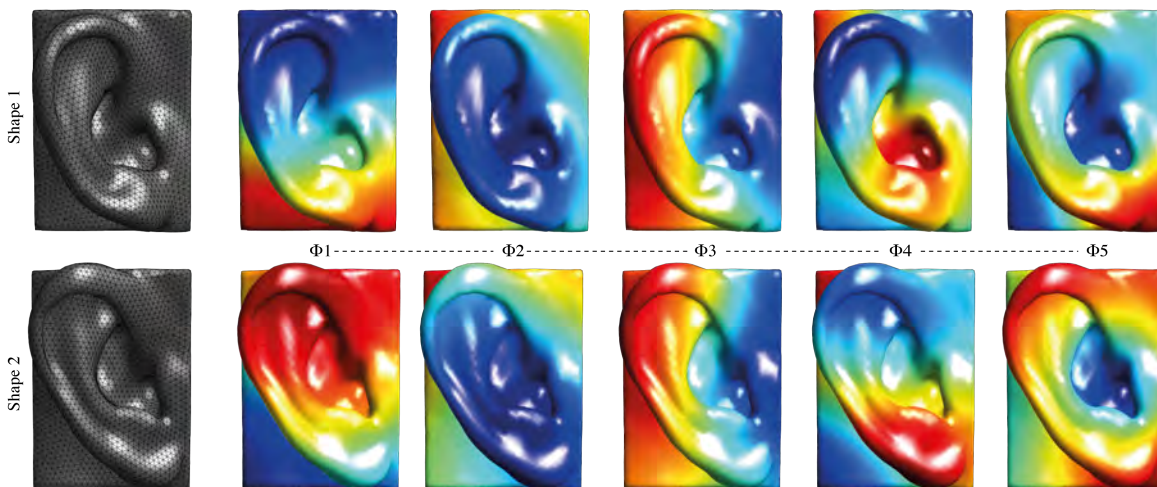


FIGURE 4.8: Example of basis functions on the surface of two ears illustrating the similarities in certain basis functions.

It can be seen in Figure 4.8 that there are some similarities between models. The colours in Figure 4.8 are representative of the basis functions on the surface of the 3D model. It should be noted that basis functions are typically unordered so generating a map between basis functions requires some refinement. Following the process of Ovsjanikov et al. (2012), 50 basis functions are chosen to estimate the functional map. It is possible to use less functions, however, decomposition of the 3D shape into basis functions is similar to the process of mesh compression. Therefore, by using less functions there is the potential to miss important information on the surface. Similarly, by using a large amount of basis functions there may be a lot of redundant information. Lévy (2006) illustrates this through reconstruction of a sample 3D model using 10-300 basis functions, as seen in Figure 4.9.

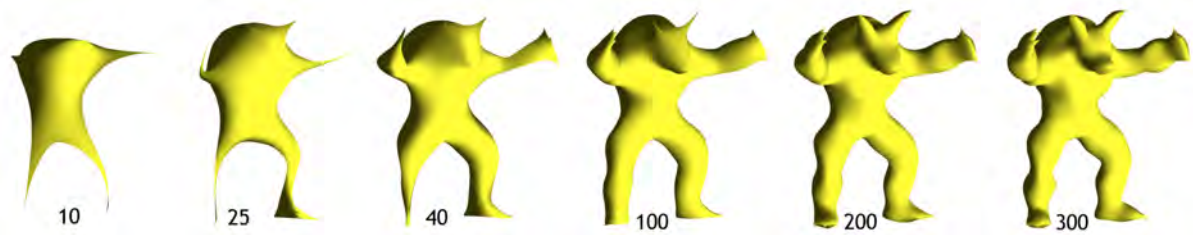


FIGURE 4.9: Reconstruction of a 3D model using the Laplace-Beltrami basis functions, showing the improved level of detail with increased basis functions (Lévy, 2006).

With the initial correspondences and the basis functions calculated it is now possible to generate the functional maps.

Consistent Functional Map Networks: For a SSM, there are a collection of shapes of the same class, therefore it is beneficial to analyze these shapes in a groupwise scenario. This research follows the functional map network approach of Huang et al. (2014); Huang and Guibas (2013) which generates consistent functional maps of a collection of shapes through joint map optimization. Functional map networks were introduced from the understanding that standard functional maps rely on clean or relatively accurate correspondences typically from feature descriptors. However, Huang et al. (2014) determined that these correspondences may not be sufficient. Cycle-consistency was introduced to rectify the noisy correspondences and produce improved results. This approach is based on the fact that, for a system to be cycle-consistent, then every function when transported along a loop, should go back to the original function.

As a SSM is generated from a collection of shapes, imposing consistency is advantageous, especially in circumstances where the shape varies significantly. Figure 4.10 shows the functional map achieved using the process of Huang et al. (2014).

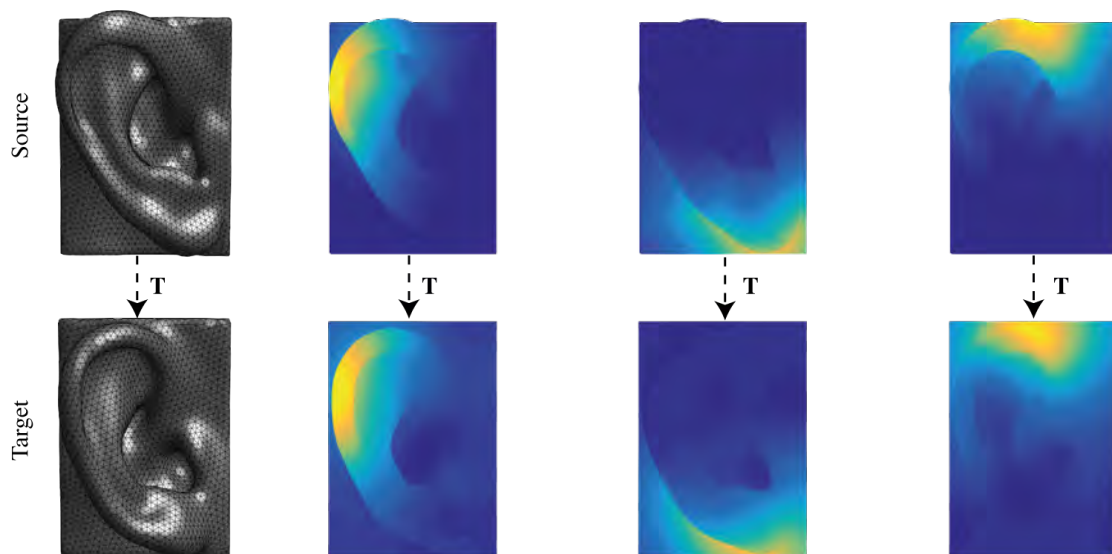


FIGURE 4.10: Showing the process of transferring a function on the source shape to the target using the calculated functional map.

Using the process by Huang et al. (2014), the functional maps are jointly optimized which instills consistency in the registration process. In Figure 4.10, the process of transferring basis functions from one shape to another using a functional map is shown.

Refinement into Point-to-Point Correspondences: Simply generating a functional map network between a collection of shapes does not allow for a SSM to be constructed. To be applicable to a SSM, the functional map network must be refined into a point-to-point correspondence. Rodola et al. (2015) uses the coherent point drift (CPD) (Myronenko et al., 2007) algorithm to generate a point-to-point correspondence from a functional map. However, this process generates a one-to-many mapping, where multiple vertices on one shape can be matched to a single vertex on another. This is not ideal for a SSM, which requires a meaningful one-to-one correspondence. If the positions of the corresponding vertices on the target surface are taken then this creates inverted faces which are not desirable in a SSM. To alleviate this issue the position of the corresponding vertices using CPD are used as an initial guess position and the mean shape is deformed to the target shape using a regularized thin-plate spline approach. This can be seen to alleviate the issue of inverted faces and one-to-many correspondences in Figure 4.11.

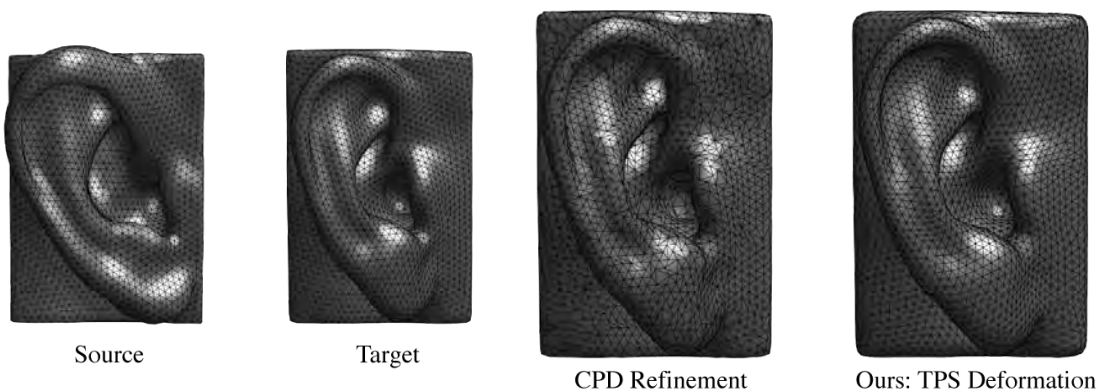


FIGURE 4.11: Consistent point-to-point refinement vs regularized thin-plate-spline: CPD refinement (Rodola et al., 2015) and our approach using regularized TPS deformation.

As can be seen in Figure 4.11, rather than taking the position of the target vertices as the final position, by deforming the source shape it creates a much more uniform face distribution. It was discussed in Section 1.1.8 that using CPD on the vertex positions, as opposed to functional maps, would not be sufficient for full 3D scan data that exhibits large surface deformations. Figure 4.12 illustrates the significance of the functional maps over the CPD method.

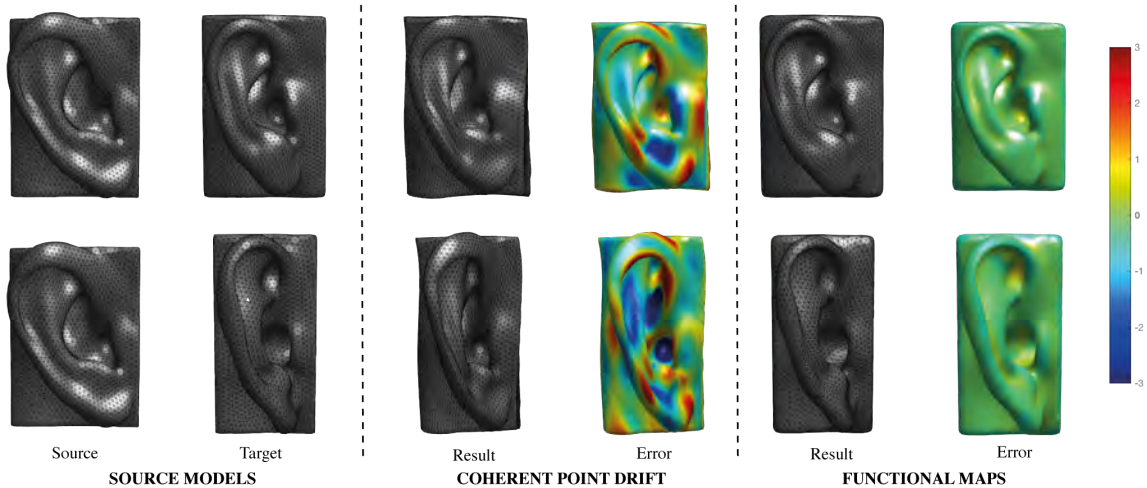


FIGURE 4.12: The registration error of the standard coherent point drift algorithm on the raw point data versus the refined correspondences using the functional maps. Scale is between -3mm and +3mm.

As can be seen in Figure 4.12, using CPD alone it is not possible to deform the source shape to accurately match the target, this could be due to the high density of the point set or the large deformation. CPD aims to physically deform the source point set whilst taking account of the overall structure. Therefore, there is a limit to how much the shape can deform and in the case of the human ear, the algorithm fails. However, in medical applications such as human organs or bones where there is a lower level of curvature or features, the CPD algorithm may perform better.

4.3.2.3 Analyzing the Registered Data using Principal Components

Once the models are completely registered it can be said that there is now a one-to-one or meaningful correspondence across each model in the dataset. What has been achieved in the previous sections is that, for each vertex on the mean shape, its position across each shape in the dataset has been recovered. From this it is possible to establish the average shape in the dataset by simply taking the mean. The mean shape is an extremely important component of the SSM and is very useful in terms of product design. Principal component analysis (PCA) models the variation in a set of variables in terms of a smaller number of independent linear combinations (principal components) of those variables, in this case the variables are the position of the corresponding points. Principal components refer to the directions where there is the most variance, i.e. the directions where the data is more spread out. The outputs of PCA are the eigenvectors and eigenvalues; an eigenvector is a principal component and an eigenvalue denotes the variance in the data in that principal component.

By taking the corresponding vertices across the models and processing them through PCA, the output will be the principal components and the eigenvalues which illustrate the variation within the dataset. Each principal component can be assigned a proportion of the variation within the dataset and can therefore be used to reduce the dimensionality. For example, if the first three out of thirty principal components constitute 96% of the total variation, then the model may be simplified or approximated by ignoring the remaining 27 components. By performing PCA, it is possible to reconstruct a set of data within a predefined standard deviation, where S is the shape, ε_{val} and ε_{vec} are the eigenvalues and eigenvectors respectively, and σ is the standard deviation.

$$S_{new} = S_{mean} + \sigma \times \sqrt{\varepsilon_{val}} \times \varepsilon_{vec} \quad (4.4)$$

For this research, it is desirable to analyze the variation in a dataset between a certain range of deviations, such as between $\pm 3\sigma$. As per Figure 4.1, by selecting $\pm 3\sigma$, a variance of 99.7% of the dataset will be covered. By varying the standard deviation it is possible to construct any number of 3D ears, however, the accuracy of which is dependent on the size, quality, and variability of the dataset. By constructing a SSM and analyzing the data in the desired standard deviation range it is possible to design a product that can be a one-size-fits-most or to develop automation algorithms for custom-fit, which is the goal of this research. The following section shows the results of the statistical shape modelling process described in the previous sections.

4.4 Resultant Statistical Shape Model of the Human Ear

By performing the process outlined in Figure 4.4, a SSM of the human ear can be constructed, which will be presented in this section. In order to construct the SSM, each 3D model from the dataset in Chapter 3 was registered to the mean shape using the functional map process discussed above. Principal component analysis (PCA) was then performed on the registered shapes to produce the eigenvectors and eigenvalues that can then be used to reconstruct any shape within the normal distribution. Using PCA there are two ways to reconstruct the data, selecting the desired principal component and selecting the level of variance. If the model contains 20 principal components, selecting a certain mode allows for the impact of individual components to be assessed. Alternatively, a level of variance can be set, for example 95%, and the number of principal components that amount to this variance are used.

4.4.1 Modes of variation of the Statistical Shape Model

By processing the 3D ear dataset in Figure 4.14, it can be seen that the first principal component accounts for 29.6% of the variation in the dataset, the second principal component accounts for 12.4% and the third component takes just 10.7%. Which cumulatively amounts to 52.8%. To account for 95% of the variation the first 27 principal components would be required. The full cumulative variance of the principal components can be seen in Figure 4.13.

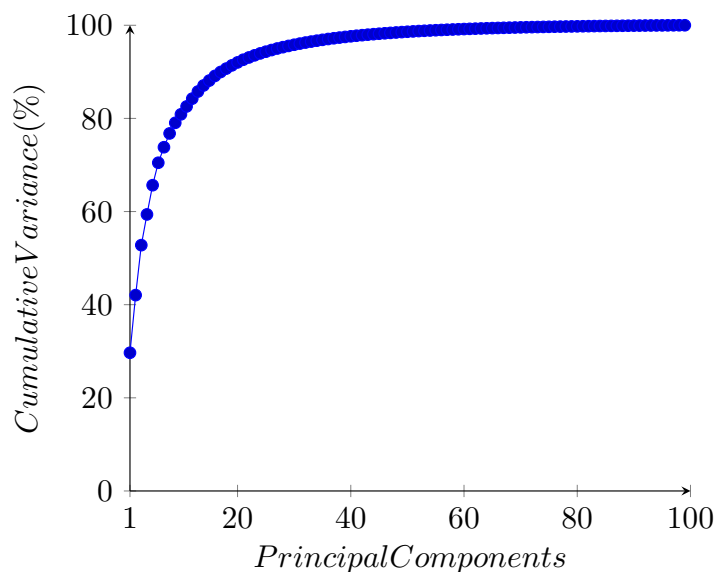


FIGURE 4.13: The cumulative variance of the principal components with 95% variance reached after 27 principal components.

Figure 4.14 shows the first three modes of variation for these principal components between $\pm 2\sigma$.

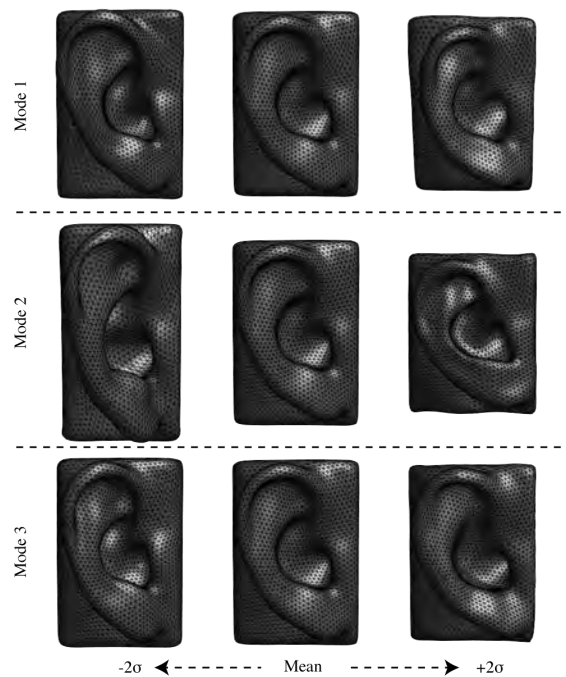
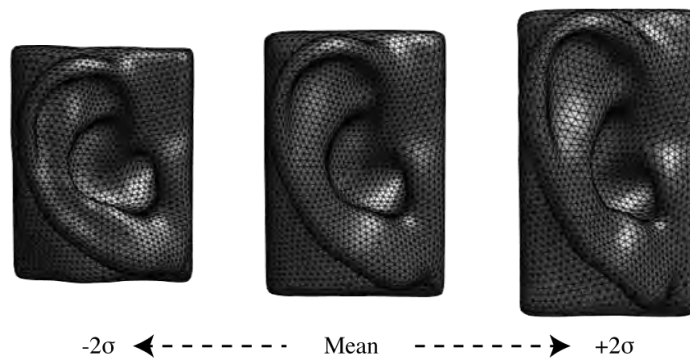


FIGURE 4.14: Statistical shape model of the human ear showing the individual modes of variation between -2σ and $+2\sigma$ standard deviations.

4.4.2 Selecting desired variance of the Statistical Shape Model

Figure 4.14 shows the individual modes of the SSM. However, the principal components can also be summed so as to account for a set level of variance. Figure 4.15 shows $\pm 2\sigma$, accounting for 95% of the total variance. In comparison to Figure 4.14, the shapes of the model show to account for scale and shape changes in the ear.

FIGURE 4.15: Accounting for 95% of the variation within the dataset between -2σ and $+2\sigma$ standard deviations



The SSM consists of 5000 points and 10,000 faces. However, the process used is relatively invariant to the density of the pointset, the only disadvantage is the increased computational cost.

4.4.3 Variational Analysis of the Human Ear

The benefit of the SSM is the ability to analyze the variance within the dataset. Traditionally, variance is measured in 2D through the use of anatomical landmarks. This variance is then used by designers through a mathematical table that establishes the planar variation between landmarks. However, now that the dataset is in 3D it is possible to establish a more visual presentation of the variation that is analogous to the 3D computer aided design approach to product design. By taking the mean shape established in the previous section it is possible to visualize a scalar field on the surface of the shape that is representative of the distance between the mean shape and the selected standard deviation. The colour fields, in Figure 4.16 and Figure 4.17, represent signed distances measured in millimetres.

FIGURE 4.16: The distance from the mean shape to $+2\sigma$, visualized as a scalar field on the mean shape. The distances are in millimetres.

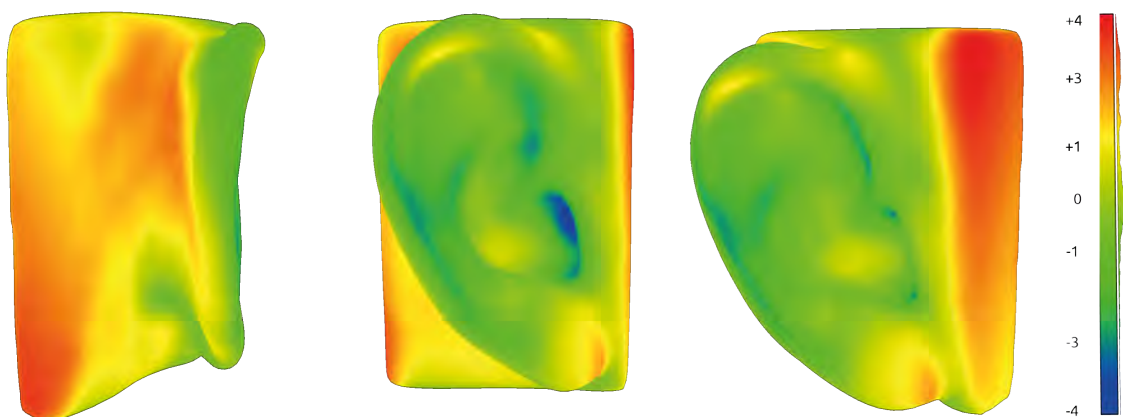
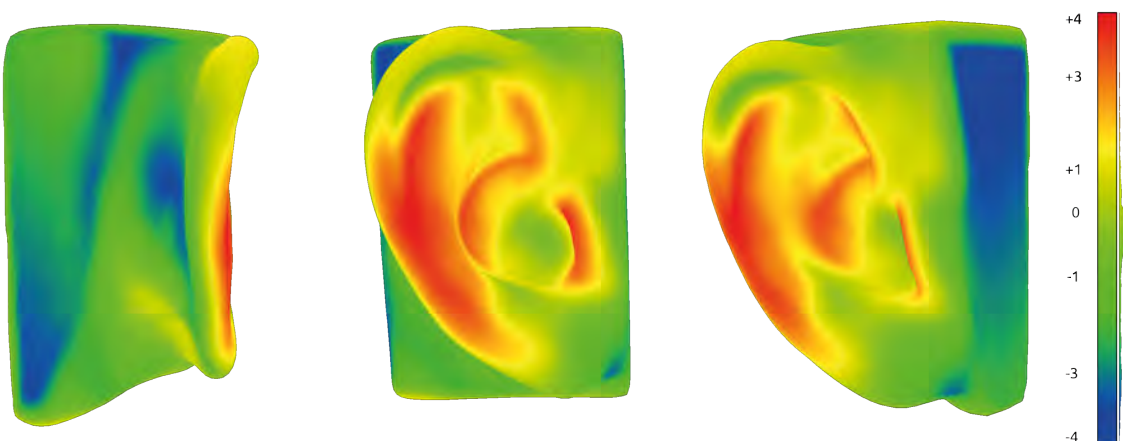


Figure 4.16 shows the distribution of distances on the surface of the mean shape. As can be seen, these distances are representative of the distance from the mean shape to the $+2\sigma$ deviation in Figure 4.15. The scale is in the range of $\pm 4\text{ mm}$. In the inner ear region the difference is relatively uniform aside from the entrance to the ear canal which exhibits a large deformation. The majority of deformation, for this deviation, is behind the ear with the angle of protrusion of the ear increasing. By performing the same analysis using the -2σ model in Figure 4.15 the scalar field in Figure 4.17 is established.

FIGURE 4.17: Distance from the mean shape to -2σ deviation, visualized as a scalar field. The distances are in millimetres.



Comparatively, Figure 4.17 contains the majority of variation in the inner ear region, as opposed to the Figure 4.16, which is primarily behind the ear.

4.5 Discussion

The importance of the SSM was established in the introduction to this chapter and the process for generating the SSM defined in the following sections. The goal of this research was to establish the base variance within a given range of 3D ears in order to answer the research question:

How can we statistically analyze the full 3D ear scan data, without the use of landmarks?

The research question was then broken down into several requirements that were required to generate a SSM using algorithms that non-rigidly determine a groupwise, dense correspondence without relying on landmarks. It can now be determined that this goal has been achieved, using a combination of technique that is relatively unique to our knowledge. The SSM process that was created is invariant to pose and deformation, robust to large point densities, and can also be adapted to incorporate incomplete data by following Rodolà et al. (2016). The process to generate the SSM is also completely automatic. While it was required to pre-process the data in order to uniformly distribute the vertices and faces on the mesh, the process can still be considered dense.

4.5.1 SSM Construction Process

The SSM process can be considered state-of-the-art in terms of registration accuracy and flexibility. Figure 4.12 shows a comparison between the functional map framework used in this research and the standard point-to-point matching using coherent point drift (CPD), which demonstrates the clear advantage of functional maps for this complex shape. In terms of quantitative analysis, the geometric reconstruction error can be seen in Figure 4.12 and for the functional maps is relatively even between $\pm 0.5mm$. In terms of processing time the method requires iterative refinement which is computationally expensive, and takes approximately 30 minutes for a dataset of 20 models. However, this is not optimized, using GPU or cloud processing there is the potential to reduce this time further. The chosen SSM process has valuable properties, that to the best of our knowledge, are not seen in any other previously reported SSM process. The unique features include invariance to pose, large deformations, and high density point sets. The joint optimisation of the functional maps also establishes consistency in the registration process. The main difficulty with the established functional map registration is the necessity to refine the functional map into a point-to-point correspondence, which is the main processing bottleneck. Following, Boscaini et al. (2014) there is the potential to use the functional maps without having to refine the point-to-point correspondence by using the functional map to deform the source shape to match the target. However, using the process outlined here, the requirements have been fulfilled and it was decided to proceed to the next stage.

4.5.2 SSM of the Human Ear

From Figure 4.15 and Figure 4.14, the SSM of the human ear can be seen. Overall the quality is very high and is on a par with the available state-of-the-art seen in Figure 4.2. The SSM of the human body consists of 6449 vertices in total, however, for the human ear SSM constructed in this research, the density is 5000 points and contains considerably more detail than the available model. The SSM construction process is invariant to the density of the input point

set, which means that the algorithm will be able to process a dataset of high density with similar quality with the only disadvantage being the increase in processing time.

Using the functional map algorithms, the natural variations in shapes of the human ear can be taken into account. From Figure 4.12 it can be seen that when compared with standard point-to-point CPD, the functional map registration of this research is able to generate a near exact match for models with large surface deformation. The colour-maps represent the distance between the deformed source shape and the target shape. CPD fails to converge to the target shape as can be seen through the large colour variation on the surface in the range of $\pm 3\text{ mm}$. Using the same scale it can be seen that the functional map based registration recovers the target shape with a relatively uniform surface registration error.

From Figure 4.16 and Figure 4.17, the distance between the mean shape and $\pm 2\sigma$ can be visualized on the surface of the mean shape as a scalar field. It was discussed previously, that by using a 3D SSM it is possible to overcome the limitations of 2D landmarking and anthropometrics by using the 3D variance in shape as a means to guide the design process in a way that is more compatible with the way in which designers work. By using the 3D scanning system developed in Chapter 3 and the SSM processing code from this chapter, it is possible to remove the complexity in generating SSMs and make 3D anthropometrics viable for industries or designers to inform the way in which they design products.

4.5.3 SSM Evaluation

Without a ground truth dataset it is difficult to quantify the accuracy of the SSM and also there is no point of comparison as this is, to the best of our knowledge, the first application of functional maps to SSM. Davies et al. (2002) introduced generic evaluation criteria for SSM's which are Generalization Ability, Specificity and Compactness. The generalization ability measures a model's ability to represent unseen instances of the dataset and is typically assessed through a leave-one out test. Specificity measures a model's ability to generate instances of the dataset that are similar to those in the training set which means to test the SSM by using the principal components to generate a shape that is close to one in the dataset and compare the difference. Compactness measures a model's ability to use as few parameters as possible to cover the same variance and is typically measured as the cumulative variance. These parameters depend on the quality of the dataset more so than the quality of the registration. The primary interest of this research is the feasibility of using a 3D SSM to guide the mass-customization of in-ear devices, with the main concern being the ability to create a SSM from the full 3D scan data. Following the steps in Figure 4.4, it can be said that it is possible to create a SSM from 3D scan data. As the dataset used for testing consists of only 100 models, a larger dataset would be required to yield good results for generalization, specificity, and compactness.

4.5.4 Limitations of the SSM process

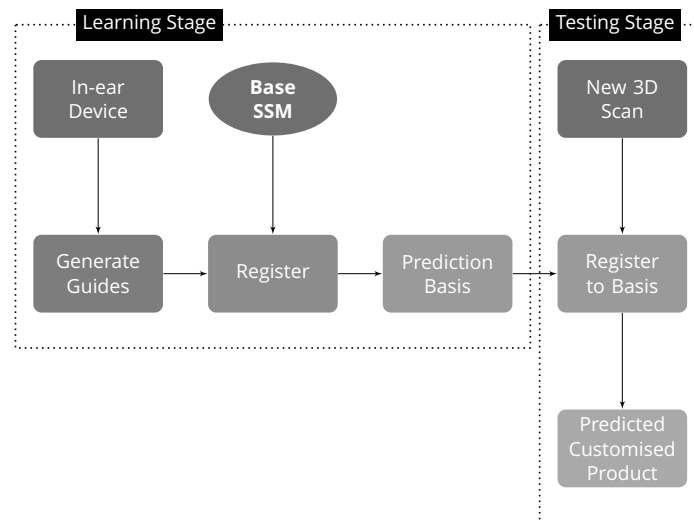
While the process in Figure 4.4 has successfully created a SSM model of the human ear and achieved the requirements set out in Section 4.2, there are limitations. Recovering the point-to-point correspondences from the functional map registration is computationally expensive and potentially unnecessary. Research by Boscaini et al. (2014) has shown that, rather than recovering the point-to-point correspondence, it is possible to deform the source shape to match the target using the functional maps and basis functions. While soft correspondences would still be required to generate the functional map, the method by Boscaini et al. (2014) would alleviate the necessity to refine a point-to-point correspondence from the functional map and would allow the functional map framework to be self-contained. As discussed in Section 4.3.2.2, refinement of the functional map to a point-to-point correspondence could result in a one-to-many mapping, by self-containing the functional map framework it prevents this issue.

The necessity to pre-process the the input data in Figure 4.5 could be inferred as a limitation due to the necessity to alter the input data. However, by distributing the faces and vertices on the surface it improves the overall registration process while maintaining the surface features. The reduction in point density also improves the overall computational time by removing redundant information. For a large database the processing time can be significant, however, due to the iterative nature of the correspondence refinement procedure there is currently no apparent alternative. By using more powerful GPU or cloud processing the construction time can be reduced. Even though the processing time is very high it only needs to be performed once. All future use of the SSM uses Equation (4.4) to generate a new 3D shape from input 3D scan data, function of which is discussed in Chapter 4.

4.5.5 Applications to the goal of this research

It was discussed at the beginning of this chapter that the SSM was needed to generate any shape along the normal distribution (see Figure 4.1). This is a very important concept for the overall goal of this research which is to automate the process of generating custom-fit in-ear devices. This research proposes the automation pipeline revolving around the SSM, shown in Figure 4.18.

FIGURE 4.18: Concept of this research showing the use of the constructed SSM as the base for a prediction framework of the customized shape.



The concept here is to use the SSM as a prediction of the overall shape of the in-ear device. The SSM encompasses the variation of the given population, therefore, given a new shape it is possible to predict where in the normal distribution that test shape lies, which is the foundation of morphable models (Bustard and Nixon, 2010). By registering an in-ear device to the SSM and then using a morphable model framework it is possible to predict the customised shape of the input device. Also, by incorporating rules detailing how the surface deforms allows the user to create functional products. The development of rules will be illustrated in the following chapter.

4.5.6 Future Research

While this research has achieved the initial requirements set out in Section 4.2, during the process of constructing the SSM, additional gaps in current knowledge were seen and there are still areas of further development that are available for future research.

Extending the SSM: One of the disadvantages of the SSM is the necessity to register all of the data to the mean. If a new model is added to the dataset it would be required to re-process the entire dataset which is a time consuming task. The algorithms developed in this research completely automate the task but it would still require computational resources. Future research could explore the development of algorithms that allow for additional models to be added to the dataset without the need to re-register the entire dataset. Research by Pereañez et al. (2014) has shown the ability to merge existing SSMs to enhance the overall informativeness. Future research would aim to extend this to allow for singular models to be added to the existing SSM. However, the results achieved in this chapter are sufficient for the current objectives.

Evaluating comfort: The SSM has been developed as a means to custom-fit in-ear devices to an individual's 3D scan data. The aspect of what metrics can be used to derive comfort from the SSM is not being discussed due to the subjectivity in the users perception of comfort. Several questions remain such as, *what accuracy is required for the SSM to give a comfortable feeling for in-ear devices?*.

4.6 Conclusion

The initial goal of this chapter was to generate a methodology to analyze the variance in the given dataset, that will be used in the remainder of this research. At the outset, requirements were established to guide the development of the statistical shape modelling (SSM) algorithms, which were dense, groupwise, non-rigid, and non-landmark based. As a result, a state-of-the-art framework for SSM using functional maps was developed which meets these requirements. This was tested on a dataset of 100 models of the human ear consisting of 5,000 vertices and 10,000 faces. The results have shown that the framework exhibits a significant improvement in terms of registration quality for models with large surface deformation. The main advantage of the algorithms developed here, is that the registration is invariant to pose, deformation, and high density point sets. The process to construct the SSM is also highly automated requiring the tuning a few parameters that control the degree of deformation, smoothness and dimensionality of the basis. It can now be said that the original goal of establishing the base variance has been accomplished and the remainder of the thesis will use this SSM for the overall goal:

How do we use already fully functional CAD designs as opposed to performing the processes after customization?

Chapter 5

Deformation Constraints in CAD Designs to Streamline the Automation Process

In Chapter 4 the proposed automation framework was outlined (see Figure 4.18). The objective of this chapter is determine how one can use the statistical shape model (SSM) as an input into a parametric/deformable model of the in-ear device. This means that when a new 3D scan is registered to the SSM it generates a deformation field which is transferred to the product, using this deformation field as a guide the CAD product is deformed into the customized shape. The cornerstone and novelty of this approach is the use of constrained 3D mesh deformation techniques guided by the change in shape from the SSM to the input 3D scan. By incorporating 3D mesh deformation techniques it allows the user to control how the product deforms such that functional or critical regions in the CAD product can be preserved. Contrary to the literature in Section 1.1.5, where the majority of automation systems use rules consisting of if-then-else statements in order to construct the functional product in a generative fashion, this research begins with the CAD designed product and applies deformation constraints such that the in-ear device's shape can adapt to an individual's 3D scan.

It is important to understand the distinction between a rule and a constraint in this research. Here a customized product being generate by a set of rules is being perceived as a step-by-step process in which raw 3D scan data is transferred into the final shape through a process of landmark detection and rule-based detailing and modelling (see Figure 1.15 and Figure 1.16). For example, if a raw 3D ear impression is being processed, a rule may be;

```

1 if Angle between Landmark A and Landmark B > 30 then
2   |   Insert Cutting Plane;
3 else
4   |   Skip this cut;
5 end

```

Any number of rules can be put in place to generate a final product from raw 3D scan data, especially when the complexity of the product increases. The use of rules relies on the accuracy of the detected landmarks and the user's knowledge of the anatomy of the target object. A constraint, on the other hand, does not require complex definitions of angles between points. For this research, a constraint can be thought of as a restriction to the deformation process. This research uses the deformations from the SSM to guide how the CAD product can deform. Without any constraints, the CAD product would be free to fully conform to the SSM. By adding constraints it allows for control of this process. The benefit of this approach is that, regardless of the deformations received from the SSM, the system will always constrain the regions defined by the user. To assist the reader, the following terminology is introduced and used throughout this chapter:

Constraint: A constraint, in this case, is a segmentation of the CAD design into relative areas such as form-preserved, free-moving, or completely-fixed, to name a few.

Form region: A form region is the area of that a constraint is applied to or in other words, it is the area that is segmented to apply a constraint.

Local rotation: The local rotation, used throughout, is referring to the normal to the surface which is preserved during the deformation process.

Preservation: It is important to differentiate between the two forms of preservation used in this chapter. The first relates to the preservation of local rotations and volume during the deformation. In this case, preservation is similar to conservation, where minimum change is allowed but not explicitly enforced. The second preservation, is the explicit preservation of form, in this case, it is enforced and there is no change in shape allowed.

Laplacian mesh deformation: This is the basis by which the 3D mesh deformation is generated. In contrast to traditional Cartesian coordinates which only rely on the spatial location of each point, Laplacian or differential surface representations carry more information about the local shape of the surface, and the size and orientation of local details. For more information on Laplacian mesh processing the reader is directed to Sorkine (2005).

By applying constraints to the CAD design, when the SSM deforms and the deformation field is transferred to the CAD design, the 3D mesh deformation algorithms deform the CAD design while taking account of the constraints. With this framework, the only extra information other than the SSM and the 3D CAD design are the constraints for how the CAD design can deform to match the 3D scan data. In order to maintain functionality of the product design, these constraints determine the rigidity and final positioning of the customized mesh elements. The theory and use of these constraints are discussed in the following sections and a practical application is explored in Chapter 6.

5.1 Sample 3D Design for Testing the Constrained 3D Mesh Deformation

To test the algorithms developed in this chapter against the available researched techniques, the 3D test mesh shown in Figure 5.1 will be used.

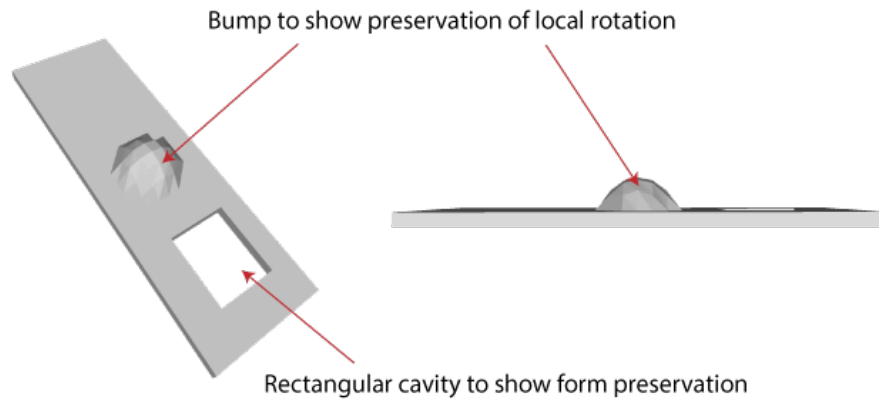


FIGURE 5.1: Sample 3D mesh design to test the mesh deformation algorithms, designed to have a hemispherical bump to evaluate the effective preservation of the local rotations and a rectangular cavity to explore preservation of the form.

With the test mesh in Figure 5.1, the aim is to show the preservation of the local rotation on the hemispherical bump and the explicit form preservation of the rectangular cavity.

5.2 As-Constrained-As-Possible (ACAP) 3D Mesh Deformation

Part of the novelty of this research is the use of deformation techniques to fit a CAD design to the new 3D scan. Therefore, how the surface is deformed becomes a critical component. This research introduces the As-Constrained-As-Possible (ACAP) 3D mesh deformation algorithm that allows for realistic and local rotation preserving deformations whilst preserving user-defined critical features. ACAP extends the As-Rigid-As-Possible (ARAP) (Sorkine and Alexa, 2007) energy minimisation framework for surface deformation to include both volume and form preservation through the use of user-defined constraints on the input 3D mesh.

5.2.1 ACAP Mathematical Background

ACAP 3D mesh deformation follows two main steps, namely the approximation of the local rotations for the vertex cell and the estimation of the vertex positions by solving a Laplacian system. The iterative estimation for the local rotations follows the same approach as Sorkine and Alexa (2007), however, the novelty of ACAP lies in the variation of the Laplacian system which has been altered to include user-defined constraints which allow for form and position constraints to be added. Similar to As-Rigid-As-Possible (Sorkine and Alexa, 2007), ACAP revolves around the concept of directly minimizing the stretching and/or bending energy to achieve a realistic surface deformation that preserves local detail (i.e. local rotations). To preserve local rigidity, the surface is split into overlapping cells and the transformation in each cell is minimized to be as-rigid-as-possible. A cell, in this case, covers the triangles incident upon a vertex, or the one-ring neighbourhood of a vertex, as depicted in Figure 5.2, and is denoted by $N(i)$.

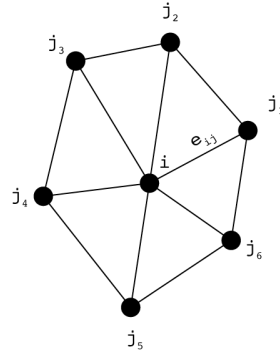


FIGURE 5.2: A one-ring neighbourhood of a vertex, i , showing the edge length, e_{ij} , to connected vertices, j .

Therefore, given the cell C_i corresponding to vertex i that deforms to C'_i , if that transformation is perfectly rigid there exists a rotation R'_i such that:

$$p'_i - p'_j = R_i(p_i - p_j), \forall j \in N(i) \quad (5.1)$$

The letter p , in this case, is referencing the position of vertex i relative to vertex j . It should be noted that $(p_i - p_j)$ is essentially the edge length e_{ij} , therefore, the ARAP surface deformation tries to preserve the edge length of the mesh. This then leads to an energy function that is at a minimum when the rigidity is maximized:

$$E(C_i, C'_i) = \sum_{j \in N(i)} w_{ij} \|(p'_i - p'_j) - R_i(p_i - p_j)\|^2 \quad (5.2)$$

The vertex weights, w_{ij} , are selected by the user and determine how the surface deforms. Selection of the vertex is discussed in Section 5.2.1.2. By summing up the energy functions from all cells, a global energy functional is obtained:

$$E(S') = \sum_{i=1}^n w_i E(C_i, C'_i) = \sum_{i=1}^n w_i \sum_{j \in N(i)} w_{ij} \|(p'_i - p'_j) - R_i(p_i - p_j)\|^2 \quad (5.3)$$

This energy functional is non-linear and depends only on p'_i , the new positions of the vertices. To solve this non-linear system, a two-stage optimization scheme is proposed to iteratively decrease the energy which is achieved by separating the optimization of R_i from the optimization of p'_i , specifically, given vertex positions, the optimal rigid transformation R_i is found, this is then back-substituted into the system and the optimal vertex positions p'_i are solved. This process is then iterated until a threshold or maximum number of iterations is reached.

5.2.1.1 Derivation of the optimal rotation

One of the critical components of ACAP, similar to ARAP, is the best approximation of the per-vertex rotation matrix, R_i , which preserves the local rigidity of the cell. The derivation follows the approach of Sorkine and Alexa (2007). For convenience, the edge $e_{ij} := p_i - p_j$ and similarly for e'_{ij} for the deformed cell C'_i .

$$\begin{aligned}
& \sum_j w_{ij} (e'_{ij} - R_i e_{ij})^T (e'_{ij} - R_i e_{ij}) = \\
& = \sum_j w_{ij} (e_{ij}^T e'_{ij} - 2e_{ij}^T R_i e_{ij} + e_{ij}^T R_i^T R_i e_{ij}) = \\
& = \sum_j w_{ij} (e_{ij}^T e'_{ij} - 2e_{ij}^T R_i e_{ij} + e_{ij}^T e_{ij})
\end{aligned} \tag{5.4}$$

The terms that do not contain R_i are constant in the minimization and therefore can be dropped. The equation then becomes:

$$\begin{aligned}
\arg \min_{R_i} \sum_j -2w_{ij} e_{ij}^T R_i e_{ij} &= \operatorname{argmax}_{R_i} \sum_j w_{ij} e_{ij}^T R_i e_{ij} \\
&= \operatorname{argmax}_{R_i} \operatorname{Tr} \left(\sum_j w_{ij} R_i e_{ij} e_{ij}^T \right) = \\
&= \operatorname{argmax}_{R_i} \operatorname{Tr} \left(R_i \sum_j w_{ij} e_{ij} e_{ij}^T \right)
\end{aligned} \tag{5.5}$$

Sorkine and Alexa (2007) denote by S_i the covariance matrix:

$$S_i = \sum_{j \in N(i)} w_{ij} e_{ij} e_{ij}^T = P_i D_i P_i^T \tag{5.6}$$

where D_i is a diagonal matrix containing the weights w_{ij} , P_i is the $3 \times |N(\nu_i)|$ containing e_{ij} 's as columns and similarly for P_i^T . The optimum rotations, R_i , can then be derived by singular value decomposition of $S_i = U_i \Sigma_i V_i^T$:

$$R_i = V_i U_i^T \tag{5.7}$$

up to changing the sign of the column U_i corresponding to the smallest singular value, such that $\det(R_i) > 0$. Equation (5.7) calculates the per-vertex rotation that best preserves the local rotation, i.e. normal to the surface. The per-vertex rotation is iteratively refined in the two-stage optimization process discussed previously.

5.2.1.2 Selection of weights

The selection of per-edge weights w_{ij} and per-cell weights w_i is important for making the deformation energy as robust against variations in topology as possible.

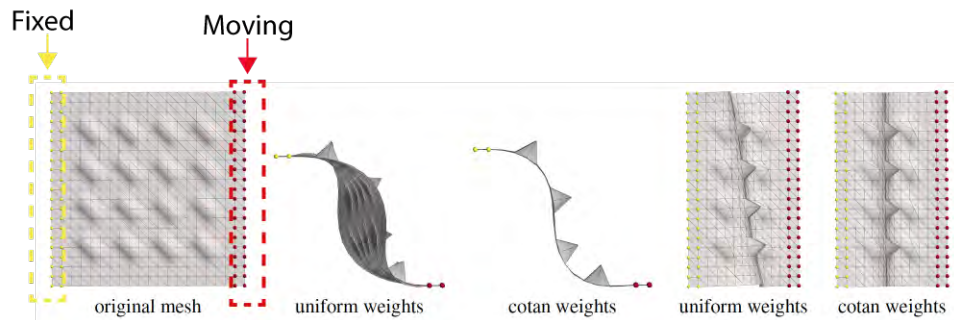


FIGURE 5.3: Test Piece Deformation: The yellow region remains fixed and the red region is deformed using uniform weights and cotan weights (Sorkine and Alexa, 2007).

Figure 5.3 shows an example of how the choice of weights can affect the deformation of the mesh under the same displacements. The selection of weights should compensate for non-uniformly shaped cells, such as coarsely meshed shapes with large triangle areas, and prevent discretization bias. Sorkine and Alexa (2007) use the cotangent weight formula for w_{ij} :

$$w_{ij} = \frac{1}{2}(\cot\alpha_{ij} + \cot\beta_{ij}) \tag{5.8}$$

From Figure 5.3 the cotangent weights provide a more reasonable deformation over the uniform weighting. In Equation (5.8), α_{ij} and β_{ij} are the angles opposite of the mesh edge (i, j) , as seen in Figure 5.4. An alternative approach is to use the area-corrected edge weights $w'_{ij} = (1/A_i)w_{ij}$, where A_i is the area of the cell C_i .

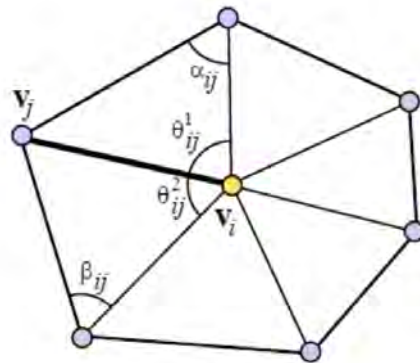


FIGURE 5.4: Cotangent weights in the one-ring neighbourhood of a vertex (Sorkine, 2005).

The ACAP process follows Sorkine and Alexa (2007) and uses the area-corrected cotangent edge weighted, and is defined as follows:

$$w_{ij} = \frac{1}{2A_i}(\cot\alpha_{ij} + \cot\beta_{ij}) \tag{5.9}$$

5.2.2 Incorporating volume preservation in ACAP

It has been discussed that ACAP 3D mesh deformation preserves local rigidity around a cell which constitutes the one-ring neighborhood of a vertex. However, while this preserves the edge length it does not the volume of the mesh. Depending on the type of object being deformed this can be a critical issue, for example, if the object being deformed is a planar surface with local detail then there is no necessity for volume preservation. However, if the object has a thickness or in the case of the in-ear device, which has a hollow region with a functional wall thickness, then it is important to preserve that volume.

Kwok et al. (2014) extended the ARAP framework to account for internal volume through the use of tetrahedral meshes. Traditionally, it is difficult to use tetrahedral meshes for surface/mesh deformation applications due to the necessity to convert between representations. However, Kwok et al. (2014) showed that a volumetric mesh, M , is compatible with the surface mesh, S , on its boundary (i.e. $\delta M = S$). The present research follows this concept of volume preservation through tetrahedral mesh generation in order to ensure that the internal volume is preserved as much as possible during the deformation stage, which is critical in the case of large deformations.



FIGURE 5.5: Tetrahedral mesh, shown in red, generated to preserve the volume of the mesh during the ACAP deformation.

Referring to Section 5.2.1, the ACAP mesh deformation aims to preserve the edge lengths of the mesh, such that the rigidity of the overall elements remains the same, ensuring a realistic deformation. However, using a standard mesh there is no means to take account of the internal volume. From Figure 5.5 (b), the original mesh when split does not have any connectivity/edges on the internal, meaning during the deformation process the algorithm will only preserve the external connectivity. While this is sufficient for standard meshes, during large and complex deformations this could result in self-intersections or failures. In Figure 5.5 (c), it can be seen that the tetrahedral mesh has the same topology as Figure 5.5 (a), but there are edges connecting the external vertices to make an internal volume. This means that the ACAP algorithm, which preserves edge-lengths, will now take account of the internal volume and prevent self-intersections during large deformations.

To generate the tetrahedral mesh the widely utilised TetGen method is used (Si, 2015). To ensure compatibility with the original surface the TetGen is restricted to not remesh the surface, meaning the algorithm will not introduce new vertices into the mesh. The outcome of this process is the original vertices and faces with another connectivity matrix that is the tetrahedrons. In regards to the ACAP process in Section 5.2.1, the tetrahedron connectivity is used in the energy minimization as opposed to the standard triangular connectivity.

5.2.3 Form Preservation for ACAP

As this research aims to preserve the shape of important features of a design, there must be the means to preserve or limit the deformation in user-defined areas. To allow for user-defined constraints the second stage of the ACAP process, solving the Laplacian system for position estimation, is replaced with a constraint-based solution with a variety of user-defined constraints which will allow for a multitude of possible designs. For ACAP, the process of Masuda et al. (2007) is adapted for form preservation with local rotation and volume preservation.

5.2.4 Form Preservation using constrained least squares Laplacian

ARAP mesh deformation minimizes the energy such that the edge-lengths of the mesh are preserved. The advantage of this approach is that it will always converge to the closest possible solution. However, this does not guarantee that the form will be preserved. As this research requires that form regions be explicitly preserved so that electronic components can be fitted, the solving of the Laplacian system is adapted to explicitly preserve form regions.

Masuda et al. (2007) use a Laplacian mesh deformation approach with rotation and form constraints that explicitly preserve pre-determined regions of a mesh. However, the difficulty with their approach is that the deformations have to be provided as quaternion (axis, angle) rotations as opposed to translational. This research uses a deformation field obtained from the

morphing of a statistical shape model (SSM), which is a three-dimensional translational deformation field. Therefore, the work of Masuda et al. (2007) is not directly compatible with this approach. Masuda et al. (2007) aim to initiate the deformation with a rotation and translation provided by the user which is then interpolated over the surface. The present research adapts the approach by Masuda et al. (2007) by incorporating an iterative rotation estimation such that the deformation field can be directly used without having to explicitly provide per-vertex rotations. Therefore only Equation 11 (b) from Masuda et al. (2007) is relevant.

$$p_i - p_j = s_f R(n_i, \theta_i)(p_i^o - p_j^o) \quad (i, j \in \bigwedge_F; (i, j) \in T_F) \quad (5.10)$$

Where $R(n_i, \theta_i)$ is the per-vertex rotation matrix that is interpolated over the surface such that the normals or frame of each cell is preserved. Recall from Equation (5.1), that ARAP finds a rotation for each vertex that preserves the rigidity of each cell, $p_i - p_j$. Equation (5.10) states that the difference in new position of vertex i and j in the minimum spanning tree \bigwedge_F , should be equal to the vertex rotation $R(n_i, \theta_i)$ times the difference in old position of the vertices. The scale factor, s_f , is used by the designer to vary the size of a form region, however, this is not necessary for this research. One of the important components of the method by Masuda et al. (2007) is the use of a minimum spanning tree to reduce the complexity of the least-squares solution. Given a pre-defined form region, \bigwedge_F consisting of vertices and connectivity information (i.e. faces), a minimum spanning tree is a path that traverses the surface in a minimal fashion such that repeated edges are excluded. In Equation (5.10), the spanning tree edges are represented by T_F and the faces in a form region by \bigwedge_F . An example of a minimum spanning tree is shown in Figure 5.6.

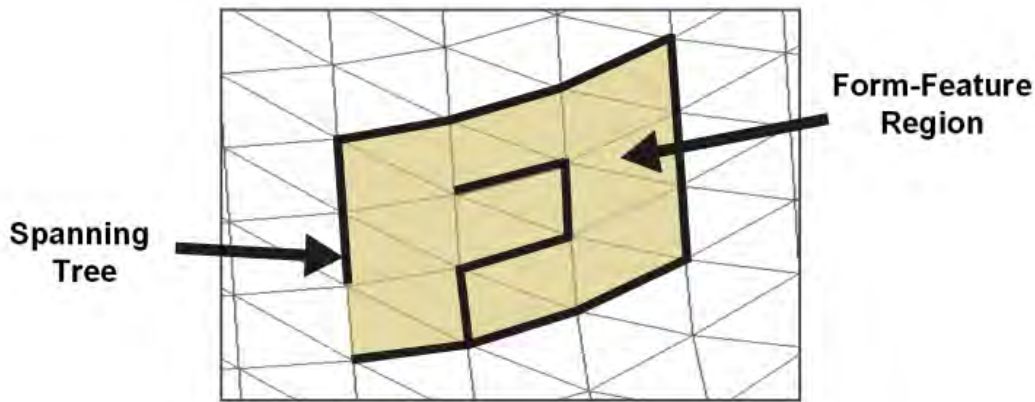


FIGURE 5.6: Spanning Tree: a minimum representation of the connectivity in a 3D mesh region such that repeated edges are eliminated in the selected region (Masuda et al., 2007).

To explicitly preserve a form region without having to define rotations for cells, this research takes the per-vertex rotation matrices from Equation (5.7) of the ACAP process and adds into Equation (5.10). Taking the rotation matrices from the ACAP process, a minimum spanning tree is generated from the user-defined form region. A Laplacian least-squares system is then solved using Equation 5.10 as soft constraints, such that the system becomes:

$$Mv' = \tilde{b}$$

$$M = \begin{bmatrix} A^t A & C^t \\ C & 0 \end{bmatrix}, \tilde{b} = \begin{bmatrix} A^t v \\ d \\ \cdot \end{bmatrix}$$

where A is the cotangent Laplacian matrix L_D . v' is the new vertex positions, $A^t v$ are the delta coordinates of the mesh, and d are the constraints from Equation (5.10). The critical components here are the C and d matrices which constitute the form matrices. Taking vertex i with corresponding edge vertex j , to preserve the form region as per Equation (5.10) the difference in position $p_i - p_j$ is taken, hence C_{i-j} becomes:

$$C = \begin{bmatrix} C_{i-j} & 0 & 0 \\ 0 & C_{i-j} & 0 \\ 0 & 0 & C_{i-j} \end{bmatrix} \quad (5.11)$$

$$C_{i-j} = (\ddot{0} \overset{i}{1} \ddot{0} \overset{j}{-1} \ddot{0})$$

Equation (5.11) represents the left hand side of Equation (5.10), where the position of the vertices are constrained. Similarly, for the d matrix, the constraints become:

$$d_{i-j} = R_i(v_i - v_j) \quad (5.12)$$

Equation (5.12) is the right hand side of Equation (5.10), notice that the scale factor s_f has been removed as it is not relevant to this research. By adding these constraints to the Laplacian system such that the M matrix is constructed, the form preserving mesh deformation can be performed using least squares, such that:

$$v' = M \setminus \tilde{b}$$

By following the process in Figure 5.7, the mesh is deformed to fit the user constraints and can preserve both volume and form in a simple and interactive manner.

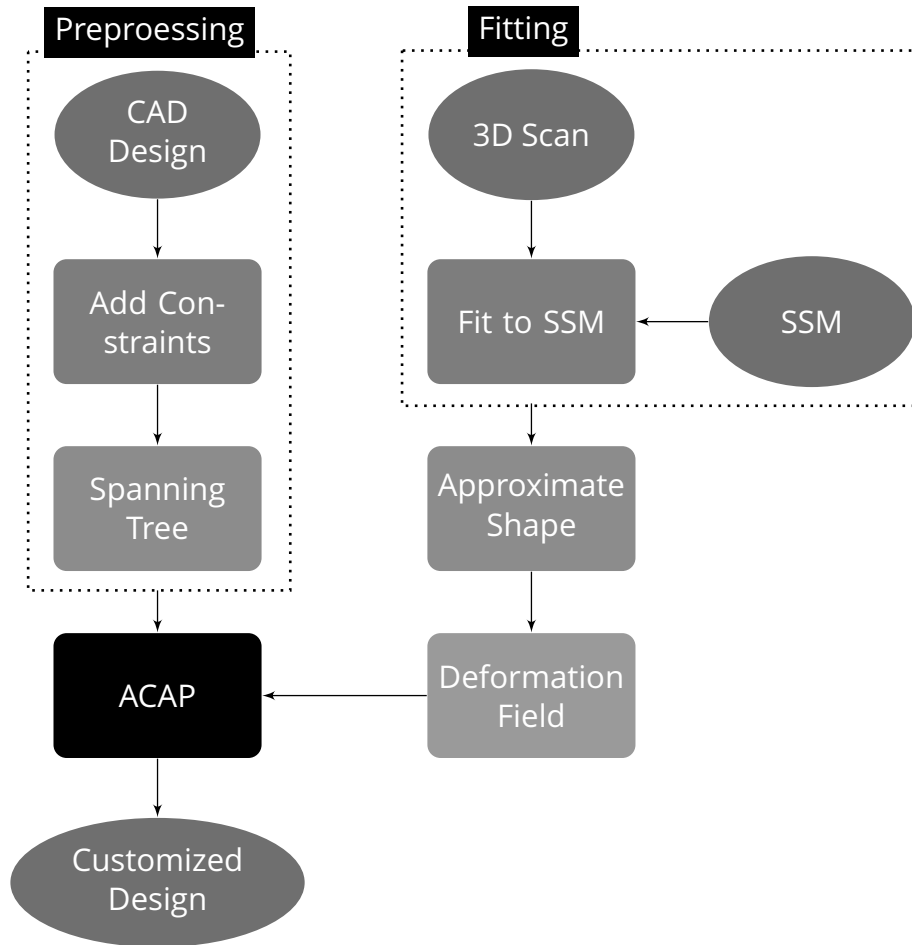


FIGURE 5.7: Process for generating a customized in-ear device from CAD data using the ACAP 3D mesh deformation process.

The following section shows the advantage of this process against standard ARAP deformation.

5.3 ACAP 3D Mesh Deformation Applied to the Test Mesh

To illustrate the ACAP approach, the sample component from Figure 5.1 is deformed as set out in Figure 5.8.

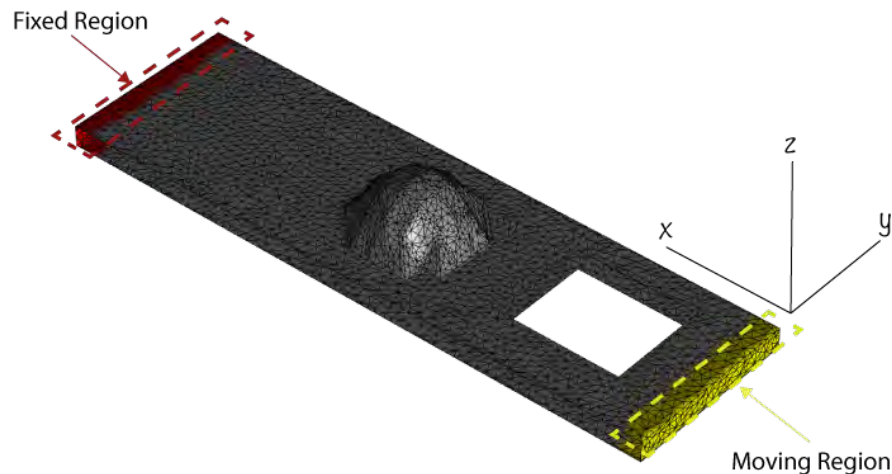


FIGURE 5.8: Test Piece Deformation: the red region remains fixed and the yellow region is deformed 0.5mm in the X-axis, and -1mm in both the Y and Z axes.

To showcase the importance of the addition of the volumetric information, the deformation is shown with the original ARAP deformation (Figure 5.9), the volume preserving ARAP (Figure 5.10), and the full ACAP process (Figure 5.11).

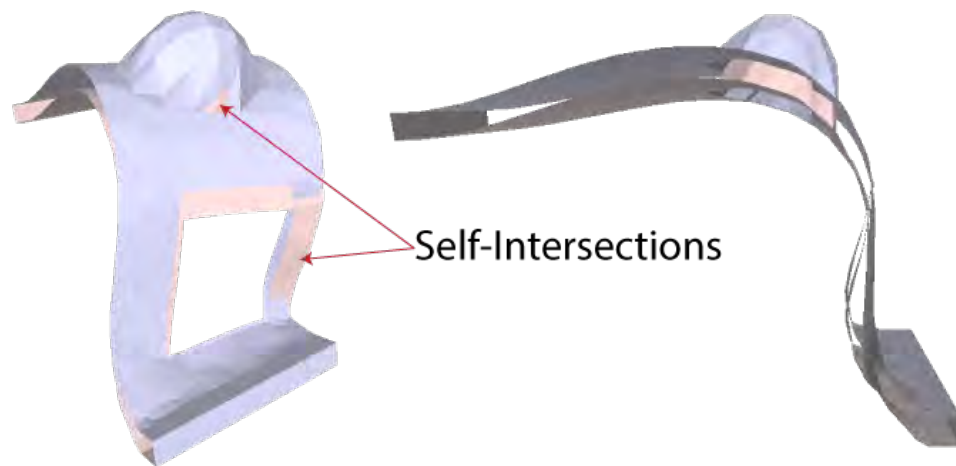


FIGURE 5.9: ARAP mesh deformation showing the self-intersections (pink) that arise due to the lack of volume information.

As can be seen in Figure 5.9, using the original ARAP system, the process has no way to identify internal volume. The algorithm simply aims to minimize the edge-lengths of adjacent vertices without taking into account the volume of the mesh. This is clearly shown by removing all internal edges of the model as the deformation exhibits self intersections, which can be seen as variations in colour on the mesh. The proposed solution is to convert the original triangular mesh into a tetrahedral volume as per Kwok et al. (2014). By restricting the TetGen algorithm to not remeshing the surface, the original vertices and faces of the mesh are maintained and the additional tetrahedral connectivity information is passed through the ARAP process, as shown in Figure 5.10.

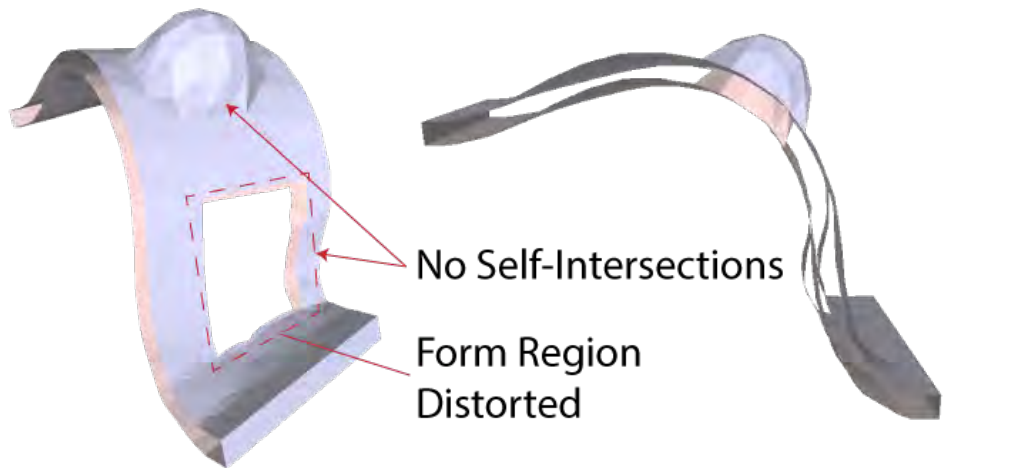


FIGURE 5.10: ARAP process including the volume information in the form of the tetrahedral connectivity, showing that self intersections are avoided, but the form region is distorted.

By adding volumetric information, the ARAP system is able to preserve the internal volume and prevent self-intersections. This is particularly important because as the complexity of models increases, it is imperative that self-intersections do not occur. However, by analyzing the form region it can be seen that it has become distorted which is not ideal for this research. It was determined that to explicitly preserve the form a post-processing stage is added that utilises the minimum spanning tree of the form region and the rotation matrices calculated from the ARAP process to determine the exact shape whilst maintaining the rotation of the original deformation.

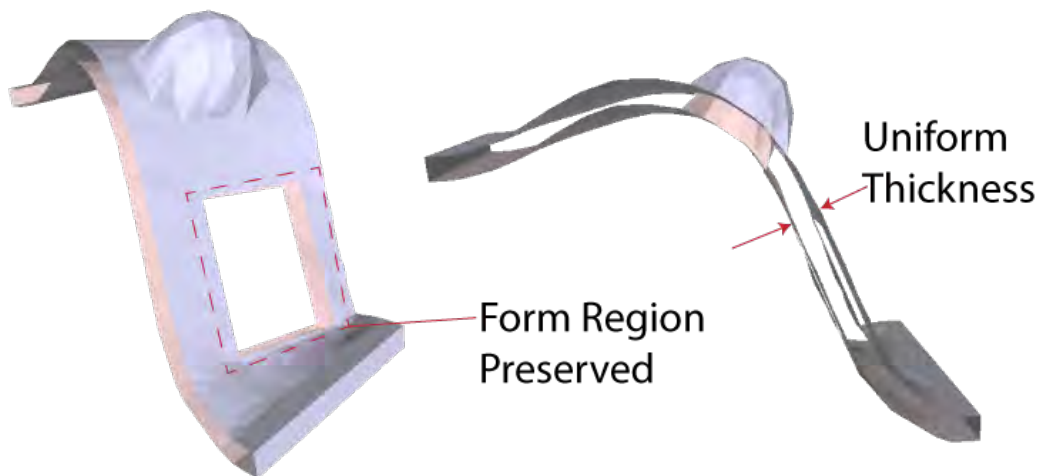


FIGURE 5.11: ACAP process showing the preservation of both volume and rotation with the critical component being the preservation of the form of the designated region.

As can be seen, both the rotation and form of the designated area are preserved. Of importance here is that the normal to the surface is preserved whilst the form regions remain the original size but follow the natural rotations of the deformation. By preserving the form region, it should be noted, that some distortion can appear on the surface due to the enforcement of the constraint. However, in practice this did not cause any issues.

5.4 Discussion

The purpose of this research is to construct an alternative approach to mass-customisation of products from 3D scan data. Contrary to the standard generative or morphometric approaches discussed in Section 1.1.5, this research opts for direct surface deformation using the SSM as the guide. By using this approach it allows the user to work with standard CAD data without the need to pre-program landmarks or cut-planes. Using a simple set of tools, discussed in this chapter, the user is able to identify form regions that preserve the functionality of a design, i.e. mounting holes for electronics or clearance holes for assemblies.

This chapter has laid out the mathematical basis for constrained mesh deformation preserving form and volume, referred to As-Constrained-As-Possible), due to the minimization of the bending energy which fits the rotations to the surface, showing its advantages over the standard ARAP process.

5.4.1 ARAP Surface Deformation

ARAP surface deformation is a widely used technique that provides realistic 3D mesh deformation without the need to provide per-vertex rotations. The two-stage optimization allows for the per-vertex rotations to be fitted such that the normal to the surface is preserved. However, as discussed, the standard ARAP process has no way to preserve internal volume and can often lead to self-intersections depending on the shape of the object being deformed. This can be clearly seen in Figure 5.9, when the sides connecting the two surfaces of the test piece (see Figure 5.1) are removed there is no way for the algorithm to know the internal volume and therefore self-intersections occur. This is detrimental to the applicability to this research as self-intersections or inversions will cause the mesh to become un-printable, meaning it will not be possible to 3D print the output of the process, and the shape may not fit the 3D scan as expected.

5.4.2 ACAP 3D Mesh Deformation - Preserving Volume and Form

As the standard ARAP is not fully applicable to this research it was determined that volume and form preserving extensions were required. Volume preservation is required such that no self-intersections occur during large deformation or with complex parts and that the overall thickness of the part remains the same where possible. As the goal of this research is to deform a functional part it is imperative that regions that have an engineered purpose remain within tolerance such that components can be fitted to the part or the part can fit within the specified region, therefore form preservation is critical.

Kwok et al. (2014) introduced a process to preserve the internal volume during the ARAP process by using a volumetric tetrahedral mesh. In their approach, the conversion between standard triangular and tetrahedral mesh is expressed on the boundary of the tetrahedral. However, for this research it was determined that by restricting the TetGen algorithm to not remesh the surface, the original vertices and faces of the triangular mesh are maintained and the generated set of tetrahedral connectivity information is used in the minimization process. This therefore allows the ARAP system to take account of that edge-length, thus preserving the internal volume as seen in Figure 5.10.

To contain volume, rotation and form preservation, the ACAP process was developed, which allows the user to add constraints to the Laplacian system such that form preservation is achieved. These constraints are simple and interactive, giving the user the ability to manually select critical regions of the design which are then automatically processed into a minimum spanning tree (see Figure 5.6). By doing this the algorithm is able to preserve the region such that it rotates with the natural rotations of the surface but does not deform. This is an ideal

scenario for in-ear device design as the form region should conform with the deformations of the SSM. It is also possible to add further constraints to the system which control the final positioning of the form region, such as restricting the motion to a certain normal angle, or following a direction to a line. However, it will be shown in Chapter 6, that for in-ear device design the form region preservation in Figure 5.11 is sufficient. This will be demonstrated by applying the full algorithm in a practical scenario with the design and testing of an in-ear device.

5.4.3 Advantages of the ACAP 3D Mesh Deformation

The advantage of the ACAP process is that it will always converge to form that is as close as possible to the desired form, due to the minimization approach. This can give information on the limitations of the design or topology of the mesh. For example, with the human ear, there is a significant amount of variation in terms of shape between extremes of the population (see Chapter 4). Therefore, there may be situations where the algorithm cannot physically deform the mesh to fit the desired target, which will give information on the limitations of the design. The ACAP process is also relatively simple and can be extended to include further constraints relating to the final positioning of the form region. By varying the edge weights it is also possible to change how the surface deforms which gives the user extra control for specialized applications, i.e. specifying custom edge weights to generate a certain deformation that may be related to material properties (e.g. Young's modulus).

5.4.4 Further Work

While this process has shown to provide acceptable results for this research, a full framework incorporating more surface controls would be ideal to cover all possible designs other than the inner-ear. Further work could also include exploration of the per-vertex weights to incorporate material properties into the deformation process.

5.5 Conclusion

The aim of this chapter was the development of a method for deformation of a 3D mesh that preserves both the internal volume and pre-defined form regions. The ACAP 3D mesh deformation algorithm was developed to allow the user to define form regions on the 3D mesh which will then be preserved during the deformation whilst still moving with the rotation of the surface. This is an ideal scenario for in-ear devices as the range of deformations can be extreme, as seen in Chapter 4. The novelty of the ACAP process is the ability to begin the customization process with a functional CAD design, and deform the model in a constrained manner, such that the model is still functional and directly 3D printable after the customization process. The ACAP process is also extendable, meaning new methods for constraining the surface can easily be added to the system, thus creating a full design and customization framework.

As the overall goal of this research is to use mesh deformation techniques for customization, this chapter has provided a cornerstone for the success of this approach. The following chapter will illustrate the application of this ACAP framework to the design of an in-ear device by showing the process from the design of the part through to realizing the customized design from 3D scan data.

Chapter 6

Automated Customization of an In-Ear Device From 3D Scan Data

Chapter 3 illustrated the design of a 3D scanner that automatically captures the 3D ear data in high resolution. Chapter 4 then used this data to construct a statistical shape model (SSM), which is a compressed representation of the variation within the dataset. Chapter 5 outlined the mathematical background and functionality of the proposed deformation constraints in manipulating the chosen CAD design. In this chapter, the application of this research will be established by combining the techniques in Chapters 3 to 5. Here, it will be shown that by using a SSM, a deformation field from the mean shape to the input 3D scan can be established. This deformation field can then be transferred to the product design and using the deformation constraints the design will be customized to fit the deformation field. In this approach there is no necessity for pre-programmed rules or detection of landmarks, all that is required is that the CAD design be registered to the SSM and the user define the deformation constraints, such that the ACAP technique from Chapter 5 can apply the deformation.

The following section discusses available consumer in-ear devices and issues that must be considered when developing a mass-customized product, together with a justification on the selected product for this research. Sections 6.2 and 6.3 then illustrate the design process using the SSM and final design that is to be tested for this research. Section 6.4 shows the steps for pre-processing a functional CAD design such that it can be used in this mass-customization framework. Section 6.5 shows how the SSM is integrated into the customization process such that it can guide where the CAD design deforms. Sections 6.6 and 6.7 show the outcome of the process with a custom-fit in-ear device that can be automatically adjusted to fit the input 3D scan data.

6.1 In-Ear Device and the Considerations For Automated Customization

One of the advantages of the proposed automation framework is that it can generalize to a wide range of products as it relies on the SSM as the basis for deformation. In order to test the automated customization process, a consumer in-ear earphone was selected as it represents a widely used product that has a significant amount of available design information from which to test.



FIGURE 6.1: Styles of in-ear earphones. Various designs aim to improve comfort or sound quality by exploiting different areas of the ear for mounting or sound isolation.

In Figure 6.1, various in-ear earphone designs are shown, with some of the variation intended to either improve the comfort, mounting in the ear, or the sound quality. Figure 6.1 (a) shows two earphones with silicone inserts, also known as canal-phones. The purpose of the silicone insert is to improve the mounting of the earphone and also the sound isolation and quality. By using a silicone insert, the aim is to compress the earphone into the users ear canal such that a tight seal is formed. This prevents external noise from polluting the sound and creates a firm mounting base for the earphone. However, there is significant bias in terms of user adoption of canal-phones due to the pressure induced on the ear canal. As the human ear is so varied there are users that may find the pressure on the ear canal painful, and while the earphone suppliers provide various size silicone inserts there will always be an issue with discomfort for a proportion of the user base. Canal-phones and in-the-canal hearing aids also suffer from occlusion due to the ear canal being sealed by the insert. The occlusion effect is a very serious issue for in-ear devices as it can cause the users voice to become 'hollow' or 'booming', and it can also increase the noise from jaw movement such as chewing or talking.

Contrary to canal-phones, there are standard "earbuds" (see Figure 6.1 (b)) which do not enter the ear canal. Standard earbuds mount in the external ear and project the sound into the canal. The benefit of these devices is that there is no occlusion or pain as a result of sealing the ear canal. However, as the ear canal is not sealed there is the possibility for sound leakage. The disadvantage of mounting in the external ear is that earphones can become unsteady for a proportion of the population, especially during dynamic motion such as exercise. Some products aim to improve this mounting through the use of hooks behind the ear (see Figure 6.1) or compression fittings within the external ear (see Figure 6.1 (d)). This research aims to solve the issues with placing objects in the canal by custom-fitting an earphone to the external ear. Using the automated customization framework, it is possible to create bespoke earphones that fit perfectly to the external ear, such that it is not necessary to fully enter the ear-canal. As this research uses the full, high resolution 3D scan data to customize the in-ear device, a seal is created from the external ear such that noise leakage is minimized, without affecting the comfort of the user.

An example of this approach in industry is given by Snugz Earphones (Snugs, 2017). In their approach, a mould is made from the individuals ear canal which is then 3D scanned and manually edited such that a custom-fit mount is produced. The benefit of their approach is the ability to use widely available and already mass-produced earphones with their custom-fit mount.



FIGURE 6.2: Custom-fit earphones produced using moulding, 3D scanning and manual processing of the scan data (Snugs, 2017).

As can be seen in Figure 6.2, the custom-fit earphones leverage the mass-produced earpieces that contain the electronics with a custom-fit shell such that the only required object to be 3D printed is the custom-shell. This research will replicate the earpiece seen in Figure 6.2 (a), where a standard earpiece containing the electronics is fitted to a custom shell such that the comfort and robustness of the mounting can be improved. As the process used by the Snugz company is manual, the porting of this design to the automation framework developed in this research will showcase its applicability to functional products.

6.1.1 Custom Shell and Electronics Module

For this research, the Beats urBeats2 earphone will be used. In terms of design, the earphone is relatively simple consisting of a metal casing shell that holds the electronics and a silicone insert that is placed in the ear canal, as annotated in Figure 6.3 (a).

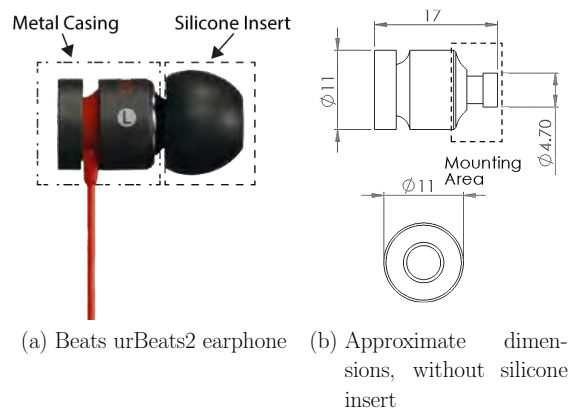


FIGURE 6.3: The Beats urBeats2 that will be used to test the customized earphone (a) and the approximate dimensions that were measured manually (b).

As can be seen in Figure 6.3 (a), the earpiece is a cylindrical metal casing containing the speaker driver and a silicone insert. As annotated in Figure 6.3 (b), the silicone insert is removed and the custom-fit earpiece is attached to the mounting location. For the shell, the mechanical properties of the material are not considered here, as the critical component for this research is the customized shape.

6.2 Design Considerations for Automation and 3D Printing

One of the advantages of the approach developed in this research is the ability to design products in the conventional way using CAD programs, meaning that the shape of the product is generated in steps using digital modelling tools. However, there are some modifications to the process due to the enhanced information from the SSM introduced in Chapter 4. With the introduction of the SSM, which is a full 3D representation of the variation in shape, there exists more information from which to guide the design of the product. When designing custom-fit products, it is important to consider how the product interacts with the human body. For example analyzing how the product will fit to the human body and also considering how the target shape deforms. The SSM is a valuable resource as it can allow for the design of parts to fit within a certain range of variation in the population. It may not be possible to design a single product that can fit to the entire population due to either the deformations not being possible on the product or the size of electronics not being viable for extreme deviations of shape. In order to achieve customized products, the following section introduces design for the mean, which uses the SSM from Chapter 4 to guide the design.

6.2.1 Design for the mean

This is an approach that uses the mean shape from the SSM that was constructed in Chapter 4. To design for the human body, designers typically use a table of anthropometric data, which is a representation of the variation in shape in planar dimensions. However, using the high resolution 3D data constructed as part of this research it is possible to advance and ease this process. By designing for the mean, the product will already fit the mean of the population in the given dataset and will then be adapted using the automation approach of this research (see Chapter 5). By beginning with the mean shape it allows the designer to assess the end shape of the product to determine appropriate localization of electronics or critical components. As the mean shape is a representation of the median in the normal distribution, the deformation will either be contraction or expansion, so designing for the mean is an optimal approach for when the device must fit to a target object.

Designing for the mean follows a similar process as outlined in Figure 1.15 and Figure 1.16, with the process slightly modified due to the type of input data. Section 6.3 shows the process of designing an in-ear device using design for the mean. It should be noted that, using the SSM it is possible to design for any number of deviations along the normal distribution, such as $\pm 3\sigma$, which will take account of the extreme variations in shape. However, for the purposes of this research, design for the mean was deemed sufficient for demonstration purposes.

6.2.2 Limitations of 3D scan data

Prior to designing the product, it is important to consider the limitations of the 3D scan data. As 3D scan data reconstructs only what is seen by the cameras, areas that are occluded cannot be reconstructed. By assessing the ear, there are numerous folds, particularly between the concha and triangular fossa that makes 3D scanning very difficult. Analyzing the custom-fit moulding in Figure 6.2, it can be seen that there is significant detail at the top of the mould which constitutes the concha-triangular fossa region. This mould is generated from a manual involving the injection of silicone into the ear canal and the 3D scanning of the hardened result. The use of this manual process allows for areas that are typically occluded to be reconstructed. While this is a limitation of the non-contact 3D scanning process, it is yet to be determined whether it is a drawback to the customization process.

6.3 In-Ear Device Design using the SSM as a Guide

For this research, due to the availability of the SSM, design for the mean is the chosen protocol. With the full 3D SSM, a robust mean shape is provided such that the design can be guided. However, there are two ways in which to use this mean shape to output a designed shape: direct and indirect design.

6.3.1 Direct and Indirect Design using the SSM

In direct design, the SSM is used from the start of the design process, such that the earpiece is specifically designed to fit to the mean shape. In this process, the mean shape is imported into the CAD program and the earpiece is designed in the standard way. As there are multiple ways in which to design a product using the same CAD software, this research will outline an approach using non-uniform rational basis spline (NURBS) modelling. However, the customization approach is not restricted to a single method.

The benefit of direct design is that, the earpiece is already registered to the SSM and can be directly exported for pre-processing into the automation framework. With indirect design, the earpiece is designed in the standard way using dimensional data and is then registered to the SSM and using snapping the earpiece is fitted to the SSM in the desired areas. The benefit of this approach is that an earpiece that was not designed for the automation framework can still be applicable. By snapping the desired areas to the SSM it also reduces the overall complexity of the shape deformation. Due to the availability of the SSM, this research will illustrate the direct design approach.

6.3.2 Direct Design of an Earphone to the Mean Shape of the SSM

As stated previously, NURBS modelling, also known as freeform Sub-D modelling, was used to construct the earphone in the direct design approach. This process is synonymous with clay modelling as the earpiece is digitally moulded to fit the 3D scan data, this process is illustrated in Figure 6.4.

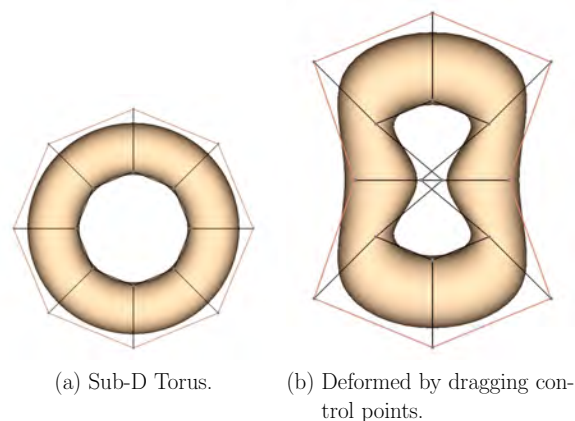


FIGURE 6.4: A Sub-D model of a torus (a), showing the control points that are used to deform the shape (b).

The benefit of Sub-D modelling is the simple creation of complex and organically shaped Class A surfaces, meaning the surface has curvature and tangency alignment or continuity.

6.3.2.1 Creating the Custom-Fit Shell Using Sub-D Modelling

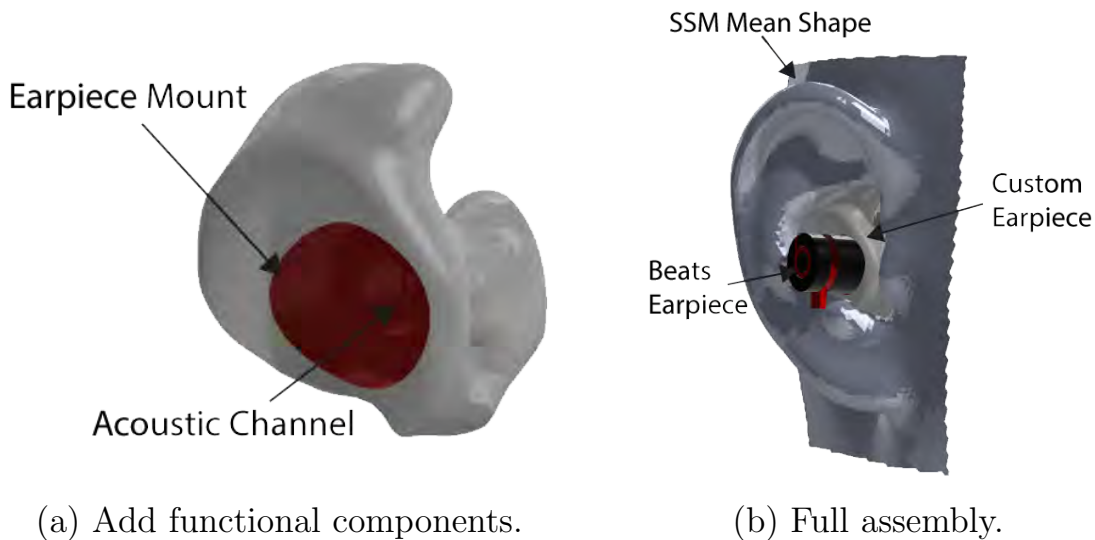
To recall, this research is aiming to produce an earphone shell similar to that seen in Figure 6.2 (a). Therefore, the earpiece is designed such that the Beats urBeats 2 earpiece can fit into the custom-shell with the mounting positions marked in Figure 6.3 (b). The process for designing the earphone can be seen in Figure 6.5.



(a) Initialize Sub-D. (b) Drag to fit shape. (c) Slight over-size. (d) Cut using SSM.

FIGURE 6.5: A Sub-D model of a torus (a), showing the control points that are used to deform the shape (b).

As can be seen in Figure 6.5, the mean shape of the SSM is used as the basis for containing the in-ear device. A simple freeform NURBS modelling toolkit is used to push and pull the earpiece to the desired shape and the SSM is as a guide for where the earpiece should fit. Alternative means to create the initial shape would be to use an interference fit, as per Harmon et al. (2011). In this approach, the model is expanded and the SSM would act as a physical barrier, however, to test the process the NURBS modelling approach is sufficient. The model in Figure 6.5 (d) contains no features other than the shape of the SSM, the next stage is to add the mounting region and acoustic channels, which can be seen in Figure 6.6.



(a) Add functional components.

(b) Full assembly.

FIGURE 6.6: A Sub-D model of a torus (a), showing the control points that are used to deform the shape (b).

Using the mean shape as a limit, it can be said that the earpiece in Figure 6.5 now fits to the exact shape of the mean of the population. Figure 6.6 (a) shows the functional regions as the earpiece mount and acoustic channel, for clarity the functional region is displayed as red. Figure 6.6 (b) shows the full assembly with the mean shape, the Beats earpiece and the customized earpiece shell. With an approximate design time of 10-15 minutes for a well-trained individual, the addition of new designs is not a time consuming task.

6.4 Pre-Processing the In-Ear Device for the Automation Framework

The earphone design from Figure 6.6 consists of a mounting region for the Beats earphone in Figure 6.3, an acoustic passage, and the custom-fit region for the ear. To incorporate the constraints into the algorithms set out in Chapter 5, a simple segmentation approach is used, wherein the designer manually annotates the regions which must be preserved. The vertex indices of these regions are then added to the constrained Laplacian system as discussed in Chapter 5. For the earphone in Figure 6.6, there is a single form region constituting the earphone mount and acoustic passage, the remainder of the earphone is unconstrained.

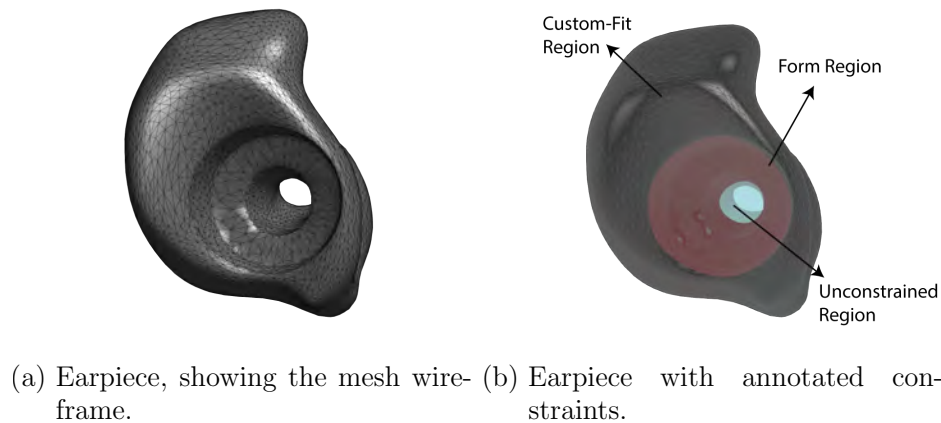


FIGURE 6.7: Preprocessing the earpiece for the ACAP customization framework, showing the segmentation of the form region in red and the black region, the custom-fit region in black and the free region in gray.

Figure 6.7 shows the segmented earpiece with the form region, custom-fit region and unconstrained region. One of the benefits of this approach is that it does not need to be known how the entire shape will deform. Using the algorithms in Chapter 5, the process is able to approximate deformations in a realistic manner, such that, a deformation that affects one side of the earpiece will affect the opposite side. In order to test the process, only form constraints are used, however, there are a multitude of possible constraints that can be used to achieve more advanced or controlled deformations, for example, normal constraint, relative position constraint, or constrain to a line. To test the process, a single form constraint was used, it should be noted that there is no limit to the number of constraints that can be used, the only consideration is processing time.

6.5 Transferring a Deformation Field from the SSM to the In-Ear Device

The first step to generate a deformation field from the SSM is to fit it to an input 3D scan. The input 3D scans in this case are taken from the 3D scanning system developed in Chapter 3. The

process for fitting the SSM to a new 3D scan was discussed in Chapter 4. To reiterate; the SSM consists of the mean shape and the set of eigenvectors and eigenvalues, known as principal components, which are a compressed representation of the variation within the dataset. Using these values it is possible to vary the SSM to any shape along the normal distribution. To fit the SSM to a new 3D scan a set of parameters are selected which scale the individual principal components such that the SSM is deformed to match the input 3D scan. For example, the SSM in this research consists of 98 principal components, however, in reality not all of the components are needed to reconstruct a shape. In actuality, the number of components needed is estimated as 95% of the total variance in the dataset, which in this case amounts to 27 principal components.

Using the first 27 principal components, the scaling vector (one per principal component) is calculated through the iterative estimation of correspondence and difference between the SSM and the input 3D scan. Figure 6.8 shows the mean shape of the SSM (a), with an input 3D scan (b), and the relative difference in position and orientation from the SSM to the input 3D scan (c).

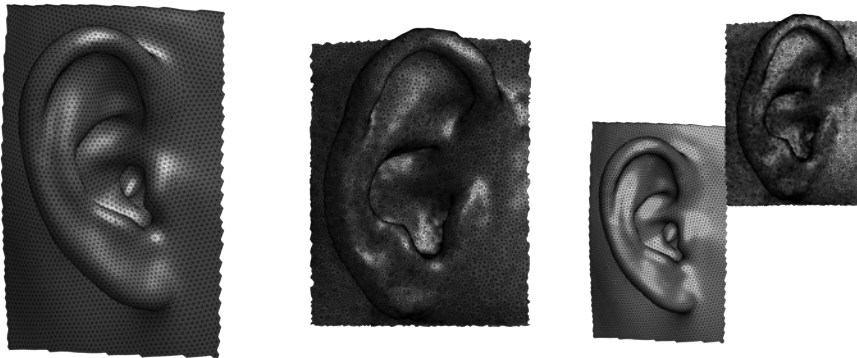


FIGURE 6.8: (a) The mean shape of the SSM with (b) an input 3D scan, showing (c) the spatial and topological difference from the scan to the SSM.

Of interest in Figure 6.8 is not only the large variation in shape but also in topology, i.e. mesh density and vertex positions. As the iterative estimation of the scaling vectors requires calculating the difference in vertex positions, the two models need to be brought as-close-as-possible. This research opts for a variant of the iterative closest point (ICP) based on finite differences which provided adequate results Kroon (2009). The registration of the input 3D scan to the SSM in Figure 6.8 can be seen in Figure 6.9.

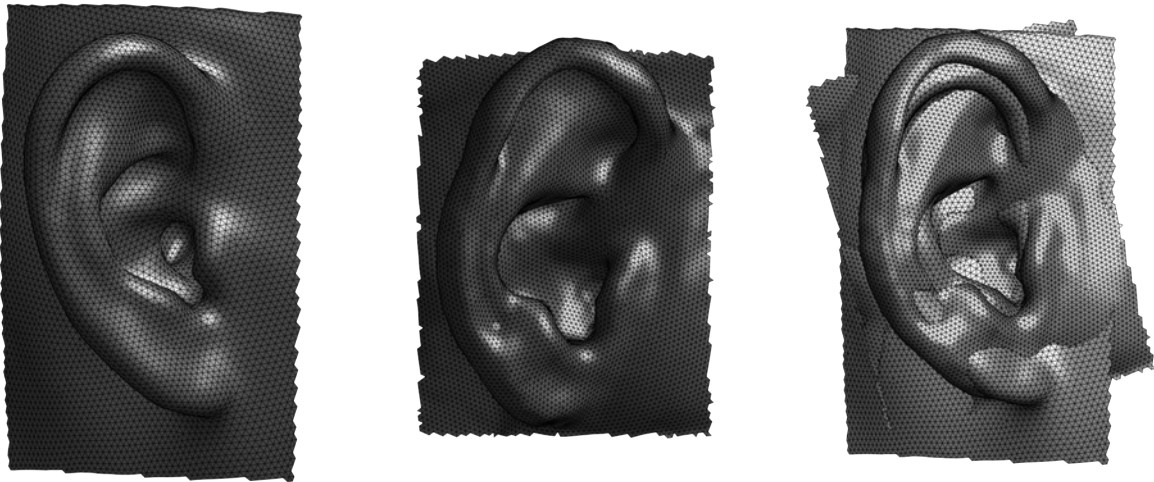


FIGURE 6.9: (Left) The mean of the SSM registered to (Middle) an input 3D scan, showing (Right) the overlapping areas after registration. Further refinement is required as the SSM did not fully predict some areas of the shape.

As can be seen in Figure 6.9, using the finite ICP method, the SSM and input 3D scan are now overlapping. The next step is to iteratively estimate the correspondence and difference from the SSM to the input 3D scan. Similar to Chapter 4, the correspondence is established using a non-rigid free form deformation (FFD). Contrary to Chapter 4, functional map refinement is not needed as the SSM can now approximate any errors or mismatches in the data. Once a one-to-one correspondence is established from the 3D scan to the SSM, the scaling vector is solved using the following formulae (Bernard et al., 2016):

$$b = X_{scan} - X_{SSM} \quad I = 1/e_{values} \quad A = e_{vectors}$$

$$\sigma_{scale} = (A * A' + I) / A' * b \quad (6.1)$$

Equation (6.1) approximates the scaling vector (σ) which best fits the shape of the SSM given the difference (b) between the SSM and the input 3D scan. The I matrix applies regularization to this shape deformation, allowing for more principal components to be used without introducing significant noise. From this approach, the SSM is able to approximate any input 3D scan relative to the dataset that was used to train the model, meaning models that are outside of the parameters of the dataset may not be accurately reconstructed. To reiterate from Chapter 4, the dataset for this database consists of 100 left and right ears. However, statistically, the ethnicity of the dataset may also skew the results. For this research, the database was constructed from primarily caucasian men and women, meaning, the data may be skewed towards caucasian people. This is assuming that variation in ear shapes can be found based on ethnicity. While this is in issue in commercial terms, in order to prove the concept it is not a critical issue. As the dataset grows and becomes more diverse, the accuracy will also increase.

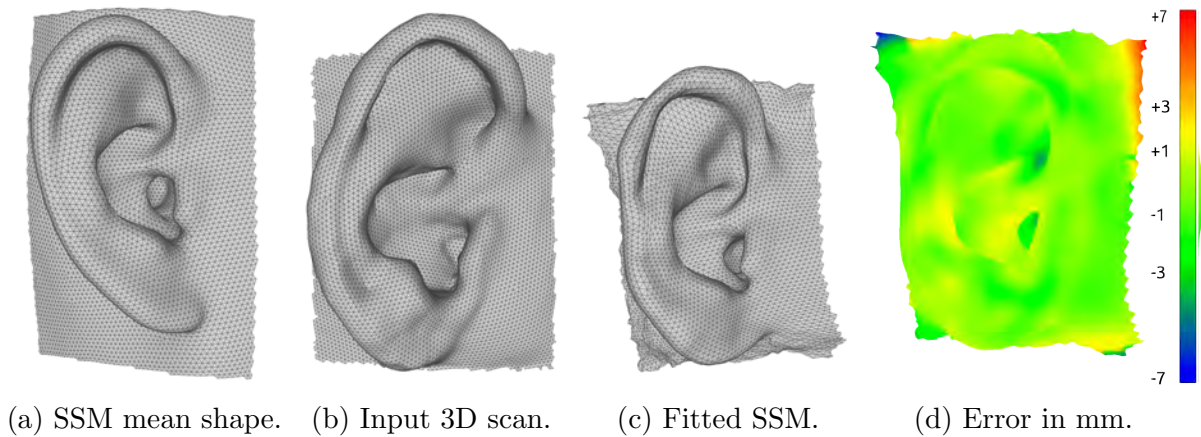


FIGURE 6.10: SSM fitting process; showing the change from the SSM (a), to the input 3D scan (b), and the fitted 3D scan (c), and finally error in the fitting process shown in mm (d).

One of the novelties of this customization approach is the use of the deformation field generated by the change in shape of the SSM to guide how the CAD design deforms. Specifically, in Section 6.2, the earphone is designed relative to the mean shape of the SSM, therefore, any change in shape of the SSM can be directly transferred to the CAD design.

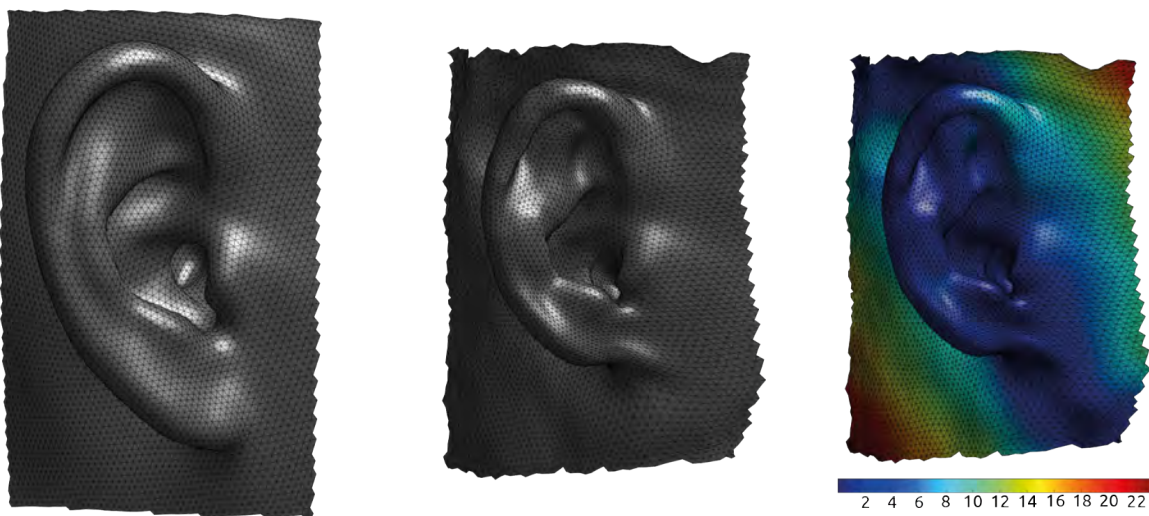


FIGURE 6.11: Generation of the deformation field, showing the change in shape from the mean (left), to the fitted input 3D scan (middle), and the deformation field (right). Colours represent the magnitude of the deformation in mm, however, the actual deformation field is in three dimensions (X,Y,Z)

In Figure 6.11, the deformation field from the change in shape of the mean shape of the SSM to an input 3D scan is shown. The colours in Figure 6.11 (right) represent the magnitude change in mm. However, the actual deformation field is in three-dimensions, i.e. X,Y, and Z. From Figure 6.5 (b), earpiece is registered to the SSM, the deformation field can therefore be transferred by simply finding the closest point from the vertices on the earpiece to the SSM. Specifically, the vertices of the earpiece are projected along their normal axis until they intersect with the SSM. The value of the deformation field at that point is then interpolated to give a more accurate deformation, see Figure 6.12. This process is required so that deformations on the SSM are only transferred to parts of the earpiece that are in contact.

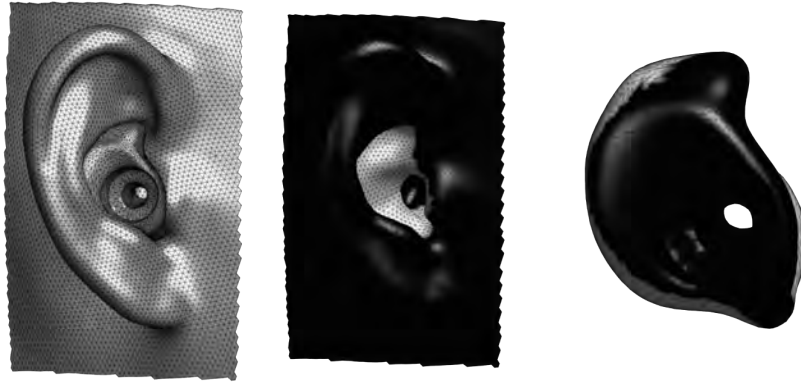


FIGURE 6.12: (a) The mean shape from the SSM with the registered earpiece, (b) the mean shape with the area in contact with the earpiece, (c) the earpiece with the area in contact with the SSM. The indices of the contact areas are used to transfer the deformation from the SSM to the earpiece.

Using the deformation field in Figure 6.11, the values can be directly related to the CAD design by interpolating the values at the projected points, as seen in Figure 6.12. One of the benefits of this approach is that the positions of the projected vertices of the CAD design onto the SSM only need to be calculated once. The only remaining processing is interpolating the deformation field.

6.6 Customized In-Ear Device using Variations in the SSM

As stated previously, by using a SSM to guide the deformation process of the product design, it allows for the designer to anticipate any errors or limitations of the design that may occur at extreme variations. For example, the earpiece in Figure 6.6, was designed relative to the mean shape of the SSM. By deforming the SSM between $\pm 3\sigma$, it will show if there are any deficiencies in the design. This could be related to the size of the acoustic passage being too large for shape variations over $+2\sigma$ or the size of the mounting position is not adequate for ears below -2σ due to the size of the concha.

By using a SSM to test this process it will allow for the designer to determine the statistical range over which the design will work for the population. It may also inform as to whether multiple designs are required which can be automatically selected by the program based on the mean deviation of the scaling vectors.

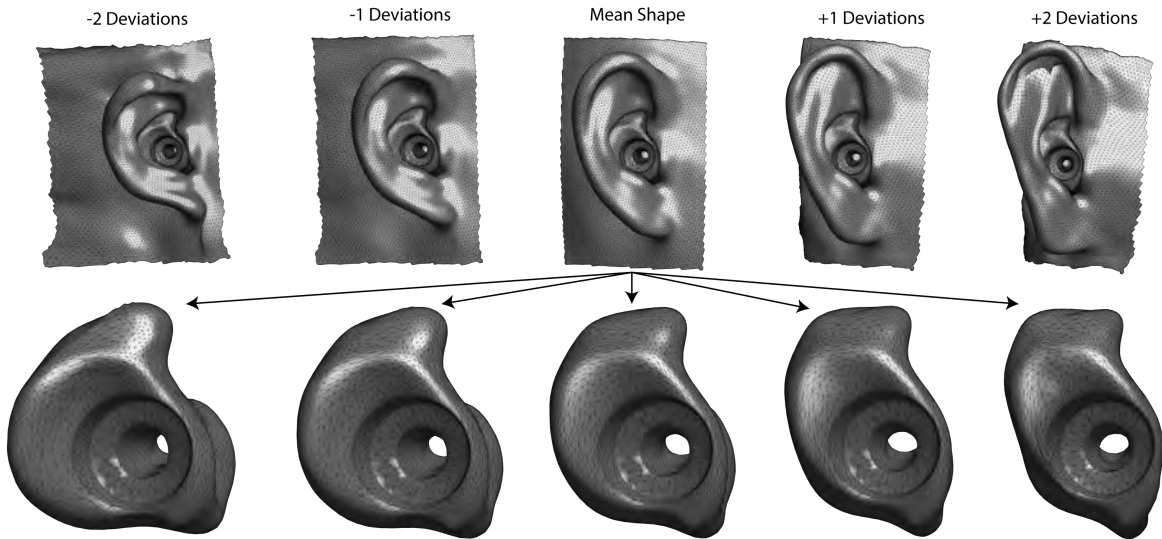


FIGURE 6.13: Testing the ACAP mesh deformation process showing the change in shape from the mean to $\pm 2\sigma$ in the SSM using 95% of the variance in the principal components.

Figure 6.13 shows the deformation from the mean shape to ± 2 standard deviations. As can be seen, while the concha, or external region, of the ear exhibits large deformation, the earpiece follows that deformation whilst maintaining the form of the designated region set out in Section 6.4. What this is showing is that designed earpiece will work for any ears that fall between the range of ± 2 standard deviations from the mean, i.e. 95% of the population at least.

6.7 Customized In-Ear Device from 3D Scan Data

The objective of this research was to establish a method for automating the customization of in-ear devices from 3D scan data. In Section 6.6, it was shown that it is possible to automatically create new earpieces using the change in shape from the SSM. To apply this to a real-life subject, the process in Section 6.5 is followed such that the input 3D scan is registered to the SSM. The SSM is then iteratively refined to be as close as possible to the input 3D scan, taking account of noise and outliers (see Figure 6.14). As such, the SSM should now be as-close-as-possible to the input 3D scan, meaning the deformation field from the mean shape to the input 3D scan is established.

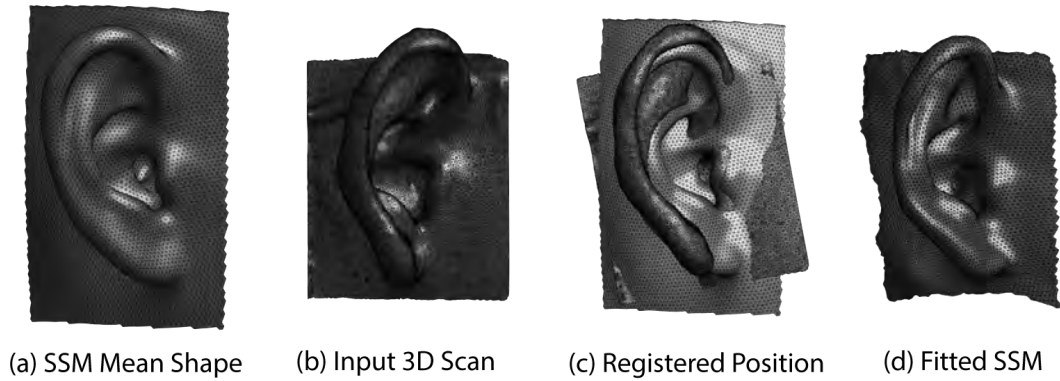


FIGURE 6.14: SSM fitting showing, (a) mean shape, (b) input 3D scan, (c) registered scan to SSM, and (d) the fitted SSM.

Figure 6.14 shows the complexity of this approach given not only the spatial variation but the difference in topology, i.e. density and positioning of the vertices. An advantage of using the entire 3D model as opposed to a sparse set of landmarks is the ability to capture the entire surface variation, however, this means that the registration and refinement becomes more complex.

As discussed in Section 6.5, the input 3D scan is registered to the SSM using a variant of the iterative closest point. As can be seen in Figure 6.14 (c), this brings the scan spatially close to the SSM based on some distance measure. With the SSM and 3D scan now spatially aligned, the iterative fitting procedure is performed to fit the SSM to the input 3D scan Figure 6.14 (d).

In Figure 6.14 (d), the fitting procedure is able to account for large deformations while also able to interpolate missing information on the 3D scan. With the SSM fitted to the input 3D scan, a deformation field is constructed which is then transferred to the CAD product. Using the ACAP mesh deformation process discussed in Chapter 5, the earpiece in Figure 6.6 (a) is deformed under the deformation field, as seen in Figure 6.15.

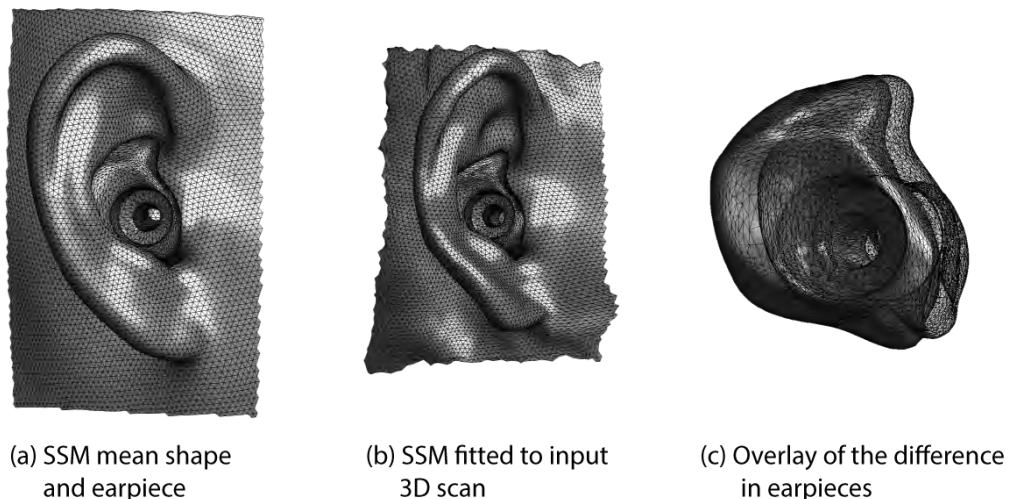


FIGURE 6.15: The full ACAP process, showing (a) the mean shape with the earpiece, (b) the input 3D scan with the deformed earpiece using ACAP, and (c) the relative change in shape with the old earpiece being shown as transparent.

As can be seen in Figure 6.15, the ACAP process is able to accurately deform a CAD design to fit an input 3D scan whilst maintaining the regions set out in Section 6.4.

6.7.1 3D Printed Customized In-Ear Device

Using the Form2 3D printer a sample of the customized earphone from the previous section was tested using the Beats earphone in Figure 6.3. For the resin, the material from 3Dresyns (2017) proved to be the most effective for direct 3D printing of the in-ear device due to the flexibility and biocompatibility. The earphone was printed at a layer resolution of 10 microns and took approximately 1 hour 20 minutes to print.

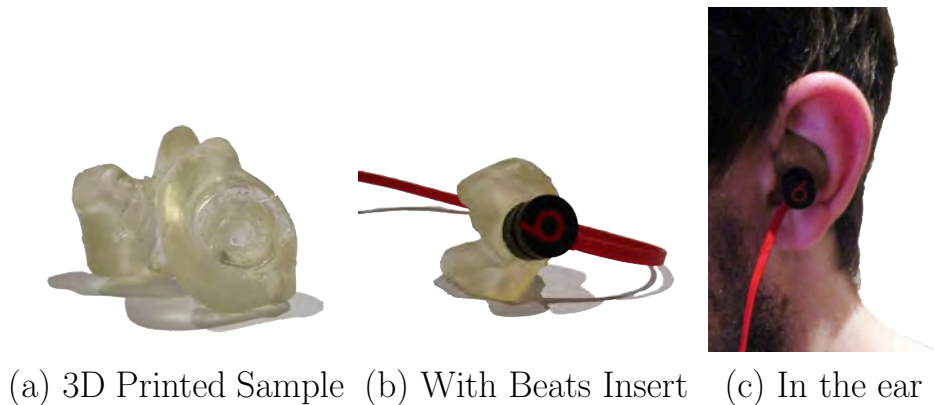


FIGURE 6.16: Sample 3D print of a customized in-ear device, showing the sample part (a), the beats insert (b), and the 3D printed in the ear (c).

The result of the 3D printing process can be seen in Figure 6.16. The use of the form-preserving 3D mesh deformation framework in Chapter 6 has been successful, which can be seen in the fitting of the Beats earphone to the form region in Figure 6.16 (b). Informal feedback has suggested that the earpiece is an excellent fit and due to the exact nature of the 3D scan data, the occlusion is minimal. Using the 3D scan data it is actually possible to selectively expand parts of the earpiece to obtain the desired level of occlusion. The testing of the audio quality is not an aspect of this research as the focus was on how to obtain a custom-fit. Nevertheless, initial impressions with the in-ear device suggests that the audio quality has moderate improvement with the sound isolation and no noticeable loss of sound transmission due to the 3D printed acoustic channels. As discussed in Section 1.1.1.1, comfort and fit are largely subjective parameters and their evaluation requires careful experimental design that is beyond the scope of this project. However, these preliminary results for a customised in-ear device are promising and may provide the basis for more comprehensive user-acceptance testing in future work.

6.8 Discussion

The goal of this chapter was to illustrate the process of automatically deforming a CAD product design based on an input 3D scan, and it can be said that this has been achieved. Using the SSM constructed in Chapter 4 and the ACAP mesh deformation discussed in Chapter 5, the process is able to take an input 3D scan and fit it to the SSM, such that a new 3D mesh is constructed with the same topology as the SSM but with the shape of the input 3D scan. This is then processed through the ACAP system and a custom-fit earphone is designed to fit the input 3D scan in a completely automatic and headless manner. Headless in this case is referring to the ability of the system to function without a trained expert. However, there are still some considerations regarding the process, as discussed below.

6.8.1 Fitting the SSM to a New 3D Scan

The use of the SSM allows for approximations to be made about the input 3D scan such that outliers, noise, and even missing information can be accounted for. This is one of the main advantages of the SSM. However, the accuracy of the SSM is dependent on the size and quality of the dataset. For this research, a database consisting of 100 3D scans of the ear was used and was predominantly caucasian. Comparatively, the publicly available SSM of the human body (Pishchulin et al., n.d.), was constructed with over 4500 3D scans. In order to ensure validity of the process a much larger dataset of 3D ears is required which contains much greater representation of variations in race and age. However, the SSM which was constructed in Chapter 4 has proved the concept of automating the customization of in-ear devices.

A novelty of the use of a SSM as the basis for the custom-fit is that it allows for some approximations or interpolations to be made about the input 3D scan. For example, if the 3D scan contains some occlusion, the SSM will be able to approximate what is missing. This can be seen in Figure 6.15 where the ear canal has been approximated to a certain degree without having any of that data in the 3D scan. This potentially allows for more complex earphone designs to be made without having to leverage more invasive moulding techniques or using expensive ear canal 3D scanning technology. While the SSM has been able to interpolate the ear canal, the validity of the resulting deformation is not being assessed as it considered beyond the scope of this research.

As was stated in Chapter 4, the SSM is constructed from full 3D scan data without the need for manual landmarking. This allows for the user to rapidly take a 3D database and process it into some thing that is useful for product design. However, this creates complications in the fitting stage as the input 3D scan now needs to be registered to the SSM and then iteratively refined. If landmark information was available, the alignment and fitting would be a relatively simple task. However, that creates difficulties in detecting the landmarks and reliably processing the database such there is consistency in the landmarking. Through the use of the algorithms in Chapter 4, the complexities of the fitting process have been minimized using advanced non-rigid registration techniques.

6.8.2 ACAP Mesh Deformation and it's Limitations

The ACAP mesh deformation process allows for a CAD design to be deformed relative to the change in shape of the SSM. The novelty here is the ability to incorporate form preservation in the deformation process. Contrary to the standard generative approach where a 3D scan is cut and modified to create the final product by detecting features on the input 3D scan, this research opts for starting with the CAD design and deforming it to fit each individual. As such, it is required that functional components such as mounting holes or acoustic cavities be preserved. Preservation in this case is referring to the overall form such as the diameter. The benefit of the ACAP process is that the user-defined form region will move with the natural deformation of the CAD design, but the form or shape of the form region will be preserved. This can be seen in Figure 6.15 (c) where the overall positioning has changed but the form of the earpiece mounting region remains the same.

Another advantage of the ACAP process is its extensibility, meaning it is possible to add further constraints to the system such as normal, relative position, or line constraints. However, in order to evaluate the overall process relating to an earphone, form preservation was the main requirement. A disadvantage of the ACAP process is its sensitivity to mesh topology. As the process can be related to a physical deformation, the more densely packed the vertices are the less space there is for the mesh to deform, this is especially important during large shape deformations. The form preservation also works through the use of a minimum spanning tree constructed on the edges of the form region, therefore, if there are closely packed

edges or erroneous topology the process will fail. The output from the majority of CAD packages is an STL (Stereolithography) file which contains the vertices and faces of the mesh. Petik (2000) outline the errors relating to the outputting of STL files from CAD packages and discusses the issues regarding tessellation or closure errors, which for this research would result in a failed customization. In order to ensure that the process was successful, a pre-processing stage is added before the segmentation of the CAD product which distributes the vertices and faces evenly over the mesh (Jakob et al., 2015).

6.8.3 3D Printed In-Ear Device

In Figure 6.16 a sample customized in-ear device is shown. For this research, it was attempted to directly 3D print the in-ear devices as opposed to casting the parts from a 3D printed shell as per Formlabs (2018). This was based on the premise of on-demand customized devices where the manufacturing time is of importance. In Section 6.7.1 the printing time was 1hr 20minutes. If a casting approach was used additional time would have to be added to the process to clean the 3D printed shell, inject the silicone resin and give it time to cure. The benefit of the casting approach is the use of soft medical grade silicone as opposed to harder 3D printing resins. Future research on the development of the 3D printing process for in-ear devices will endeavour to reduce the 3D printing time while allowing for a wider range of biocompatible materials to be used. It was discussed in Section 1.1.9 that ultra-fast 3D printers have the potential to produce an in-ear device in under 20 minutes and could be an opportunity for this automated customization process, however, access to this equipment was not possible during this research.

6.9 Conclusion

The original aim of this thesis was the development of a method for automatic customization of in-ear devices from 3D scan data. From Figure 6.15, it can be seen that this aim has been achieved in principle. In the process outlined in this chapter, an input 3D scan was taken and fitted to the SSM, creating a deformation field which was transferred to a registered CAD design. Using the novel ACAP process, the CAD design was deformed to fit the new 3D scan incorporating a set of constraints that relate to how the CAD design can deform. In order to achieve mass-customization, the automatic nature of the system requires that there be no trained expert at any stage of the process. Aside from the design and pre-processing of the actual CAD design, the fitting of the SSM and deformation of the CAD design are all fully automatic. It can be said that this system is the first step towards mass-customization of in-ear devices.

Chapter 7

Discussion and Conclusion

The aim of this research was the development of a method for the automated customization of in-ear devices from 3D scan data. Through considerable research and experimentation a method for generating custom-fit in-ear devices from 3D scan data was constructed, using a 3D statistical shape model (SSM) and as-constrained-as-possible (ACAP) mesh deformation to achieve a completely automated and standalone system. Four primary research questions were discussed in Chapter 1;

RQ1: What is the most applicable method for 3D scanning the human ear?

RQ2: How do we statistically analyze the full 3D scan data, without the use of landmarks?

RQ3: How do we use already fully functional CAD designs as opposed to performing the processes after customization?

RQ4: What are the limitations, for design, using this customization process?

Research question 1 aimed to establish the most applicable 3D scanning system for the human ear in the context of mass-customization. Through this it was established that a 3D scanning system based on the principles of photogrammetry provided the best results. The outcome of this approach is discussed in Section 7.1.

Research question 2 formed the cornerstone of this research, which was the statistical analysis of 3D scan data. The SSM was used to establish the variation from the dataset to a new 3D scan, such that the resultant deformation field would deform a CAD design. The use of the SSM in both the 3D scanning and the automated customization shows the importance of generating an accurate model. Chapter 4 established the mathematical basis for the SSM and posed the advantages over the current methods. The outcome of this approach is discussed in Section 7.2.

Research question 3 is the main aim of this thesis as it generates the customized shape. Contrary to the methods in the literature in Section 1.1.5, this research uses a fully functional CAD design as the input to the customization process. Coupling this CAD design with the SSM and the constrained 3D mesh technique developed in Chapter Chapter 5, it was possible to deform the functional CAD design to fit the new input 3D scan data while preserving the user-defined features. This approach, named As-Constrained-As-Possible (ACAP) 3D mesh deformation, is discussed in Section 7.3.

Research question 4 aims to understand the limitations of the proposed customization process. As with any new processes, there are advantages and limitations and in order to understand the future direction of this research it is important to assess the extent to which it can be used in a practical scenario. This research questions is partially answered in Chapter 6 and is discussed in Section 7.4.

In combination, these questions combined aim to assess the entire mass-customization infrastructure from obtaining 3D scan data to processing it into something fit-for-purpose and suitable for 3D printing. From Chapter 1, the research background was established and the

gaps in the literature were critically assessed. By understanding the shortcomings of the customization methods in the literature, it was determined that the requirements in Figure 7.1 were needed to reliably generate custom-fit in-ear devices.

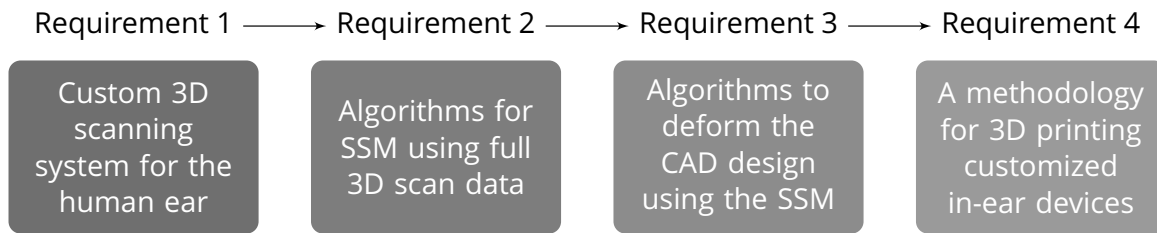


FIGURE 7.1: Requirements for automating the customization of in-ear devices relating to 3D scanning, statistical shape model (SSM) development, customization algorithms, and 3D printing.

Using the requirements in Figure 7.1 as guides this research developed an automation system for the direct 3D printing of in-ear devices from 3D scan data, with the following contributions:

1. Design and testing of an automated 3D scanning system for the human ear based on low-cost multiple-camera photogrammetry.
2. Development of a 3D database of the human ear that can be used for SSM and anthropometric analysis.
3. Development of a state-of-the-art framework for non-rigid Statistical Shape Model (SSM) generation; circumventing the complications with currently available systems (outlined in Chapter 4).
4. Development of a 3D mesh deformation based automation framework for design of custom-fit in-ear devices that does not rely on prior knowledge of anthropometrics and is completely automatic (detailed in Chapter 5).

7.1 3D Scanning the Human Ear

In order to 3D scan the human ear a number of experiments were performed using available 3D scanning system, both passive and active (see Chapter 2). Through this it was established that active 3D scanning system, while highly accurate, were highly sensitive to occlusion and therefore unsuitable for this research. It should be noted that since the initial experimentation several new active 3D scanning systems have been released which may be less prone to occlusion. However, referring back to the original goal of this research, which was the establishment of an automation framework, the hand-held manual operation of the active systems also limited their applicability to this research.

It was therefore determined that a passive system, using solely images, was required to reconstruct the human ear. Passive systems consist of a single moving camera or a series of cameras placed around the viewing sphere of the target subject. Chapter 3 gives a detailed description of the design and construction of a passive 3D scanning system for the human ear that is completely automatic. The system consists of two DSLR cameras moving around the arc of the subject's ear, capturing 76 images. Photogrammetry software, Photoscan3D, was then used to reconstruct the 3D shape of the ear. The advantage of this approach is the low cost and modular nature of the system, however, the disadvantage is the requirement to move the cameras. It should be noted that passive systems can have an arbitrary number of cameras and

the choice of two in this case was primarily related to cost. Due to the multiple view angles of the passive system, a relatively occlusion free 3D scan was obtained. However, the process contains more surface noise than active 3D scanning systems due to the approximation of the surface from possibly noisy images. While this is an issue if the 3D scan data was to be used in its natural state for customization, the noise did not appear to be an issue when used with the SSM as the basis for customization .

7.1.1 Improvement in Processing and Capture Time

Future improvements of this system relate to the processing and capture time of the system. With the current system, the processing time was approximately 20-30 minutes for a single 3D scan on an ear, primarily due to the large number of images. Compared to active systems which have near real-time reconstruction, this is a disadvantage. For commercial systems, it will be required to reduce the processing time. A potential method for reducing the processing time is to make the system stationary, i.e. increase the number of cameras and calibrate the system such that the positions and overlap of each camera is known prior to reconstruction, therefore alleviating the initial processing stage of structure from motion. The difficulty with this approach is the multiplicity of the DSLR cameras, which can cost up to \$1000 per camera. In industry, a passive 3D scanning system for the human body that contains 40 dedicated cameras for the head would cost approximately \$40,000 just to scan the head. Based on the understanding that a CCD/CMOS sensor has a very long life cycle, approximately 10 years, this cost can be spread out. However, future research will endeavour to find a lower cost alternative to passive 3D scanning of the human ear. This may involve lower-cost point-and-shoot cameras with dedicated passive 3D reconstruction algorithms for the ear.

7.1.2 Dedicated 3D Reconstruction Algorithms

A commercial software package, *Photscan3D*, was used to reconstruct the 3D shape from the input 2D images. Due to the nature of the software, it is designed to reconstruct a wide range of objects. However, for this research there is a specific object that is to be reconstructed. An improvement would therefore be the development of specific algorithms for the reconstruction of the human ear. An advantage of passive 3D scanning is the ability to use software to improve or tailor the overall 3D reconstruction process without having to change the cameras or imaging setup. As discussed in Section 1.1.7, there are multiple areas of passive 3D scanning (Pears et al., 2012), including:

- Shape from shading:** varies the camera focus and estimates the depth pointwise from image sharpness.
- Shape from focus:** uses the shadows in a grayscale image to infer the shape of surface, based on the reflectance map.
- Shape from texture:** assumes to object is covered by a regular surface pattern. Surface normal and distance are then estimated from the perspective effects in the images.
- Shape from stereo disparity:** uses correspondences from two distinct viewpoints to estimate 3D position, which is the process of this research.
- Volumetric space carving:** uses the silhouette of the target shape from multiple views to "carve" the outline of the 3D shape.

While each one the processes above has advantages and disadvantages, with passive 3D imaging there is the potential to improve upon a selected category or even combine to leverage

multiple aspects of 2D imagery (White and Forsyth, 2006). With the structure from motion (SFM) approach proving to be successful in Chapter 3, future development will entail the advancement of passive 3D imaging algorithms specifically relating to the 3D reconstruction of the ear. Using the 3D scanning system in Chapter 3, a database of ears was constructed was used to analyze the data to construct a statistical shape model which formed the cornerstone for this research.

7.2 Statistical Shape Models and their Application to Product Design and Customization

Statistical shape modelling is the process of analyzing the variance within a given dataset, for example the variance in shape of a database of ears as shown in Chapter 5. The 3D scan database in its normal state is just a collection of 3D points and faces, for product design this can provide some guidance for designers. However, it would be difficult to ascertain which end of the shape range you are designing for. Statistical shape analysis compresses the variance in the given dataset such that it is possible to generate the mean of the dataset and by varying a simple set of parameters any shape can be constructed along the normal distribution.

Traditionally, statistical shape analysis is performed on a sparse set of landmark points, such as anatomical landmarks which are manually annotated on the surface of the 3D scan dataset. This research opted to use the entirety of the 3D scan for the statistical shape analysis as opposed to abstracting a sparse set of landmarks due to two issues; the first being that landmarking 3D scan data requires sufficient knowledge of the anatomy of the subject, which was not available; second, the use of landmarks requires detecting said landmarks on the input 3D scan data, which can be unreliable.

7.2.1 Establishing Correspondences Using the Full 3D Scan Data

The complexity of using the entire 3D scan as opposed to just landmark data is in generating correspondences across the dataset. With 3D scan data, there is no consistency in point distributions on the surface over consecutive 3D scans, this means that a vertex that was located on one 3D scan, may not be in the same position on the next. In order to construct a SSM, there need to be meaningful correspondences across each model in the dataset, and so vertices must be in the same position. To circumvent this, correspondences are typically established through the use of feature description and matching, or through the use of spatial deformation and matching. In Chapter 4, it was shown that by employing state-of-the-art non-rigid 3D shape matching techniques, known as functional maps, it was possible to generate the required correspondences to a high degree of accuracy when compared with standard non-rigid spatial deformation (Coherent Point Drift, CPD), as seen in Figure 4.11. Spatial deformation using CPD was seen to fail to establish an accurate correspondence for the human ear due to the large shape variation.

7.2.2 Quantitative Assessment of the SSM

In terms of quantitative assessment, there are various measures for assessing the performance of statistical shape models, including generalization ability, specificity, and compactness. The generalization ability of a model measures its capability to represent unseen instances of the class of the object modelled. Specificity is the ability to measure whether the model can generate instances of the object that are close to those in the training set. Finally, compactness is the ability to use fewer parameters to cover more shape instances in the training sets. These measures are more indicative of the quality of the dataset than the quality of the registration.

The objective in developing the SSM, for this research, was to determine the feasibility in using the full 3D scan data. Therefore, the results in Chapter 4 are based on the registration accuracy rather than the generalization, specificity, and compactness of the SSM. To quantitatively assess the SSM using the new non-rigid 3D shape matching approach would require a larger dataset. Comparatively, the SSM by Pishchulin et al. (2015) was constructed from a dataset of approximately 4500 3D scans of the human body, whereas, the dataset in this research only contained 100 3D scans of the ear. The dataset, for this research, was also constructed from primarily caucasian males and females which may skew the data. While there is no known data determining ear shape variations across ethnicities, it would be statistically relevant to have a more varied dataset to do a full quantitative analysis.

7.2.3 Relevance to the Overall Aim of this Thesis

Assessing the aim of the thesis, which was the automation of the customization process for in-ear devices, it can be said that the functional map approach for generating the SSM fits this aim. Aside from capturing the 3D data, which could come from any source, the process for registering and generating the correspondences is completely automatic. This allows for rapid adaptation of the customization framework to new areas aside from the human ear, assuming that the data is highly detailed, relatively occlusion free, and varied. By processing the 3D ear database from Chapter 3, a high resolution SSM of the human ear was constructed, and could then be applied to the customization and product design aspect of this research. Assessing research question 2, *how do we statistically analyze the full 3D scan data, without the use of landmarks?*, it has been shown that any dataset of 3D scans can be analyzed by gathering a 3D scan database, generating correspondences using the non-rigid functional map framework, and processing this using principal component analysis.

7.3 ACAP Mesh Deformation for Automatic Customization

The SSM in Chapter 4 formed the basis for how the CAD design deforms to fit the input 3D scan. As detailed in Chapter 6, when a new 3D scan is fitted to the SSM it generates a deformation field from the mean shape to this new 3D scan. As the CAD designed earpiece, developed in Chapter 6 is registered to the SSM, this deformation field can be directly applied to the earpiece. The novelty of this approach is the use of constrained 3D mesh deformation, known as as-constrained-as-possible (ACAP), to deform the earpiece while preserving user-defined form regions. With any product design, there are regions that must remain the same shape due to their functionality, for example mounting holes, acoustic cavities, or push-fit regions. By incorporating form preservation in the mesh deformation it allows for the CAD design to be deformed under the deformation field whilst preserving key features.

7.3.1 Applying Constraints using ACAP

In Chapter 5 the mathematical background and operation of the algorithm was discussed. Extending the widely used as-rigid-as-possible (ARAP) mesh deformation framework to incorporate user constraints has led to a new approach in customized design. By segmenting a standard CAD design, such that the indices of the form regions are recorded, the algorithms are able to process them and apply constraints to the Laplacian deformation system. Contrary to the approaches seen in Section 1.1.5, the application of segmentation to mesh constraints is a very simple process. In this research, the user manually selected the faces of the mesh where the form region was required. While this allows for simple selection of key features, a difficulty was established in the selection of internal cavities. Due to the manual selection, using brush-like tools, the form region needs to be visible to the user. This makes the selection of

internal cavities or obstructed areas difficult to manually annotate. While this was not an issue for the earpiece design in Figure 6.5, it could potentially be an issue for hearing aid design which contains vents to relieve pressure. Future research could explore advanced selections and visualization tools to assist the user in selecting more complex form regions.

7.3.2 Advantages and Disadvantages of ACAP

The advantage of ACAP 3D mesh deformation is the realistic deformations achieved through the local rotation preservation, but also the simplicity and extensibility of the constraint system. For the in-ear device in Chapter 6, only one form region was required, but there is no upper limit. The only complexity is the increase in processing time. Considering the complexity of some in-ear devices, the ACAP customization process also allows for further constraints that control how the surface can deform, including normal constraint, relative position, and on-line constraints. The combination of these constraints with the standard form constraints should account for the full device catalogue for the human ear.

A disadvantage of the ACAP process was the sensitivity to variations in topology. It was discussed in Chapter 5 and Chapter 6 that due to the nature of the mesh deformation, the density of vertices and the topology of the mesh is critical. In this case, the topology is referring to the distribution of faces and edges on the mesh. As the ACAP deformation algorithm aims to preserve the edge lengths, their distribution on the surface needs to be optimized. This is also the case for the form preservation as the spanning tree is constructed on the mesh edges. To alleviate this issue a pre-processing step was introduced in Chapter 6, which distributes the vertices and faces on the surface of the CAD design, such that a more uniform distribution is achieved (Jakob et al., 2015). This approach circumvents possible errors in exporting CAD designs from the wide-range of available softwares.

7.3.3 Relevance to the Aim of this Thesis

Referring to research question 3, *How do we use already fully functional CAD designs as opposed to performing the processes after customization?* it can be said that by applying the ACAP 3D mesh deformation process described in Chapter 5 and Chapter 6, it is possible to control the deformation of a CAD design such that user-defined form regions can be preserved and the newly customized device can be directly 3D printed. In Chapter 5 the functionality of this ACAP process was detailed with a sample mesh and comparing against the standard ARAP process. Chapter 6 then determined the feasibility of the ACAP process to a functional earpiece.

7.4 Automated Customization of In-Ear Devices

In Chapter 6, an in-ear device was designed using the urBeats2 earphone as the base model. The in-ear device consisted of a shell that fits to the outer-ear and a form region that allows for the earphone to be mounted in the custom shell. Chapter 6 combined the research from Chapter 3 to Chapter 5, showing the use of the SSM and the application of the ACAP 3D mesh deformation process. Through experimentation it was seen that the SSM can fit accurately to the given input 3D scans, which in turn creates a deformation field that is transferred to the in-ear device, the ACAP process then deforms the device to fit the input 3D scan preserving the user-defined form regions.

7.4.1 Advantages of the ACAP Automated Customization Process

The simplicity of the segmentation approach to adding constraints allows for CAD designs to be pre-processed in a very efficient manner. Following the preprocessing, i.e. retopologization and segmentation, the ACAP process is relatively fast; it takes less than 1 minute to process a custom-fit in-ear device. This is not including the time taken to fit the SSM to the input 3D scan, which takes approximately 2 minutes.

The main advantage of the proposed automated customization process is the degree to which automation has been achieved. While there are aspects of the 3D scanning from Chapter 3 that require further work, mainly related to processing time and noise, it has been shown that as long as the data is relatively occlusion free and of high quality then the proposed automated customization framework will still work. To process the 3D scan data, a completely automatic system has been developed which can process not only the SSM but also the customized design of the earpiece.

7.4.2 Limitations of the ACAP Automated Customization Process

The limitation of the proposed automated customization framework is in the sensitivity of the ACAP processes to variations in topology. While this is a limitation, a pre-processing stage was added which alleviates the issue. At this stage of the research, the main limitations are found in processing time, i.e. the time to process a 3D scan in Chapter 3 and the time to 3D print a set of customized earphones in Chapter 6. While this is a current limitation, improvements have been proposed which could potentially solve these issues. For 3D scanning, altering the system to a stationary setup would allow for faster processing times. The development of dedicated reconstruction algorithms for the human ear would also allow for more efficient processing. For 3D printing, changing from a laser-based SLA to a mask-based system would allow for faster processing times. However, further research would be required to determine if there is any surface degradation as a result of pixelation. It was also discussed that by using the emerging ultra-fast SLA 3D printing technology, it would be possible to reduce the printing time to approximately 10-15 minutes.

7.4.3 Quantitative Assessment of the Automated Customization Process

The ultimate motivation for custom-fitting in-ear devices is to achieve a greater level of comfort and fit while also improving the sound quality by filtering out ambient noise. Quantitatively, there are not many known measures by which to assess the performance of the ACAP process. There are standard measures such as processing time or surface distortion, but, these measures do not relate to comfort and fit. While it is a simple matter to measure the time it takes to process a custom-fit in-ear device from scan to print, this aspect of the research is not of primary importance. Beyond the goal of automating the process, the critical criteria revolve around the ability to accurately and reliably fit the in-ear device to input 3D scan. Through user studies it would be possible to ascertain a subjective measure of the performance of products manufactured with the ACAP process. This is outside of the scope of this research but remains an aspect of future work.

7.5 3D Printing and Mass-Customization

Section 1.1.9 discussed the processes for 3D printing an in-ear device and the SLA-based 3D printing technology was selected due to the high surface quality when compared with FDM or SLS based 3D printing.

7.5.1 3D Printing Time and the Potential for Improvement

Within the field of SLA, it was seen that there are variations in printing technology that can be used depending on the application. For this research, the laser-based SLA system was selected due to its availability and wide range of compatible materials. It was discussed that a potential improvement in time could stem from the use of a DLP or mask based system. However, further research is required to quantify the impact of pixelation on the surface quality.

A new area of ultra-fast SLA-based 3D printing has the potential to reduce the 3D printing time from 1 hr 30 minutes to approximately 10-15 minutes. While these types of machines are not accessible at the moment due to cost, future research could involve the testing of these machines to determine the achievable surface quality and assess the available materials for in-ear devices.

7.5.2 3D Printing Materials for In-Ear Devices

This research opted for direct 3D printing of the in-ear devices which means the 3D printing material and achievable quality of the machine is critical. From the 3D printing process, the main limitation for direct 3D printing was the need for support structures. The support structures seen in Figure 8.4 (b), adhere to the surface in order to prevent warping or sagging during the 3D print process. The removal of the supports is a manual operation which requires a trained individual, and to our knowledge there is no known method for automating this at the moment. Removing the supports creates protrusions on the surface of the part and these have to be sanded, which has the potential to create issues in terms of aesthetics. A key area for future research is the improvement of the surface quality using direct 3D printing and the assessment of consumer opinions about directly 3D printed devices versus indirect.

7.6 Automated Customization and the Research Questions

The initial aim of this thesis was the development of a method for automated customization of in-ear devices from 3D scan data. By assessing the results in Chapter 6 it can be said that this aim has largely been achieved. Using the 3D scanning system developed in Chapter 3, with the SSM in Chapter 4, and the ACAP mesh deformation process in Chapter 5, a completely automated customization framework from scan to print has been developed. This framework can operate without the need for a trained expert at any stage of the customization process. During the initial design stages, a trained individual is required to design the in-ear device and provide the segmentations that determine how the in-ear device can deform. However, this is a standard process in the design of any device and only needs to be performed once. Following this the automated customization system is able to output customized in-ear devices from the input 3D scan, and pre-processed CAD design. The SLA 3D printer then automatically processes the part for 3D printing. However, the post-processing, as discussed in Section 1.1.9, is predominantly manual with no currently known method of automation. This has effectively answered research questions 1-3, while the limitations of the approach (research question 4) have been discussed in this chapter.

7.7 Future Research

While the ACAP process has proven to be able to automatically produce custom-fit in-ear devices, there are areas which can be improved.

7.7.1 Soft Body Modelling for In-Ear Device Design

The in-ear device in Chapter 6 was constructed from the mean shape of the SSM using standard CAD applications. This assumes that the ear is a rigid shape, however, in reality the ear is able to non-linearly deform. Therefore, by designing products that fit directly to the mean shape of the SSM it doesn't allow for any holding pressure to be applied to the ear. While it is relatively simple to expand the earpiece to apply some pressure, a more intuitive approach would be to model the deformation of the object during the design stage. In this way, it will be clearly seen where the ear will deform under certain pressures, allowing for a more accurate pressure profile to be constructed from the in-ear device.

7.7.2 Further Constraints for the ACAP Process

For the earphone in Chapter 6 the only constraint used was the form constraint. Incorporation of further constraints such as normal, relative position, and on-line constraints will open up more possible designs with this process.

7.7.3 Functional Map Based Statistical Shape Modelling

Rustamov et al. (2013) have shown that functional maps can provide information on shape variability, without having to process each functional map back into a point-to-point correspondence as shown in Chapter 4. The only detracting factor of this approach is the inability to take the shape variability from the functional map representation back to a point based representation. In Boscaini et al. (2014), the functional map based statistical shape variation is converted back to a point-based representation, however, under certain conditions that make it not applicable to this research. Future research will involve the in-depth analysis of this approach in order to apply it to statistical analysis of the human ear. One of the computational bottlenecks of the SSM process in Chapter 4 is the computation of the point-to-point correspondence from the functional map representation, should it be possible to remove the point-to-point conversion, a considerable time saving will be achieved.

7.7.4 User Studies on Comfort for In-Ear Devices

This thesis has been proposed to establish the feasibility of using automation tools for the customization of in-ear devices. It can be said that it is possible to automatically produce customized in-ear devices directly from 3D scan data. However, questions still remain on the level of comfort that can be achieved through this process. Due to ethical and time restrictions it was not possible to perform a full user study during this research. However, user studies are being performed as part of further development of this process and it is anticipated that it will be possible to quantify the improvement this process makes over standard moulding procedures.

7.7.5 Automatic Post-Processing of SLA-Based 3D Printed Parts

Post-processing is one of the main limitations of the 3D printing process for automation. This involves, cleaning, support removal, post-curing, sanding, and optional surface treatments. To the best of our knowledge, the cleaning and post-curing processes have successfully been automated but there is no known method for the automation of support removal or sanding. Future research will involve the development of methods to either ease the process of removing the supports through the use of software or completely automating the removal process using robotics.

7.8 Conclusion

The aim of this thesis was the development of a method for automated customization of in-ear devices from 3D scan data. By reviewing the results in Chapter 6, it can be said that this has been achieved. Throughout the research, the goal of automation has been a critical theme, from the development of the 3D scanning, to the processing of the statistical shape model, and finally to the customization of the CAD design. As such, a customization framework has been developed which can operate without the input of a trained expert. A major novelty of this system is the use of a full 3D statistical shape model, as opposed to a sparse set of landmarks, working together with algorithms that control how the CAD design can deform. The headless nature of the system is a step forward towards the goal of mass-customization, where customized products are not a novelty but a standard process. While the customization framework is functional in its current state, there are areas remaining for future research, predominantly relating to improvements in processing time and quality for 3D scanning, the design of the CAD product relative to statistical shape model, and the extension of the customization framework to incorporate more advanced deformations.

Bibliography

- 3Dresyns (2017), 'Otoplastic 3dresyn oto-s basic color and synthetic'.
URL: <https://www.3dresyns.com/collections/otoplastic-3dresyns-oto-sf-clear-and-basic-colors/products/otoplastic-3dresyn-oto-s-basic-color-syntehtic>
- Agisoft (2006), 'Agisoft photoscan'.
URL: <http://www.agisoft.com/>
- Agisoft (2014), 'Tutorial (intermediate level): Coded targets & scale bars in agisoft photoscan pro 1.0.0', Online.
- Artec (2012), 'Artec eva: Fast 3d scanner for professionals'.
URL: <https://goo.gl/hQJVCj>
- Artec3D (2015), 'Robotic arm scans motorcycle engine with artec spider'.
URL: <https://www.artec3d.com/news/robotic-arm-scans-motorcycle-engine-artec-spider>
- Baloch, S., Sickel, K., Bubnik, V., Melkisetoglu, R., Azernikov, S., Reh, A., Boltyenkov, A. and Fang, T. (2010), Feature driven rule based framework for automatic modeling of organic shapes in the design of personalized medical prosthetics, *in* 'International Workshop on Medical Imaging and Virtual Reality', Springer, pp. 128–138.
- Bernard, F., Gemmar, P., Hertel, F., Goncalves, J. and Thunberg, J. (2016), Linear shape deformation models with local support using graph-based structured matrix factorisation, *in* 'Proceedings of the IEEE Conference on Computer Vision and Pattern Recognition', pp. 5629–5638.
- Besl, P. J. and McKay, N. D. (1992), Method for registration of 3-d shapes, *in* 'Sensor Fusion IV: Control Paradigms and Data Structures', Vol. 1611, International Society for Optics and Photonics, pp. 586–607.
- Beyeler, M. (2015), *OpenCV with Python Blueprints*, Packt Publishing, chapter 4.
- Blom, J. (2000), Personalization: a taxonomy, *in* 'CHI'00 extended abstracts on Human factors in computing systems', ACM, pp. 313–314.
- Boscaini, D., Eynard, D. and Bronstein, M. M. (2014), 'Shape-from-intrinsic operator', *arXiv preprint arXiv:1406.1925*.
- Bronstein, M. M., Bruna, J., LeCun, Y., Szlam, A. and Vandergheynst, P. (2017), 'Geometric deep learning: going beyond euclidean data', *IEEE Signal Processing Magazine* **34**(4), 18–42.
- Brown, Z. and Cole, R. J. (2009), 'Influence of occupants' knowledge on comfort expectations and behaviour', *Building Research & Information* **37**(3), 227–245.
- Burge, M. and Burger, W. (1997), 'Ear biometrics for machine vision'.
- Bustard, J. D. and Nixon, M. S. (2010), 3d morphable model construction for robust ear and face recognition, *in* 'Computer Vision and Pattern Recognition (CVPR), 2010 IEEE Conference on', IEEE, pp. 2582–2589.

- Cadavid, S. and Abdel-Mottaleb, M. (2008), '3-d ear modeling and recognition from video sequences using shape from shading', *IEEE Transactions on Information Forensics and Security* **3**(4), 709–718.
- CameraGrip (2017), 'Tracking systems.'
URL: <https://www.cameragrip.com/camera-tracking-systems/>
- Campbell, R. (2006), 'Customer input and customisation', *Rapid manufacturing: An industrial revolution for the digital age* pp. 19–37.
- Choudhari, C. and Patil, V. (2016), Product development and its comparative analysis by sls, sls and fdm rapid prototyping processes, in 'IOP Conference Series: Materials Science and Engineering', Vol. 149, IOP Publishing, p. 012009.
- Coward, T. J., Scott, B., Watson, R. and Richards, R. (2002), 'Identifying the position of an ear from a laser scan: The significance for planning rehabilitation', *International journal of oral and maxillofacial surgery* **31**(3), 244–251.
- Coward, T., Scott, B., Watson, R. and Richards, R. (2000), 'Laser scanning of the ear identifying the shape and position in subjects with normal facial symmetry', *International journal of oral and maxillofacial surgery* **29**(1), 18–23.
- Coward, T., Watson, R. and Scott, B. (1997), 'Laser scanning for the identification of repeatable landmarks of the ears and face', *British journal of plastic surgery* **50**(5), 308–314.
- Creaform (2012), 'Goscan 3d g1 scanner'.
URL: <https://www.creaform3d.com/en/customer-support/legacy-products/goscan-3d-g1-scanner>
- Crunchbase (2013), 'Metamason: Truly personalized respiratory devices via 3d scanning and printing'.
URL: <https://www.crunchbase.com/organization/metamason>
- Dalal, P., Munsell, B. C., Wang, S., Tang, J., Oliver, K., Ninomiya, H., Zhou, X. and Fujita, H. (2007), A fast 3d correspondence method for statistical shape modeling, in 'Computer Vision and Pattern Recognition, 2007. CVPR'07. IEEE Conference on', IEEE, pp. 1–8.
- Dalal, P. and Wang, S. (2012), 'Landmark sliding for 3d shape correspondence', *Intelligent Data Analysis for Real-Life Applications: Theory and Practice: Theory and Practice* **57**.
- Davies, R. H., Twining, C. J., Cootes, T. F., Waterton, J. C. and Taylor, C. J. (2002), 3d statistical shape models using direct optimisation of description length, in 'European conference on computer vision', Springer, pp. 3–20.
- Defferrard, M., Bresson, X. and Vandergheynst, P. (2016), Convolutional neural networks on graphs with fast localized spectral filtering, in 'Advances in Neural Information Processing Systems', pp. 3844–3852.
- Dreyfuss, H. (1960), *The measure of man: human factors in design*.
- Fang, Y., Xie, J., Dai, G., Wang, M., Zhu, F., Xu, T. and Wong, E. (2015), 3d deep shape descriptor, in 'Proceedings of the IEEE Conference on Computer Vision and Pattern Recognition', pp. 2319–2328.
- Formlabs (2017a), '3d printing technology comparison: Sla vs. dlp'.
URL: <https://formlabs.com/blog/3d-printing-technology-comparison-sla-dlp/>

- Formlabs (2017b), 'Form cell: Automated 3d print production, powered by the form 2.'.
URL: <https://formlabs.com/3d-printers/form-cell/>
- Formlabs (2017c), 'Laser sla vs dlp vs masked sla 3d printing technology'.
URL: <https://formlabs.com/3d-printers/form-2/>
- Formlabs (2018), 'Formlabs white paper: Custom silicone ear molds with the form 2'.
- Frey, S. (2017), 'Laser sla vs dlp vs masked sla 3d printing technology'.
URL: <http://theorthocosmos.com/laser-sla-vs-dlp-vs-masked-sla-3d-printing-technology-compared/>
- Furukawa, Y. and Ponce, J. (2010), 'Accurate, dense, and robust multiview stereopsis', *IEEE transactions on pattern analysis and machine intelligence* **32**(8), 1362–1376.
- Geoface (2016), 'Anatomy of outer ear diagram'.
URL: <http://www.flspinalcord.us/anatomy-of-outer-ear/best-25-external-ear-anatomy-ideas-on-pinterest-ear-anatomy-anatomy-of-outer-ear-2/>
- Gilmore, J. and Pine, B. (1997), 'The four faces of mass customization.', *Harvard business review* **75**(1), 91.
- Gizmo3DPrinters (2017), 'The worlds first super speed, high quality and affordable top down sla dlp 3d printer.'.
URL: <https://www.gizmo3dprinters.com.au/>
- Gray, E. (2018), 'The exposure triangle – a beginner's guide'.
URL: <https://photographylife.com/what-is-exposure-triangle>
- Hardawar, D. (2014), 'Normal's 3d-printed headphones are a great custom fit — but aren't for everyone (review)'.
URL: <https://venturebeat.com/2014/08/28/normals-3d-printed-headphones-are-a-great-custom-fit-but-arent-for-everyone-review/>
- Harmon, D., Panozzo, D., Sorkine, O. and Zorin, D. (2011), Interference-aware geometric modeling, in 'ACM Transactions on Graphics (TOG)', Vol. 30, ACM, p. 137.
- Harris, C. and Stephens, M. (1988), A combined corner and edge detector., Citeseer.
- hear.com (2018), 'Hearing aid innovations for 2018'.
URL: <https://www.hear.com/hearing-aids/innovations-2018/>
- Heimann, T. and Meinzer, H.-P. (2009), 'Statistical shape models for 3d medical image segmentation: a review', *Medical image analysis* **13**(4), 543–563.
- Huang, Q., Wang, F. and Guibas, L. (2014), 'Functional map networks for analyzing and exploring large shape collections', *ACM Transactions on Graphics (TOG)* **33**(4), 36.
- Huang, Q.-X. and Guibas, L. (2013), Consistent shape maps via semidefinite programming, in 'Computer Graphics Forum', Vol. 32, Wiley Online Library, pp. 177–186.
- Iannarelli, A. V. (1964), *The Iannarelli system of ear identification*, Police science series, Foundation Press, Brooklyn., 64004959 illus., port. 24 cm. Police science series (Foundation Press).
- iTranslate (2018), 'The ear translator has arrived'.
URL: <http://www.itranslate.com/ear-translator>
- Jakob, W., Tarini, M., Panozzo, D. and Sorkine-Hornung, O. (2015), 'Instant field-aligned meshes.', *ACM Trans. Graph.* **34**(6), 189.

- Konkle, D. F. and Bess, F. H. (1974), 'Custom-made vs stock earmolds in hearing aid evaluations', *Archives of Otolaryngology* **99**(2), 140–144.
- Kroon, D.-J. (2009), 'Finite iterative closest point'.
URL: <https://au.mathworks.com/matlabcentral/fileexchange/24301-finite-iterative-closest-point>
- Kwok, T.-H., Yeung, K.-Y. and Wang, C. C. (2014), 'Volumetric template fitting for human body reconstruction from incomplete data', *Journal of Manufacturing Systems* **33**(4), 678–689.
- Laganière, R. (2014), *OpenCV Computer Vision Application Programming Cookbook Second Edition*, Packt Publishing, chapter 10.
- Lantos Technologies (2018), '3d ear scanning'.
URL: <http://www.lantostechnologies.com/>
- Lee, W., Jung, H., Bok, I., Kim, C., Kwon, O., Choi, T. and You, H. (2016), Measurement and application of 3d ear images for earphone design, in 'Proceedings of the Human Factors and Ergonomics Society Annual Meeting', Vol. 60, SAGE Publications Sage CA: Los Angeles, CA, pp. 1053–1057.
- Lévy, B. (2006), Laplace-beltrami eigenfunctions towards an algorithm that "understands" geometry, in 'Shape Modeling and Applications, 2006. SMI 2006. IEEE International Conference on', IEEE, pp. 13–13.
- Li, C. and Hamza, A. B. (2013), 'A multiresolution descriptor for deformable 3d shape retrieval', *The Visual Computer* **29**(6-8), 513–524.
- Li, C., Mu, Z., Zhang, F. and Wang, S. (2012), A novel 3d ear reconstruction method using a single image, in 'Intelligent Control and Automation (WCICA), 2012 10th World Congress on', IEEE, pp. 4891–4896.
- Li, C., Wei, W. and Mu, Z. (2015), Improved 3d ear reconstruction based on 3d emm, in 'Information and Automation, 2015 IEEE International Conference on', IEEE, pp. 2842–2847.
- Liu, H. and Yan, J. (2007), Multi-view ear shape feature extraction and reconstruction, in 'Signal-Image Technologies and Internet-Based System, 2007. SITIS'07. Third International IEEE Conference on', IEEE, pp. 652–658.
- Liu, Y., Lu, G. and Zhang, D. (2015), 'An effective 3d ear acquisition system', *PloS one* **10**(6), e0129439.
- Mandad, M., Cohen-Steiner, D., Kobbelt, L., Alliez, P. and Desbrun, M. (2017), 'Variance-minimizing transport plans for inter-surface mapping', *ACM Transactions on Graphics (TOG)* **36**(4), 39.
- Mansurov, N. (2018), 'Understanding iso for beginners – photography basics'.
URL: <https://photographylife.com/what-is-iso-in-photography>
- Masuda, H., Yoshioka, Y. and Furukawa, Y. (2007), 'Preserving form features in interactive mesh deformation', *Computer-Aided Design* **39**(5), 361–368.
- Modat, M., Ridgway, G. R., Taylor, Z. A., Lehmann, M., Barnes, J., Hawkes, D. J., Fox, N. C. and Ourselin, S. (2010), 'Fast free-form deformation using graphics processing units', *Computer methods and programs in biomedicine* **98**(3), 278–284.

- Mugge, R., Schoormans, J. P. L. and Schifferstein, H. N. J. (2009), 'Emotional bonding with personalised products', *Journal of Engineering Design* **20**(5), 467–476.
URL: <http://dx.doi.org/10.1080/09544820802698550>
- Myronenko, A. and Song, X. (2010), 'Point set registration: Coherent point drift', *IEEE transactions on pattern analysis and machine intelligence* **32**(12), 2262–2275.
- Myronenko, A., Song, X., Carreira-Perpinán, M. A. et al. (2007), 'Non-rigid point set registration: Coherent point drift', *Advances in Neural Information Processing Systems* **19**, 1009.
- Naddeo, A., Cappetti, N., Califano, R. and Vallone, M. (2015), 'The role of expectation in comfort perception: the mattresses' evaluation experience', *Procedia Manufacturing* **3**, 4784–4791.
- Nakamura, T., Goverdovsky, V. and Mandic, D. P. (2018), 'In-ear eeg biometrics for feasible and readily collectable real-world person authentication', *IEEE Transactions on Information Forensics and Security* **13**(3), 648–661.
- Netter, F. H. (2017), *Atlas of Human Anatomy*, Elsevier Health Sciences.
- Nguyen, A., Alqurashi, R., Raghebi, Z., Banaei-Kashani, F., Halbower, A. C. and Vu, T. (2016), A lightweight and inexpensive in-ear sensing system for automatic whole-night sleep stage monitoring, in 'Proceedings of the 14th ACM Conference on Embedded Network Sensor Systems CD-ROM', ACM, pp. 230–244.
- Nogneng, D., Melzi, S., Rodolà, E., Castellani, U., Bronstein, M. and Ovsjanikov, M. (2018), 'Improved functional mappings via product preservation'.
- Ouji, K., Ardabilian, M., Chen, L. and Ghorbel, F. (2013), '3d deformable super-resolution for multi-camera 3d face scanning', *Journal of mathematical imaging and vision* **47**(1-2), 124–137.
- Ovsjanikov, M., Ben-Chen, M., Solomon, J., Butscher, A. and Guibas, L. (2012), 'Functional maps: a flexible representation of maps between shapes', *ACM Transactions on Graphics (TOG)* **31**(4), 30.
- Ovsjanikov, M., Corman, E., Bronstein, M., Rodolà, E., Ben-Chen, M., Guibas, L., Chazal, F. and Bronstein, A. (2016), Computing and processing correspondences with functional maps, in 'SIGGRAPH ASIA 2016 Courses', ACM, p. 9.
- Ownphones (2014), 'Ownphones: Wireless, custom-fit, 3d printed earbuds'.
URL: <https://www.kickstarter.com/projects/ownphones/ownphones-the-worlds-first-custom-fit-3d-printed-e>
- Palladino, V. (2016), 'Hear the pulse: Heart rate monitoring fitness earbuds tested'.
URL: <https://arstechnica.com/gadgets/2016/12/hear-the-pulse-heart-rate-monitoring-fitness-earbuds-tested/>
- Park, J.-H., Jang, D.-G., Park, J. W. and Youm, S.-K. (2015), 'Wearable sensing of in-ear pressure for heart rate monitoring with a piezoelectric sensor', *Sensors* **15**(9), 23402–23417.
- Paulsen, R., Larsen, R., Nielsen, C., Laugesen, S. and Ersbøll, B. (2002), Building and testing a statistical shape model of the human ear canal, in 'International Conference on Medical Image Computing and Computer-Assisted Intervention', Springer, pp. 373–380.
- Pears, N., Liu, Y. and Bunting, P. (2012), *3D imaging, analysis and applications*, Vol. 3, Springer.

- Pereañez, M., Lekadir, K., Butakoff, C., Hoogendoorn, C. and Frangi, A. F. (2014), 'A framework for the merging of pre-existing and correspondenceless 3d statistical shape models', *Medical image analysis* **18**(7), 1044–1058.
- Petik, A. (2000), Some aspects of using stl file format in cae systems.
- Piller, F. and Tseng, M. (2010), Introduction: Mass customization thinking: Moving from pilot stage to an established business strategy, in 'Handbook of Research in Mass Customization and Personalization: (In 2 Volumes)', World Scientific, pp. 1–18.
- Pine, B. J. (1993), 'Mass customisation', *Harvard Business School Press. Boston, Massachusetts* .
- Pishchulin, L., Wuhrer, S., Helten, T., Theobalt, C. and Schiele, B. (2015), 'Building statistical shape spaces for 3d human modeling', *arXiv preprint arXiv:1503.05860* .
- Pishchulin, L., Wuhrer, S., Helten, T., Theobalt, C. and Schiele, B. (n.d.).
- RedStack (2017), 'Selecting the right 3d printing technology: Fdm vs. sla vs. sls'.
URL: <https://goo.gl/Fs4FGr>
- Rodolà, E., Cosmo, L., Bronstein, M. M., Torsello, A. and Cremers, D. (2016), Partial functional correspondence, in 'Computer Graphics Forum', Wiley Online Library.
- Rodolà, E., Cosmo, L., Bronstein, M. M., Torsello, A. and Cremers, D. (2017), Partial functional correspondence, in 'Computer Graphics Forum', Vol. 36, Wiley Online Library, pp. 222–236.
- Rodola, E., Moeller, M. and Cremers, D. (2015), 'Point-wise map recovery and refinement from functional correspondence', *arXiv preprint arXiv:1506.05603* .
- Rustamov, R. M. (2007), Laplace-beltrami eigenfunctions for deformation invariant shape representation, in 'Proceedings of the fifth Eurographics symposium on Geometry processing', Eurographics Association, pp. 225–233.
- Rustamov, R. M., Ovsjanikov, M., Azencot, O., Ben-Chen, M., Chazal, F. and Guibas, L. (2013), 'Map-based exploration of intrinsic shape differences and variability', *ACM Transactions on Graphics (TOG)* **32**(4), 72.
- Salti, S., Tombari, F. and Di Stefano, L. (2014), 'Shot: Unique signatures of histograms for surface and texture description', *Computer Vision and Image Understanding* **125**, 251–264.
- Si, H. (2015), 'Tetgen, a delaunay-based quality tetrahedral mesh generator', *ACM Transactions on Mathematical Software (TOMS)* **41**(2), 11.
- Sickel, K., Baloch, S., Melkisetoglu, R., Bubnik, V., Azernikov, S. and Fang, T. (2011), 'Toward automation in hearing aid design', *Computer-Aided Design* **43**(12), 1793–1802.
- Slabaugh, G., Fang, T., McBagonluri, F., Zouhar, A., Melkisetoglu, R., Xie, H. and Unal, G. (2008a), '3-d shape modeling for hearing aid design [applications corner]', *IEEE Signal Processing Magazine* **25**(5).
- Slabaugh, G., Fang, T., McBagonluri, F., Zouhar, A., Melkisetoglu, R., Xie, H. and Unal, G. (2008b), '3d shape modeling for hearing aid design'.
- Snugs (2017), 'Create your unique earphones'.
URL: <https://snugs.com/>
- Sorkine, O. (2005), Laplacian mesh processing.

- Sorkine, O. and Alexa, M. (2007), As-rigid-as-possible surface modeling.
- Sun, C., Mu, Z.-c. and Zeng, H. (2009), Automatic 3d ear reconstruction based on epipolar geometry, *in* 'Image and Graphics, 2009. ICIG'09. Fifth International Conference on', IEEE, pp. 496–500.
- Sun, J., Zheng, N.-N. and Shum, H.-Y. (2003), 'Stereo matching using belief propagation', *IEEE Transactions on pattern analysis and machine intelligence* **25**(7), 787–800.
- Tam, G. K., Cheng, Z.-Q., Lai, Y.-K., Langbein, F. C., Liu, Y., Marshall, D., Martin, R. R., Sun, X.-F. and Rosin, P. L. (2013), 'Registration of 3d point clouds and meshes: a survey from rigid to nonrigid', *IEEE transactions on visualization and computer graphics* **19**(7), 1199–1217.
- Tanenbaum, M. and Hollstein K, W. (2016), 'Mass production'.
URL: <https://www.britannica.com/technology/mass-production>
- Ten-24 (2009), '3d scan store'.
URL: <http://www.3dscanstore.com/>
- Tola, E., Lepetit, V. and Fua, P. (2010), 'Daisy: An efficient dense descriptor applied to wide-baseline stereo', *IEEE transactions on pattern analysis and machine intelligence* **32**(5), 815–830.
- Tumbleston, J. R., Shirvanyants, D., Ermoshkin, N., Januszewicz, R., Johnson, A. R., Kelly, D., Chen, K., Pinschmidt, R., Rolland, J. P., Ermoshkin, A. et al. (2015), 'Continuous liquid interface production of 3d objects', *Science* **347**(6228), 1349–1352.
- Unal, G. (2010), 'Nonparametric joint shape learning for customized shape modeling', *Computerized Medical Imaging and Graphics* **34**(4), 298–307.
- Unal, G., Nain, D., Slabaugh, G. and Fang, T. (2011), 'Generating shapes by analogies: An application to hearing aid design', *Computer-Aided Design* **43**(1), 47–56.
- UND (2007), 'Biometric datasets'.
URL: <https://sites.google.com/a/nd.edu/public-cvrl/data-sets>
- Van Kaick, O., Zhang, H., Hamarneh, G. and Cohen-Or, D. (2011), A survey on shape correspondence, *in* 'Computer Graphics Forum', Vol. 30, Wiley Online Library, pp. 1681–1707.
- Varotsis, A. (2017), 'Introduction to sla 3d printing'.
URL: <https://www.3dhubs.com/knowledge-base/introduction-sla-3d-printing>
- Vestner, M., Litman, R., Rodolà, E., Bronstein, A. and Cremers, D. (2017), Product manifold filter: Non-rigid shape correspondence via kernel density estimation in the product space, *in* 'Proceedings of CVPR'.
- VMC (2018), 'Ear anatomy and physiology'.
URL: <https://www.myvmc.com/anatomy/ear/>
- White, R. and Forsyth, D. A. (2006), Combining cues: Shape from shading and texture, *in* 'Computer Vision and Pattern Recognition, 2006 IEEE Computer Society Conference on', Vol. 2, IEEE, pp. 1809–1816.
- Wickramaratne, V. D. W., Ryazanov, V. and Vinogradov, A. (2009), 'Analysis of a 3d face-scanning system by active triangulation', *Pattern Recognition and Image Analysis* **19**(1), 78–83.
- Wijenayake, U., Choi, S.-I. and Park, S.-Y. (2014), Automatic detection and decoding of photogrammetric coded targets, *in* 'Electronics, Information and Communications (ICEIC), 2014 International Conference on', IEEE, pp. 1–2.

- Yan, P. and Bowyer, K. W. (2007), 'Biometric recognition using 3d ear shape', *IEEE Transactions on pattern analysis and machine intelligence* **29**(8), 1297–1308.
- Zeng, H., Mu, Z.-C., Wang, K. and Sun, C. (2009), Automatic 3d ear reconstruction based on binocular stereo vision, in 'Systems, Man and Cybernetics, 2009. SMC 2009. IEEE International Conference on', IEEE, pp. 5205–5208.
- Zhang, S. and Yau, S.-T. (2007), 'High-speed three-dimensional shape measurement system using a modified two-plus-one phase-shifting algorithm', *Optical Engineering* **46**(11), 113603–113603.
- Zouhar, A., Baloch, S., Azernikov, S., Bahlmann, C., Unal, G., Fang, T. and Fuchs, S. (2009), Freeform shape clustering for customized design automation, in 'Computer Vision Workshops (ICCV Workshops), 2009 IEEE 12th International Conference on', IEEE, pp. 1590–1597.